2 March 2007 | S10

Science

AAAS

Volume 315, Issue 5816

COVER

In adult humans, newly born brain cells travel in the rostral migratory streams (orange bands) from the fluid-filled lateral ventricles (pink structures at top) to the olfactory bulbs, along hollow tubelike extensions of the ventricles. See page 1243.

Image: Jonathan Westin

DEPARTMENTS

1187 *Science* Online
1189 This Week in *Science*
1194 Editors' Choice
1196 Contact *Science*
1199 Random Samples
1201 Newsmakers
1287 New Products
1288 *Science* Careers

EDITORIAL

1193 Animal Health Research
by Jakob Zinsstag

NEWS OF THE WEEK

Tight Budget Takes a Toll on U.S.–Funded Clinical Trials 1202
Dreams Collide With Reality for International Experiment 1203
African Penguin Populations Reported in a Puzzling Decline 1205
SCIENCESCOPE 1205
Mystery Towers in Peru Are an Ancient Solar Calendar 1206
>> *Research Article p. 1239*
Democrats Rescue Technology Research Program 1206
Data on Adult Stem Cells Questioned 1207

NEWS FOCUS

Brain Evolution Studies Go Micro 1208
Recruiting the Cell's Own Guardian for Cancer Therapy 1211
A Healthy Tan? 1214
Why I Have Red Hair, Need to Avoid the Sun, and Shouldn't Commit a Crime
Pollutant Hazes Extend Their Climate-Changing Reach 1217

1208

LETTERS

To Sleep, Perchance to Dream *R. Conduit* 1219
Response *C. Adami; H. Lipson, V. Zykov, J. Bongard*
Online Versus Hardcopy Textbooks *R. I. Dorn*
Is the EC Afraid of Its Own Visions? *J. Settele* et al.
CORRECTIONS AND CLARIFICATIONS 1220

BOOKS *ET AL.*

The Omnivore's Dilemma A Natural History of Four Meals *M. Pollan, reviewed by T. Plieninger* 1222
Skin A Natural History *N. G. Jablonski, reviewed by Q. Al-Awqati* 1223

POLICY FORUM

Consequences of Regional-Scale Nuclear Conflicts *O. B. Toon* et al. 1224

PERSPECTIVES

Negative Refraction for Electrons? *J. B. Pendry* 1226
>> *Report p. 1252*
Keep It Local *A. Buckling* 1227
>> *Report p. 1284*
Water from First Principles *A. J. Stone* 1228
>> *Report p. 1249*
A Missing Link in Membrane Protein Evolution *B. Poolman, E. R. Geertsma, D.-J. Slotboom* 1229
>> *Report p. 1282*
How the Wood Moves *K. Shea* 1231
Forecasting Hurricane Intensity and Impacts *H. E. Willoughby* 1232
>> *Research Article p. 1235*

1231

CONTENTS continued >>

Science

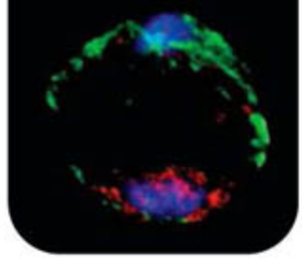

SCIENCE EXPRESS

www.sciencexpress.org

CLIMATE CHANGE

Discovery of Till Deposition at the Grounding Line of Whillans Ice Stream
S. Anandakrishnan, G. A. Catania, R. B. Alley, H. J. Horgan
Sediments have been accumulating beneath a major Antarctic ice stream where it begins to float over water, implying that the glacier is extensively eroding its bed.
10.1126/science.1138393

CLIMATE CHANGE

Effect of Sedimentation on Ice-Sheet Grounding-Line Stability
R. B. Alley, S. Anandakrishnan, T. K. Dupont, B. R. Parizek, D. Pollard
Accumulation of sediments where glaciers begin to float stabilizes them against changes in sea level, implying that changes in temperature, not sea level, have driven past melting.
10.1126/science.1138396

IMMUNOLOGY

Asymmetric T Lymphocyte Division in the Initiation of Adaptive Immune Responses
J. T. Chang et al.
Upon antigen binding, immune cells generate pathogen-fighting cells from daughters arising close to the antigen and memory cells from daughters away from it.
10.1126/science.1139393

MEDICINE

CREB-Binding Protein Modulates Repeat Instability in a *Drosophila* Model for PolyQ Disease
J. Jung and N. Bonini
Transgenic fruit flies show many features of a human triplet repeat disease, including expansion of the repeats, and thus can provide clues for therapeutic intervention.
10.1126/science.1139517

TECHNICAL COMMENT ABSTRACTS

PSYCHOLOGY

Comment on "Detecting Awareness in the Vegetative State" 1221
P. Nachev and M. Husain
full text at www.sciencemag.org/cgi/content/full/315/5816/1221a

Comment on "Detecting Awareness in the Vegetative State"
D. L. Greenberg
full text at www.sciencemag.org/cgi/content/full/315/5816/1221b

Response to Comments on "Detecting Awareness in the Vegetative State"
A. M. Owen et al.
full text at www.sciencemag.org/cgi/content/full/315/5816/1221c

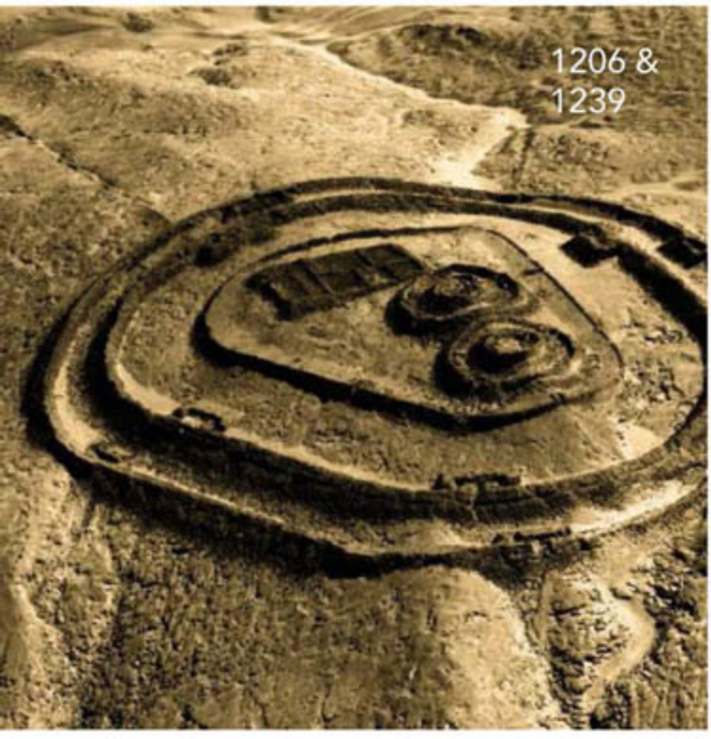

BREVIA

GEOCHEMISTRY

Was There Really an Archean Phosphate Crisis? 1234
K. O. Konhauser, S. V. Lalonde, L. Amskold, H. D. Holland
High silica concentrations in Archean oceans may have prevented iron oxyhydroxides from depleting the oceans of nutritionally essential phosphate, as had been thought.

RESEARCH ARTICLES

ATMOSPHERIC SCIENCE

Hurricane Intensity and Eyewall Replacement 1235
R. A. Houze Jr. et al.
Aircraft observations of Hurricane Rita show that downward winds outside the eye wall led to its replacement by a new outer eye wall, causing cyclic strengthening of the storm.
>> Perspective p. 1232

ARCHAEOLOGY

Chankillo: A 2300-Year-Old Solar Observatory in Coastal Peru 1239
I. Ghezzi and C. Ruggles
Stone towers built on a hill in a 2300-year-old Peruvian temple imply that careful observations of the Sun were made in the New World long before the Inca civilization.
>> News story p. 1206

NEUROSCIENCE

Human Neuroblasts Migrate to the Olfactory Bulb via a Lateral Ventricular Extension 1243
M. A. Curtis et al.
As in rodents, adult human neurons born along the fluid-filled ventricles in the brain migrate to the olfactory bulb along a tubelike extension of the ventricle.

CONTENTS continued >>

REPORTS

CHEMISTRY

Predictions of the Properties of Water from First Principles 1249

R. Bukowski et al.

A purely quantum mechanical potential energy function accurately predicts many features of water in forms ranging from an isolated pair of molecules to the bulk liquid. *>> Perspective p. 1228*

PHYSICS

The Focusing of Electron Flow and a Veselago Lens in Graphene *p-n* Junctions 1252

V. V. Cheianov, V. Fal'ko, B. L. Altshuler

Balancing the densities of electrons and holes across a graphene-based junction can focus an electric current, potentially leading to electronic lenses and electron beam-splitters. *>> Perspective p. 1226*

PALEONTOLOGY

Halwaxiids and the Early Evolution of the Lophotrochozoans 1255

S. Conway Morris and J.-B. Caron

A new species from the Burgess Shale unites two enigmatic groups important in the early evolution of bilateria and implies that mollusks diverged early in the Cambrian.

ATMOSPHERIC SCIENCE

Rethinking Organic Aerosols: Semivolatile Emissions and Photochemical Aging 1259

A. L. Robinson et al.

Organic aerosols, thought to be unmodified from their sources, instead typically evolve through a cycle of evaporation, oxidation, and reformation in urban atmospheres.

NEUROSCIENCE

Anti-Hebbian Long-Term Potentiation in the Hippocampal Feedback Inhibitory Circuit 1262

K. P. Lamsa et al.

In an unusual form of plasticity, certain synapses in rat interneurons are strengthened if presynaptic activity occurs while the postsynaptic cell is at rest or hyperpolarized.

NEUROSCIENCE

Nucleus Accumbens D2/3 Receptors Predict Trait Impulsivity and Cocaine Reinforcement 1267

J. W. Dalley et al.

Rats that tend to abuse cocaine have lower dopamine receptor availability even before drug exposure, suggesting that this trait is preexisting and not a result of drug abuse.

CELL BIOLOGY

Reconstitution of DNA Segregation Driven by Assembly of a Prokaryotic Actin Homolog 1270

E. C. Garner, C. S. Campbell, D. B. Weibel, R. D. Mullins

DNA movement during prokaryotic cell division can be reconstituted in a cell-free system by an actin-like protein and a DNA binding protein, which form a bipolar spindle.

IMMUNOLOGY

Multiple Functions of the IKK-Related Kinase IKKε in Interferon-Mediated Antiviral Immunity 1274

B. R. tenOever et al.

A kinase activated in response to viral infection unexpectedly acts directly on a transcription factor for antiviral genes.

GENETICS

***LRP6* Mutation in a Family with Early Coronary Disease and Metabolic Risk Factors** 1278

A. Mani et al.

A mutation in a key signaling pathway causes both coronary artery disease and a metabolic syndrome, explaining why these disorders are often associated with one another.

BIOCHEMISTRY

Emulating Membrane Protein Evolution by Rational Design 1282

M. Rapp, S. Seppälä, E. Granseth, G. von Heijne

Stepwise modifications to a drug efflux pump show how the bacterial dimeric pump may have evolved through duplication and inversion of an ancestral protein domain. *>> Perspective p. 1229*

EPIDEMIOLOGY

Local Interactions Select for Lower Pathogen Infectivity 1284

M. Boots and M. Mealor

Among caterpillars harboring a virus, the least mobile individuals harbor the least infective viruses, confirming a basic hypothesis about disease transmission. *>> Perspective p. 1227*

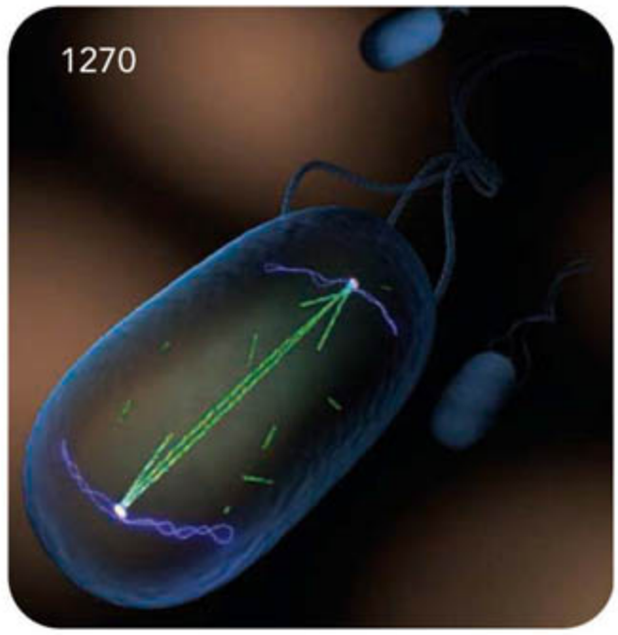

AAAS
ADVANCING SCIENCE, SERVING SOCIETY

SCIENCE (ISSN 0036-8075) is published weekly on Friday, except the last week in December, by the American Association for the Advancement of Science, 1200 New York Avenue, NW, Washington, DC 20005. Periodicals Mail postage (publication No. 484460) paid at Washington, DC, and additional mailing offices. Domestic individual membership and subscription (51 issues): $142 ($74 allocated to subscription). Domestic institutional subscription (51 issues): $710; Foreign postage extra: Mexico, Caribbean (surface mail) $55; other countries (air assist delivery) $85. First class, airmail, student, and emeritus rates on request. Canadian rates with GST available upon request, GST #1254 88122. Publications Mail Agreement Number 1069624. **Printed in the U.S.A.**

Change of address: Allow 4 weeks, giving old and new addresses and 8-digit account number. **Postmaster:** Send change of address to AAAS, P.O. Box 96178, Washington, DC 20090–6178. **Single-copy sales:** $10.00 current issue, $15.00 back issue prepaid includes surface postage; bulk rates on request. **Authorization to photocopy** material for internal or personal use under circumstances not falling within the fair use provisions of the Copyright Act is granted by AAAS to libraries and other users registered with the Copyright Clearance Center (CCC) Transactional Reporting Service, provided that $18.00 per article is paid directly to CCC, 222 Rosewood Drive, Danvers, MA 01923. The identification code for *Science* is 0036-8075. *Science* is indexed in the *Reader's Guide to Periodical Literature* and in several specialized indexes.

CONTENTS continued >>

SCIENCENOW

www.sciencenow.org DAILY NEWS COVERAGE

Anti-HIV Strategy Backfires in Botswana
Switch from breast-feeding to infant formula leads to pathogen outbreak.

Fish Mix-Up Complicates Conservation Efforts
Mysterious spearfish may be inflating numbers of threatened white marlin population.

Evolution: It Does a Body Good
Study of ancient skeletons reveals ability to digest milk arose relatively recently.

Common network motifs.

SCIENCE'S STKE

www.stke.org
SIGNAL TRANSDUCTION KNOWLEDGE ENVIRONMENT

PERSPECTIVE: Book Review—Understandable Complexity
J. Stelling
The book "An Introduction to Systems Biology" offers a look at the design principles of biological control circuits.

FORUM
Share your thoughts in the "Open Discussion of Modeling and Computational Approaches to Cellular Signaling."

The big jump to independence.

SCIENCE CAREERS

www.sciencecareers.org CAREER RESOURCES FOR SCIENTISTS

MISCINET: Priming the Mind
P. Shulman
Grad student Lawrence Williams studies factors we aren't aware of that influence thoughts and decisions.

GLOBAL: Mind Matters—Making the Leap to Independence
I. S. Levine
Scientists need a mix of science and business skills, plus the right attitude, to start up their own labs.

US: A "Hippocratic Oath" for Scientists?
B. L. Benderly
Ethical commitments could improve the practice of science and the treatment of early-career scientists.

GRANTSNET: March 2007 Funding News
GrantsNet Staff
Learn about the latest research funding opportunities, scholarships, fellowships, and internships.

SCIENCEPODCAST

Listen to the 2 March *Science* Podcast to hear about how a microview of neuroanatomy is spurring new insights on brain evolution, the human and environmental consequences of regional nuclear conflicts, and other stories.
www.sciencemag.org/about/podcast.dtl

Separate individual or institutional subscriptions to these products may be required for full-text access.

EDITED BY STELLA HURTLEY AND PHIL SZUROMI

CREDITS (TOP TO BOTTOM): JEAN-BERNARD CARON WITH PERMISSION OF THE ROYAL ONTARIO MUSEUM AND PARKS CANADA; CHEIANOV ET AL.

<<Bring Some Order to an Explosion

The Lophotrochozoa, which comprise mollusks, worms, brachiopods, bryazoans, and several other animals, played a large role in the Cambrian explosion. Their origins and early relations are uncertain, but bear on the pace and magnitude of Cambrian evolution, and a key issue has been the origin of several enigmatic lophotrochozoans from the Burgess Shale, principally the halkieriids and wiwaxiids. **Conway Morris and Caron** (p. 1255) describe several examples of a new fossil species from the Burgess Shale that seems to unite these two groups and implies an early evolution of mollusks.

Insights into Hurricane Intensity

Predicting how a hurricane's intensity will change duing its lifetime is challenging, in part because of difficulties in forecasting how the internal structure of the storm will evolve. **Houze *et al.*** (p. 1235; see the Perspective by **Willoughby**) examine a key component of that process, "eyewall replacement." They document in great detail the eyewall-replacement cycle in Hurricane Rita using high-resolution airborne radar observations of wind speed as well as temperature, humidity, and pressure data, and develop a conceptual model for this process. They also suggest how obtaining specific data on small-scale structure of hurricanes could improve forecasting of intensity changes.

Water from the Ground Up

The simple structure of the water molecule belies the extreme complexity of the interactions responsible for the properties of the bulk liquid. In general, theoretical analysis of liquid water relies on potential energy functions derived at least in part from experimentally measured parameters. **Bukowski *et al.*** (p. 1249; see the Perspective by **Stone**) present a water potential function derived purely from quantum-mechanical interaction forces, with no experimental inputs. Using this function, they calculate the absorption spectrum of the water dimer to high accuracy, and also reproduce the radial distribution functions and thermodynamic properties of the bulk liquid relatively well.

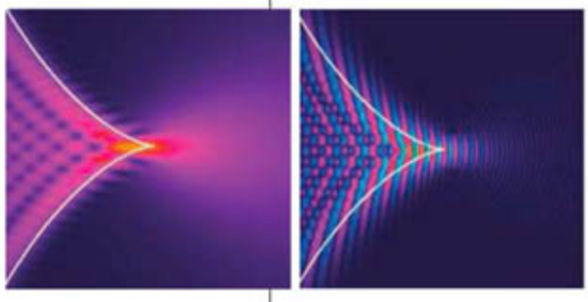

Electrons in Sharper Focus

The fabrication of metamaterials that give rise to negative refractive index for electromagnetic radiation has been used to image objects smaller than the conventional diffraction limit, and such materials hold the promise of creating the "perfect lens" that could achieve extremely fine focusing. **Cheianov *et al.*** (p. 1252; see the Perspective by **Pendry**) carry over the principle of the perfect lens and negative refraction to electron flow. They show theoretically that a graphene sheet, which makes electrical contacts such that one side is *p*-type and the other *n*-type, should be able to focus the flow of electrons as they pass through the *pn*-junction. They argue that such an effect could lead to novel applications in electron optics such as electron-beam splitters and lenses.

Towers to Track the Sun

Both archaeological sites and written and spoken records document that the Incas were making careful solar observations about 500 years ago, but evidence for earlier observational activity has been difficult to obtain. **Ghezzi and Ruggles** (p. 1239; see the news story by **Mann**) now describe a series of 13 stone towers that date to 2400 years ago that are arrayed north-south along a hill in the center of a temple complex in coastal Peru, and show that these towers marked the annual rising and setting arcs of the Sun and served as a calendar accurate to a few days. Thus, these towers and the surrounding temple evidently served as an early solar observatory.

Organic Aerosol Evolution

The abundance and chemical nature of most urban organic aerosols have been thought to be primary in nature—that is, determined at their sources—and essentially static. **Robinson *et al.*** (p. 1259) combine observations and models to show that the life histories of organic aerosols are much more complex, and that large numbers of those particles have gone through a cycle of evaporation, photooxidation, and recondensation. Thus, existing theories of organic aerosol distributions, while in many cases match observations fairly well, may often be getting the right answers fortuitously. This improved understanding of organic aerosol behavior could lead to important changes in the ways that they are measured and emissions are regulated.

Rejuvenating the Human Sense of Smell

Active neurogenesis from neural progenitors continues throughout life in discrete regions of the central nervous system of most mammals. However, human adult neurogenesis is still a

Continued on page 1191

Continued from page 1189

contentious issue. Signs of adult neurogenesis have been reported in the hippocampus, but a second neurogenic niche described in rodents has not been found in recent human studies. Now, however, using multiple techniques, **Curtis *et al.*** (p. 1243, published online 15 February; see the cover) not only describe this missing rostral migratory stream in great detail but also show that it is organized around a tubular extension of the lateral ventricle that reaches into the olfactory bulb.

Prokaryotic DNA Segregation

The prokaryotic actin-like protein ParM is dynamically unstable and is thought to play a role in DNA segregation. **Garner *et al.*** (p. 1270) describe the complete reconstitution of DNA segregation in vitro using purified components. ParM, together with DNA and a DNA-binding protein, generate a bipolar spindle that can promote the directional movement of DNA and can explain in vivo DNA movements. Thus, a dynamic filament protein can mediate DNA movement in prokaryotes.

Drugs, Dopamine, and Disposition

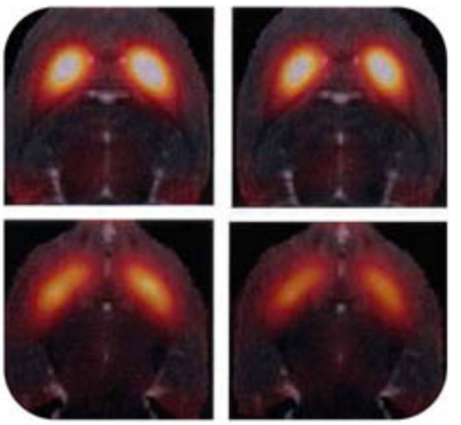

CREDIT: DALLEY *ET AL.*

Individual differences in drug abuse reflect distinct behavioral and physiological traits. **Dalley *et al.*** (p. 1267) found that, compared to controls, spontaneously impulsive rats had decreased dopamine D2/3 receptors in the nucleus accumbens even before exposure to cocaine. Trait impulsivity in rats was predictive of subsequent high rates of intravenous cocaine self-administration. Impulsivity is thus an important mediator of drug abuse vulnerability and not a consequence of chronic drug exposure.

The Heart of Metabolic Syndrome?

Patients with coronary artery disease (CAD) often have accompanying hypertension, diabetes, and aberrant levels of cholesterol and triglycerides. This diverse group of risk factors is collectively known as "metabolic syndrome," but the underlying molecular mechanisms that link these disorders are still poorly understood. **Mani *et al.*** (p. 1278), have now identified the causative mutation in a family afflicted with a rare, inherited form of early-onset CAD that cosegregates with many features of metabolic syndrome. The culprit gene encodes low-density lipoprotein receptor–related protein 6 (LRP6), a co-receptor in the Wnt cellular signaling pathway.

Reconstituting Transport Proteins

The few available crystal structures of membrane-transport proteins generally reveal internal symmetry, either about an axis perpendicular to the membrane or, somewhat more surprisingly, about an axis within the plane of the membrane. Transporters in the first class contain two structurally similar domains that exhibit the same membrane topology, which yields an even ($2n$) number of membrane-spanning helices, whereas those in the second class have oppositely oriented domains and an odd ($2n+1$) number of helices. By making stepwise modifications to the bacterial drug efflux pump EmrE, **Rapp *et al.*** (p. 1282, published online 25 January; see the Perspective by **Poolman *et al.***) show how a functional dimer might evolve from a monomer (containing n helices) that can have either membrane topology.

Local Affects on Virulence

For public health purposes, controlling infectious diseases requires a clear idea of the processes that select parasite infectivity and virulence. One key assumption is that parasites that are circulating locally in slowly mixing populations will evolve to be less infective and virulent. The converse is that as the host-parasite world becomes more connected and populations more mixed, more dangerous parasite strains will be selected. **Boots and Mealor** (p. 1284; see the Perspective by **Buckling**) test the first assumption in an easily manipulated system using a virus that infects caterpillars and verify that the host populations least able to move harbor the least infective strains of virus.

Jakob Zinsstag is an assistant professor at the Swiss Tropical Institute in Basel, Switzerland. E-mail: jakob.zinsstag@unibas.ch

Animal Health Research

TODAY'S INTIMATE AND RAPID GLOBAL INTERCONNECTIONS MEAN THAT UNCONTROLLED infectious diseases in one part of the world threaten animal and public health everywhere. The good news is that animal health sciences are technologically better equipped than ever before for detecting new disease outbreaks almost in real time. The bad news is that despite this, there is a daunting gap in converting these advances into effective actions and policies, particularly in developing countries. What can be done to remedy this lack of cohesion?

Some problems and possible solutions were recently discussed at a conference held in Hinxton, United Kingdom.* Experts in animal health research and policy-makers from high- and low-income countries reviewed developments and challenges in the field, including vaccine design, the analysis of host responses to infection, and disease transmission from wild and domestic animals to humans. There is much to laud. New approaches underlie recent progress, including genome-based vaccine discovery for treating *Anaplasma* and post-genomic selection for vaccine response in chickens. We can also predict the size of outbreaks of emerging pathogens on the basis of their reproductive ratio. Even economic losses from livestock deaths may be prevented by a detailed understanding of the cyclical transmission of pathogens (such as African *Trypanosoma*) at the livestock/wildlife interface.

Nevertheless, the conference revealed a growing divide between knowledge and application. Many strategies to detect and control disease are adequate in industrialized countries but not transferable to developing countries, namely sub-Saharan Africa. These countries often lack trained personnel and infrastructure (such as labs with water and electricity) and thus have no basic diagnostic and surveillance capacity. This includes genome-based surveillance for avian influenza, which is encroaching on the industrialized and developing world. Control strategies cannot be transferred because of insufficient funds to compensate farmers for culled stock. These deficiencies have resulted in the emergence and reemergence of infectious diseases in the developing world.

Could this frustrating gap be bridged through improved public engagement? As discussed at Hinxton, programs such as the National Centre of Competence in Research North-South, which brings together research institutions in Europe, Africa, Asia, and America, indicate that public participation is key for effective interplay among international scientists, local and national authorities, and populations confronted with animal diseases. This program, among others, has shown that by connecting these entities, long-term North-South and South-South partnerships can surpass results achieved by any institution alone. Scientists can also be effective advocates for private and public investment in the control of disease transmission [take the scientists who motivated a private donor to invest in the control of sleeping sickness (trypanosomiasis) in Uganda]. But animal health researchers should also consider new ways of knowledge-brokering to promote evidence-based policy-making. The Regional East African Community Health Policy Initiative of Kenya, Uganda, and Tanzania is one example of how scientists and policy-makers can establish priorities for research and interventions through a cyclical process of negotiation. Moreover, periodic communication of research findings by scientists to local communities leads to a more integrated research process, assuring its validity and social relevance in a given context. Just such a public engagement approach led the Chad government to propose a new policy for providing social services to nomadic pastoralist populations, including education, health, animal health, food security, and water.

Although there is no doubt that progress in animal health research must continue, it must also respond to societal needs and lead to solutions that can be delivered quickly. When science engages more with society, neither time nor resources are sacrificed. We can't afford to lose either.

– Jakob Zinsstag

10.1126/science.1141278

*The Wellcome Trust and *Science* hosted the conference "Animal Health Research: Recent Developments and Future Directions" in Hinxton, UK, from 24 to 26 January 2007.

CREDIT: FRANS LEMMENS/GETTY IMAGES

EDITED BY STELLA HURTLEY AND JAKE YESTON

BIOMEDICINE

To Splice or Be Spliced?

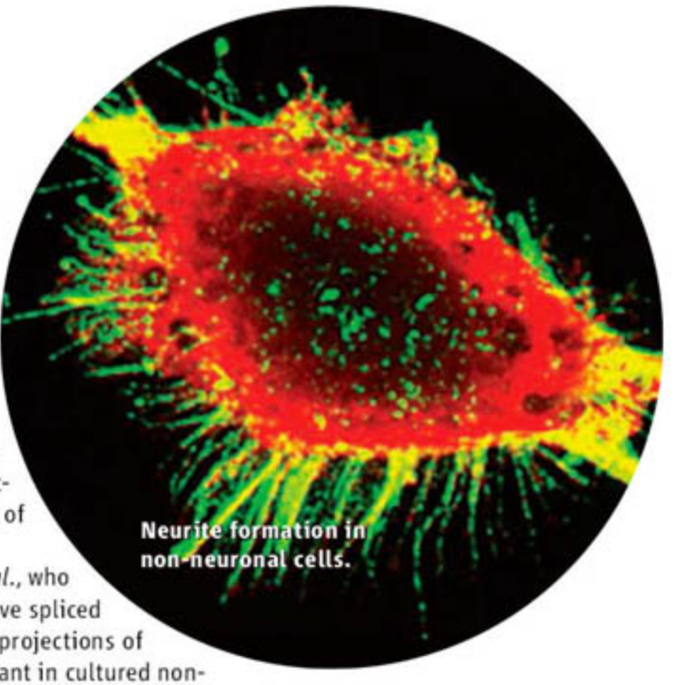

Spinal muscular atrophy (SMA) is an inherited disease characterized by the selective death of motor neurons, resulting in generalized muscle weakness that is often fatal in infancy or early childhood. SMA is caused by deletions or mutations in the gene encoding survival motor neuron 1 protein (SMN1), whose function is unclear. SMN1 contributes to the assembly of the pre-mRNA splicing machinery, and loss of SMN1 has been hypothesized to cause disease through disruption of mRNA splicing. However, this cannot readily explain the selective effect of SMN1 loss on motor neurons.

An intriguing clue to this selectivity is provided by Setola *et al.*, who identify a truncated form of SMN1 that arises from an alternative spliced *SMN1* transcript that is preferentially expressed in the axonal projections of developing motor neurons. Forced expression of this SMN1 variant in cultured non-neuronal cells induces the formation of neurite-like extensions, a change in cell shape reminiscent of that occurring when motor neurons send out axons to their muscle targets. Whether this new variant of SMN1 affects axonal growth in vivo and plays a causal role in SMA remains to be investigated. — PAK

Proc. Natl. Acad. Sci. U.S.A. **104**, 1959 (2007).

BIOPHYSICS

Diffusion Flashing into View

Kinetic measurements with microsecond resolution have offered substantial insight into the folding mechanisms of proteins. However, before the folding event, protein chains undergo diffusional motion on a time scale of tens of nanoseconds that has proven challenging to probe. This time window is of particular interest because of its ready accessibility to theory. Nettels *et al.* have used single-molecule spectroscopy to resolve the nanosecond dynamics of unfolded cold-shock protein from *Thermotoga maritima*. They labeled the protein's ends with fluorophores and then detected changes in the chain geometries through shifts in the emitted photon statistics due to Förster resonance energy transfer. By comparing the resulting autocorrelation functions with model calculations, they could extract diffusion coefficients and reconfiguration times, which in turn contribute to a quantitative picture of the free-energy landscape. A significant (fivefold) decrease in the diffusion coefficient was observed on chain collapse, a pre-folded state induced by lowering the concentration of denaturant. — JSY

Proc. Natl. Acad. Sci. U.S.A. **104**, 2655 (2007).

GEOLOGY

Superplume in Silico

Rising beneath South Africa from the base of Earth's mantle is a giant plume of hot material: the African superplume. This feature has distinct edges and rises buoyantly like a plume of smoke from the core/mantle boundary, reaching a height of 1500 km beneath the continent. Simmons *et al.* have constructed a theoretical model of the African superplume incorporating seismic observations, motions of the overlying tectonic plates, and the elongated shape of the core/mantle boundary, as well as detailed mineral physics. They find that temperature effects can reproduce most of the plume's properties, but there remain some anomalies that must be due instead to chemical differences. Notably, a denser material

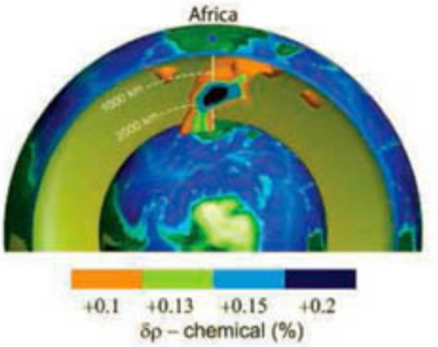

3D Model of the African superplume.

seems to lie in the mid-mantle region of the plume, 1000 km above the core/mantle boundary, which is also the site where the temperature is highest. Thus, this density anomaly counteracts the density drop that the heat would naturally produce. This anomaly may be the remnant of a pile of dense material entrained from the superplume's base. — JB

Geophys. Res. Lett. **33**, 10.1029/2006GL028009 (2007).

MOLECULAR BIOLOGY

Reading Chromatin Signatures

Regulated gene expression requires a highly choreographed assembly and disassembly of transcription factors to segments of DNA. This process must occur both near gene promoters and at enhancers, which can be present upstream or downstream of the gene being expressed. Specific epigenetic features also mark the degree of activity of the transcribing unit. Genes that are being actively transcribed generally contain nucleosomes with acetylated histone proteins, H3 and H4, as well as methylated H3; in contrast, DNA segments with inactive expression normally have deacetylated histones. Heintzman *et al.* used a combination of chromatin immunoprecipitation and microarray analysis to map histone modifications, transcription-factor binding, and nucleosome density within 30 Mb of the human genome. The study revealed that active human promoters were nucleosome-depleted. Furthermore, these promoters also showed enrichment of trimethylation of Lys^4 of histone H3 (H3K4), whereas the enhancers showed enrichment of monomethylated H3K4.

The authors went on to incorporate these distinct promoter and enhancer chromatin signatures into a computational algorithm. Analysis with this model allowed them to successfully predict the identities of several hundred promoters and enhancers of other genes in the 30-Mb region. — BAP

Nat. Genet. **39**, 10.1038/ng1966 (2007).

CREDITS (TOP TO BOTTOM): SETOLA *ET AL.*, *PROC. NATL. ACAD. SCI. U.S.A.* **104**, 1959 (2007); SIMMONS *ET AL.*, *GEOPHYS. RES. LETT.* **33**, 10.1029/2006GL028009 (2007)

CLIMATE SCIENCE

Overturning Ocean Circulation

It has been suggested that Atlantic meridional overturning circulation (MOC; the northward flow of water in the upper kilometer of the north Atlantic Ocean and southward flow below) could be affected by global warming, in turn substantially affecting the climate of the Northern Hemisphere, particularly in Europe. Observations of the strength of the circulation, taken over ~1-month periods in different seasons of each of the years 1957, 1981, 1992, 1998, and 2004, have been used to argue that the MOC has slowed by about 30% over that interval. Searl *et al.* have now analyzed simulations of the MOC from the HadCM3 climate model and found no significant trend in the strength of the MOC over the period in question. Furthermore, variations in the MOC as large as 30% were very unusual.

The discrepancy between the model and measurements may be due not to inherent limitations of the model, but rather to the small number of observations, short-term variability of the MOC, and measurement errors, which together inhibit accurate estimates of multidecadal trends from the data. Indeed, after taking all such factors into account, the HadCM3 results are fully consistent with the observations. To determine with confidence how the MOC may be changing on interannual and seasonal time scales in the warming world, continuous monitoring of water transport appears to be needed. — HJS

Geophys. Res. Lett. **34**, L03610 (2007).

PLANT BIOLOGY

Cell Fate and Gametes

Most eukaryotes, including plants, form female gametes or eggs. In *Arabidopsis thaliana,* the egg is formed from a haploid spore that undergoes multiple division cycles to create a structure known as a gametophyte that contains eight nuclei in four different cell types, including the egg. By examining egg-specific mutants, Gross-Hardt *et al.* were able to identify a gene, *LACHESIS* (*LIS*), that controls cell fate in egg development, independent of other gametophytic tissues. In heterozygote plants lacking one functional copy of *LIS*, 50% of the resulting gametophytes are malformed with multiple eggs, suggesting that *LIS* functions in the developmental specification of the egg. Furthermore, these eggs derive from a specific gametophytic cell type, the accessory cell, which forms next to the egg, potentially acting as a reserve in case of reproductive failure. *LIS* encodes a WD40 repeat protein homologous to a yeast splicing factor, which suggests that some aspects of cell fate may be controlled by the spliceosome. — LMZ

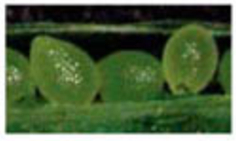

Wild-type set of seeds.

PLoS Biol. **5** e47 (2007).

Science STKE AAAS

www.stke.org

<< The Queen of Dopamine

The queen bee controls the physiology and behavior of her fellow bees and essentially determines the workings of the entire society of insects. The queen exerts this influence by producing a cocktail of pheromones known as queen mandibular pheromone (QMP), but it has not been clear just how the mixture produces its effects. Beggs *et al.* noted that one component of QMP, homovanillyl alcohol (4-hydroxy-3-methoxyphenylethanol or HVA) has a chemical structure similar to that of the neurotransmitter dopamine. The authors therefore tested the effects of the pheromone on dopaminergic function in worker bees. Exposure of newly emerged adult bees to QMP for 2 days decreased the amount of mRNA transcript encoding one of the bee's dopamine receptors. Cultured neurons from the bees' mushroom body normally respond to dopamine with an increase in production of cAMP (adenosine 3′-5′monophosphate), but neurons taken from bees exposed to QMP showed a small decrease in the production of cAMP. HVA produced responses similar to those evoked by dopamine. Total amounts of dopamine in the brain were reduced in bees exposed to HVA for 2 days. Thus, the HVA in the QMP mixture may interact directly with dopamine receptors in the bee nervous system, perhaps decreasing the expression of dopamine receptors and thus altering the response of the neurons to endogenous dopamine. — LBR

Queen bee surrounded by workers.

Proc. Natl. Acad. Sci. U.S.A. **104**, 2460 (2007).

CREDITS (TOP TO BOTTOM): GROSS-HARDT *ET AL.*, *PLOS BIOL.* **5** E47 (2007); BEGGS *ET AL.*, *PROC. NATL. ACAD. SCI. U.S.A.* **104**, 2460 (2007)

www.sciencemag.org

Science

1200 New York Avenue, NW
Washington, DC 20005
Editorial: 202-326-6550, FAX 202-289-7562
News: 202-326-6500, FAX 202-371-9227

Bateman House, 82-88 Hills Road
Cambridge, UK CB2 1LQ
+44 (0) 1223 326500, FAX +44 (0) 1223 326501

Subscription Services For change of address, missing issues, new orders and renewals, and payment questions: 866-434-AAAS (2227) or 202-326-6417, FAX 202-842-1065. Mailing addresses: AAAS, P.O. Box 96178, Washington, DC 20090-6178 or AAAS Member Services, 1200 New York Avenue, NW, Washington, DC 20005

Institutional Site Licenses please call 202-326-6755 for any questions or information

Reprints: Author Inquiries 800-635-7181
Commercial Inquiries 803-359-4578
Corrections 202-326-6501

Permissions 202-326-7074, FAX 202-682-0816

Member Benefits Bookstore: AAAS/BarnesandNoble.com bookstore www.aaas.org/bn; Car purchase discount: Subaru VIP Program 202-326-6417; Credit Card: MBNA 800-847-7378; Car Rentals: Hertz 800-654-2200 CDP#343457, Dollar 800-800-4000 #AA1115; AAAS Travels: Betchart Expeditions 800-252-4910; Life Insurance: Seabury & Smith 800-424-9883; Other Benefits: AAAS Member Services 202-326-6417 or www.aaasmember.org.

science_editors@aaas.org (for general editorial queries)
science_letters@aaas.org (for queries about letters)
science_reviews@aaas.org (for returning manuscript reviews)
science_bookrevs@aaas.org (for book review queries)

Published by the American Association for the Advancement of Science (AAAS), *Science* serves its readers as a forum for the presentation and discussion of important issues related to the advancement of science, including the presentation of minority or conflicting points of view, rather than by publishing only material on which a consensus has been reached. Accordingly, all articles published in *Science*—including editorials, news and comment, and book reviews—are signed and reflect the individual views of the authors and not official points of view adopted by the AAAS or the institutions with which the authors are affiliated.

AAAS was founded in 1848 and incorporated in 1874. Its mission is to advance science and innovation throughout the world for the benefit of all people. The goals of the association are to: foster communication among scientists, engineers and the public; enhance international cooperation in science and its applications; promote the responsible conduct and use of science and technology; foster education in science and technology for everyone; enhance the science and technology workforce and infrastructure; increase public understanding and appreciation of science and technology; and strengthen support for the science and technology enterprise.

Information for Authors

See pages 120 and 121 of the 5 January 2007 issue or access www.sciencemag.org/feature/contribinfo/home.shtml

EDITOR-IN-CHIEF **Donald Kennedy**
EXECUTIVE EDITOR **Monica M. Bradford**
DEPUTY EDITORS **R. Brooks Hanson, Barbara R. Jasny, Katrina L. Kelner**
NEWS EDITOR **Colin Norman**

Editorial supervisory senior editor Phillip D. Szuromi; **senior editor/perspectives** Lisa D. Chong; **senior editors** Gilbert J. Chin, Pamela J. Hines, Paula A. Kiberstis (Boston), Marc S. Lavine (Toronto), Beverly A. Purnell, L. Bryan Ray, Guy Riddihough, H. Jesse Smith, Valda Vinson, David Voss; **associate editors** Jake S. Yeston, Laura M. Zahn; **online editor** Stewart Wills; **associate online editor** Tara S. Marathe; **book review editor** Sherman J. Suter; **associate letters editor** Etta Kavanagh; **editorial manager** Cara Tate; **senior copy editors** Jeffrey E. Cook, Cynthia Howe, Harry Jach, Barbara P. Ordway, Jennifer Sills, Trista Wagoner; **copy editors** Lauren Kmec, Peter Mooreside; **editorial coordinators** Carolyn Kyle, Beverly Shields; **publications assistants** Ramatoulaye Diop, Chris Filiatreau, Joi S. Granger, Jeffrey Hearn, Lisa Johnson, Scott Miller, Jerry Richardson, Brian White, Anita Wynn; **editorial assistants** Maris M. Bish, Emily Guise, Patricia M. Moore, Jennifer A. Seibert; **executive assistant** Sylvia S. Kihara; **administrative support** Maryrose Police

News senior correspondent Jean Marx; **deputy news editors** Robert Coontz, Eliot Marshall, Jeffrey Mervis, Leslie Roberts; **contributing editors** Elizabeth Culotta, Polly Shulman; **news writers** Yudhijit Bhattacharjee, Adrian Cho, Jennifer Couzin, David Grimm, Constance Holden, Jocelyn Kaiser, Richard A. Kerr, Eli Kintisch, Andrew Lawler (New England), Greg Miller, Elizabeth Pennisi, Robert F. Service (Pacific NW), Erik Stokstad; John Simpson (intern); **contributing correspondents** Barry A. Cipra, Jon Cohen (San Diego, CA), Daniel Ferber, Ann Gibbons, Robert Irion, Mitch Leslie, Charles C. Mann, Evelyn Strauss, Gary Taubes, Ingrid Wickelgren; **copy editors** Linda B. Felaco, Rachel Curran, Sean Richardson; **administrative support** Scherraine Mack, Fannie Groom; **bureaus** Berkeley, CA: 510-652-0302, FAX 510-652-1867, New England: 207-549-7755, San Diego, CA: 760-942-3252, FAX 760-942-4979, Pacific Northwest: 503-963-1940

Production director James Landry; **senior manager** Wendy K. Shank; **assistant manager** Rebecca Doshi; **senior specialists** Jay Covert, Chris Redwood; **specialist** Steve Forrester; **Preflight director** David M. Tompkins; **manager** Marcus Spiegler; **specialist** Jessie Mudjitaba

Art director Kelly Buckheit Krause; **associate art director** Aaron Morales; **illustrators** Chris Bickel, Katharine Sutliff; **senior art associates** Holly Bishop, Laura Creveling, Preston Huey; **associates** Nayomi Kevitiyagala, Jessica Newfield; **photo editor** Leslie Blizard

***Science* International**

Europe (science@science-int.co.uk) **editorial: international managing editor** Andrew M. Sugden; **senior editor/perspectives** Julia Fahrenkamp-Uppenbrink; **senior editors** Caroline Ash (Geneva: +41 (0) 222 346 3106), Stella M. Hurtley, Ian S. Osborne, Stephen J. Simpson, Peter Stern; **associate editor** Joanne Baker **editorial support** Alice Whaley; Deborah Dennison **administrative support** Janet Clements, Jill White; **news: europe news editor** John Travis; **deputy news editor** Daniel Clery; **correspondent** Gretchen Vogel (Berlin: +49 (0) 30 2809 3902, FAX +49 (0) 30 2809 8365); **contributing correspondents** Michael Balter (Paris), Martin Enserink (Amsterdam and Paris), John Bohannon (Vienna); **intern** Krista Zala

Asia Japan Office: Asca Corporation, Eiko Ishioka, Fusako Tamura, 1-8-13, Hirano-cho, Chuo-ku, Osaka-shi, Osaka, 541-0046 Japan; +81 (0) 6 6202 6272, FAX +81 (0) 6 6202 6271; asca@os.gulf.or.jp; **asia news editor** Richard Stone +66 2 662 5818 (rstone@aaas.org); **japan news bureau** Dennis Normile (contributing correspondent, +81 (0) 3 3391 0630, FAX 81 (0) 3 5936 3531; dnormile@gol.com); **china representative** Hao Xin, + 86 (0) 10 6307 4439 or 6307 3676, FAX +86 (0) 10 6307 4358; cindyhao@gmail.com; **south asia** Pallava Bagla (contributing correspondent +91 (0) 11 2271 2896; pbagla@vsnl.com)

Africa Robert Koenig (contributing correspondent, rob.koenig@gmail.com)

EXECUTIVE PUBLISHER **Alan I. Leshner**
PUBLISHER **Beth Rosner**

Fulfillment & Membership Services (membership@aaas.org) **director** Marlene Zendell; **manager** Waylon Butler; **systems specialist** Andrew Vargo; **customer service supervisor** Pat Butler; **specialists** Laurie Baker, Tamara Alfson, Karena Smith, Vicki Linton, Latoya Casteel; **circulation associate** Christopher Refice; **data entry supervisor** Cynthia Johnson; **specialists** Tomeka Diggs, Tarrika Hill, Erin Layne

Business Operations and Administration director Deborah Rivera-Wienhold; **business manager** Randy Yi; **senior business analyst** Lisa Donovan; **business analyst** Jessica Tierney; **financial analysts** Michael LoBue, Farida Yeasmin; **rights and permissions: administrator** Emilie David; **associate** Elizabeth Sandler; **marketing: director** John Meyers; **marketing managers** Darryl Walter, Allison Pritchard; **marketing associates** Julianne Wielga, Mary Ellen Crowley, Catherine Featherston, Alison Chandler, Lauren Lamoureux; **international marketing manager** Wendy Sturley; **marketing executive** Jennifer Reeves; **marketing/member services executive** Linda Rusk; **japan sales** Jason Hannaford; **site license sales: director** Tom Ryan; **sales and customer service** Mehan Dossani, Kiki Forsythe, Catherine Holland, Wendy Wise; **electronic media: manager** Lizabeth Harman; **project manager** Trista Snyder; **assistant manager** Lisa Stanford **production associates** Nichele Johnston, Kimberly Oster

Advertising director worldwide ad sales Bill Moran

Product (science_advertising@aaas.org): **midwest** Rick Bongiovanni: 330-405-7080, FAX 330-405-7081 • **west coast/w. canada** Teola Young: 650-964-2266 **east coast/e. canada** Christopher Breslin: 443-512-0330, FAX 443-512-0331 • **uk/europe/asia** Julie Skeet: +44 (0) 1223-326-524, FAX +44 (0) 1223-325-532 **japan** Mashy Yoshikawa: +81 (0) 33235 5961, FAX +81 (0) 33235 5852 **traffic manager** Carol Maddox; **sales coordinator** Deiandra Simms

Commercial Editor Sean Sanders: 202-326-6430

Classified (advertise@sciencecareers.org): **u.s.: recruitment sales manager** Ian King: 202-326-6528, FAX 202-289-6742; **u.s./industry:** Darrell Bryant: 202-326-6533; **midwest/canada:** Daryl Anderson: 202-326-6543; **northeast:** Allison Millar: 202-326-6572; **southeast:** Fernando Junco: 202-326-6740; **west:** Katie Putney: 202-326-6577; **sales coordinators** Erika Bryant, Rohan Edmonson, Shirley Young; **international: sales manager** Tracy Holmes: +44 (0) 1223 326525, FAX +44 (0) 1223 326532; **sales** Christina Harrison, Svitlana Barnes; **sales assistant** Louise Moore; **japan:** Jason Hannaford: +81 (0) 52 757 5360, FAX +81 (0) 52 757 5361; **advertising production operations manager** Deborah Tompkins; **associates** Christine Hall, Amy Hardcastle; **publications assistants** Robert Buck, Mary Lagnaoui

AAAS Board of Directors **retiring president, chair** John P. Holdren; **president** David Baltimore; **president-elect** James J. McCarthy; **treasurer** David E. Shaw; **chief executive officer** Alan I. Leshner; **board** John E. Dowling, Lynn W. Enquist, Susan M. Fitzpatrick, Alice Gast, Linda P. B. Katehi, Cherry A. Murray, Thomas D. Pollard, Kathryn D. Sullivan

AAAS
ADVANCING SCIENCE, SERVING SOCIETY

ETS Spies Literacy Trouble Ahead

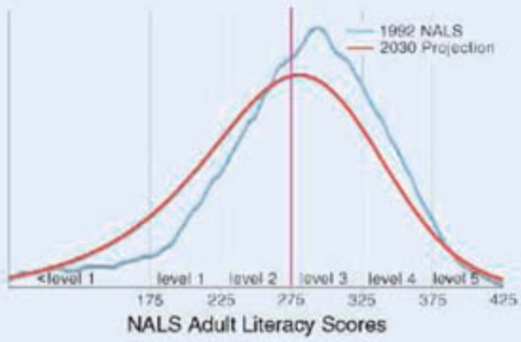

NALS Adult Literacy Scores

Literacy in the U.S. workforce is eroding and will continue to do so at least through 2030, according to the Educational Testing Service (ETS) in a gloomy report issued last month.

The economy is becoming more knowledge-intensive—only about 10% is now manufacturing-based compared with one-third in 1950. But workers are getting less literate—defined by the National Adult Literacy Survey (NALS), in part, as "using [English] printed and written information to function in society." The uneducated immigrant population is growing: Hispanics, who have the lowest high school graduation rate (50%) of any group, will go from 14% of the population to 20% in 2030. And according to U.S. Census projections, 60% of the Hispanic working population is expected to remain foreign-born, says ETS's Kentaro Yamamoto.

Hopeful trends are hard to find, says the report. High school graduation rates for both Hispanics and African Americans peaked in 1969. And college attendance among these minorities has been "stagnant" for more than a decade. ETS labels the confluence of economic and demographic factors "a perfect storm [which] continues to gain strength with no end in sight."

Whale Sensing

Research on cosmic neutrinos has led to the discovery of a sperm whale hot spot in the Mediterranean.

The Italian National Institute of Nuclear Physics plans to build a giant neutrino detector, called NEMO, 3500 meters deep off the coast of Catania, Sicily. Ordinary detectors look for the elusive Čerenkov-light signature. But in 2005, Italian physicists decided to test a new method: acoustic sensing. They deployed an array of four sensors off Sicily to see whether background noise is low enough to allow for acoustic detection.

As it happens, sound frequencies of interest for neutrino detection overlap with those from sperm-whale and dolphin calls. So marine biologists from the University of Pavia piggybacked a sea mammal–monitoring experiment on the array. The ensuing log, which is still being analyzed by both biologists and physicists, indicates hundreds of sperm-whale transits per year over an area of about 1000 square kilometers—far more than have been supplied by visual sightings. Scientists are thrilled with the new tool. Cruise-based missions provide data from only a small time window, points out Giuseppe Notarbartolo di Sciara of the conservation agency ACCOBAMS. "We still don't know how many whales live in the Mediterranean," he says. "But listening posts like this would be great for monitoring their seasonal movements."

Nuclear Hazard Has a New Face

After a 5-year, $200,000 search, the International Atomic Energy Agency (IAEA) in Vienna, Austria, has picked a red triangle showing a person fleeing from a skull and bones while being showered with wobbly rays.

A new symbol was needed, says Carolyn MacKenzie, an IAEA radiation source specialist, because no one gets the yellow trefoil anymore. She says tests in 11 countries found that "people do not know what the trefoil stands for." The old symbol will remain on containers and the entrances to radiation facilities. But the new one will go on dangerous items the public is commonly exposed to, such as food irradiators, radiation sources for cancer treatment, and x-ray units.

NET WATCH

The Nano Beat >>

This new series of podcasts from the Exploratorium in San Francisco, California, is definitely for the small-minded. Small Talk offers monthly programs on the present and promise of nanotechnology for a general audience. Hosted by a physicist and a science writer, the shows feature conversations with scientists, artists, and other nano nabobs.

Already on the record is IBM researcher Donald Eigler, who in 1989 became the first person to manipulate individual atoms, arranging them to spell out "IBM." And chemist James Tour of Rice University in Houston, Texas, chats about the nanocars (right) and other minute vehicles his team has designed. No wider than a strand of DNA, the machines might be able to truck around atoms during, for example, the manufacture of computer chips. The podcasts will run at least through May, with future programs delving into nanotech products already on the market, nanomedicine, and other topics. >> www.nisenet.org/publicbeta/podcasts

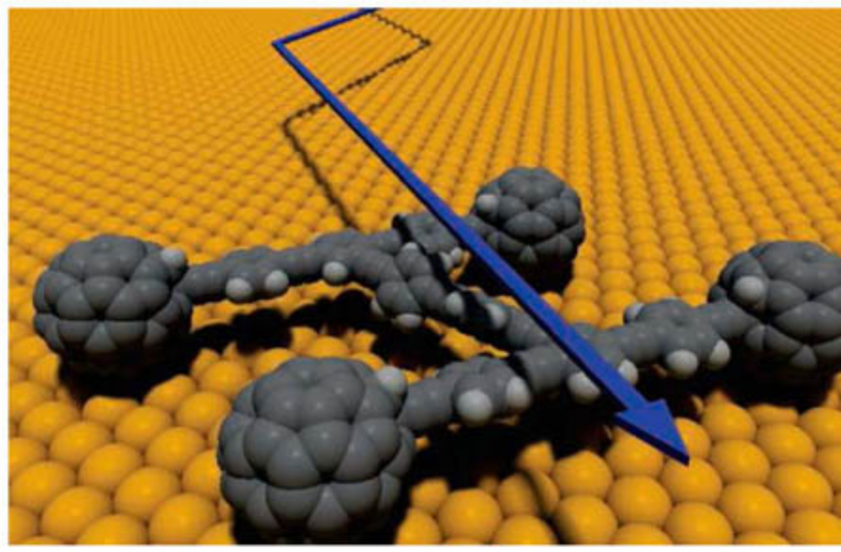

CREDITS (TOP TO BOTTOM): NALS; GIANNI PAVAN, IAEA; Y. SHIRAI/RICE UNIVERSITY

EDITED BY YUDHIJIT BHATTACHARJEE

All in the Family

SYMBIOSIS. In 1989, Niles Eldredge of the American Museum of Natural History in New York City collaborated with his sons Greg and Doug to write a children's book called *The Fossil Factory*. Now the 63-year-old evolutionary biologist is teaming up with Greg to edit a new journal from Springer titled *Outreach and Education in Evolution*.

Father and son have benefited professionally from each other over the years. While writing *The Fossil Factory*, Niles recalls, "my kids made it clear to me what kids could actually respond to. Now they're teachers and can tell me what teachers can respond to."

Greg, who teaches learning-disabled children in New York City, says his father has always been a "fantastic resource." A favorite family story relates to a class visit to the 2005 Darwin exhibit Niles curated. Seeing a case displaying various mammalian skeletons, one student was particularly impressed by the hand of a chimp. "That's it, I believe the whole thing," the student exclaimed.

The quarterly journal, which will feature articles by both biologists and teachers, could debut as early as this fall.

RISING STARS

UP AND UP. What began as an entry for a campus competition has earned Nathan Ball an innovation prize from the Lemelson Foundation and his start-up company a $120,000 contract from the U.S. Army.

The 23-year-old graduate student at the Massachusetts Institute of Technology (MIT) in Cambridge hopes that his invention—a device that can rapidly raise heavy loads hundreds of meters above the ground—will help firefighters and first responders save more lives.

More than 2 years ago, Ball and three MIT colleagues conceived of the "rope ascender," in which a rotating spindle continuously pulls rope through the machine. In addition to its military and rescue applications, the device can be used to trim trees, wash windows, and assist recreational climbers. His 2-year-old company, Atlas Devices, is now building prototypes for the Army. Last month, he won the $30,000 Lemelson-MIT Student Prize.

Ball also hopes to inspire youngsters to follow his innovative spirit by co-hosting *Design Squad*, an engineering-based reality show for preteens that debuted last month on PBS.

POLITICS

NOT OFFICIAL. George Taylor is the state climatologist of Oregon. Or is he?

Since 1991, Taylor has headed the Oregon Climate Service, which is based at Oregon State University (OSU) in Corvallis. In that capacity, he holds the title of "state climatologist." But Taylor's opinion that humans are not the dominant cause of global warming has prompted a move by Oregon Governor Ted Kulongoski to take away that title.

Kulongoski—who has made reduction of greenhouse gases a priority—is concerned that the public will mistake Taylor's contrarian view on global warming as that of the government. So last month, he asked OSU's president to change Taylor's title to put an end to the confusion. OSU hasn't decided how it will respond, but one option may be to transfer the title to the head of a new climate change center on campus. The state climatologists of Virginia and Delaware are in a similar fix.

On Campus >>

UNIFIED FIELD. Nine years after anthropologists at Stanford University split into two separate departments amid bitter infighting, university administrators want to reunite them. The unenviable task of overseeing the merger—announced last month—has fallen upon James Ferguson, current chair of cultural and social anthropology.

The 50-year-old department split in 1998 after cultural and biological anthropologists parted company on methodology, values, new hires, and the department's future (*Science*, 20 June 1997, p. 1783). The fighting got so intense that a law school professor was brought in to run the department briefly.

The reunification plan has come as a surprise to many faculty members, who would have liked a heads-up. "The two departments are further apart than ever," says biological anthropologist Arthur Wolf. "I am very upset by this decision." Ferguson says the merger was not his idea but that he's optimistic "things will turn out much better." He's hoping that the faculty turnover that occurred during the estrangement will bring "a fresh attitude."

CREDITS (TOP TO BOTTOM): MICHELLE ELDREDGE; LEMELSON-MIT PROGRAM; STEVE CASTILLO

Got a tip for this page? E-mail people@aaas.org

Penguin declines in South Africa 1205

Ancient solar observatory 1206

CANCER RESEARCH

Tight Budget Takes a Toll on U.S.–Funded Clinical Trials

Cancer specialists are reeling from deep cuts now being made in clinical trials, including what they say is the first-ever request from the U.S. National Cancer Institute (NCI) in Bethesda, Maryland, to slash patient enrollment. They are anxiously waiting to learn in the coming weeks precisely how 2007 funding will be divvied up. But already among the 10 U.S. cooperative groups that run large-scale cancer trials, many are implementing an NCI recommendation to trim their costs by 10% because of growing pressure on NCI's budget. Roughly 95 trials are at risk, and the number of open slots for patients is being reduced by 3000.

Trials for children have been hit hard, according to pediatric oncologists. Over several decades, they have built up an efficient network to wring data from a relatively small number of patients. More than 50% of children with cancer enroll in a clinical trial, compared with about 3% of adults, says Gregory Reaman, a pediatric oncologist and head of the Children's Oncology Group (COG) that runs pediatric trials.

COG's leaders expect to receive the next installment of their 5-year grant on 1 March, as in the past, but Reaman is still waiting to hear precisely how much they'll get. NCI officials have told him to expect about $24.9 million, down from $27 million last year. "The sense is that things will continue to get worse for the next several years," says Reaman, who has targeted 16 of 94 trials to be put on indefinite hold or to undergo cuts in enrollment levels.

"We had to play Solomon and try to figure out which kids would we affect the least," says William Woods, a member of COG's scientific council and president of the American Society of Pediatric Hematology/Oncology. Affected studies included protocols for relapsed T-cell leukemia, the brain tumor medulloblastoma, the kidney cancer Wilms tumor, and a rare infantile sarcoma.

NCI declined to make officials available for this story. Press officer Michael Miller said that the cooperative groups were advised to "prepare for various contingencies," and that the details were left up to them. In an October 2006 letter sent to one of the groups, however, NCI wrote, "we ask that you submit a plan for an approximate 10.28% budget reduction." According to Robert Comis, president and chair of the Coalition of Cancer Cooperative Groups, 9 of the 10 groups received similar instructions.

Shrinking Support for Pediatric Cancer Trials

YEAR	FUNDING ($million)
2003	$29.1
2004	$29.0
2005	$27.7
2006	$27.0
2007	*$24.9

* Anticipated.

NCI's 2007 budget held steady at $4.8 billion, but it will have $43 million more to spend than last year because it won't have to contribute to the "common fund" of the National Institutes of Health. The institute will be determining the 2007 budget for the cooperative groups and other NCI programs in the next month, said Miller. But no one is expecting good news. Although the groups are hoping that NCI's slight increase will stabilize funding at last year's level, "we have received no word from the NCI in this regard, and in some instances have begun implementing the reductions," says Comis.

"Even though many trials are still moving forward, they're really stripped down," says John Maris, a pediatric oncologist at Children's Hospital of Philadelphia and head of COG's neuroblastoma committee. Maris is streamlining a study in high-risk neuroblastoma, eliminating plans to test blood levels of chemotherapy drugs.

None of the neuroblastoma studies were among the 16 targeted by COG. But pediatric oncologist April Sorrell of the Cancer Institute of New Jersey in New Brunswick was "blindsided" to learn from COG in December that a leukemia trial that she'd spent more than 4 years developing along with 17 other researchers wasn't going to happen. The trial sought to enroll 180 infants with Down syndrome who had developed a preleukemia disease. Sorrell planned to test whether low doses of chemotherapy could prevent cancer among these children. "It's the first study that we've been able to develop that is asking, 'Can we prevent leukemia in high-risk kids?' " she says. "I've been given very dismal possibilities" about the likelihood of the trial launching in the near future.

Radiation oncologist Jeff Michalski of Washington University School of Medicine in St. Louis, Missouri, learned last week that his medulloblastoma study would have to reduce its enrollment goal to 455 from 600. Like some other COG trials impacted by the budget cuts, Michalski's was designed to reduce the intensity of treatment—in this case, radiation—to ease devastating long-term effects in cancer survivors. "There is some concern," he says, that with fewer patients, the study might not be able to detect whether lower radiation doses are appropriate for this cohort.

COG isn't the only clinical program facing cuts. Another cooperative group. ▶

CREDIT: (PHOTO) EZRA SHAW/GETTY IMAGES; SOURCE: CHILDREN'S ONCOLOGY GROUP

Fine-scale brain evolution
1208

Protecting redheads from the sun
1214

Cancer and Leukemia Group B (CALGB), has dropped or delayed roughly 12 trials, including programs in melanoma, which it has shut down. CALGB is also capping the number of lung tumor samples collected each month for its tissue bank. The Eastern Cooperative Oncology Group, which Comis chairs, is dismantling its brain cancer and sarcoma programs and delaying activation of most phase II studies by at least 3 months. The Gynecologic Oncology Group is putting on hold its collection of ovarian tumor samples, which normally number about 750 a year.

"Not in … almost 13 years as the chairman of my group have we been asked to plan for a substantial reduction in budget," says Richard Schilsky, associate dean for clinical research at the University of Chicago in Illinois and chair of CALGB. "It's a bizarre turn." **–JENNIFER COUZIN**

PARTICLE PHYSICS

Dreams Collide With Reality for International Experiment

U.S. high-energy physicists are scrambling to plug a hole in the long-range plans of the U.S. Department of Energy (DOE) for their field after the department's top scientist warned them that they may have to wait years longer than they'd hoped for their dream machine.

Three weeks ago, an international team released a design and cost estimate for the International Linear Collider (ILC) (*Science*, 9 February, p. 746). American physicists want to build the ILC at Fermi National Accelerator Laboratory (Fermilab) in Batavia, Illinois, and researchers had hoped to break ground in 2012 and fire up the ILC's beams of electrons and positrons in 2019. But last week, DOE Under Secretary for Science Raymond Orbach told the government's High Energy Physics Advisory Panel to add 5 years or more to that timeline, extending a projected gap during which the United States will not have a particle smasher (see table, right). Orbach asked the panel to bridge the gap with smaller-scale projects, a request that vexes researchers whose experiments were canceled in part to free up resources for the ILC.

"Even assuming a positive decision to build an ILC, the schedules will almost certainly be lengthier than the optimistic projections," Orbach told the panel at its meeting in Washington, D.C. "Completing the R&D and engineering design, negotiating an international structure, selecting a site, obtaining firm financial commitments, and building a machine could take us well into the mid-2020s, if not later," he added.

Scientists at the meeting put the best face on that hard-nosed assessment. Orbach's promise to continue R&D and engineering for the ILC is his most important message, says Barry Barish, a physicist at the California Institute of Technology in Pasadena, who leads the ILC design effort. "If you're saying, 'Put [the project] on the shelf for 5 years and then come back,' then of course, you lose momentum. But he isn't saying that at all." At the same time, Barish and others warn that talk of delay "has the danger of becoming a self-fulfilling prophecy."

Meanwhile, Orbach's call for a program of smaller projects evoked jeers from researchers whose experiments had been cut. "This is really stupid and very frustrating because we *had* a program," says Sheldon Stone, a physicist at Syracuse University in New York who worked on an experiment called BTeV that would have run at the Tevatron collider at Fermilab. In 2005, DOE nixed BTeV (*Science*, 11 February 2005, p. 832), and months later the National Science Foundation killed a pair of experiments known as RSVP that would have run at DOE's Brookhaven National Laboratory in Upton, New York (*Science*, 19 August 2005, p. 1163). Last April, DOE joined a Chinese neutrino experiment rather than backing one at a nuclear reactor in Braidwood, Illinois.

After decades of leadership, the United States by 2010 will be left with just a few accelerator-based experiments to study neutrinos. By then, the action will have shifted to the Large Hadron Collider at the European lab, CERN, near Geneva, Switzerland. Physicists expect the world's new highest-energy collider to open a realm of discovery that the ILC would later probe in detail.

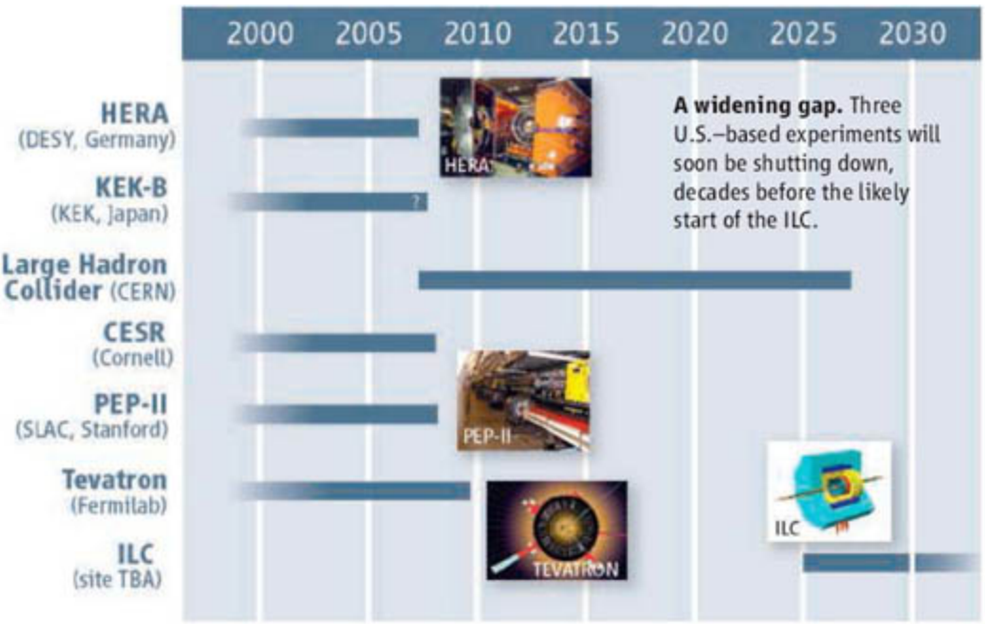

A widening gap. Three U.S.–based experiments will soon be shutting down, decades before the likely start of the ILC.

CREDIT: J. NEWFIELD/*SCIENCE* (IMAGES: DESY; SLAC/STANFORD UNIVERSITY; FERMILAB; ILC)

Fermilab Director Pier Oddone calls Orbach's request for input "an opportunity" to set out in new directions, including, perhaps, pursuing the lab's idea for an intense proton source. But Edward Blucher, a physicist at the University of Chicago who worked on the Braidwood neutrino experiment, says "many of us who have had the experience [of getting a project cut] are going to think twice before trying again." **–ADRIAN CHO**

With reporting by Jeffrey Mervis.

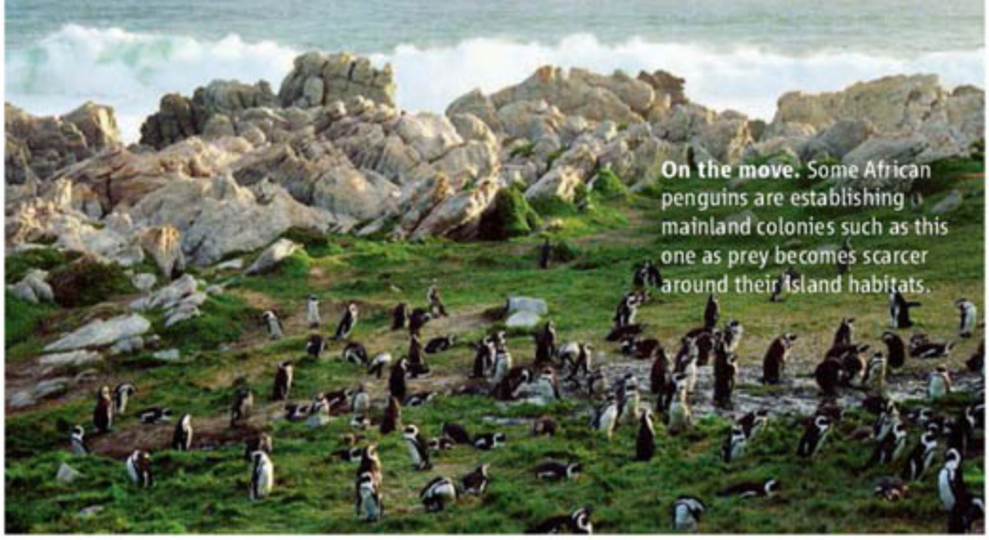

On the move. Some African penguins are establishing mainland colonies such as this one as prey becomes scarcer around their island habitats.

CREDIT: R. KOENIG/SCIENCE

ZOOLOGY

African Penguin Populations Reported in a Puzzling Decline

PRETORIA, SOUTH AFRICA—African penguin populations, on the upswing since the mid-1990s, appear to have gone into a surprising nosedive. New data indicate that their numbers may have dropped in the past few years by as many as 50,000—40% of the population. And the birds, which normally breed on island colonies, have puzzled scientists by establishing a growing number of new colonies on the mainland.

Marine zoologists see this population pattern reflected in several observations. "Every piece of information we have—breeding success, breeding counts, diet sample analysis, and [a bird census during molting season]—all show the same trend and are serious cause for concern," says Samantha Petersen, who manages BirdLife South Africa's seabird conservation program.

Zoologist Rob Crawford, a penguin expert with South Africa's Environmental Affairs Department, agrees that the trend is "quite disturbing." He believes that the birds' prime food sources—sardines and anchovies—are becoming scarce around established colonies. Although overfishing may be part of the problem, Crawford and South African fish experts also blame "a large eastward shift" in the distribution of the fish. In a recent study, they found that the biomass of those fish species in the region near the penguins' largest breeding islands west of Cape Town fell sharply after 2002.

In what Crawford suspects is a "desperation move" to get closer to their fish prey, some penguins—apparently from island colonies—have been moving eastward and settling on the mainland, most recently at the De Hoop Nature Reserve. They normally shun these locations because of predators. Les Underhill, who directs the University of Cape Town's avian demography unit, agrees that the new colonies reflect a trend of penguins moving eastward toward the current fish biomass center, near Mossel Bay.

African penguins, called jackass penguins because of their braying, once numbered more than 1.5 million on islands off South Africa's western coast. But guano and egg harvesting a century ago led to a 90% decline in the population; oil spills in 1994 and 2000 also held them back. Even so, South African penguins climbed to about 120,000 earlier in this decade before the most recent downturn.

Long-term oceanographic studies are needed to assess whether climate change could be a factor. For now, South Africa's environment department is considering various short-term options to try to protect the penguins, including establishing no-fishing zones around several breeding islands. Underhill contends that "setting up areas around breeding colonies which are closed to fishing is *the* critical issue facing penguin conservation today."

This month, Crawford's group will begin a new count of nests and, later, of penguins themselves during molting. Researchers are also using satellite-tracking and transponders to analyze the birds' feeding habits. Parallel efforts are ongoing in Namibia, where the number of penguins is now about 24,000, down from 100,000 in 1956.

Life is not likely to get easier for South Africa's penguins, threatened by oil spills, predators, and habitat changes. But Underhill says the new colony at De Hoop offers some hope: It shows that the penguins might be safely relocated. If scientists could figure out how to start colonies, "then we could secure a piece of coastline from land predators and get a colony going near the fish."

–ROBERT KOENIG

SCIENCESCOPE

Speaking of Intellectual Property ...

NEW DELHI—A controversial report arguing that India's patent laws are out of line with global norms has been withdrawn under a charge of plagiarism. One paragraph of the report, delivered to the government late last year by a blue-ribbon panel chaired by India's top expert on intellectual property, Raghunath Anant Mashelkar, states that incremental innovations to a patented product "may be of tremendous value ... [and] ought to be encouraged." Analysts say that statement favors pharmaceutical companies and could sway a case in Madras High Court in which the drug giant Novartis has challenged India's rejection of its patent application for the cancer drug Gleevec.

Mashelkar has acknowledged that the paragraph on incremental innovations was copied verbatim, unacknowledged, from another source: "A slip did happen, and I deeply regret it." Last week, he offered to submit a new version in 3 months that would follow "best ethical practices." Some in Parliament have demanded that the government scrap the Mashelkar committee and start over. The government earlier this week said it is still weighing its response. **–PALLAVA BAGLA**

Europe Launches Its Own NSF

BERLIN—In what many describe as a fresh start for European science policy, hundreds of scientists and politicians celebrated the launch of Europe's new research funding agency here at a meeting on 27–28 February. Modeled on U.S. agencies such as the National Science Foundation (NSF), the European Research Council (ERC) will focus on funding basic research and rewarding proposals according only to their quality—characteristics that set it apart from the E.U.'s existing funding schemes. "This is a revolutionary development," says Imperial College London biologist Fotis Kafatos, who chairs ERC's Scientific Council. He hopes ERC, whose annual budget is set to grow to €1.3 billion, will help retain Europe's top talent and lure back scientific stars working abroad.

Staff members at ERC's Brussels bureau are still working frantically to prepare for the expected flood of grant applications. The agency can handle up to 3000 proposals for the 200 grants it has available in 2007, says Vice President Helga Nowotny. "If it's twice that number, we'll have a problem," she adds. This year's grants, worth €1.5 million on average, will go to young scientists; larger grants for senior researchers will become available in 2008.

–MARTIN ENSERINK

ARCHAEOLOGY

Mystery Towers in Peru Are an Ancient Solar Calendar

Since the 19th century, archaeologists have puzzled over Chankillo, a massive, 2300-year-old ruin 400 kilometers north of Lima, with a walled hilltop center and an enigmatic line of 13 small, rectilinear towers. Scientists have variously interpreted the complex "as a fort, a redoubt, a temple, and even as the setting for ceremonial battles," says archaeologist Iván Ghezzi of the Pontificia Universidad Católica del Perú (PUCP) in Lima.

Now, on page 1239, Ghezzi and archaeoastronomer Clive Ruggles of the University of Leicester, U.K., demonstrate that Chankillo was, in part, a solar observatory. In what Luis Guillermo Lumbreras of the Universidad Nacional Mayor de San Marcos in Lima calls "an excellent scientific contribution, very serious and informative," Ghezzi and Ruggles show that the sequence of towers marked the summer and winter solstices.

Jokingly dubbed "the Norelco ruin" for the distinctive shaverlike shape of its three concentric walls, Chankillo was built during the collapse of a major Andean religious center called Chavín de Huántar, in a time when many population centers were emptied and others were fortified. Among the most visible of the latter is Chankillo, which was erected between 200 and 300 B.C.E. according to new radiocarbon dates also provided in the paper.

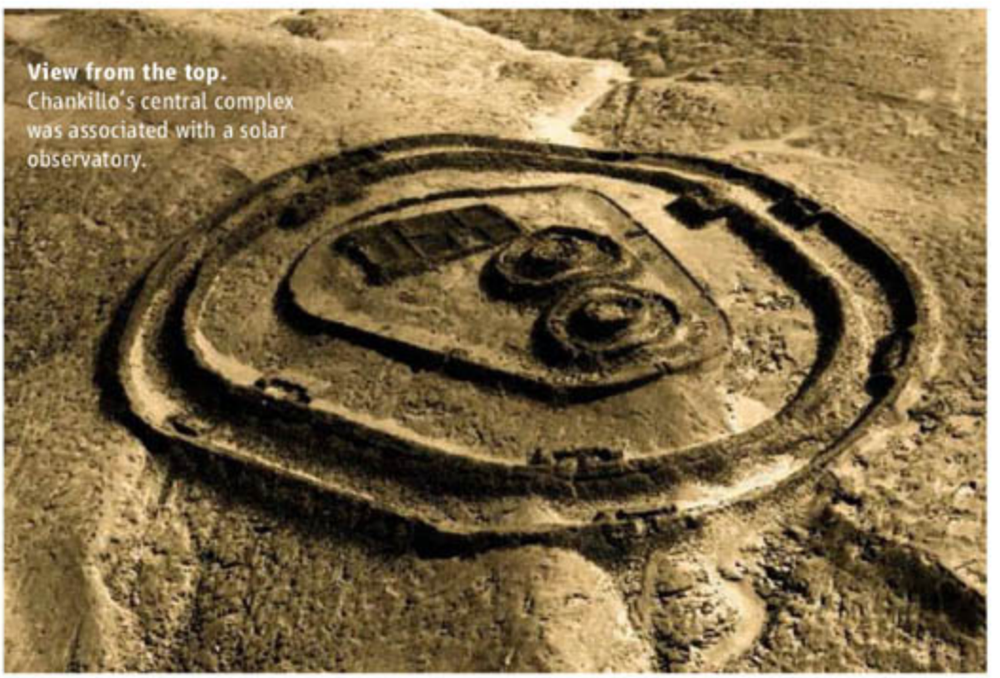

View from the top. Chankillo's central complex was associated with a solar observatory.

CREDIT: IVÁN GHEZZI/PUCP

Chankillo's commanding location and thick walls suggest a martial purpose, but its elegant design, many gates, and lack of water supply raise doubts that it was a fort. Working with Ruggles, Ghezzi uncovered two artificial observation points constructed about 200 meters away from and on opposite sides of the line of towers, which run along the top of a ridge east of the main complex. The eastern viewpoint was partly wrecked, but the western viewpoint was both well-preserved and, to Ghezzi and Ruggles, unambiguous in function: The two viewpoints are positioned so that on the winter and summer solstices the sun rises and sets over the towers on the opposite end of the line, establishing the beginning and midpoint of the solar year. The western viewpoint was at the end of a 40-meter-long, windowless corridor that wrapped around the outside wall of a structure filled with ceremonially displayed ceramic figurines of soldiers.

Because the heavens are filled with celestial objects, researchers often fool themselves with coincidental astronomical alignments. "When Iván said I had to come and see this site that might be an observatory," Ruggles says, "inside I was thinking, 'Yeah, yeah, yeah'—people are always saying this to me." But instead, he found what PUCP archaeologist Luis Jaime Castillo calls an "absolutely clear-cut" example of a monumental calendar. "It is difficult to imagine what other function the observation structures could have served," says Castillo. ▶

U.S. INNOVATION

Democrats Rescue Technology Research Program

Written off as dead by critics and fans alike, the Advanced Technology Program (ATP) has been given a $79 million lifeline from Democrats in the U.S. Congress.

Run by the National Institute of Standards and Technology (NIST), ATP was begun in the early 1990s as a way to help companies conduct research aimed at commercializing new products. It has supported everything from genomics to materials science. Republicans—including the current Bush Administration—have long derided it as so-called corporate welfare, however, and neither the Senate nor the House included money in NIST's 2007 spending bills for the program. But after Republicans left Democrats with the job of finishing this year's budget (*Science*, 22 December 2006, p. 1862), staffers staved off ATP's demise in the spending bill President George W. Bush signed 2 weeks ago.

"This was under the radar," says lobbyist Robert Boege of the Alliance for Science & Technology Research in America in Washington, D.C., of the turnaround, which he says "defied even metaphysics." Congressional aides and lobbyists say top Democrats on Capitol Hill, including House Speaker Nancy Pelosi (D–CA), view the program as an essential piece of the House Democrats' "Innovation Agenda" introduced nearly a year before they won control of Congress.

Last week, NIST officials said that details of the competition, including how much money will be available, will be announced in the spring. "I am actually very proud, as NIST's director, to be hearing about [ATP] success stories," NIST head William Jeffrey told a House science committee panel last week in testimony on the agency's 2008 budget request, which once again zeroes out the program. But, he added, "the issue is, in the Administration's viewpoint, whether or not [ATP] is the appropriate role for the federal government."

–ELI KINTISCH

The practical need for the Chankillo observatory is evident, notes Daniel Sandweiss of the University of Maine, Orono: agriculture, which required "solar observation to know when to plant." Along the bone-dry Peruvian coast, where farming has long depended on irrigating rivers, "people need to know the date with some precision."

Until recently, the first complex states in northern Peru were dated to the rise of the Moche in about 400 C.E. "Now we find very sophisticated measurement techniques 600 years before Moche," says Castillo. "It says to us that there may have been more going on than we thought."

Most important, says Clark Erickson of the University of Pennsylvania, "this kind of discovery really begins to get into the minds of people in the past." The long hallway to the western observation point, he notes, "only provides space for a few people to be brought there and dazzled." Understanding this piece of architectural theater, he says, "helps make the past come alive." **–CHARLES C. MANN**

STEM CELLS

Data on Adult Stem Cells Questioned

Just as her team is preparing some long-awaited follow-up papers on multipotent adult progenitor (MAP) cells, stem cell researcher Catherine Verfaillie is dealing with accusations that her landmark study, published in *Nature* in 2002, contains "flaws" that could jeopardize its conclusions. *Nature* has decided to rereview the work. Verfaillie, now at the Catholic University of Leuven, Belgium, says that although some data are puzzling, the problems do not affect her findings.

The accusations were raised last summer but became widely known only last week following an article in *New Scientist*. They've received a flurry of attention because of the big splash Verfaillie made when she originally reported that her team had cultivated a new type of cell that appeared to have the potential to grow into most cell types in the body (*Science*, 9 February, p. 760).

Hot seat. Catherine Verfaillie sticks up for her cells.

CREDIT: UNIVERSITY OF MINNESOTA

Last year, two *New Scientist* reporters noticed that the *Nature* paper and another the team published at the same time in the *Journal of Experimental Hematology* contained identical data on flow cytometry—a technique for identifying cells—even though the two papers described different cell populations. They notified Verfaillie, who in turn notified the journal editors and the University of Minnesota (UMN), Twin Cities, where she did the research.

At Verfaillie's request, UMN convened three experts to review the flow-cytometry data. They concluded last August that the duplication was an "honest error." Verfaillie subsequently had an erratum published in the hematology journal.

However, the panel also said it had reservations about the "validity" of the flow-cytometric analysis data in the *Nature* paper. Flow cytometry involves the use of antibodies to recognize proteins on cell membranes. Some of the fluorescent signatures generated by antibodies showed a variability "far outside what would be expected for this kind of experiment," said the panel. If those data are unreliable, it could mean that the MAP cells do not have all the characteristics described in the paper.

The experts said they couldn't judge whether the problem would affect the paper's conclusions about the versatility of MAP cells. One of them told *Science* that "problems are rampant" in flow cytometry, and it would be hard to find a paper without some flaw.

UMN then asked two unnamed stem cell experts to address the validity of the conclusions of the *Nature* paper. Their comments have not been made public, but the university's vice president for research, Tim Mulcahy, says that one of the experts felt the problematic data "weakened" the paper. The other said the data were "not critical" to the conclusions. Mulcahy says the university plans no further action and will let the scientific community judge the matter for itself.

Verfaillie says her team has "no explanation for why" the data turned out as they did. "I personally don't think it affects the conclusion of the paper, and I've spoken to many people who personally don't think so," she says. But it's "up to *Nature* to decide." **–CONSTANCE HOLDEN**

SCIENCESCOPE

Ethics at Issue in China

BEIJING—China's largest research body is getting serious about misconduct. Earlier this week, the Chinese Academy of Sciences (CAS) unveiled guidance on what constitutes misconduct and set up a high-level academy committee to investigate allegations.

In recent months, a series of high-profile misconduct cases has tarnished the reputation of China's scientific community (*Science*, 9 June 2006, p. 1464). CAS this week ordered each of its 100 institutes to set up their own committees to probe allegations against their researchers and to educate staff about ethical behavior. The CAS panel will investigate higher profile allegations. With Chinese science becoming more competitive and well-funded, the new rules should deter misconduct, says Zhou Xingjiang of CAS's Institute of Physics in Beijing. **–JIA HEPENG**

Those Crafty Europeans

Next stop for the European Space Agency (ESA): Mercury, perhaps the least well known of the planets. Coming on the heels of recent missions to Mars, Venus, and Saturn's moon Titan, ESA last week approved construction of BepiColombo, which will launch in 2013 and reach Mercury 6 years later. Only NASA's Mariner 10 spacecraft has visited Mercury before, in 1974–75, and NASA has dispatched another craft, dubbed Messenger, to arrive in 2011. BepiColombo is designed to split into two orbiters upon arrival at Mercury: one to study the planet and the other—provided by Japan—its magnetosphere. **–DANIEL CLERY**

South Africa Listens Hard

PRETORIA, SOUTH AFRICA—South Africa's new proposed budget aims to improve the country's chances of beating out Australia for the world's most powerful radio telescope, the Square Kilometre Array (SKA). About 40% of the government's proposed $172 million budget increase for science and technology (S&T) would fund an upgraded pilot instrument, the Karoo Array Telescope (KAT).

The nation's SKA project manager, Bernie Fanaroff, says an expanded version of the demonstrator array, called the MeerKAT, will "optimize the science we can do" with available funds. Although some scientists question devoting so much of the budget to KAT, zoologist Robin Crewe, who is president of South Africa's leading science academy, predicts that a successful bid's information network would benefit other areas of South African research.

–ROBERT KOENIG

Brain Evolution Studies Go Micro

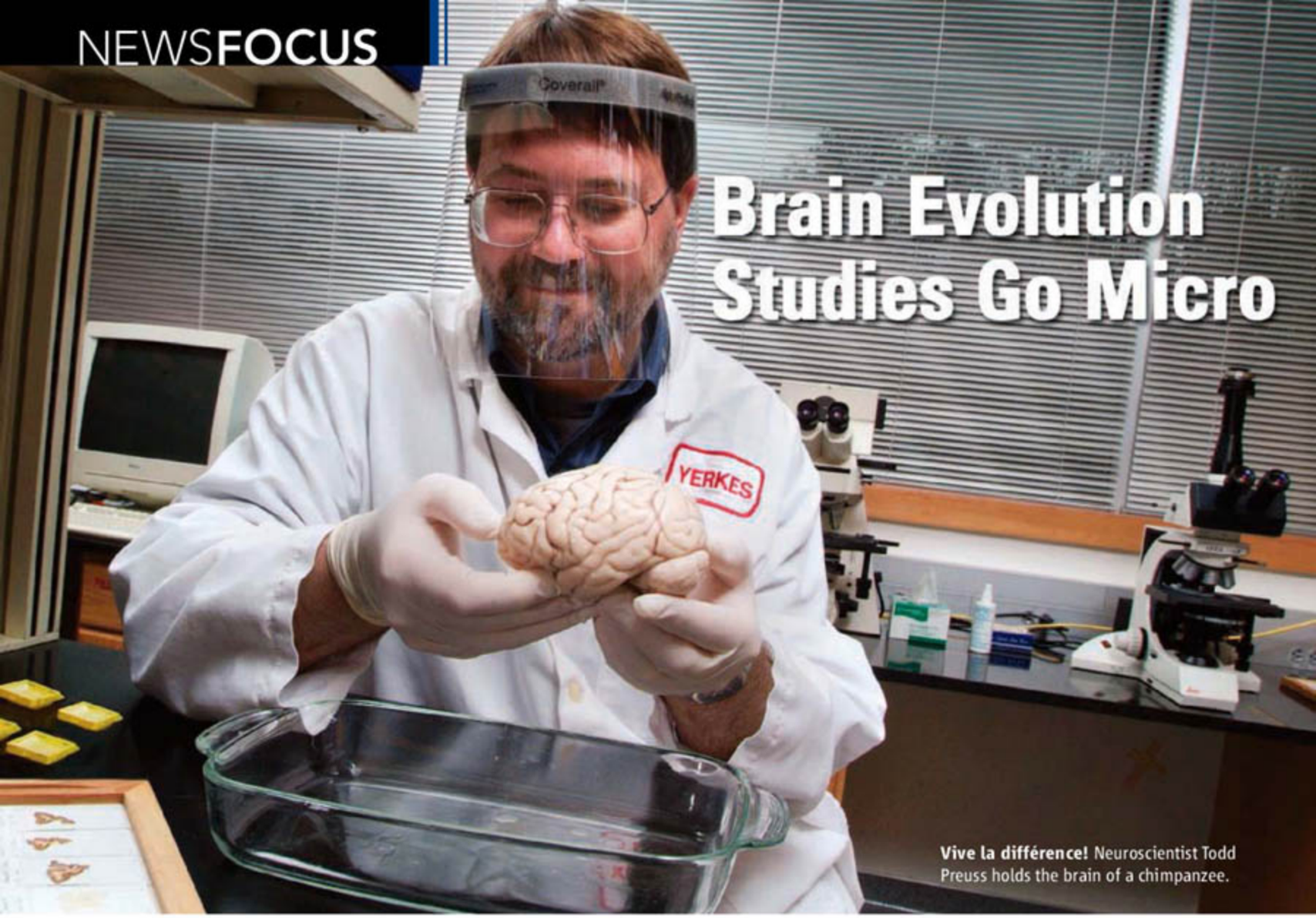

Vive la différence! Neuroscientist Todd Preuss holds the brain of a chimpanzee.

CREDIT: JACK KEARSE/EMORY UNIVERSITY

What makes the human brain unique? Researchers are coming up with new answers to that question as they shift their focus from large-scale brain structures to individual neurons and their complex wiring

NEW YORK CITY—When it comes to brains, Patrick Hof has plenty. Plastic containers filled with the brains of macaques, gorillas, chimpanzees, bonobos, and humans cram the shelves of the walk-in refrigerator in his lab at Mount Sinai School of Medicine here. During the 1990s, Hof and his team were studying human brains when they spotted a type of nerve cell they had never seen before, in a small area associated with higher cognition. At first they thought the long, narrow cell was an artifact. But then they realized that they had rediscovered a cell type first described during the 1920s. So Hof turned to his collection and got an even bigger surprise: These cells were found only in apes and humans, not other primates.

His discovery was the first demonstration that the ape lineage had evolved an entirely new type of brain cell. Since then, he and other neuroscientists have been putting primate brains under the microscope, looking for clues to how the extraordinary information-processing capabilities of the human brain evolved.

On the macro level, many of the differences between human and other primate brains have long been obvious. Researchers have known since the early 19th century that the average human brain is nearly four times as large as that of a chimpanzee. And for decades, anthropologists have analyzed the relative sizes and visible structures of brain regions such as the frontal and temporal lobes in humans and in other living and fossil primates.

Yet in recent years, a growing number of researchers have become convinced that size isn't the whole story. Work over the past decade by Katerina Semendeferi, an anthropologist at the University of California, San Diego (UCSD), suggests that the human frontal lobes, the seat of many advanced cognitive functions, are not proportionately larger than those of other apes (*Science*, 5 May 2000, p. 798). Her work remains controversial, but it has spurred many scientists to look elsewhere for explanations. "Having a big brain is necessary but not sufficient" to explain human cognition, says UCSD glycobiologist Ajit Varki. "Neandertals had brains bigger than ours, but they did not paint on cave walls."

Now, armed with new histological and imaging techniques to identify and trace individual nerve cells, a growing number of researchers have begun looking for signs of human uniqueness that can only be spotted under the microscope. They are discovering microanatomical structures and enhancements in the wiring and connectivity of nerve cells that our ape cousins lack. "Brain size is one thing, and brain organization is something else," says neuroscientist Todd Preuss of Emory University in Atlanta, Georgia, a leading member of this avant-garde movement in evolutionary neuroanatomy. "There is a whole microuniverse of human nature for us to explore."

Like Hof's slender neuron, some small-scale innovations are shared by humans and

great apes but not other primates, implying that they arose after the great apes evolved about 15 million years ago but before humans came on the scene, about 5 million to 7 million years ago. Yet in nearly all cases—including Hof's discovery—these novelties show additional differences between apes and humans. Indeed, most of the ape-human distinctions are seen in parts of the brain implicated in advanced functions such as social cognition and language. "This is the first set of [microscopic] differences that define the human brain as more than just another great ape brain," says Chet Sherwood, an evolutionary neuroanatomist at George Washington University in Washington, D.C.

Despite considerable progress, the field is still in the basic discovery stage, identifying new features and trying to decipher their functions. Researchers can't point to a recently evolved nerve cell type and say with confidence that it helps humans to plan ahead or negotiate delicate social situations, for example. On the other hand, the emerging micro differences are encouraging new hypotheses about brain evolution. These studies "have a beautiful potential and open a whole new window on the evolutionary history of [primates] that we never had before," says anthropologist Ralph Holloway of Columbia University.

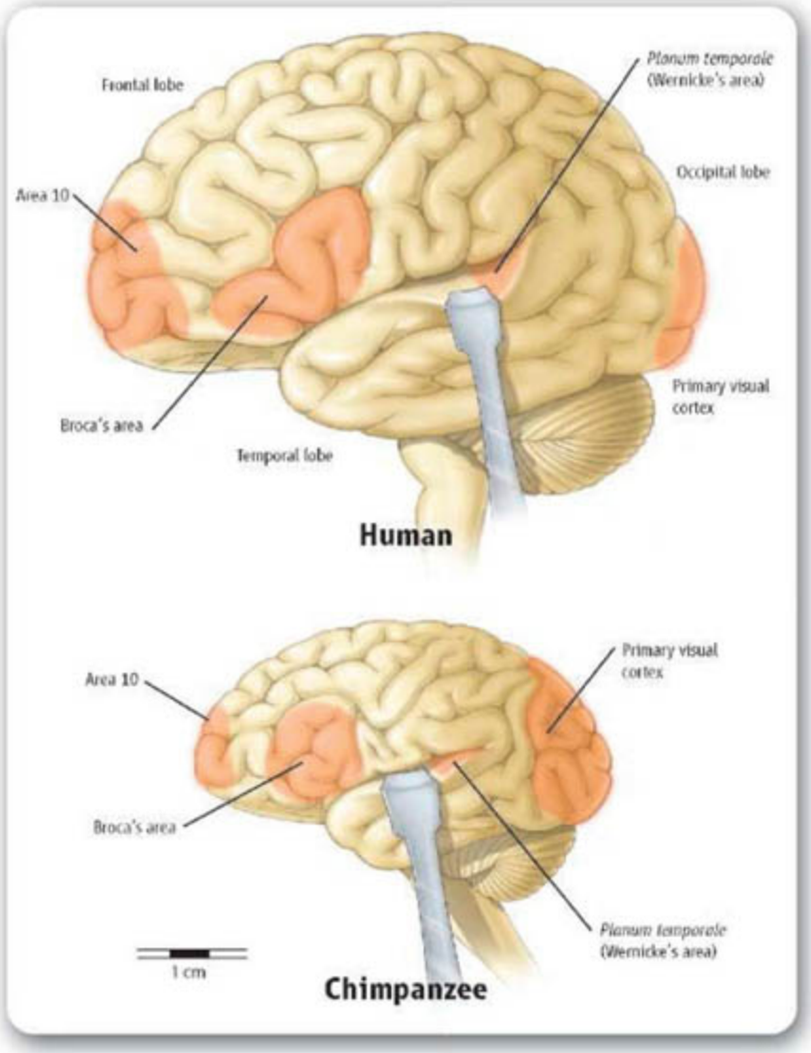

Of apes and whales

Although researchers have long studied the anatomy of the brain, until recently many had assumed that all mammalian brains are basically the same at the microscopic level. "Many neuroscientists haven't wanted to imagine that the human brain is anything more than a rat or mouse brain done a little differently," Varki says. As a result, researchers have overlooked important differences between humans and their close primate kin, Preuss says. He adds that the roots of the problem go all the way back to Charles Darwin, who argued that humans were essentially big-brained apes. Well into the 1980s, he says, neuroscientists continued to argue for what they called the "basic uniformity" of the mammalian brain.

This simple picture began to change during the 1990s, when researchers began to find subtle differences in the shapes and biochemical properties of neurons across mammalian species. They were greatly aided by new histological techniques that allowed them to label specific nerve cells and neurotransmitters. In 1999, Preuss and his coworkers were the first to show more significant microscopic differences in brain organization between apes and humans. They reported in the *Proceedings of the National Academy of Sciences* that one layer of the human primary visual cortex, which is located in the occipital lobe in the back of the brain (see diagram), differs markedly from that of monkeys as well as apes such as chimps and orangutans. In this layer, which helps relay visual information from the retina to the parietal lobe, nerve cells are organized in a complex meshlike pattern very different from the simpler vertical arrays of cells found in other primates. Preuss's team concluded that the meshlike arrangement was an evolutionary innovation on the human line and might help explain humans' superior ability to detect objects against a background. "This was very nice work," says Holloway.

Built for speed. Slender Von Economo neurons may relay nerve impulses swiftly.

That was the same year Hof reported the elongated neurons he had rediscovered, called spindle neurons because of their tapered shape or Von Economo neurons (VENs) after the Austrian neurologist who originally spotted them. Work by Hof, neuroscientist John Allman of the California Institute of Technology in Pasadena, and Semendeferi has shown that these neurons are located in only two parts of the brain: the anterior cingulate cortex, deep in the center of the brain, and the frontoinsular cortex, located inside the frontal lobes. In humans, both of these structures appear to be involved in aspects of social cognition such as trust, empathy, and feelings of guilt and embarrassment. Not only were VENs unique to great apes, but humans had many more VENs than other apes. And the human VENs were markedly larger.

What do humans use those big VENs for? No one knows for sure, but a few hints are emerging. Last year, Allman's team reported in *Neuroscience* that human VENs seem to make fewer connections with adjacent nerve cells than do other types of neurons. And because the speed of nerve impulse conduction generally increases with the diameter of a nerve fiber, Allman hypothesizes that the large VENs might relay information rapidly from the anterior cingulate and frontoinsular cortices to other parts of the brain. "We think of them as a Ferrari relative to a Chevrolet," Allman says. "They are really stripped-down, high-performance kinds of cells."

CREDITS (TOP TO BOTTOM): C. BICKEL/SCIENCE (SOURCE: T. PREUSS); J. ALLMAN/CALIFORNIA INSTITUTE OF TECHNOLOGY

Brains aplenty. Patrick Hof's extensive collection helped him rediscover a specialized nerve cell.

He and others think that one target for nerve impulses from the VENs is a part of the frontal lobes called area 10 (see diagram, p. 1209), which is involved in taking initiative and advance planning; Semendeferi has argued that this region, unlike the frontal lobe as a whole, is expanded in the human line relative to its counterpart in other apes. Allman hypothesizes that the big VENs might help humans adjust behavior swiftly in response to rapidly changing social situations.

New data on dementia seem to fit that notion. Last December, a team led by William Seeley at UC San Francisco reported in *Annals of Neurology* that subjects afflicted with a type of dementia that causes inappropriate and impulsive social behavior had 74% fewer VENs in their anterior cingulate cortex compared to normal controls.

But other researchers note that it's too early to draw functional conclusions about the role of VENs in the normal brain. "They do have a [shape] that suggests they are designed for conduction of more rapid output than surrounding cells," Sherwood says. "But what they are connected to we don't know yet."

Whatever the VENs do, primates may not be the only creatures doing it. In a surprise finding last year, Hof and his Mount Sinai co-worker Estel Van der Gucht found that some large whales—including humpbacks and fins—have VENs too, as they reported in the *Anatomical Record*. This apparent case of parallel or convergent evolution could help explain the cognitive talents of some whale species, including singing and other forms of complex communication, says Hof.

Marching in column

Whereas VENs seem to be restricted to certain mammal species and specific brain regions, other researchers are exploring the uniquely human specializations of a feature shared by all mammals: the minicolumn. Discovered in the 1950s, each minicolumn is comprised of 80 to 100 nerve cells bundled together vertically in the cerebral cortex. Most neuroscientists now consider the minicolumn to be the basic modular unit of neural information processing, one that can respond to many simultaneous stimuli at once. "The minicolumn serves as a parallel processor in the brain," explains neurologist Manuel Casanova of the University of Louisville in Kentucky.

And certain human minicolumns apparently have unusually great processing capacities. In 2001, Casanova and biological anthropologist Daniel Buxhoeveden, now at the University of South Carolina in Columbia, examined minicolumns in the left planum temporale, a part of the temporal lobe involved in uniquely human activities such as language and perhaps music. As they reported in the *American Journal of Physical Anthropology*, they found that human minicolumns in this region were organized much differently than those of chimps and rhesus monkeys. Human minicolumns were much wider, an average of 51 micrometers compared to about 36 micrometers in both chimps and monkeys. This increased size was apparently due to an increase in the so-called neuropil space at the minicolumn's periphery, which contains the axons, dendrites, and synapses that make neural connections. The neuropil space was expanded even more by a tighter packing of nerve cells in the center of the minicolumn in humans compared to other primates.

This suggests that the organization of nerve cells in the planum temporale has evolved since the human-chimp split, says Casanova. In a follow-up study, the team also showed that in humans, the minicolumns of the left planum temporale are wider and have more neuropil space than those of the right planum temporale, whereas in chimps and rhesus monkeys the left and right sides are similar. And recent unpublished work by Semendeferi's graduate student Natalie Schenker shows a significant enlargement of minicolumns in area 10 as well as Broca's area, an area on the left side of the brain involved in language processing.

These microlevel asymmetries fit with macrolevel results: In most humans, certain areas are bigger on the left side of the brain than on the right, and some of the left-side regions, such as Broca's area, are apparently involved in language. Sherwood suggests that

CREDIT: M. BALTER/SCIENCE

the macrolevel asymmetries may reflect an underlying left bias at the micro level.

All this work suggests that the human minicolumn has reorganized during evolution to allow greater connectivity, says Casanova. That reorganization may have helped make the expansion of the human brain possible, he says: "To have a big brain, you need more connections."

Making connections

In the nervous system, making connections is everything—and usually, the more the better. Until recently, however, little was known about what triggered the formation of synapses between neurons. Then in 2001, a team led by neurobiologist Ben Barres of Stanford University in Palo Alto, California, reported that specialized neural cells called astrocytes—which make up nearly half the cells in the human brain, but whose functions had remained a mystery—must be present for synapses to form. Astrocytes do not form synapses themselves, but Barres's work showed that they play some sort of supporting role in creating synapses between the axons and dendrites of impulse-carrying nerve fibers. Later, Barres and his colleagues reported that astrocytes trigger synapse formation by secreting large proteins called thrombospondins (*Science*, 21 November 2003, p. 1323).

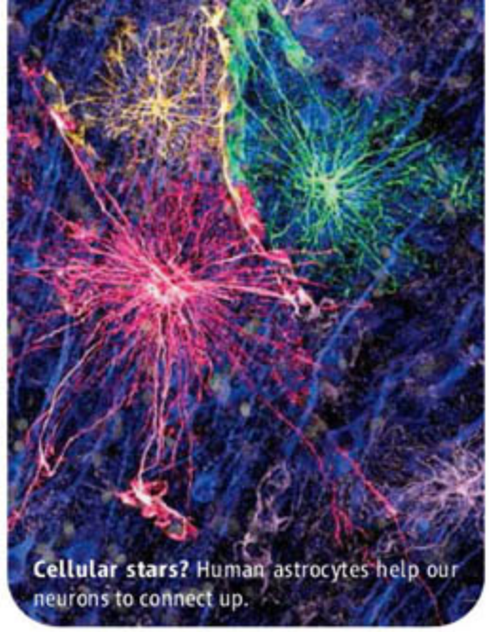

Cellular stars? Human astrocytes help our neurons to connect up.

"Thrombospondin secretion is an astrocyte function with a high impact on the capacity for neural processing," agrees Maiken Nedergaard, a neurologist at the University of Rochester Medical Center in New York. In general, the more synapses, the greater the brain's ability to transmit messages and process information.

Intrigued by Barres's results, Preuss wondered whether there were any differences in thrombospondin secretion among primates. He and co-workers looked at the gene expression of thrombospondins in the brains of humans, chimps, and macaques. The team hit the jackpot: As reported online last December in *Cerebral Cortex*, human brains produce up to six times as much thrombospondin messenger RNA and protein than do either chimps or macaques. Moreover, the differences were seen in the cerebral cortex but not in the cerebellum and nonbrain tissues.

"Todd's findings are extremely interesting," Barres says. "They raise the question of whether the human brain can form more synapses," at least in adulthood. Varki agrees: "This work is excellent. It is exactly the kind of approach needed for the future." Semendeferi adds that these results are completely consistent with her lab's finding that minicolumns in area 10—one region where Preuss found enhanced thrombospondin expression—have larger neuropil space and thus more room for synaptic connections.

Just how much the relatively new field of comparative microneuroanatomy will contribute to our understanding of human brain evolution remains to be seen. "Some of it may work out, and some might not," Holloway says. "What we need now is to establish a solid relationship between these structural elements and actual behavioral variations" between humans and other primates. Nevertheless, says Holloway, a pioneer in macrostudies of brain evolution, "If I were 42 years old instead of 72, I would throw all my brain endocasts away and get right into this new field."

–MICHAEL BALTER

ONCOLOGY

Recruiting the Cell's Own Guardian for Cancer Therapy

Reactivating the *p53* tumor suppressor gene has given promising results in mice, reversing and even temporarily eradicating some tumors

Within the past few years, biologists have begun to see their study of cancer cell genetics pay off in the best way possible: through the development of new drugs that can improve patient survival. Some specifically block the oncogenic proteins that drive tumor growth; Herceptin is a recent example. But oncogenes are only one part of the equation. Many if not all human cancers also have defects in so-called tumor suppressor genes that would normally restrain cancer development. And now, researchers are increasingly turning their attention to the tumor suppressor genes to see whether it's possible to develop therapies that work by restoring their activity.

The lion's share of attention has focused so far on the tumor suppressor gene known as *p53*. This work, still in its very early preclinical stages, looks promising. One line of evidence comes from three recent studies showing that restoring *p53* activity can halt the growth of cancerous tumors in mice, and in some cases, even cause tumors to disappear. The papers "eloquently show that restoration of *p53* function in every cell is effective in suppressing tumors," says Wafik El-Deiry of the University of Pennsylvania School of Medicine in Philadelphia.

In addition, researchers are hot on the trail of the field's Holy Grail: the development of small molecule drugs that reactivate the p53 protein. Some of this work was sparked by the discovery 3 years ago of a drug called nutlin that has shown promise in preclinical testing; now several additional drugs are also in the pipeline. "The whole field is in a stage of very serious optimism," says *p53* pioneer David Lane of the Institute of Cell and Molecular Biology in Singapore.

The reason drug developers are so interested in *p53* is that mutations in the gene contribute to the development of about 50% of all human cancers. In addition, tumors lacking mutations in *p53* itself often carry mutations in other genes that produce proteins that interact with and regulate p53. Indeed, Lane says, one way or another, the *p53* pathway may be inactivated in all human cancers.

The *p53* pathway may have evolved as a protection against cancer, helping cells cope with stresses such as DNA damage triggered by exposure to environmental toxins or radiation. When activated, the p53 protein turns on genes that can halt cell division until the DNA damage is repaired, or it can set off a form of cell suicide called apoptosis. Thus, *p53* can help prevent the accumulation of potentially cancer-causing mutations and also put the brakes on abnormal cell growth. That's why Lane once christened *p53* "the guardian of the genome."

CREDIT: N. OBERHEIM/T. TAKANO/M. NEDERGAARD/UNIVERSITY OF ROCHESTER

The cancer cells didn't laugh

Although a great deal of evidence links inactivated *p53* to cancer, researchers were unsure whether turning the tumor suppressor gene back on would actually halt tumor growth once it was under way. "*p53* mutations could simply set the stage for other [cancer-causing] mutations," says Tyler Jacks of the Massachusetts Institute of Technology in Cambridge. If so, he adds, "you could put *p53* back into cancer cells, and the cells would simply laugh." There was also the possibility that tumors could lose other proteins needed for normal *p53* pathway function, and that these would need repair, too.

Three independent teams, one led by Jacks and the others by Gerard Evan of the University of California, San Francisco, and Scott Lowe of Cold Spring Harbor Laboratory in New York, have now found that *p53* reactivation can indeed halt tumor growth. (Evan's results appeared in the 29 December 2006 issue of *Cell* and those of Jacks and Lowe were published online by *Nature* on 24 January and also appear in the 8 February issue.)

Both Evan's and Jacks's teams used mice that had been genetically engineered so that the *p53* gene could be turned on and off at will in the animals' cells. The mice also carried oncogene mutations to facilitate the development of cancers—lymphoma in the case of the Evan team's mice, and lymphomas and sarcomas in the Jacks team's animals. Lowe and his team took a somewhat different tack, genetically engineering liver tumor cells so that the researchers could turn the cells' *p53* gene on and off. These cells were then transplanted into the livers of mice.

In all cases, the researchers kept the *p53* gene "off" until the tumors grew to an advanced stage in the animals. Then, they turned the gene back on. "We all came to the same conclusion. … When *p53* is restored to the system, [cancer] cells respond," Jacks says. Depending on the tumor type, the exact mode of the responses differed, however.

The lymphoma cells in the Evan team's mice died by apoptosis, with the tumors beginning to shrink in about 12 hours. "The effect on the tumor appears to be quite catastrophic," Evan says. The effect was not permanent, however. Eventually the tumors grew back in all the animals, and this time *p53* could not be reactivated, either because that gene or the one for a protein called MDM2 that's known to inhibit p53 had been lost. This adds a cautionary note to efforts to treat human cancers by activating p53. Assuming that can be done, Evan says, "we don't know how long a remission will last."

Jacks and his team also saw lymphoma cells die by apoptosis. But the cells of the sarcomas went into growth arrest. The liver tumor cells in the Lowe team's mice stopped growing and became senescent. The Cold Spring Harbor group saw an additional feature as well: The changes that occurred in the senescent cells triggered a strong inflammatory attack on—and the destruction of—the tumor cells.

Early clinical trials

These results clinched the case that p53 activity can squelch tumor growth at least temporarily—a possibility hinted at by early gene therapy efforts to restore *p53* in human cancers. Clinical trials conducted about 10 years ago, which used adenovirus to carry a normal copy of *p53* into the tumors of patients with head and neck cancer or non–small cell cancer of the lung, led to reduced tumor growth in some patients and even tumor shrinkage in a few.

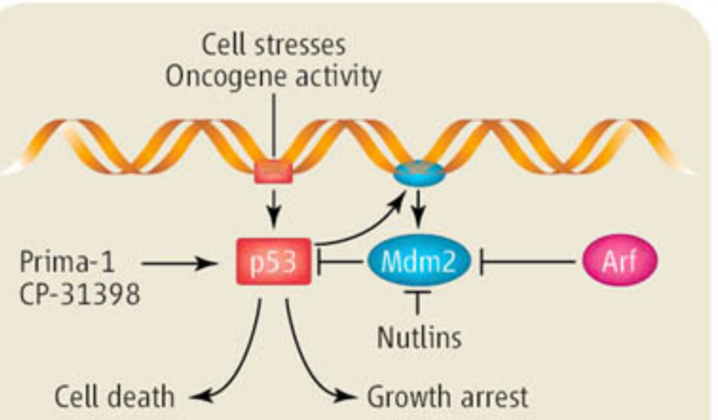

Drug targets in the p53 pathway. Some of the drugs being developed to fight cancer, including PRI MA-1 and CP-31398, aim to reactivate mutant p53 proteins, possibly by helping them fold more normally. Others, like nutlins, were designed to foster p53 activity by preventing its interaction with the natural inhibitor MDM2.

Another approach using adenovirus doesn't try to reactivate *p53* but instead takes advantage of the virus's ability to kill the cells it infects. To achieve this cell-killing, the virus must replicate. Normally, p53 can inhibit that replication, but adenovirus has a defense: a gene that makes a protein that stops p53 from doing that. In work also done in the mid-1990s, Frank McCormick and his colleagues, then at Onyx Pharmaceuticals in Richmond, California, identified a natural adenovirus mutant that can't inhibit p53. This virus, they reasoned, should only be able to replicate in, and kill, cancer cells that lack p53, whereas the active p53 of normal cells should block the mutant virus's replication, thus sparing the cells from its lethal effects.

Although later research showed that the mutant adenovirus's failure to replicate in normal cells was due to a different defect, the virus has shown promise in early clinical trials, including one from a team led by Tony Reid of Stanford University in Palo Alto, California, that was published online on 1 December 2006 by *Cancer Gene Therapy*. In that study, the liver tumors of seven of 17 patients with metastatic colorectal cancer who were treated with the virus either stopped growing or shrank, and there were few signs of liver toxicity.

Even so, these viral-based therapies aren't ideal, mainly because the agents have to be injected directly into the tumors or, as in the case of the liver tumors, into the artery leading to the liver. Cancer surgeon Gary Clayman of M. D. Anderson Cancer Center in Houston, Texas, who conducted an early trial of *p53* gene therapy, says that one of the problems with this approach is that it's not possible to get sufficient quantities of the virus into every cell of every tumor a patient might carry. "More effective delivery systems are needed," Clayman says.

Small is beautiful

To avoid such drug-delivery problems, researchers are now concentrating more on the development of small-molecule drugs that can be taken by mouth and transported by the bloodstream to the entire body. "You really need systemic delivery to reach all the targets," says Klas Wiman of the Karolinska Institute in Stockholm, Sweden. Some of this work aims to block the natural p53 inhibitor, MDM2.

A few years ago, researchers including Lane showed that small peptides that bind to MDM2 can prevent its interaction with p53, thus turning up the activity of the tumor suppressor protein. But the biggest boost came 3 years ago with the discovery of nutlins by Lyubomir Vassilev and colleagues at Hoffmann–LaRoche's labs in Nutley, New Jersey.

These compounds, called imidazolines, fit neatly into the small pocket where MDM2 contacts p53 and prevent the interaction between the two proteins. In experiments conducted at the time, the Roche team found that nutlins inhibit the growth of human tumors transplanted into mice by 90%, apparently without

CREDIT: P. HUEY/SCIENCE

causing harmful side effects. That's an important issue because a few months ago Evan and his colleagues reported that activating p53 in mice lacking a functional *mdm2* gene is fatal to the animals. (The results appeared in the December issue of *Cancer Cell*.)

In the absence of this natural brake on p53 activities, the tumor suppressor triggered massive apoptosis and growth arrest. "A drug that completely took out MDM2 would be disastrous to the patient," Evan says. He and others note, however, that a drug is unlikely to be that efficient, and it may be possible to adjust the dose of a nutlin or other MDM2 inhibitor so that it works in the tumor without causing unacceptable side effects.

Roche spokesperson Darien Wilson says that for competitive reasons, the company does not want to discuss its current work on nutlins, but that it is "still very involved in doing research" on the compounds and hopes to initiate clinical trials at some point.

Because the nutlins are directed at MDM2, they will only work on tumors that still retain functional *p53*. That, of course, is not the case for the 50% of cancers in which the p53 gene itself is mutated, but researchers are also identifying small-molecule drugs that can restore p53 activity in such cells. Mutated p53 proteins often fold abnormally and thus lose the ability to regulate their target genes. Some of the new p53 activators are thought to work partly by helping p53 fold into a more normal configuration.

These include two drugs, called MIRA-1 and PRIMA-1, that Wiman and his colleagues identified by screening a library of low-molecular-weight compounds from the U.S. National Institutes of Health in Bethesda, Maryland. The Karolinska team found that tumor cells, both in culture and transplanted into mice, respond to the drugs with increased p53 activity and tumor shrinkage. "We've shown that we can restore wild-type activity to some p53 [mutant] proteins," Wiman says. Provided the needed regulatory approvals come through, he hopes to start clinical trials with PRIMA-1 in about a year and has also started a company to commercialize the drug.

Another small-molecule activator of p53, a drug called CP-31398, was identified 8 years ago by Farzan Rastinejad and colleagues at Pfizer Central Research in Groton, Connecticut. Researchers originally thought that it, too, helps mutant p53 fold more normally. That would require that the drug bind to the tumor suppressor, but studies by Alan Fersht of Cambridge University in the United Kingdom failed to detect such binding. Despite that, "this compound has antitumor effects and may have potential for clinical development," says El-Deiry, who has done some work on CP-31398.

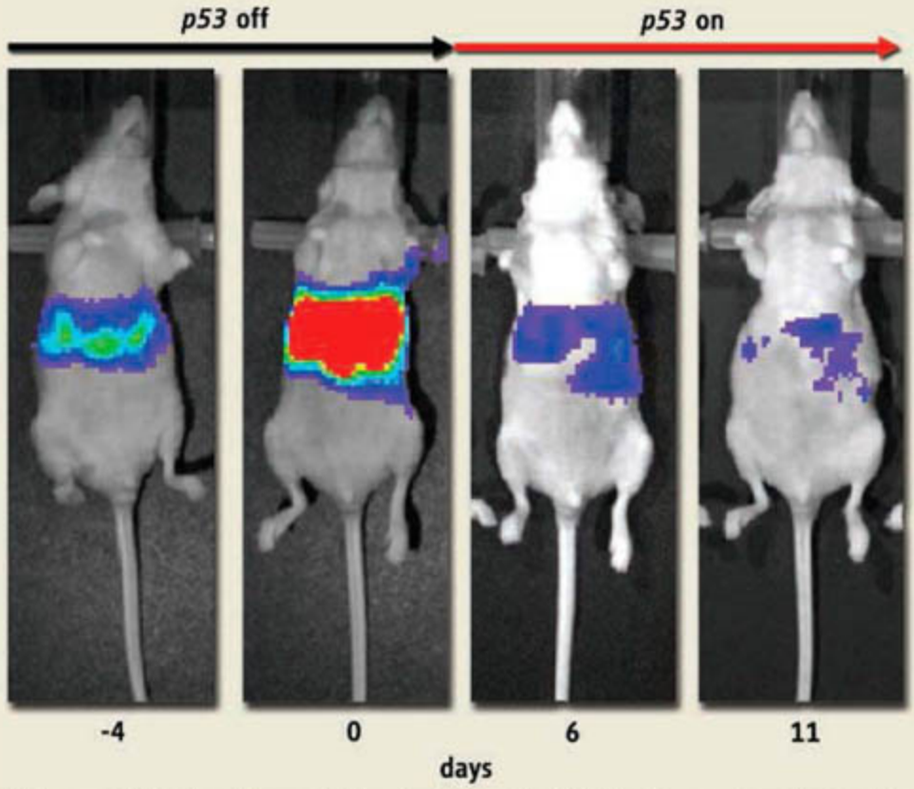

Melting away. With the *p53* gene off, liver tumors transplanted into mice grow to an advanced stage as indicated by the red color, but the tumors begin to shrink as soon as *p53* is activated.

It presumably has other mechanisms of action. For example, El-Deiry's team, working with the Pfizer group, has shown that it stabilizes both normal and mutated p53, apparently by inhibiting its degradation. Currently, however, Pfizer has no plans to develop the drug.

Still, these early successes in identifying activators of the p53 pathway have encouraged other researchers to attempt their own screens. Last summer, for example, El-Deiry and his colleagues reported on a search for drugs that mimic p53's effects in activating gene transcription. The screen turned up more than two dozen candidates. Some of them worked even in cells that lack p53 expression altogether because they increase production or stabilization of a p53 relative called p73, which also has tumor suppressive effects. Lane says that, in as-yet-unpublished work, his team has also screened for, and identified, candidate drugs that activate the p53 system.

As things are shaping up, researchers now have several p53 activators in hand, with more on the way. But not everyone is trying to activate p53 to help fight cancer. In some circumstances inhibiting its actions, particularly its ability to induce apoptosis, could be beneficial. The side effects of gene-damaging cancer therapies, including radiation and some types of chemotherapy, are largely due to cell death triggered in normal tissue by p53 activation. Last September, Evan and his colleagues reported evidence that tumor suppression by p53 does not depend on this response to gene damage but is instead due to its activation by a different path triggered by oncogene activity.

If so, Evan says, "we might be able to split the bad effects of p53 away from tumor suppression and protect cancer patients during therapy" by temporarily shutting down p53. Andrei Gudkov and colleagues at the Cleveland Clinic Foundation in Ohio have come to a similar conclusion. This team has identified a drug called pifithrin that can inhibit p53-induced apoptosis without altering its effects on gene transcription.

Much more work will be required before cancer therapies targeting the p53 pathway make it to the clinic. And if they do make it, clinicians will likely need to fine-tune therapeutic regimens to the specific p53 mutations being treated. But that may not be too much of an obstacle, because the field of cancer therapy is headed in that direction; indeed, "personalized medicine" is already a buzz phrase. "You might have to genotype the tumor [to decide on a therapy]," Jacks says. "But I expect that you're going to have to do that anyway."

–JEAN MARX

CREDIT: W. XUE *ET AL.*, *NATURE* **445**, 656 (2007)

Skin problem. There are a variety of human skin types, but pale people who don't tan seem to have the least protection from sun-induced skin cancers, including deadly melanomas.

SKIN BIOLOGY

A Healthy Tan?

A dark natural tan offers unparalleled protection against skin cancer. So scientists are developing compounds that trigger tanning without the sun's damaging effects

Anyone who relies on sunscreen knows it is sticky, inconvenient, and easy to forget. But sunscreen has a lesser known, and more serious, downside: It doesn't adequately protect against the deadliest form of skin cancer.

Although ultraviolet (UV)-blocking sprays and creams protect people against sunburn and the milder forms of skin cancer—squamous cell and basal cell carcinoma—they do not form an effective shield against melanoma, which doctors diagnose in 132,000 people worldwide each year. Ironically, says a growing cadre of skin biologists, what seems to protect best against melanoma is something that sunscreens efficiently thwart: a deep, dark tan.

Dark-skinned people, who also tend to tan well, are up to 500 times less likely to get melanoma and other skin cancers than are fair-skinned individuals. The ability to tan confers protection, researchers say, regardless of the skin's background level of pigmentation. This is due in part to the UV-shielding effect of melanin, the pigment that makes skin cells dark, and perhaps in part to an acceleration of DNA repair that some believe accompanies tanning. But tanning in the sun is a fool's wager, dermatologists say, because it causes dangerous DNA damage, which may lead to cancer before it can be fixed. To provide a sun-independent alternative, scientists are now developing compounds that trigger tanning and DNA repair by acting on molecules that control the melanin production pathway.

One key molecule is the melanocortin 1 receptor (MC1R), a protein on the surface of melanocytes that heads a major tanning pathway. Some researchers are targeting MC1R directly to stimulate tanning, whereas others are bypassing it and aiming at downstream targets in that pathway—a strategy that could help fair-skinned people who have mutations in the receptor's gene and thus normally don't tan (see sidebar, p. 1215). Still other investigators are concocting skin-cancer preventatives that promote MC1R-independent DNA repair within the skin, in some cases while also promoting melanin production.

"We hope to develop something that works far better than a sunscreen," says pigment cell researcher Zalfa Abdel-Malek of the University of Cincinnati College of Medicine in Ohio, who is developing an MC1R stimulator. "It will allow your pigment cells to make melanin and protect themselves against subsequent sun exposure." Adds pediatric oncologist David Fisher of Harvard Medical School in Boston, who is aiming elsewhere in the same pathway: "By switching on pigmentation, we may be able to mimic the epidemiological groups that have the lowest risk of melanoma," which are people with dark skin or who tan easily.

None of the candidate tanning compounds or DNA-repair agents has yet been proven safe and effective in large numbers of people. And there remain some who question the cancer-protective aspects of tanning alone, noting that tanned skin has a sun protection factor (SPF) of just 2 to 4. These skeptics argue that dark-skinned people may have other physiological features that protect them from skin cancer and that a pale person with an artificially induced tan may enjoy minimal cancer protection. "Even if you increase tanning, the improvement in photoprotection is likely to be small," suggests dermatologist Jonathan Rees of the University of Edinburgh, U.K.

Tanning tales

Cosmetic companies as well as researchers have been experimenting with skin-darkening agents for decades. There are many tanning agents on the market today, but they only dye the skin without engaging the natural tanning process or protecting the skin from UV rays.

The first scientific step toward a true artificial tanning agent came in the 1960s, when Yale University dermatologist Aaron Lerner discovered that injecting people with crude extracts from the hypothalamus containing the newly discovered melanocyte-stimulating hormone (MSH) increased skin pigmentation. Then in 1991, a team led by biologist Mac Hadley of the University of Arizona, Tucson, reported that injecting a long-lived analog of MSH increased skin pigmentation without sun exposure in 28 Caucasian men.

But no one understood how MSH acted on skin cells. In 1992, Roger Cone and his colleagues at Oregon Health Sciences University in Portland reported cloning the hormone's receptor, MC1R, in humans and mice. They also showed that mutations in that receptor gene underlie varying coat colors in mice: If mice inherited two defective receptors, they were yellow, whereas mice with at least one

CREDITS: JUPITER IMAGES

highly efficient MC1R protein were black or partially black. In 1995, Rees and several colleagues reported a similar association between aberrant forms of the receptor and variations in skin and hair color in people.

But it wasn't clear until recently that MSH and MC1R play an integral role in the skin's natural tanning response. In a report in the 21 September 2006 issue of *Nature*, Fisher, along with John D'Orazio, then a postdoc in Fisher's lab at the Dana-Farber Cancer Institute in Boston, and other colleagues, proved that connection. They studied a mouse that, like redheaded people, has two defective copies of the gene for MC1R. Unlike mice with working receptors, the pink-skinned "redheaded" mice could not tan at all, showing that a functioning MC1R is necessary for the process, at least in rodents.

In cell culture experiments, the group demonstrated that UV radiation prompts the release of MSH from keratinocytes, the dominant cell type in skin. The MSH then triggers MC1R on melanocytes, which produce melanin after a cascade of chemical reactions that begins with the activation of the enzyme adenyl cyclase, yielding an upsurge in cyclic adenosine monophosphate. Once melanocytes transfer the melanin to keratinocytes, the pigment forms caps over cell nuclei, shielding their DNA and creating the skin's tanned look. The pigmented keratinocytes protect the melanocytes below them as well.

Activation of the tanning pathway by MSH also seems to initiate DNA repair. Skin biologists Markus Böhm and Agatha Schwarz of the University of Münster in Germany and their colleagues reported in 2005 in the *Journal of Biological Chemistry* that the application of MSH reduced amounts of cyclobutane pyrimidine dimers, a sign of DNA damage, in cultured melanocytes exposed to UVB rays. These results and others indicating an enhanced DNA repair ability in tanned skin may explain its protective capacity beyond its simple SPF. "If you are genetically blessed with skin that tans well, only part of that is the melanin; you also have a repair mechanism that jumps to the challenge," says Barbara Gilchrest, a dermatologist at Boston University (BU) School of Medicine. "When you tan, you increase the level of DNA repair proteins by a factor of 2 or 3."

Protective potions

An agent targeting MC1R or other molecules in the tanning pathway might confer both advantages: the protection provided by pigment production and better DNA repair. For example, scientists at Clinuvel Pharmaceuticals, based in Melbourne, Australia, are testing a slow-release formulation of one of Hadley's injected MSH analogs, with the idea of initially using it as a preventive treatment for various sun-related ailments such as the common sun rash called polymorphous light

Why I Have Red Hair, Need to Avoid the Sun, And Shouldn't Commit a Crime

I am a redhead who cannot tan, and so are my two children. My husband, on the other hand, has dark brown hair and tans reasonably well. Surprisingly, red hair and the inability to tan are largely endowed by variations in a single gene: one for a receptor on the surface of melanocytes dubbed MC1R. Epidemiologists have discovered about 75 alleles for the *MC1R* gene, a handful of which disrupt the function of the receptor. In 1995, Jonathan Rees of the University of Edinburgh, U.K., and his colleagues reported that more than 80% of the people with red hair or fair skin they tested had such defective *MC1R* alleles. By contrast, these versions of the gene were present in fewer than 20% of study participants with dark hair and in less than 4% of those who tanned well.

Since then, larger studies, including one by Richard Sturm at the University of Queensland in Australia, have confirmed the association between faulty *MC1R* alleles and light skin and red hair. Redheads like me almost always have two alleles encoding defective MC1R proteins.

As part of my reporting on artificial tanning agents (see main text), geneticist Greg Barsh of Stanford University in Palo Alto, California, agreed to help me learn my *MC1R* genotype. Barsh's postdoc, Linda Ste. Marie, identified what appear to be two different alleles for a malfunctioning receptor, suggesting that I am a so-called compound heterozygote. One of these alleles, known as R151C, is fairly common, appearing in 10% to 20% of people with European ancestry. It is caused by a single-nucleotide exchange that inserts the amino acid cysteine in place of the usual arginine at codon 151. The result is that cells produce fewer of the receptor or it has diminished function, or both.

Barsh had never heard of my other allele, in which a single-nucleotide swap at position 456 produces a genetic stop sign that would halt MC1R's manufacture early. A receptor that is missing half of its amino acids can hardly be expected to work.

In 2000, Sturm's group reported that any of three alleles associated with red hair, including my R151C, double a person's risk of melanoma. To me and other redheads, this is not a big surprise, because dermatologists have already shown that our typical pale skin color is a reliable predictor of increased skin cancer risk.

CREDIT: VICTORIA VERNON

More important, *MC1R* status may help size up melanoma risk in people who do not have the physical characteristics associated with that greater cancer threat. In the 28 July 2006 issue of *Science* (p. 521), Maria Teresa Landi of the U.S. National Cancer Institute in Bethesda, Maryland, and her colleagues reported that possessing just one allele for a poorly functioning MC1R raises the risk of a dangerous type of melanoma more than threefold in people who have darker skin or hair. My husband may be one of these people, because my redheaded children presumably received one of their inactive MC1R proteins from their father.

MC1R genotype might also inform decisions about which of the experimental tanning compounds could work best. In theory, MSH analogs might not be the choice in people like me with defective MC1R receptors. Mysteriously, however, redheads have responded with tans in trials of such drugs. Spelling out a person's *MC1R* genes could also help crime-scene investigators, Rees suggests. If the analysis of biological tissue left at the scene reveals two aberrant versions of *MC1R* alleles, there is a 90% chance that its owner has red hair. That little fact should keep me on the straight and narrow. **–I.W.**

eruption. In the August 2006 *Journal of Investigative Dermatology*, a team led by dermatologist Ross StC. Barnetson of Royal Prince Alfred Hospital in Camperdown, Australia, reported that three 10-day cycles of the Clinuvel treatment increased skin melanin content by 41% in 47 healthy, fair-skinned people, preventing them from sunburn and significantly reducing signs of DNA damage in their skin. The drug will soon be tested in fair-skinned organ-transplant recipients to see whether it reduces the number of precancerous lesions such patients typically develop from the transplant's regimen of immune-suppressing drugs.

Clinuvel's drug must be injected every 2 months to maintain a tan. By contrast, Cincinnati's Abdel-Malek and her colleagues have developed potent MSH analogs small enough that they might be administered topically. Two such peptides stimulated melanin production, reduced programmed cell death, and enhanced DNA repair in melanocytes exposed to UV light, the researchers reported in the July 2006 *FASEB Journal*.

MSH analogs may not work in redheads with two damaged genes for MC1R proteins, however. Other teams are therefore aiming compounds downstream in the MC1R pathway. Fisher, D'Orazio, now at the University of Kentucky College of Medicine in Lexington, and their colleagues created a spectacular artificial tan in their redheaded rodents by smearing the shaved animals daily with the small molecule forskolin, a natural product in some teas that stimulates adenyl cyclase activity in cells. The forskolin-induced tan protected UV-exposed mice against sunburn and the production of DNA adducts, a sign of DNA damage. In redheaded MC1R-lacking mice that also had defective DNA repair enzymes, and thus are prone to UV-induced tumors, forskolin significantly reduced the number of such tumors compared to similar mice in a control group, Fisher says. Fisher has co-founded a firm, Magen Biosciences in Cambridge, Massachusetts, that is now trying to develop drugs that hit molecules more specific to the tanning pathway, because virtually all cells contain adenyl cyclase.

Damage signal

The MC1R pathway is not the sole arbiter of tanning. In addition to stimulating release of MSH, UV light triggers DNA damage, and many researchers believe that such damage can itself induce tanning and DNA repair by a separate mechanism. Gilchrest theorizes that this DNA-damage response revolves around telomeres, looplike structures at the ends of chromosomes that contain repetitive DNA sequences.

Starting in the 1990s, Gilchrest and her colleagues found that exposing skin cells to DNA fragments with specific sequences triggered both tanning and DNA repair. Gilchrest concluded that the fragments that triggered tanning, which she dubbed T-oligos, were eliciting restorative DNA-damage responses in healthy skin cells by imitating the exposed end of damaged telomeres that had lost its loop structure.

An earful. This mouse's right ear darkened after a compound that triggers the tanning pathway was applied to the skin.

CREDIT: DR. JOHN D'ORAZIO/UNIVERSITY OF KENTUCKY

In a recent study reported in the September 2006 *FASEB Journal*, the BU researchers applied T-oligos over 5 days to patches of human skin in culture from 18 Caucasian donors. The treatment boosted the melanin content of the skin samples three- to fivefold, comparable to UV's effects, and greatly accelerated the removal of markers of DNA damage in the skin after exposure to UV light compared to untreated, UV-exposed skin samples from the same donors. The T-oligos also increased levels of the cancer-suppressor protein p53 after UV irradiation. These findings, Gilchrest says, support the idea that sunscreen lotions incorporating T-oligos could produce tans in people, protecting them against sun damage and skin cancer. BU has patented this strategy, and Gilchrest is now trying to get funding for additional animal tests that could pave the way for human trials.

Meanwhile, other researchers are experimenting with lotions that trigger DNA repair without promoting a tan. Scientists at AGI Dermatics in Freeport, New York, have been testing a skin lotion called Dimericine that contains a bacterial DNA repair enzyme, T4N5, packaged into liposomes, microscopic lipid spheres that help cells absorb the enzyme. Molecular biologist and AGI head Daniel Yarosh envisions his product as a "morning-after cream" that could reduce the risk of cancer and other skin problems after a person has spent too long in the sun. Sunburned skin cells ordinarily repair half the DNA damage within 24 hours, whereas Yarosh cites published studies indicating that Dimericine-treated cells eliminate most of the damage within 6 hours.

In 2001, AGI Dermatics reported in the *Lancet* on a study of the lotion in people with a rare disease called xeroderma pigmentosum (XP), in which a lack of DNA repair enzymes leads to very high skin cancer rates. Compared to 10 XP patients who received a placebo lotion, a year of Dimericine treatment in 20 XP patients lowered the rate of precancerous lesions and basal cell carcinomas by 68% and 30%, respectively. (Currently under way are company-sponsored skin-cancer prevention trials in renal transplant patients and people with a history of skin cancer.)

A skin lotion instead of an injected drug like Clinuvel's, Dimericine has displayed few side effects so far in its tests on people, although some could crop up in larger trials. Some experts worry about artificially triggering the tanning response using agents that target players in the MC1R pathway, especially via drugs administered to the whole body and not just the skin. The Clinuvel compound, for instance, has caused nausea and vomiting in study subjects. There are more serious hypothetical concerns as well. "If you add MSH to melanocytes, they divide more quickly" in culture, raising the specter of cancer, Rees says. Then, of course, there's a sociological question of how many pale-skinned people would actually darken their skin to protect themselves against skin cancer.

On the other hand, the incidence of melanoma has tripled in the past 40 years despite the increased use of traditional sunscreens. Given that, D'Orazio, for one, thinks it's worth trying to develop novel ways to protect people against a ubiquitous, known mutagen—that is, UV light.

–INGRID WICKELGREN

Hazy climate driver. The cloud of pollutant particles over Asia may shift climate over Australia.

CREDIT: V. RAMANATHAN, FROM NSF C-130 DURING THE INDIAN OCEAN EXPERIMENT, 1999

CLIMATE CHANGE

Pollutant Hazes Extend Their Climate-Changing Reach

New studies show aerosols from burning fuels altering everything from rainfall to great ocean currents, with effects that can girdle the globe

The microscopic aerosol particle has long been recognized as a mighty agent of climate change. At a micrometer or less in size, this bit of combustion crud from power plant, tailpipe, or farmer's fire can reflect sunlight back to space and cool the polluted eastern United States. Or it could suppress rainfall over smoggy Houston, Texas. But for years, atmospheric scientists generally assumed that pollutant aerosols worked locally or regionally. Most dramatically, the brown haze over Asia weakens both the Indian and Asian monsoons that bring essential rains to the continent.

Now, scientists are finding that the effects of aerosols can range far from their source region and well beyond the wind-blown travels of the aerosols themselves. The trick lies in the well-known heating and cooling effects of aerosols, which in turn can shift the way the wind blows. For example, "Australians have tended to assume [pollutant aerosols] are a Northern Hemisphere phenomenon, [because] our skies are quite blue here," says climate modeler Leon Rotstayn of Commonwealth Scientific and Industrial Research Organisation (CSIRO) Marine and Atmospheric Research in Aspendale, Australia. Yet Rotstayn sees signs in his model that heavy aerosol pollution over Asia is increasing rainfall over distant Australia. Such aerosol action-at-a-distance is turning up in the Western Hemisphere as well.

So far, the expanding reach of aerosols is being documented primarily in global climate models, with tantalizing parallels with what's been happening in the real world in recent decades. In the case of Australia, Rotstayn and colleagues ran a global climate model to simulate the changing climate of the 20th century. In the past decade or two, production of aerosols over Asia has soared as developing economies cranked up, especially those of India and China. When Rotstayn and colleagues plugged increasing Asian aerosols into their model along with increasing greenhouse gases, rainfall and cloud cover increased over Australia, especially in the northwest. Yet when they omitted the distant aerosols, rainfall and cloudiness decreased, contrary to observations.

In the model, at least, the aerosols increase Australian rain and clouds by altering atmospheric and oceanic circulation, as the group will soon report in the *Journal of Geophysical Research*. Differences in atmospheric pressure can drive winds, and pressure can depend on temperature. So when aerosols produced in Asia blow downwind toward the Pacific and intercept sunlight, they can warm the surrounding air. At the same time, they cool the surface by blocking sunlight. Both those effects, in turn, can change how the winds blow, especially the rising air of atmospheric convection and the horizontal flow of air toward that convection. Around Asia, aerosols' net effect was to move more moisture-laden marine air into Australia, especially the northwest part of the continent, and thus increase cloudiness and rainfall.

North American aerosols seem to hold sway over a far more massive moisture flow: the great "conveyor belt" of currents that carries heat from the Southern Hemisphere into the far North Atlantic, called the meridional overturning circulation (MOC). That's according to modeling reported in a January 2006 paper in *Geophysical Research Letters* (*GRL*) by Thomas Delworth and Keith Dixon of the Geophysical Fluid Dynamics Laboratory in Princeton, New Jersey. Increasing greenhouse gases should be slowing the MOC, according to a raft of models, but in their model, Delworth and Dixon found that aerosols counter the effect of the strengthening greenhouse on the MOC. By counteracting the greenhouse's warming and its enhancement of precipitation at high latitudes, the aerosols have delayed the MOC's slowing by roughly 40 years, they find. Modeler Wenju Cai of CSIRO Aspendale and colleagues found a similar aerosol-induced MOC slowing in their model, as they reported last November in *GRL*.

The record for long-range effects may go to natural, dusty aerosols over the Sahara, abetted by sooty aerosols over East Asia, according to a report last September in the *Journal of Climate* by Maeng-Ki Kim of Kongju National University in South Korea and colleagues. The group found that in their model, dust raised over the springtime Sahara warms in sunlight, inducing air to rise there. That air eventually falls over southern Europe, warming the region. Then, much as an El Niño's tropical warmth can form an "atmospheric bridge" to change distant weather, this aerosol-induced circulation transmits some of its energy eastward. That shift alters atmospheric circulation to the east, bringing unusually cold air down to the Caspian Sea region.

The sunlight-absorbing aerosols of East Asia extend this atmospheric bridge as far as the western Pacific, bringing added warmth to central and northeastern Asia. The model's resulting pattern of springtime cooling and warming relative to broader trends bears a strong resemblance to actual trends, say Kim and his colleagues. Perhaps the thickening brew over Asia is also driving temperature changes over Eurasia, they say.

Untangling the web of aerosol effects will take a while. In the meantime, aerosol emissions are changing. North American and western European hazes have faded as developed countries reduced their emissions for health reasons. When will the developing nations of Asia follow suit? What will be the effects? Researchers will likely still be playing catch-up as the air clears.

–RICHARD A. KERR

Between us and the world 1223

Buckling 1227

Modeling water 1228

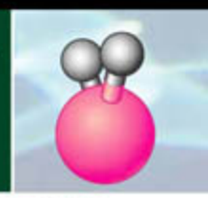

LETTERS | BOOKS | POLICY FORUM | EDUCATION FORUM | PERSPECTIVES

LETTERS

edited by Etta Kavanagh

To Sleep, Perchance to Dream

IN HIS PERSPECTIVE "WHAT DO ROBOTS DREAM OF?" (17 NOV. 2006, p. 1093), C. Adami provides an interesting interpretation of the Report "Resilient machines through continuous self-modeling" by J. Bongard *et al.* (17 Nov. 2006, p. 1118). Bongard *et al.* designed a robot with an algorithm of its stored sensory data to indirectly infer its physical structure. The robot was able to generate forward motion more adaptively by manipulating its gait to compensate for simulated injuries. Adami equates this algorithm to "dreams" of prior actions and asks whether such modeling could extend to environmental mapping algorithms. If this were possible, then a robot could explore a landscape until it is challenged by an obstacle; overnight, it could replay its actions against its model of the environment and generate (or synthesize) new actions to overcome the obstacle (i.e., "dream up" alternative strategies). It could then return the next day with a new approach to the obstacle.

This work in robotics complements current findings regarding sleep and dreaming in humans. There is now strong evidence in human sleep research showing that performance on motor (*1*) and visual (*2*) tasks is strongly dependent on sleep, with improvements consistently greater when sleep occurs between test and retest. This is generally believed to be related to neural recoding processes that are possibly connected to dreaming during sleep (*3*). However, when one considers human dreaming, it is not a simple replay of daily scenarios. It has complex, distorted images from a vast variety of times and places in our memory, arranged in a random, bizarre fashion (*4*). If we are to model such activity in robots, we would need to have some form of "sleep" algorithm that randomizes memory and combines it in unique arrays. This could be a way to generate unique approaches to scenarios that could be simulated. Otherwise, how else would scenario replay be an improvement over repeated trials in the environment?

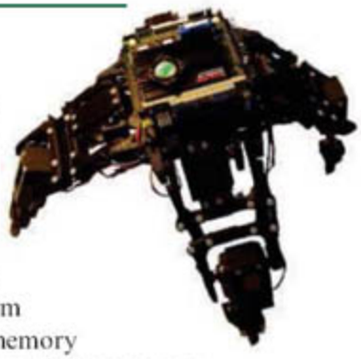

The study of human phenomena can be extremely difficult, and the study of sleep and dreaming is no exception (*5*). Robots would be ideal experimental subjects in many ways. Robots do not forget things, do not censor what they report, will not have problems sleeping, will not be bored by the tasks, are not going through life crises, and are not distracted by the laboratory or experimenter.

Adami states that the discipline of experimental robot psychology may not be far off. I say, "Bring it on!"

RUSSELL CONDUIT

Lecturer, School of Psychology, Psychiatry and Psychological Medicine, Monash University, Clayton, VIC 3800, Australia.

References

1. M. P. Walker, R. Stickgold, *Annu. Rev. Psychol.* **57**, 139 (2006).
2. S. Mednick, K. Nakayama, R. Stickgold, *Nat. Neurosci.* **6**, 697 (2003).
3. J. D. Payne, L. Nadel, *Learn. Mem.* **11**, 671 (2004).
4. J. A. Hobson, E. F. Pace-Schott, R. Stickgold, *Behav. Brain Sci.* **23**, 793 (2000).
5. R. Conduit *et al.*, *Conscious Cognit.* **13**, 484 (2004).

Response

CONDUIT DISCUSSES RECENT WORK BY Bongard *et al.* in light of dream research. I argued in my Perspective that the periods of action synthesis that are interspersed with periods of physical testing of actions could be interpreted as "robotic dreams" and speculated about a future discipline of experimental robotic psychology. Conduit suggests that, more than replaying the past days' events, human sleep consists of arrays of apparently randomly juxtaposed memories from different times and places in memory, and that these unique experiences (that do not exist in reality) are perhaps the reason for the "creative leap" that sometimes follows restful sleep.

But the periods between physical actions in the algorithm of Bongard *et al.* are by no means just replays of the previous days' events. Rather, during those periods the robot is evaluating candidate models of itself and its ability to respond, that is, it is checking whether a particular physical action (say, "move leg forward") is compatible with the remembered result (say, "tilt sensor 1 increases, all others the same") given the robot's self-modeling. In other words, the robot is not rethinking the day's events, but rather imagining possible self-models in light of the day's events. Only after this phase does the robot look for actions that could discriminate between models. If we would translate this algorithm into one where a robot is to infer a model of the environment rather than self, it would be necessary to generate as wide a variety of environments as possible, so that mental trials of actions would have a better chance of generating a response compatible with what is remembered. In such a case, perhaps the jagged and discontinuous nature of dreams can be viewed as a combinatorial algorithm designed to create as much diversity in environment models as possible. But to generate behaviors that discriminate between these

CREDITS: (TOP) BONGARD *ET AL.*; (BOTTOM) PHOTOS.COM

potential models, we would have to imagine living and navigating in them. Which, it seems to me, we do, but only in our dreams.

CHRISTOPH ADAMI

Keck Graduate Institute, Claremont, CA 91711, USA.

Response

THE ANALOGY BETWEEN MACHINE AND human cognition may suggest that reported bizarre, random dreams may not be entirely random. The robot we described did not just replay its experiences to build consistent internal self-models and then "dream up" an action based on those models. Instead, it synthesized new brief actions that deliberately caused its competing internal models to disagree in their predictions, thus challenging them to falsify less plausible theories and, as a result, improving its overall knowledge of self. It is possible that the mangled experiences that people report as bizarre dreams correspond to this unconscious search for actions able to clarify their self-perceptions. Many of the intermediate candidate models and actions developed by the robot (as seen in Movie S1 in our Supporting Online Material) were indeed very contorted, but were optimized nonetheless to elucidate uncertainties. Edelman (*1*), Calvin (*2*), and others have suggested the existence of competitive processes in the brain. Perhaps the fact that human dreams appear mangled and brief is exactly because they are—as in the robot—"optimized" to challenge and improve these competing internal models?

Indeed, analogies between machines learning from past experiences and human dreaming are potentially very fruitful and may be applicable in both directions. Although robots and their onboard algorithms are clearly simpler and may bear little or no direct relation to humans and their minds, it may be much easier to test hypotheses about humans in robots. Conversely, ideas from human cognition research may help direct robotic research beyond merely serving as inspiration. Specifically, it is likely that as robots become more complex and their internal models are formed indirectly rather than being explicitly engineered and represented, indirect probing techniques developed for studying humans may become essential for analyzing machines too.

HOD LIPSON,[1] VICTOR ZYKOV,[1] JOSH BONGARD[2]

[1]Department of Mechanical and Aerospace Engineering, Cornell University, Ithaca, NY 14853, USA. [2]Department of Computer Science, University of Vermont, Burlington, VT 05405, USA.

References

1. G. Edelman, *Neural Darwinism: The Theory of Neuronal Group Selection* (Basic Books, New York, 1988).
2. W. H. Calvin, *A Brief History of the Mind: From Apes to Intellect and Beyond* (Oxford Univ. Press, Oxford, 2004).

Online Versus Hardcopy Textbooks

SEVEN YEARS (2000–2006) OF ANALYSIS OF 1751 introductory lab science students in 10 separate semesters at Arizona State University reveals no statistically significant differences in class performance between online (81.2 ± 11.0) and hardcopy (80.8 ± 10.8) textbook users. In a required physical geography lab science class, students were given the option of using either an online (n = 760) or a hardcopy (n = 991) text to reinforce learning such topics as Wien's law, invading species, dissolution of minerals, Chezy-Manning equation, and glacial processes. By any measure, the hardcopy texts were more sophisticated than the online alternative, even though the basic information remained similar. Yet, even after disaggregating data into different semesters, texts, disciplines, class, GPA, age, ethnicity, and whether the student is a first-generation college student, no statistically significant differences emerged. Given the importance of required lab courses in shaping opinions of college-educated citizens about the importance of science, and given the growing resentment expressed by students over increasingly high-priced textbooks, similar studies in other general education lab science disciplines would seem justified.

RONALD I. DORN

School of Geographical Sciences, Arizona State University, Tempe, AZ 85287–0104, USA.

Is the EC Afraid of Its Own Visions?

IN A VISIONARY PHASE OF POLITICAL decision-making, the European Commission (EC) initiated new instruments of research funding within its 6th Framework Programme (FP 6), including the Integrated Projects (IPs), large-scale interdisciplinary programs. The first ones started in early 2004 with several tens of partner organizations and funding beyond 10 million Euro. In FP 7, launched on 22 December 2006, this instrument was scaled down and—at least for the first funding cycle—nearly abandoned.

Why has this change been made? Will most of these IPs, which have at least two more years to go, be failures?

Since February 2004, we have coordinated the IP ALARM (*1*), which is made up of 67 partner organizations and 250 scientists from 35 countries and receives EC funding of nearly 13 million Euro. ALARM focuses on some of the main drivers of biodiversity change [climate and land use change, environmental chemicals, invasive species, and loss of pollinators (*2*)] and combines ecological, environmental, and economic research. The consortium includes many leading scientists, who increasingly appreciate the opportunities offered through a project of such size and scope, e.g., by forming new teams conducting inter- and transdisciplinary research.

This is exactly what is urgently needed in science, as expressed by Carpenter *et al.* (*3*): "Meeting the research needs described will require new coalitions among disciplines that traditionally have been isolated….The [Millennium Ecosystem Assessment] has provided a road map; now, we need to start the journey." We think that large integrated projects have the clear potential to fulfil these requirements.

By initiating the IP instrument, the European Commission created considerable support to get the journey started. Do they now intend to stop halfway?

JOSEF SETTELE, INGOLF KÜHN, STEFAN KLOTZ, VOLKER HAMMEN, JOACHIM SPANGENBERG

Helmholtz Centre for Environmental Research–UFZ, Theodor-Lieser-Strasse 4, Halle (Saale) D-06120, Germany.

References

1. J. Settele *et al.*, *GAIA* **14**, 69 (2005) (see www.alarmproject.net).
2. J. C. Biesmeijer *et al.*, *Science* **313**, 351 (2006).
3. S. R. Carpenter *et al.*, *Science* **314**, 257 (2006).

CORRECTIONS AND CLARIFICATIONS

News of the Week: "New Swiss influenza database to test promises of access" by M. Enserink (16 Feb., p. 923). Amos Bairoch is not the director of the Swiss Institute of Bioinformatics (SIB), as the article stated, but director of the Swiss-Prot group at SIB, as well as director of the Structural Biology and Bioinformatics department of the University of Geneva. The SIB's director is Ernest Feytmans.

Special Section: Sustainability and Energy: News: "Catalyzing the emergence of a practical biorefinery" by A. Cho (9 Feb., p. 795). The Pacific Northwest National Laboratory is in Richland, Washington, not Hanford.

News Focus: "Judging Jerusalem" by A. Lawler (2 Feb., p. 588). Dr. Eilat Mazar is a senior fellow at the Shalem Center, an academic research institute in Jerusalem. She heads its archaeology institute, which sponsored the dig in the City of David.

Reports: "Highly siderophile element constraints on accretion and differentiation of the Earth-Moon system" by J. M. D. Day *et al.* (12 Jan., p. 217). In the first sentence of the second full paragraph on page 218, LaPaz, Bolivia, was incorrectly named as the location of meteoritic samples. The corrected sentence should read, "We report precise

Os-isotope– and HSE-abundance data (table S1) for five basalts from the Apollo 15 mission, six from Apollo 17, and six lunar basalts of meteoritic origin from LaPaz Icefield, Antarctica, that were obtained by using an ultra-low–blank, isotope-dilution digestion technique (*12*)."

This Week in *Science*: "Rubidium-rich stars" (15 Dec. 2006, p. 1653). Both instances of "^{87}Ru" should have read "^{87}Rb." Rb is the symbol for the element rubidium.

News Focus: "Getting a read on Rett syndrome" by G. Miller (8 Dec. 2006, p. 1536). Due to an editorial error, the article implied that a genetic manipulation that restored *Mecp2* gene expression in mice could potentially be used to treat people with the disorder. This manipulation was only possible because of the way the gene was initially turned off in the mice. It could not be used to undo the mutations that cause Rett syndrome in humans.

Letters to the Editor

Letters (~300 words) discuss material published in *Science* in the previous 3 months or issues of general interest. They can be submitted through the Web (www.submit2science.org) or by regular mail (1200 New York Ave., NW, Washington, DC 20005, USA). Letters are not acknowledged upon receipt, nor are authors generally consulted before publication. Whether published in full or in part, letters are subject to editing for clarity and space.

Perspectives: "Breaking the H_2 marriage and reuniting the couple" by G. J. Kubas (17 Nov. 2006, p. 1096). In line 8 of the first paragraph, "10^{10} tons of ammonia fertilizer" should instead read "10^8 tons of ammonia fertilizer."

Brevia: "The 160-kilobase genome of the bacterial endosymbiont *Carsonella*" by A. Nakabachi *et al.* (13 Oct. 2006, p. 267). The last sentence of the second paragraph is incorrect. It should read, "The genome size, which was further confirmed by long-range electrophoresis, is only about one-third that of the archaeal parasite *Nanoarchaeum equitans* (which is 491 kb) (*3*) and that of a *Buchnera* strain (which has the second smallest bacterial genome, at 422.4 kb) (*4*)." The current reference (*4*) should be replaced by the following reference: V. Pérez-Brocal *et al.*, *Science* **314**, 312 (2006).

TECHNICAL COMMENT ABSTRACTS

Comment on "Detecting Awareness in the Vegetative State"

Parashkev Nachev and Masud Husain

In a report of a single patient in a persistent vegetative state, Owen *et al.* (Brevia, 8 September 2006, p. 1402) claimed that the presence of task-specific brain activation in response to verbal command implies both covert conscious awareness and a capacity for intention. We argue that neither can be securely inferred from the evidence presented.

Full text at www.sciencemag.org/cgi/content/full/315/5816/1221a

Comment on "Detecting Awareness in the Vegetative State"

Daniel L. Greenberg

Owen *et al.* (Brevia, 8 September 2006, p. 1402) claimed that a patient's brain activity revealed that she was consciously responding to commands despite being in a vegetative state. However, several alternative explanations were not eliminated. Specifically, the activity could reflect unconscious reactions to the last word in the command, not conscious decisions to respond. A refined experimental design could clarify these issues.

Full text at www.sciencemag.org/cgi/content/full/315/5816/1221b

Response to Comments on "Detecting Awareness in the Vegetative State"

Adrian M. Owen, Martin R. Coleman, Melanie Boly, Matthew H. Davis, Steven Laureys, Dietsje Jolles, John D. Pickard

Additional data, supported by relevant functional neuroimaging literature, confirm that the "normal" patterns of brain activity reported in a patient who was clinically diagnosed as vegetative could not have occurred "automatically" in the absence of conscious awareness. The most parsimonious explanation remains that this patient was consciously aware despite her diagnosis of vegetative state.

Full text at www.sciencemag.org/cgi/content/full/315/5816/1221c

AGRICULTURE

Looking Beyond Corn and Petroleum

Tobias Plieninger

Few North Americans would consider corn their staple food of choice. But a look at some figures suggests a different reality: cornfields cover around 330,000 km^2 of U.S. farmland, corn production amounts to 430 million m^3 per year, and one out of four supermarket items are based on corn. The only thing that seems more impressive than the extent to which corn has found its way into our food is the subtlety of this process. People do not directly consume most of their corn; instead, it appears as a component in the production of steaks, hamburgers, milk, soft drinks, snacks, and countless other foods. Recently, it has entered the production stream in another form, as the source of ethanol for fuel.

In *The Omnivore's Dilemma*, Michael Pollan explores the food chains that link two biological systems, the soil and the human body, to address the question of what to eat. Noting the conflict between "neophilia" (the comfort of variety) and "neophobia" (the fear of ingesting anything new), he examines the pleasures and pains that flow from our having a wide range of diet options. Pollan (a professor of environmental and science journalism at the University of California, Berkeley) begins by describing America's "national eating disorder," manifest in "a notably unhealthy people obsessed by the idea of eating healthily." Using his personal experiences and a review of ecological and anthropological literatures, he tries to help orient disoriented consumers by tracing the origins of three dramatically different diets: the industrial, organic, and hunter-gatherer diets. With the help of three protagonists—Iowa corn farmer George Naylor, Shenandoah Valley "grass farmer" Joel Salatin, and Italo-American food aficionado Angelo Garro—Pollan devotes each section of this multifaceted book to tracing a complete food chain from the earth to the plate.

I particularly enjoyed the first chapter's comprehensive analysis of the political ecology of corn. Corn, the "keystone species of the industrial food chain," scored a triumph unchallenged in the plant world by both colonizing agricultural landscapes and inhabiting human bodies. It has become a basic commodity for animal feed, complex foods, fiber, and fuels. As Pollan shows, our interdependency with corn is so tightly woven that it seems a question whether we really have domesticated corn or whether corn has changed us to distribute its genes across the globe and to dedicate large areas of land to its cultivation—a thought that he elaborated on in his previous book, *The Botany of Desire* (*1*).

The Omnivore's Dilemma
A Natural History of Four Meals

by Michael Pollan

The Penguin Press, New York, 2006. 463 pp. $26.95, C$38. ISBN 9781594200823.

The journey along the industrial food chain starts in a cornfield in Iowa, a state that has seen an astounding increase of agricultural productivity and efficiency over the last 100 years. Pollan notes that despite (or perhaps because of) corn yields increasing 10-fold since 1920, today's corn prices are consistently low. But he argues convincingly that this cheap corn comes at a steep price: farmers go bankrupt in the footrace to break even. When corn prices decrease, taxpayers bear the burden of the federal farm policy subsidizing corn production, while the environment has to endure land degradation and water pollution.

At an important stopover on the way along the industrial food chain, corn is refined to meat. This occurs in places so different from the traditional understanding of a farm that a discrete term had to be invented: the confined animal feeding operation. These feedlots exhibit alarming parallels to a medieval city before the days of modern sanitation (with the exhaustive application of antibiotics being the main difference). They are highly efficient in the production of cheap meat. But again, Pollan presents a persuasive case that this meat is not cheap at all, if the societal costs (e.g., antibiotic resistance and the environmental costs of animal wastes) are considered.

Another iconic strand of the industrial food chain that Pollan traces throughout the book is petroleum. We learn that U.S. agriculture, once fully dependent on the energy from the sun, has become so reliant on fossil fuels that it now takes more than a calorie of fossil fuel to produce a calorie of food. Nearly 20% of the current U.S. consumption of fossil fuels goes to the production and distribution of food.

The author presents a variety of visions for alternative agriculture as countermeasures to the conventional corn- and petroleum-fed food chain. He outlines compelling advantages to a comprehensively sustainable, "pastoral" farming system for human health and the environment: Monocultures can be replaced by polycultures; soil nutrition can be derived from farm wastes instead of from imported fertilizer; entire agricultural systems can be oriented on biological rather than mechanical principles. However, the book leaves unanswered the crucial question of how alternative farming models can be scaled up to supply a growing and increasingly urbanized population.

It is clear from *The Omnivore's Dilemma* that Pollan favors more sustainable and nutritious agriculture, but he leaves the choice of food chains open to his readers—albeit he

Endless rows of corn.

CREDIT: CORBIS

The reviewer is in the Rural Land Uses Research Group, Berlin-Brandenburg Academy of Sciences and Humanities and Brandenburg University of Technology, Jägerstraße 22/23, 10117 Berlin, Germany. E-mail: plieninger@bbaw.de

does not hide his preference for grass farming. He acknowledges that food consumption is a trade-off that one has to personalize according to one's ethical standards. However, that personal approach is complicated by the fact that the average consumer rarely has the information necessary to reach a carefully considered decision. Therefore Pollan argues in favor of the "right to look" and advocates shorter, less complex, and more visible food chains: "Were the walls of our meat industry to become transparent … we would not long continue to raise, kill, and eat animals the way we do."

Reference

1. M. Pollan, *The Botany of Desire: A Plant's-Eye View of the World* (Random House, New York, 2001).

10.1126/science.1138399

ANTHROPOLOGY

Showing Some Skin

Qais Al-Awqati

No organ reflects our inner life and culture more than the skin. Our heart may race on seeing our beloved, but it is our flushed face that gives our emotions away; although you might convince your neighborhood surgeon to tattoo your liver as a way of advertising that you belong to some gang, that won't protect you from being knifed. Nina Jablonski's *Skin* promises to show how skin reflects our age, state of health, ancestry, and cultural identity.

Skin
A Natural History
by Nina G. Jablonski
University of California Press, Berkeley, CA, 2006. 293 pp. $24.95, £15.95. ISBN 9780520242814.

An author contemplating writing a book about an organ is faced by two choices. Does she want to write a guided tour of its structure and functions? Or would she prefer to concentrate on a few things she thinks are emblematic? Jablonski, a physical anthropologist at Pennsylvania State University, chose the former. She has written what can be described as an introductory text to the study of the skin, a slim volume of 175 pages of text supplemented with an additional 65 pages of notes, glossary, and bibliography. The reader learns, for example, the skin's cellular components, the role of sweat in human evolution, and the importance of touch in human communication. The author also discusses the consequences, good and bad, of having different skin colors and the many ways humans have used the skin as billboards of the self to advertise group solidarity or difference.

In its discussion of the human skin, the book's principal theme is evolution, and almost every page contains that word. There have been many splendid examples of books focused on the evolution of an organ or one of its functions. One that comes to mind is Ashley Montagu's *Touching: The Human Significance of the Skin*, an insightful and influential account of the cultural aspects of the sense of touch (*1*). A best seller in its time, it remains in print decades after its publication. One reason for its success is that Montagu avoided writing a "textbook," with all its connotations of dry academic prose and a lack of narrative drive. Jablonski, on the other hand, seems to lack a clear view of the level of expertise of her intended audience. Too often, technical medical terms pop up in the text never to be mentioned again.

Although the author wants to provide an evolutionary perspective on all attributes of skin biology, the accounts she provides seldom rise above the provision of plausible hypotheses. Is it really true that we were selected to be hairless sweaty creatures? That sounds possible, but what is the actual evidence for such an assertion? Is it also true that vitamin D synthesis, a major locus of interaction between sunlight and diet, is the dominant factor in the natural selection of skin color? This idea is simply presented without any of the documentation that would make a convincing story. One would like to see the evidence of how rickets (vitamin D deficiency) might act as an agent of evolutionary selection.

For many subjects where an anthropologist could have provided an exciting narrative—such as the roles of tattoos, body piercing, scars, or henna drawing—the book offers something closer to extended definitions than to in-depth considerations of their roles in social interaction. I would have loved, for example, a riff on the recent explosion of tattoos and piercings among young people from economically privileged backgrounds. The topic is only touched on in the chapter "Statements," and the search for individual difference is not placed in its social context. The thorny issue of the social construction of the roles of skin color is reduced again to a brief survey of skin color biology and its evolutionary implications.

Scientists writing for broad audiences tend to write about the focus of their own work. Although only a few of Jablonski's research papers address skin evolution, the lack of deep expertise need not prevent a nonspecialist from pulling together findings from different fields to generate an exciting, even fresh view of nature. An enviable example is Jared Diamond's *Guns, Germs, and Steel* (*2*). (Diamond, incidentally, has provided a very positive blurb for the book jacket.) Unfortunately, *Skin* suffers by comparison, as it lacks the narrative drive, coherent theme, and telling anecdotes that so enrich Diamond's book. However, the book's extensive notes and references testify to Jablonski's hard work and wide reading; their diversity encompasses the mutational analysis of the melanocortin-1 receptor, identification of new genes in zebrafish, chemistry of melanin, and anthropological studies of warriors. That breadth may be the book's principal strength. *Skin* offers an accessible and well-referenced overview of many aspects of the biology of human skin. Although none of the sections is comprehensive enough to serve as a primary resource, the book as a whole explains why we should care about its subject. Beauty may only be skin deep, but Jablonski shows us that the skin, be it thin or thick, is the true mirror of the soul.

Skin shaped through time.

CREDIT: FRANS JANSEN/GETTY IMAGES

The reviewer is in the Department of Medicine and the Department of Physiology, College of Physicians and Surgeons, Columbia University, 630 West 168th Street, New York, NY 10032, USA. E-mail: qa1@columbia.edu

References

1. A. Montagu, *Touching: The Human Significance of the Skin* (Columbia Univ. Press, New York, 1971).
2. J. M. Diamond, *Guns, Germs, and Steel: The Fates of Human Societies* (Norton, New York, 1997).

10.1126/science.1138921

NUCLEAR WAR

Consequences of Regional-Scale Nuclear Conflicts

Numerous deaths and dangerous climate effects would result from use of low-yield nuclear weapons being stockpiled in many parts of the world.

Owen B. Toon,[1]* Alan Robock,[2]* Richard P. Turco,[3] Charles Bardeen,[1] Luke Oman,[2,4] Georgiy L. Stenchikov[2]

The world may no longer face a serious threat of global nuclear warfare, but regional conflicts continue. Within this milieu, acquiring nuclear weapons has been considered a potent political, military, and social tool (1–3). National ownership of nuclear weapons offers perceived international status and insurance against aggression at a modest financial cost. Against this backdrop, we provide a quantitative assessment of the potential for casualties in a regional-scale nuclear conflict, or a terrorist attack, and the associated environmental impacts (4, 5).

Eight nations are known to have nuclear weapons. In addition, North Korea may have a small, but growing, arsenal. Iran appears to be seeking nuclear weapons capability, but it probably needs several years to obtain enough fissionable material. Of great concern, 32 other nations—including Brazil, Argentina, Japan, South Korea, and Taiwan—have sufficient fissionable materials to produce weapons (*1*, *6*). A de facto nuclear arms race has emerged in Asia between China, India, and Pakistan, which could expand to include North Korea, South Korea, Taiwan, and Japan (*1*). In the Middle East, a nuclear confrontation between Israel and Iran would be fearful. Saudi Arabia and Egypt could also seek nuclear weapons to balance Iran and Israel. Nuclear arms programs in South America, notably in Brazil and Argentina, were ended by several treaties in the 1990s (*6*). We can hope that these agreements will hold and will serve as a model for other regions, despite Brazil's new, large uranium enrichment facilities.

Nuclear arsenals containing 50 or more weapons of low yield [15 kilotons (kt), equivalent to the Hiroshima bomb] are relatively easy to build (*1*, *6*). India and Pakistan, the smallest nuclear powers, probably have such arsenals, although no nuclear state has ever disclosed its inventory of warheads (*7*). Modern weapons are compact and lightweight and are readily transported (by car, truck, missile, plane, or boat) (*8*). The basic concepts of weapons design can be found on of the Internet. The only serious obstacle to constructing a bomb is the limited availability of purified fissionable fuels.

There are many political, economic, and social factors that could trigger a regional-scale nuclear conflict, plus many scenarios for the conduct of the ensuing war. We assumed (*4*) that the densest population centers in each country—usually in megacities—are attacked. We did not evaluate specific military targets and related casualties. We considered a nuclear exchange involving 100 weapons of 15-kt yield each, that is, ~0.3% of the total number of existing weapons (*4*). India and Pakistan, for instance, have previously tested nuclear weapons and are now thought to have between 109 and 172 weapons of unknown yield (*9*).

Fatalities were estimated by means of a standard population database for a number of countries that might be targeted in a regional conflict (see figure, above). For instance, such an exchange between India and Pakistan (*10*) could produce about 21 million fatalities—about half as many as occurred globally during World War II. The direct effects of thermal radiation and nuclear blasts, as well as gamma-ray and neutron radiation within the first few minutes of the blast, would cause most casualties. Extensive damage to infrastructure, contamination by long-lived radionuclides, and psychological trauma would likely result in the indefinite abandonment of large areas leading to severe economic and social repercussions.

Fires ignited by nuclear bursts would release copious amounts of light-absorbing smoke into the upper atmosphere. If 100 small nuclear weapons were detonated within cities, they could generate 1 to 5 million tons of carbonaceous smoke particles (*4*), darkening the sky and affecting the atmosphere more than

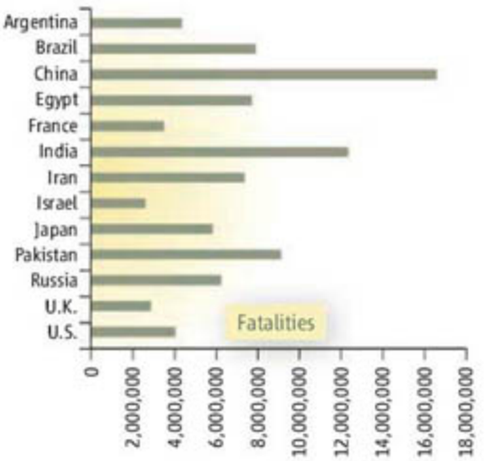

Fatalities predicted due to immediate radiation, blast, and fire damage from an attack using 50 nuclear weapons with 15-kt yield on various countries. Airbursts were assumed. Estimates for ground bursts, including early radioactive fallout, are about 25% less (*4*).

major volcanic eruptions like Mt. Pinatubo (1991) or Tambora (1815) (*5*). Carbonaceous smoke particles are transported by winds throughout the atmosphere but also induce circulations in response to solar heating. Simulations (*5*) predict that such radiative-dynamical interactions would loft and stabilize the smoke aerosol, which would allow it to persist in the middle and upper atmosphere for a decade. Smoke emissions of 100 low-yield urban explosions in a regional nuclear conflict would generate substantial global-scale climate anomalies, although not as large as in previous "nuclear winter" scenarios for a full-scale war (*11*, *12*).

However, indirect effects on surface land temperatures, precipitation rates, and growing season lengths (see figure, page 1225) would be likely to degrade agricultural productivity to an extent that historically has led to famines in Africa, India, and Japan after the 1783–1784 Laki eruption (*13*) or in the northeastern United States and Europe after the Tambora eruption of 1815 (*5*). Climatic anomalies could persist for a decade or more because of smoke stabilization, far longer than in previous nuclear winter calculations or after volcanic eruptions.

Studies of the consequences of full-scale

[1]Department of Atmospheric and Oceanic Sciences, Laboratory for Atmospheric and Space Physics, University of Colorado, Boulder, CO 80309, USA. [2]Department of Environmental Sciences, Rutgers University, New Brunswick, NJ 08901, USA. [3]Department of Atmospheric and Oceanic Sciences, University of California, Los Angeles, CA 90095, USA. [4]Department of Earth and Planetary Sciences, Johns Hopkins University, Baltimore, MD 21218, USA.

*Authors for correspondence. E-mail: toon@lasp.colorado.edu, robock@envsci.rutgers.edu

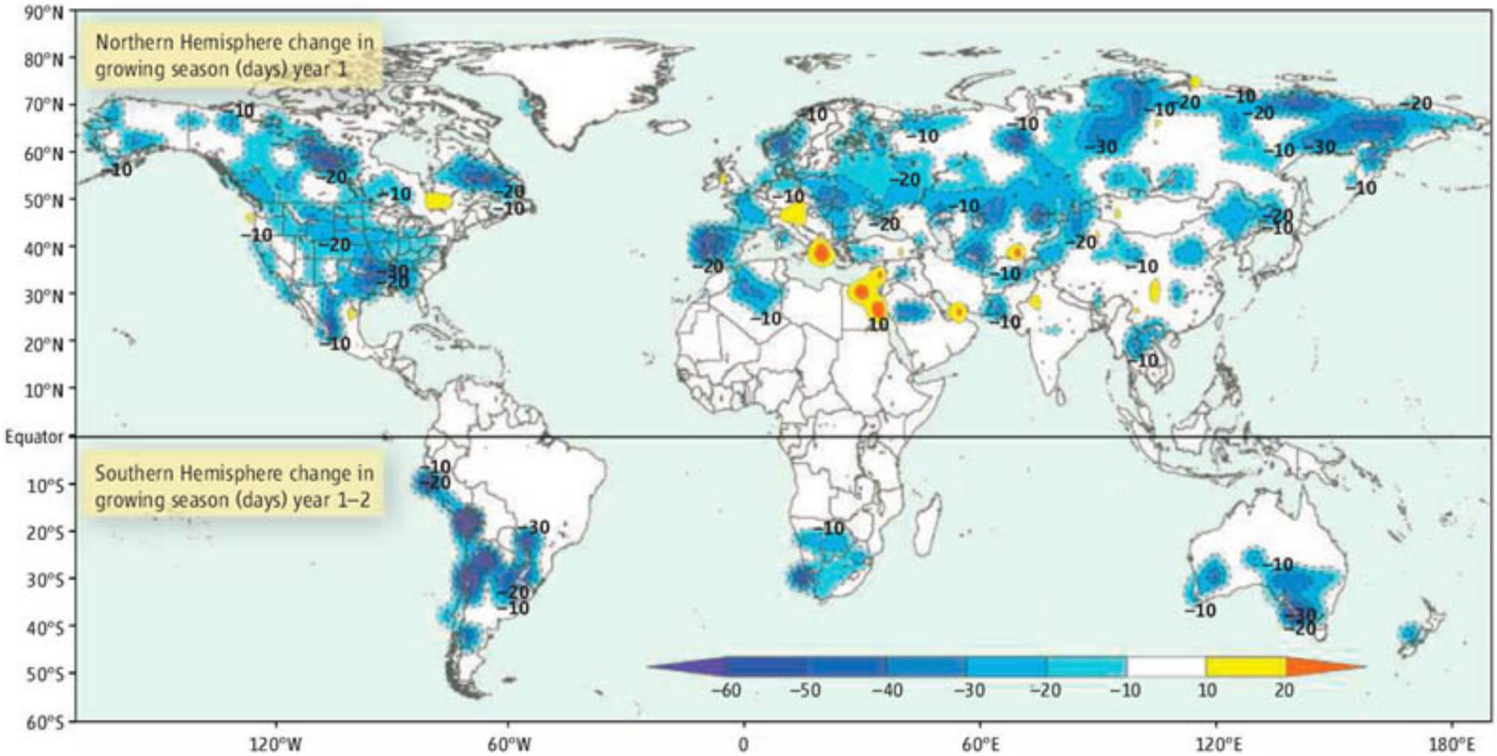

Change in growing season (period with freeze-free days) in the first year after smoke release from 100 15-kt nuclear explosions [modified from figure 11 in (*5*)].

nuclear war show that indirect effects of the war could cause more casualties than direct ones, perhaps eliminating the majority of the world's population (*11*, *12*). Indirect effects such as damage to transportation, energy, medical, political, and social infrastructure could be limited to the combatant nations in a regional war. However, climate anomalies would threaten the world outside the combat zone. The predicted smoke emissions and fatalities per kiloton of explosive yield are roughly 100 times those expected from estimates for full-scale nuclear attacks with high-yield weapons (*4*).

Unfortunately, the Treaty on Non-Proliferation of Nuclear Weapons has failed to prevent the expansion of nuclear states. A bipartisan group including two former U.S. secretaries of state, a former secretary of defense, and a former chair of the Senate Armed Services Committee has recently pointed out that nuclear deterrence is no longer effective and may become dangerous (*3*). Terrorists, for instance, are outside the bounds of deterrence strategies. Mutually assured destruction may not function in a world with large numbers of nuclear states with widely varying political goals and philosophies. New nuclear states may not have well-developed safeguards and controls to prevent nuclear accidents or unauthorized launches. This bipartisan group detailed numerous steps to inhibit or prevent the spread of nuclear weapons (*3*). Its list, with which we concur, includes removing nuclear weapons from alert status to reduce the danger of an accidental or unauthorized use of a nuclear weapon; reducing the size of nuclear forces in all states; eliminating tactical nuclear weapons; ratifying the Comprehensive Test Ban Treaty worldwide; securing all stocks of weapons, weapons-usable plutonium, and highly enriched uranium everywhere in the world; controlling uranium enrichment along with guaranteeing that uranium for nuclear power reactors could be obtained from controlled international reserves; safeguarding spent fuel from reactors producing electricity; halting the production of fissile material for weapons globally; phasing out the use of highly enriched uranium in civil commerce and research facilities and rendering the materials safe; and resolving regional confrontations and conflicts that give rise to new nuclear powers.

The analysis summarized here shows that the world has reached a crossroads. Having survived the threat of global nuclear war between the superpowers so far, the world is increasingly threatened by the prospects of regional nuclear war. The consequences of regional-scale nuclear conflicts are unexpectedly large, with the potential to become global catastrophes. The combination of nuclear proliferation, political instability, and urban demographics may constitute one of the greatest dangers to the stability of society since the dawn of humans.

References and Notes

1. S. D. Drell, J. E. Goodby, *The Gravest Danger: Nuclear Weapons* (Hoover Institution Press, Stanford, CA, 2003), 134 pp.
2. S. Kothari, Z. Mian, Eds., *Out of the Nuclear Shadow* (Zed Books, London, 2001), 525 pp.
3. G. P. Shultz, W. J. Perry, H. A. Kissinger, S. Nunn, *Wall Street Journal*, 4 January 2007, p. A15.
4. O. B. Toon *et al.*, *Atmos. Phys. Chem. Disc.* **6**, 11745 (2006).
5. A. Robock *et al.*, *Atmos. Phys. Chem. Disc.* **6**, 11817 (2006).
6. D. Albright, F. Berkhout, W. Walker, *Plutonium and Highly Enriched Uranium 1996: World Inventories, Capabilities, and Policies* (Oxford Univ. Press, New York, 1997), 502 pp.; www.isis-online.org/global_stocks/end2003/tableofcontents.html.
7. National Academy of Sciences, *Monitoring Nuclear Weapons and Nuclear-Explosive Materials* (National Academy Press, Washington, DC, 2005), 250 pp.
8. J. N. Gibson, *Nuclear Weapons of the United States* (Schiffer, Atglen, PA, 1996),
9. By comparison, China has roughly 400 and the United States has more than 10,000 warheads. For more information, see the supporting online material.
10. P. R. Lavoy, S. A. Smith, *Strategic Insights* **II**(2) (2003); www.ccc.nps.navy.mil/si/feb03/southAsia2.asp.
11. A. B. Pittock *et al.*, *Environmental Consequences of Nuclear War, SCOPE 28*, vol. 1, *Physical and Atmospheric Effects* [Scientific Committee on Problems of the Environment (SCOPE), of the International Council of Scientific Societies, Wiley, Chichester, England, ed. 2, 1989).
12. M. A. Harwell, T. C. Hutchinson, *Environmental Consequences of Nuclear War, SCOPE 28*, vol. 2, *Ecological and Agricultural Effects* (SCOPE, Wiley, Chichester, England, ed. 2, 1989), 523 pp.
13. L. Oman, A. Robock, G. L. Stenchikov, T. Thordarson, *Geophys. Res. Lett.* **33**, L18711, doi:10.1029/2006GL027665 (2006).

14. A.R., G.L.S., and L.O. were supported by NSF grants ATM-0313592 and ATM-0351280.

10.1126/science.1137747

Supporting Online Material
www.sciencemag.org/cgi/content/full/315/5816/1224/DC1

PHYSICS

Negative Refraction for Electrons?

The peculiar properties of graphene, which is neither semiconductor nor metal, may allow its electrons to be focused like light.

J. B. Pendry

Chance or cleverness sometimes brings together two exciting research areas that otherwise would proceed along separate paths. In the world of optics, for example, researchers have been studying negative refraction, a phenomenon that allows "perfect" optical lenses (*1*, *2*) that can focus light beams to extremely fine points. Condensed matter physicists, on the other hand, are unraveling the unusual properties of graphene, a material that consists of single sheets of carbon atoms (*3*). Now, a report by Cheianov *et al.* on page 1252 of this issue (*4*) combines these two areas in a potentially fruitful way. On the basis of theoretical results, the authors claim that the electron equivalent of negative refraction can be achieved in a monolayer of graphite (graphene) and exploited to focus electrons with high precision.

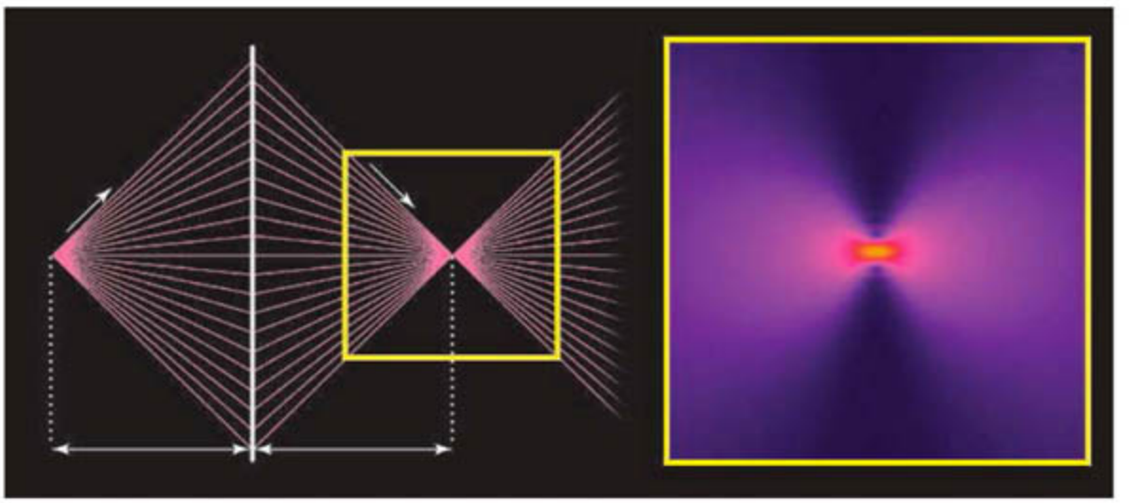

Focusing electrons. (**Left**) Veselago's lens: A negative refractive index medium ($n = -1$) bends light to a negative angle relative to the surface normal. Light formerly diverging from a point source in the object plane is set in reverse and converges back to a point. (**Right**) Computer simulation of electron charge density on graphene showing similar focusing. [Adapted from (*4*)]

In graphite, carbon atoms are arranged as sheets comprising planar hexagons, each atom connected by three bonds to its neighbors. The bonding between the sheets is relatively weak, however, so that graphite is easily sheared, which is what makes it a good lubricant. Recently, it has been reported that individual sheets of graphene can be isolated (*3*) and sophisticated experiments can be performed on them.

Graphene is an ideal two-dimensional system, and interest in it is compounded by the unusual nature of its electronic spectrum. The basic concept that physicists use to understand such electron behavior in solids is called the Fermi surface. This is a boundary that separates the unfilled orbitals from the occupied ones and has a structure that depends on the symmetry of the atomic lattice. Metals are conductive because the Fermi surface intersects a set of electronic energy bands (the continuous ranges of allowed energy created when many atoms having discrete energy levels are joined together). That is, the electrons can flow easily among the orbitals. In semiconductors, two energy bands interact with one another and split apart generating an energy gap. The Fermi level lies in this gap, making them insulators, unless the semiconductor is doped or heated so as to fill the conduction band with a few electrons.

However, graphene is neither metal nor semiconductor. A semiconductor can be doped with impurity atoms, creating two different types of materials, *p*-type or *n*-type, essentially forming the basis for all semiconductor technology. But the peculiar hexagonal symmetry of graphene, in which the unit cell contains two equivalent carbon atoms, means that symmetry forbids the interaction and bands cross at the Fermi energy without creating a gap. An infinitesimal perturbation will move the Fermi energy into either the upper or the lower band, making the system either a *p*-type conductor if the Fermi energy is lowered into the valence band or an *n*-type conductor if it is raised into the conduction band. In fact, the Fermi energy can be moved simply by applying a gate voltage to the graphene layer.

Symmetry has another consequence in the graphene system. If we launch a pulse of electrons into a conventional material such as copper, the maxima and minima of individual wavelets making up the pulse move in the same direction as the pulse. Technically speaking, the group velocity and the wave velocity have the same sign. This statement is also true if we launch electrons into the conduction band of graphene. However, although the valence band is closely related to the conduction band by symmetry, there is a twist: States in the valence band have a group velocity antiparallel to the wave vector. This provides the link with the optical effect of negative refraction, which requires group and waves velocities to be oppositely directed.

In 1968 (*1*), Veselago investigated the properties of a medium that showed negative refraction of light. Under conditions in which both the magnetic (μ) and electric (ε) responses are negative, he showed that the group and phase velocities point in opposite directions, just as is the case for the valence electrons in the new material. He went on to show that a negative angle of refraction gives rise to focusing of light by a simple slab of the material. The Veselago lens was later shown to have the extraordinary property that the perfection of its focus is limited not by the wavelength, as in a conventional lens, but by the degree of perfection in its manufacture (*2*). The lens is sometimes referred to as a "perfect lens." Several experiments have now demonstrated that the lens is capable of subwavelength resolution (*5*, *6*).

In their report, Cheianov *et al.* examine a *pn* junction in graphene. These kinds of structures are among the most basic electronic devices and are usually made with semiconductor materials. Such a junction could be made by two almost-touching metal plates above a graphene sheet, one biasing the sam-

The author is at the Blackett Laboratory, Imperial College London, London SW7 2AZ, UK. E-mail: j.pendry@imperial.ac.uk

ple to a positive voltage (*n*-type), the other to a negative voltage (*p*-type). A point source of electron current in the *n*-type half (see the figure) radiates electrons to the interface, where they are negatively refracted into the *p*-type medium and brought to a focus, just as light is focused in Veselago's lens.

The analogy with Veselago's lens is not complete: His lens matched both the refractive index and the impedance of the two media, and as a result the interface between them was perfectly transmitting. This perfect transmission also led to the property of a perfect focus. The *pn* interface in the new graphene lens is perfectly transmitting only when electrons strike the surface exactly at a perpendicular angle, but otherwise not so. As a result, the graphene lens does not show subwavelength resolution. In fact, it is a requirement that the *pn* junction be as sharp as possible because the resolution of the lens is related to the diffuseness of this interface. However, because electron wavelengths are generally very small, subwavelength resolution is less of an issue than it is for photons.

This remarkable theoretical result now stands as a challenge to experimentalists. We know that graphene can be prepared in a rather perfect form, but can a sharp, straight *pn* junction be prepared and its imaging demonstrated?

References

1. V. G. Veselago, *Sov. Phys. Usp.* **10**, 509 (1968).
2. J. B. Pendry, *Phys. Rev. Lett.* **85**, 3966 (2000).
3. K. Novoselov *et al.*, *Science* **306**, 666 (2004).
4. V. V. Cheianov *et al.*, *Science* **315**, 1252 (2007).
5. A. Grbic, G. V. Eleftheriades, *Appl. Phys. Lett.* **82**, 1815 (2003).
6. N. Fang *et al.*, *Science* **308**, 534 (2005).

10.1126/science.1140178

EPIDEMIOLOGY

Keep It Local

Studies of virus evolution within caterpillars and bacteria show that greater host mobility is associated with the emergence of more infective parasites.

Angus Buckling

Why are some parasites more infectious than others? This much debated question has spawned several theories about parasite transmission and virulence. A study by Boots and Mealor on page 1284 in this issue (*1*) indicates that the social network of host organisms is a key determinant of how parasite infectivity evolves. This implies that as the world become more connected and human populations more mixed, more dangerous parasites could be selected for.

The study was motivated by theoretical work predicting that parasite infectivity should decrease when host (and parasite) movement is restricted. Under these conditions, the theory predicts that infected hosts soon become surrounded by other infected hosts, described as "self-shading" (*2*). Once this happens, infected hosts rarely encounter susceptible hosts, so the average rate at which current infections lead to new infections (transmission) dramatically decreases. A mutant parasite that is intrinsically less infectious is predicted to cause less self-shading, thereby increasing the average contact rate between infected and susceptible hosts. The mutant parasite would therefore spread throughout the whole host population more efficiently than a highly infectious parasite, despite having reduced short-term and localized transmission. This contrasts with conditions in which host and parasites can freely mingle. In this case, the theory predicts that parasites are much less likely to be surrounded by hosts that they have already infected, and the most infectious parasites will spread more rapidly both locally and throughout the whole host population.

Boots and Mealor put this theory to the test by studying the real-time evolution of a parasitic virus that infects, primarily through cannibalism, caterpillars (see the figure). The authors manipulated the social network of the caterpillars by allowing them to live in their own food (a wholesome blend of organic cereal, yeast, glycerol, and honey). The unadulterated food had a thin consistency, allowing caterpillars to interact with each other throughout the food box. By adding water to the food, a thicker texture was created that greatly limited caterpillar movement, resulting in caterpillar clusters. Both uninfected and parasite-infected caterpillars were added to the different food boxes. After 40 weeks, the authors extracted virus from the current crop of caterpillars and measured infectivity by treating uninfected caterpillars with the harvested pathogen. The results are entirely consistent with theory: Virus in the denser food that restricted caterpillar movement evolved to be approximately one-third as infectious as viruses harvested from caterpillars in the less viscous food source.

Despite the quirkiness of the experimental system, these results are likely to have very broad applicability. The behavior of less infectious viruses in the more viscous food source can be viewed as "prudence." That is, viruses are trading off short-term competitiveness with the long-term productivity (*3*). Such a strategy works when movement is limited because prudent viruses reap their own reward by creating an environment with more available hosts. If movement is unrestricted, everyone will gain equally from the behavior of prudent individuals, in which case prudence versus imprudence carries a short-term cost, but no long-term benefit.

The importance of restricted movement for the evolution of prudent parasites was recaptured in another recent

Prudent parasites. By studying a virus that infects the larva of the moth *Plodia interpunctella*, Boots and Mealor (*1*) determine that parasites evolve to more infectious forms when their hosts are more mobile and disperse within a population. Less infectious, more "prudent" parasites result when potential host movement is restricted within a population.

The author is in the Department of Zoology, University of Oxford, Oxford OX1 3PS, UK. E-mail: angus.buckling@zoology.oxford.ac.uk

experimental evolution study of viral parasites (bacteriophage) of bacteria (*4*). Bacteriophage invade bacteria after a random encounter, reproduce inside the host, and then burst out, killing the bacteria in the process. The experimental design for this study involved nearly 200 individual media-filled "wells," some of which were inoculated with either bacteria or bacteriophage. Dispersal was manipulated by moving samples of bacteria and phage between different wells. Where dispersal was limited to only neighboring wells, clusters of wells containing only phage formed. This reflects "self-shading" by the phage, because they quickly killed bacteria in a well. As expected, this favored the evolution of prudent phage, which in turn reduced the rate of phage reproduction. Because this allowed more growth of the bacterial "resource," there was an increase in total bacteriophage yield from a well. This in turn increased the probability of bacteriophage infecting new bacterial wells. In contrast, when the bacteriophage and bacteria could disperse to any well, the authors argue that there was a much higher chance of encountering a bacterial well, so prudence was less beneficial.

Prudence, when considered a form of cooperation, is open to cheating. Regardless of the long-term benefits to the group of prudent behavior, a faster exploiting "cheat"—an individual that reproduces more rapidly in the short term—that invades a patch of prudent individuals is likely to have an advantage. What prevents such cheats from joining patches of prudent individuals in the limited-dispersal conditions in the above examples? On the one hand, it could be chance; some pathogen populations simply don't contain cheats. However, limited dispersal also means that viruses within a localized patch are more likely to share the same immediate ancestors than would viruses between patches. The benefits of prudent behavior are therefore most directed toward close kin, which themselves are likely to be cooperators, causing genes for cooperation to spread throughout a population (*5*, *6*). This process of kin selection (*7*) is likely to be an important determinant of many cooperative traits.

However, when there is greater dispersal, there will be much more interaction between individuals of different immediate ancestry, and hence between cheats and cooperators. Of course, it is impossible to know the importance of kin selection in explaining the results of Boots and Mealor because dispersal and the likelihood of viruses interacting with their closest relatives are necessarily correlated. Independent manipulation of these two variables would provide fascinating insights into the mechanisms responsible for the evolution of parasite infectivity.

Regardless of the precise details of the theoretical explanation, there is now, for the first time, some very convincing experimental data that parasites are likely to evolve to be less prudent when they get to travel. Less prudent can mean various things: more infectious, more disease-causing, and more likely to kill. None of which is likely to be very good for hosts.

References

1. M. Boots, M. Mealor, *Science* **315**, 1284 (2007).
2. M. Boots, A. Sasaki, *Proc. R. Soc. B* **266**, 1933 (1999).
3. M. Keeling, *Proc. R. Soc. B* **267**, 385 (2000).
4. B. Kerr, C. Neuhauser, B. J. M. Bohannan, A. M. Dean, *Nature* **442**, 75 (2006).
5. W. D. Hamilton, *Am. Nat.* **97**, 354 (1963).
6. W. D. Hamilton, *J. Theor. Biol.* **7**, 1 (1964).
7. J. Maynard-Smith, *Nature* **201**, 1145 (1964).

10.1126/science.1139839

CHEMISTRY

Water from First Principles

It has been hard to reproduce some of the properties of water starting only with the basic laws of physics. A description of water derived entirely from theory now succeeds in this task.

Anthony J. Stone

The water molecule is very simple, yet water in its various forms is one of the most complicated substances. Its anomalous behavior, such as its expansion on freezing and other more subtle properties, is related to the detailed form of the interaction between its molecules, which is still imperfectly understood. For more than 70 years, scientists have been trying to understand the behavior of water in its different forms from first principles—that is, based on the fundamental properties of the water molecule. Much progress has been made in this task in recent years, and the report by Bukowski *et al.* on page 1249 of this issue (*1*) marks an important step.

For some substances, the properties of the bulk solid, liquid, or gas can be deduced with reasonable accuracy once one knows the pair potential—that is, the function that describes how the energy of a pair of molecules depends on their relative geometry. For molecules like water, this function depends on six coordinates: the position (three coordinates) and orientation (three more) of either molecule relative to the other. The energy of an assembly of molecules is then taken to be a sum of all pair interactions in the assembly.

For water, and for many other substances, however, the pair potential is not enough. The energy of an assembly of water molecules cannot be described adequately as a sum of pair potentials. The interaction between any two molecules leads to a distortion of both molecules, which in turn modifies their interactions with a third molecule (see the figure). A three-body function is needed to take such effects into account. The three-body correction is a function of 12 coordinates: the position and orientation of two molecules relative to the third. Even this is not enough: In principle, there are four-body and five-body corrections, and so on. These are smaller, but are thought to be important for the tetrahedral structure of liquid water (*2*). Most of these many-body corrections can be accounted for by a careful description of the polarization of each molecule by its neighbors (*3*). There are other many-body effects that are not included in this way—for example, the three-body correction to the van der Waals attraction (*4*)—but they are smaller and can often be ignored.

For simulations of liquid water and of biological systems in the presence of water, very simple descriptions are needed because of computational constraints. They usually approximate the many-body effects by modifying the pair potential, typically by enhancing the molecular dipole moment. These models are quite successful in modeling liquid water at ambient temperature and pressure, but give a very poor account of the water dimer, because the modified pair potential is incorrect.

In recent years, several research groups have tried to obtain a description of water that gives a good account of the water dimer, small clusters of water molecules, and the bulk liquid (*5*–*7*). Such a comprehensive task requires a much more elaborate potential. Traditionally, the intermolecular potential has been determined from experimental data, but experimen-

The author is with the University Chemical Laboratory, Lensfield Road, Cambridge CB2 1EW, UK. E-mail: ajs1@cam.ac.uk

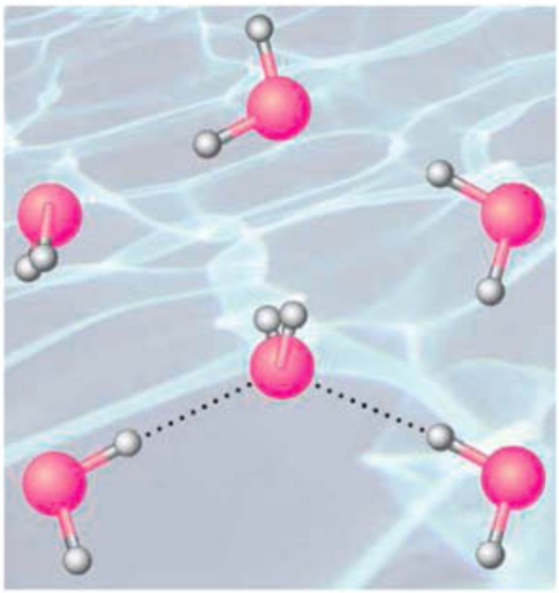

Three-body effects. The two hydrogen bonds may act cooperatively, each reinforcing the other (**top**), or they may oppose each other (**bottom**). The top configuration is bound more strongly than the bottom one. Three-body effects of this kind play an important role in water clusters and liquid water. Bukowski *et al.* (*1*) describe a potential derived entirely from first principles that captures these and other properties of water.

tal properties are averages over the potential surface, and it is difficult or impossible to extract the details of the potential surface unambiguously from such properties. Alternatively, the intermolecular potential can be calculated from first principles. The most accurate method in current use is coupled-cluster theory with inclusion of single, double, and triple excitations, the triples noniteratively. Unfortunately, this CCSD(T) method gives only the total pair potential energy, and only at isolated points. It provides no information about the functional form of the pair potential, which is needed for most applications.

Perturbation theory, on the other hand, does give information about the functional form, but is very complex and computationally demanding, and cannot yet achieve the same accuracy. Recent practice has been to refine the details of the potential by fitting to experimental data.

Fitting is a well-established technique in many fields of science, but it has pitfalls: It may improve some properties at the expense of others. For example, in the case of the simple potentials mentioned above, enhancement of the molecular dipole moment improves the calculated properties of the liquid but ruins the description of the dimer. In that case, however, the form of the potential is known to be inadequate. Careful use of perturbation theory can give the right functional form, and the numerical parameters can be refined by fitting to the very accurate experimental data that have been obtained from high-resolution spectroscopy on the dimer and small clusters. This approach can lead to potentials that give a good account of both small clusters and the bulk liquid (*7*).

Nevertheless, the challenge to obtain a good intermolecular potential energy function entirely by calculation from first principles, using experimental data only as a test of its quality, has not been met. This is what Bukowski *et al.* have been able to do. They have used perturbation theory to determine the form of the potential function, and fitted the parameters in it using data points for the water dimer calculated by the CCSD(T) method.

An advantage of this approach is that the CCSD(T) data points cover the energy surface much more completely than the spectroscopic data, which describe only the region in the neighborhood of the energy minimum and the barriers to neighboring minima. The CCSD(T) calculations were carried out only for the dimer, but with a good functional form the resulting potential is able to give a good account of the many-body interactions and hence of the liquid properties as well as the dimer spectrum.

This work is not the end of the story. The calculated properties are good, but leave room for improvement. The form of the potential function omits some of the smaller terms. Ideally, one would wish to obtain accurate numbers as well as the functional form from perturbation theory. Nevertheless, Bukowski *et al.* have been able to show that a good description of water from first principles is becoming feasible.

References

1. R. Bukowski, K. Szalewicz, G. C. Groenenboom, A. van der Avoird, *Science* **315**, 1249 (2007).
2. R. Bukowski, K. Szalewicz, G. C. Groenenboom, A. van der Avoird. *J. Chem. Phys.* **125**, 044301 (2006).
3. M. P. Hodges, A. J. Stone, S. S. Xantheas. *J. Phys. Chem. A* **101**, 9163 (1997).
4. P. M. Axilrod, E. Teller, *J. Chem. Phys.* **11**, 299 (1943).
5. C. Millot, A. J. Stone. *Mol. Phys.* **77**, 439 (1992).
6. E. M. Mas *et al.*, *J. Chem. Phys.* **113**, 6687 (2000).
7. N. Goldman, C. Leforestier, R. J. Saykally. *Philos. Trans. R. Soc. A* **363**, 493 (2005).

10.1126/science.1140758

BIOCHEMISTRY

A Missing Link in Membrane Protein Evolution

Bert Poolman, Eric R. Geertsma, Dirk-Jan Slotboom

Discerning the orientation of subunits of an unusual bacterial membrane protein suggests how the particular topology of other membrane proteins may have evolved.

Most proteins embedded in biological membranes have vectorial functions, such as transporting molecules into or out of cells or transducing signals. It is thus essential that these membrane proteins have unique orientations in the lipid bilayer. To achieve a unique orientation, membrane proteins carry signals in their amino acid sequences that are recognized during the membrane insertion process. Intriguingly, some membrane proteins have structurally similar, homologous regions with opposite orientations in the membrane, raising questions about their evolution. On page 1282 of this issue, Rapp *et al.* (*1*) offer a compelling explanation for how such proteins may have evolved.

One of the best-understood signals for membrane protein topology is the "positive-inside rule": Positively charged residues such as lysine (K) and arginine (R) tend to be most abundant ("K+R bias") in loops located at the cytoplasmic side of plasma and endoplasmic reticulum membranes (*2*). Crystallography has shown that many membrane proteins contain homologous domains with opposite (antiparallel) membrane orientation, leading to proteins with a quasi–two-fold axis in the plane of the membrane. Well-known examples are the members of the aquaporin family, in which the first three transmembrane segments are homologous to the last three but with opposite membrane orientation. Exactly how such quasi-symmetrical proteins have come about has been puzzling. Rapp *et al.*

The authors are in the Department of Biochemistry, Groningen Biomolecular Sciences and Biotechnology Institute, and Zernike Institute for Advanced Materials, University of Groningen, Nijenborgh 4, 9747 AG Groningen, Netherlands. E-mail: b.poolman@rug.nl

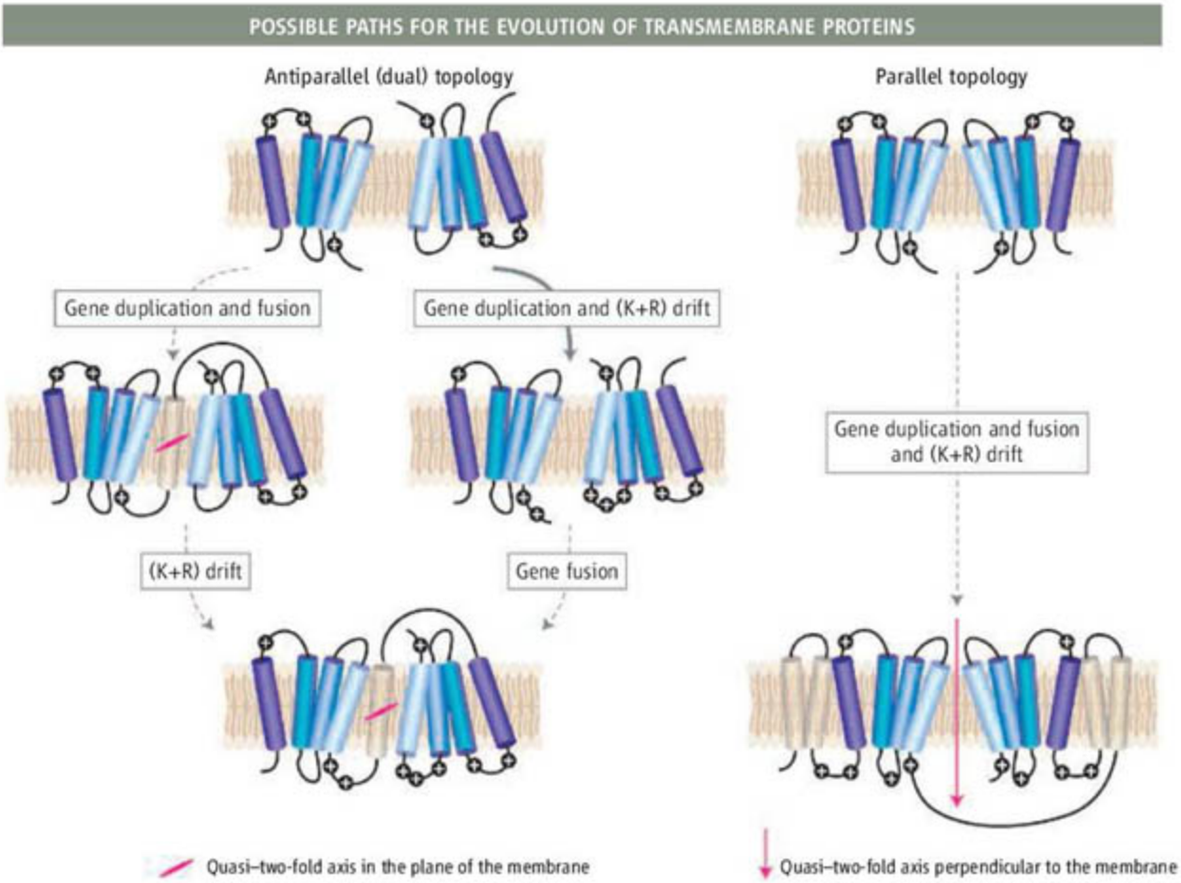

Plausible evolutionary paths. Membrane proteins with multiple homologous domains may have evolved through gene duplication, gene fusion, and drift events [bias to lysine (K) and arginine (R) residues in cytoplasmic regions of the protein]. The resulting proteins have similar domains with either antiparallel topologies (**bottom left**), or parallel topology (**bottom right**). Shaded cylinders depict additionally inserted transmembrane segments. Bold arrow indicates the evolutionary path simulated by Rapp *et al.* (*1*); dashed arrows indicate hypothetical events.

reinforce their earlier proposal that rare "dual-topology" proteins form a missing link in the evolution of membrane proteins with antiparallel domains. They trace the evolutionary path by examining the multidrug transporter EmrE from *Escherichia coli* and demonstrate that antiparallel dual topology of the transporter's subunits is required for its functioning.

EmrE is a well-characterized protein with four transmembrane segments. Its functional unit is a homodimer, but the membrane orientation of the two subunits of EmrE is a matter of fierce debate. The protein does not have strong topological signals (weak K+R bias), and evidence has been presented for both an antiparallel (dual topology) and parallel orientation of the subunits (see the figure) (*3*–*7*). The possibility of oppositely oriented subunits in EmrE was first proposed by Tate and colleagues (*7*) on the basis of a cryo–electron microscopy analysis of two-dimensional (2D) crystals. A model consistent with most of the available biochemical and biophysical data was proposed in which EmrE could be arranged as an antiparallel homodimer (*8*). On the other hand, a rigorous cross-linking study pointed toward a parallel orientation of the EmrE subunits (*5*). Regrettably, some of the assumptions in the latter work were based on a structural model that has recently become obsolete (*9*).

Rapp *et al.* now present strong evidence for dual topology of the EmrE subunits as a requirement for its function. They forced the subunits to insert into the membrane in a single orientation [with the carboxyl terminus either inside, EmrE(C_{in}), or outside, EmrE(C_{out})] by manipulating the number of positive charges in the loops connecting the transmembrane segments, resulting in a stronger K+R bias. EmrE(C_{in}) and EmrE(C_{out}) were inactive when expressed independently in bacteria. However, expression of both subunits simultaneously restored drug resistance to the level observed with the wild-type EmrE, which is indicative of a functional transporter. Thus, oppositely oriented subunits of EmrE are required for its drug efflux activity.

This work explains the occurrence of antiparallel domains observed in the 3D structures of many membrane proteins by providing a plausible path for the evolution of such transmembrane proteins: After gene duplication, a dual-topology protein could evolve via genetic drift toward a K+R bias, whereby the subunits obtain a fixed orientation (see the figure). A subsequent gene fusion event would allow a single polypeptide to accommodate all functionalities. For proteins with an even number of transmembrane segments, this requires the insertion or deletion of a transmembrane segment. In principle, the order of these events could be reversed. Either pathway leads to a membrane protein with a quasi–two-fold axis in the plane of the membrane (see the figure).

For comparison, a protein with a quasi–two-fold axis perpendicular to the membrane plane could evolve from the fusion of proteins with a parallel topology (see the figure). Prototypic of this class are the members of the major facilitator superfamily. The currently available 3D structures of channels and transporters indicate that proteins with quasi-symmetry, resulting from the duplication and fusion of ancestral proteins with either parallel or anti-parallel topologies, are the rule rather than the exception.

In a proteome-wide screen of the topology of transmembrane proteins in *E. coli*, von Heijne and colleagues previously showed that the vast majority of the proteins exhibit a unique topology (*10*). Obviously, for many membrane proteins, a unique orientation is required. For instance, domains that bind to ligands, possess certain enzymatic activities, or are chemically modified (such as by phosphorylation) need to be located on the physiologically relevant side of the membrane. However, the EmrE case shows that in principle, transporters could have dual topology.

So why are dual-topology proteins so rare? EmrE is a dimeric protein, and ideally, the subunits for such a dual-topology dimer should insert exactly 50% EmrE(C_{in}) and 50% EmrE(C_{out}). A large excess of either orientation would be a waste of cellular resources and might exert a detrimental effect if "unpaired" subunits are toxic to the cell. The realization of equal amounts of oppositely oriented subunits may well be beyond the control of the membrane insertion machinery and, in

addition, would put strong constraints on the evolution of such proteins. Any mutation that would alter the optimal insertion ratio would be a selective disadvantage, even though it could improve the catalytic activity. The dual-topology organization of EmrE likely represents an evolutionary transitional form. The work by Rapp *et al.* tips the balance in the controversy about one protein's unusual orientation in the membrane. A broader consequence of this observation may be a plausible evolutionary path for membrane proteins with antiparallel domains.

References

1. M. Rapp, S. Seppälä, E. Granseth, G. von Heijne, *Science* **315**, 1282 (2007); published online 25 January 2007 (10.1126/science.1135406).
2. G. von Heijne, *EMBO J.* **5**, 3021 (1986).
3. D. O. Daley *et al.*, *Science* **308**, 1321 (2005).
4. S. Ninio, Y. Elbaz, S. Schuldiner, *FEBS Lett.* **562**, 193 (2004).
5. M. Soskine *et al.*, *J. Biol. Chem.* **281**, 36205 (2006).
6. A. Rath, R. A. Melnyk, C. M. Deber, *J. Biol. Chem.* **281**, 15546 (2006).
7. I. Ubarretxena-Belandia *et al.*, *EMBO J.* **22**, 6175 (2003).
8. S. J. Fleishman *et al.*, *J. Mol. Biol.* **364**, 54 (2006).
9. G. Chang *et al.*, *Science* **314**, 1875 (2006).
10. M. Rapp *et al.*, *Nat. Struct. Mol. Biol.* **13**, 112 (2006).

11. We acknowledge the EU E-Mep program for funding.

10.1126/science.1140073

ECOLOGY

How the Wood Moves

Recent studies show that the movement of plant genes across the landscape involves a complex web of pollinators and fruit-eating animals.

Katriona Shea

At first glance, an obvious difference between animals and plants is movement: Elephants move, trees don't. This is in part why Tolkien's ents (*1*), Wyndham's triffids (*2*), and the march of Birnam Wood in Shakespeare's *Macbeth* (*3*) elicit such a strong response. But in fact plants do move, although only at certain life stages and usually with outside help. For example, dandelion seeds blow and sycamore samaras helicopter in the wind, acorns and berries are moved by mammals and birds, and pollen is spread by wind and insects. These movements spread plant genes across the landscape, generating the spatial patterns of distribution and abundance of species that we observe in nature. Recent work demonstrates just how complex the web of pollinators and fruit-eating animals that determine tree gene flow can be (see the figure).

The author is in the Department of Biology and the Intercollege Graduate Degree Program in Ecology, Pennsylvania State University, 208 Mueller Laboratory, University Park, PA 16802, USA. E-mail: k-shea@psu.edu

For both plants and animals, studying movement is just as difficult as it seems. Animal ecologists have radio-collared cheetahs and lions, attached satellite-linked tracking devices to seals, and painted marks on beetles to track their movements. Plant ecologists, however, are usually faced with a problem of scale. How can we follow the movement of smaller diaspores (dispersal units), such as seeds and pollen grains? Approaches broadly fall into two categories—tracking of diaspores from a source, or relocation of diaspores at different distances from parent plants (*4*)—and scientists have become very creative in their quest (*5*). Notable approaches include observational studies of dispersers at the parent plant for animal-dispersed species; studies of the environmental conditions promoting seed release of wind-dispersed species; trapping of seeds at different distances from possible parents; marking of seeds on the parent plant with ink, fluorescent powder, or radioactive markers to allow later relocation and identification of seeds; genetic methods to link seeds or pollen to possible parents; and even chasing individual seeds as they blow across the landscape.

Over the past decade, Jordano and collaborators have been patiently disentangling the gene flow story for a key tree species in southeastern Spain by combining several of these methods (*6*). Mahaleb cherry, *Prunus mahaleb*, is a tree with delicate white flowers and black fruits. Some trees are hermaphrodites (with both male and female functions); others are functionally female. Thus, both types of trees are potential seed sources, but only the hermaphrodites can provide pollen. Jordano *et al.* have studied nine distinct populations of these trees and determined the genotypes of all reproductive individuals. Their observational studies show that mahaleb cherry fruits (each contain-

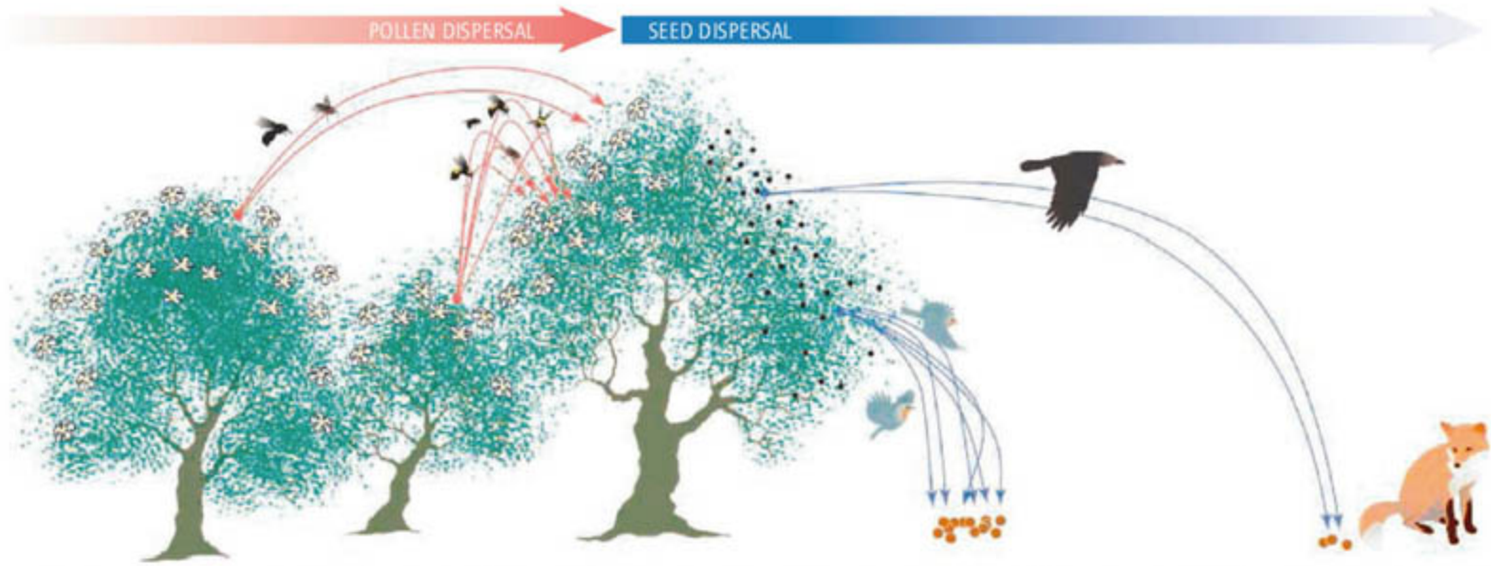

Gene flow in trees. Mahaleb cherry pollen and seeds are moved over short and long distances by strikingly different assemblages of pollinators and fruit-eating animals. This has important implications for gene flow within and between populations and for the establishment of new populations.

ing a single seed) are consumed by a wide variety of animals. Most seeds are eaten by frugivorous (fruit-eating) birds such as warblers, robins, redstarts, mistle thrushes, woodpigeons, and carrion crows. However, a small proportion of fruits are also eaten by otherwise carnivorous mammals such as badgers, stone martens, and red foxes. Pollen is dispersed by a wide range of bees and flies.

A seed contains a mix of genes from both its mother and father and, as potential parents in a population may themselves be related, it can be hard to work out parentage with any degree of certainty, even with the latest molecular genetic methods. Jordano *et al.* exploited a key factor to get around this problem. In some species, maternal tissue is attached to the seed. For example, the samara or "propeller" of a sycamore is actually made up of maternal tissue. Similarly, mahaleb cherry seeds have a maternally derived seed coat, the endocarp, which is not digested with the rest of the fruit. Analysis of the seed coat by molecular genetic techniques allows direct identification of the mother tree.

Jordano *et al.* trapped or collected seeds from animal feces across the landscape. From this they recorded which dispersal agents excreted each seed, directly identified the mother tree, and hence determined the distance the seed was dispersed. By combining these complementary methods, this work has been able to document what moves seeds, how far they are moved, and even into what sorts of habitats they are deposited by different dispersers (*6*). Similarly, they have studied the pollinators and the pollen they deposit on the two sexes of tree (*7*). Eventually, they will be able to link the two components directly, by genotyping both seeds and their endocarps. This unusually thorough understanding of seed and pollen movement is a real breakthrough for the study of gene flow in trees.

As expected, birds remove most mahaleb cherry fruits, whereas mammals take relatively few. However, smaller birds move seeds only relatively short distances (usually depositing them within the boundaries of the local population); larger birds and mammals are overwhelmingly responsible for longer-distance dispersal, particularly movement between populations (*6*). Additionally, larger birds and mammals are more likely to disperse seeds to open habitat, where new populations may establish. Pollinators prefer female trees, and different assemblages of pollinators visit the two sexes. As a result, pollen on female trees on average comes from farther away and from more pollen donors (*7*). Intriguingly, there is much less long-distance pollen movement than long-distance seed dispersal.

The implications for this species are noteworthy. Although smaller birds dominate the dispersal system numerically, loss or extinction of carnivorous mammals in this system would have serious consequences for gene flow (with a large reduction in interpopulation movement) and would likely lead to increased isolation of populations (with fewer new populations being initiated). The ramifications for other ecosystems are also considerable. It is not only the obvious or putative dispersal mechanisms that are important (*4*), and the composite patterns arising from these multiple dispersal vectors may be very complex indeed (*8*). Relatively rare events may dominate certain critical processes such as establishment of new populations, range expansions, or invasions. Particularly large effects may be seen in tropical rainforests, where rapid fragmentation dramatically influences loss of large frugivores. Jordano *et al.* show the way forward: Only with a multipronged and synthetic approach can we hope to disentangle the multiple drivers of observed plant genetic diversity or to identify possible consequences of changes in animal communities or habitats on plant populations.

References and Notes

1. J. R. R. Tolkien, *The Lord of the Rings: The Two Towers* (George Allen & Unwin, London, 1954).
2. J. Wyndham, *The Day of the Triffids* (Michael Joseph, London, 1951).
3. W. Shakespeare, *Macbeth* (Blackie, Glasgow, 1969).
4. J. M. Bullock, K. Shea, O. Skarpaas, *Plant Ecol.* **186**, 217 (2006).
5. A. Sugden, E. Pennisi, Eds., special section on Migration and Dispersal, *Science* **313**, 775 (2006).
6. P. Jordano, C. García, J. A. Godoy, J. L. García-Castaño, *Proc. Natl. Acad. Sci. U.S.A.* **104**, 3278 (2007).
7. C. García, J. M. Arroyo, J. A. Godoy, P. Jordano, *Mol. Ecol.* **14**, 1821 (2005).
8. R. Nathan, *Science* **313**, 786 (2006).
9. I thank O. Bjørnstad, E. Jongejans, and S. Yang for comments. Supported by NSF grants DEB-0315860 and DEB-0614065 and USDA grant USDA-CSREES NRI 2002-35320-12289.

10.1126/science.1136096

ATMOSPHERE

Forecasting Hurricane Intensity and Impacts

Hurricane structure and intensity can now be predicted with sufficient accuracy to support quantitative assessment of human and economic impacts.

Hugh E. Willoughby

In 2005, meteorologists embarked on an ambitious hurricane research project, RAINEX, to investigate how rainbands affect hurricane intensity. Flying radar-equipped aircraft right into the storms—including the infamous Hurricane Katrina—before they made landfall, the scientists recorded wind speed and direction, temperature, humidity, and other data. On page 1235 of this issue, Houze *et al.* report exciting results from this project (*1*). The authors observed Hurricanes Katrina, Ophelia, and Rita and then simulated them numerically on spatial scales of less than 2 km. These highly realistic simulations represent substantial progress on the vexing problem of hurricane intensity prediction.

In the United States, 2004 and 2005 were the most devastating seasons as measured by inflation-adjusted damage, and 2005 was the deadliest since 1928. Forecasts of U.S. hurricane landfalls made as long as 60 hours before the event were excellent, but Earth's atmosphere is still fiendishly unpredictable. It was a meteorologist who instigated the modern appreciation of sensitivity to initial conditions in deterministic mathematical systems (*2*). Thus, both uncertainties in the initial state of the atmosphere and limitations of the numerical models can cause forecasts that started from nearly identical representations of today's weather to diverge after just 3 to 10 days. Hurricane prediction remains an unforgiving enterprise with constant threat of public and costly failure.

There are two crucial aspects to hurricane prediction: forecasting the path it will take (the hurricane track) and forecasting the strongest wind anywhere in the storm (the hurricane intensity). Track forecasts have

The author is in the Department of Earth Sciences, Florida International University, Miami, FL 33199, USA. E-mail: hugh.willoughby@fiu.edu

improved steadily over the years, but intensity predictions have lagged a generation behind track forecasts.

Track forecasts are important, because storm surge—flooding by wind-driven water from the sea or lakes—usually causes most hurricane deaths; this was the case also for Hurricane Katrina. Timely evacuation from the surge zone based on track forecasts therefore has the potential to save many lives. Hurricane tracks depend mainly on the steering flow, that is, the prevailing wind around the storm.

Numerical weather prediction models form the basis of modern forecasting. They tabulate meteorological variables on rectangular grids and use the dynamical equations of motion to advance them forward in time. The steering flow has characteristic spatial dimensions of more than 1000 km and takes over 24 hours to change appreciably. Progress in numerical weather prediction and remote sensing has focused on these scales, facilitating advances in track forecasting.

In contrast, to simulate hurricane intensity changes, numerical models need finer grid resolution to represent the small-scale, rapidly evolving organization of convection in the hurricane core. For this reason, improvements of intensity forecasts have been slower. Numerical hurricane simulations (*3*) of individual hurricanes with resolutions of over 5 km predict cyclones that are geometrically larger, weaker cartoons of their counterparts in nature. Intensification and weakening also depend on ocean temperature beneath the storm (*4*), interactions with vertical shear of the steering flow (*5*), and rainbands, eye structure, and other manifestations of the internal dynamics of the storm.

Eyewall replacements, in which a ring of new thunderstorms forms around a preexisting eye, are probably the most difficult phenomena to model. The outer eyewall supplants the inner by intercepting the energy-laden air as it converges toward the original eyewall in contact with the warm ocean. Collapse of the inner eyewall reduces intensity. Subsequently, the hurricane may reintensify if conditions remain favorable.

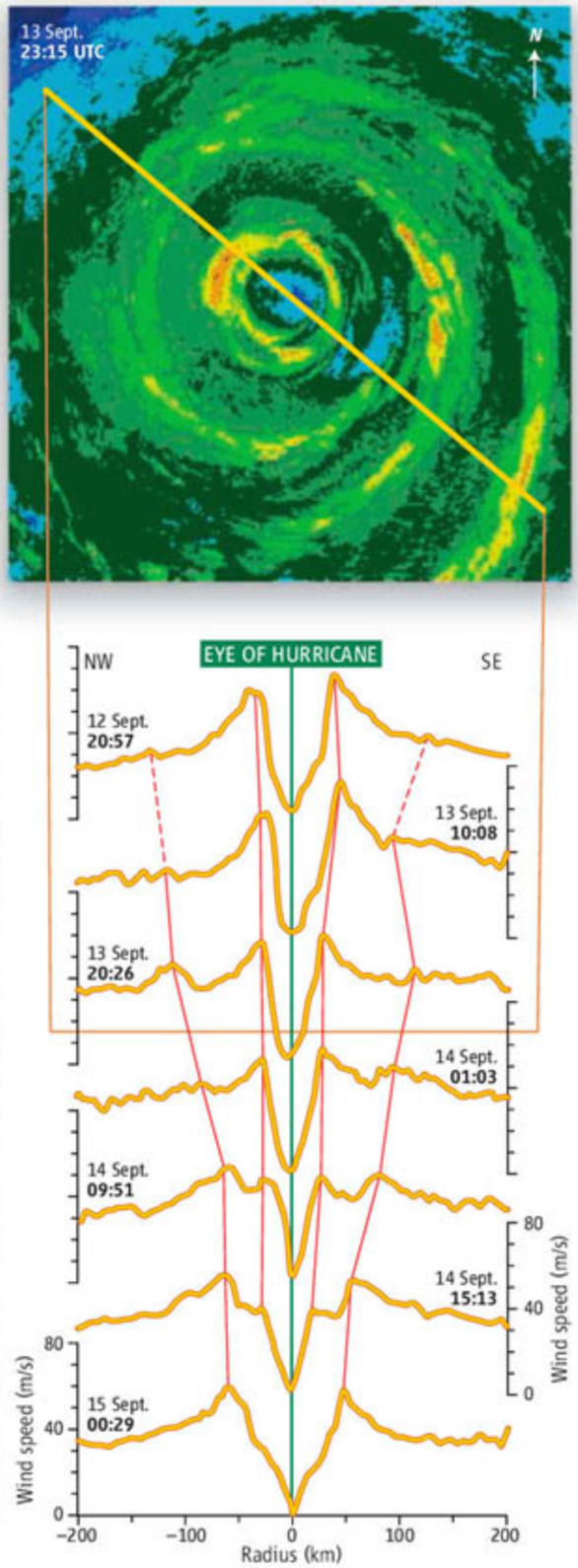

CREDIT: NOAA HURRICANE RESEARCH DIVISION

Hurricane eyewall replacement. (**Top**) This radar image of Hurricane Floyd shows the eye surrounded by outer and inner concentric eyewalls. The yellow line indicates the approximate aircraft track for the wind profiles below. Image dimensions, 360 km by 360 km. (**Bottom**) Successive profiles in Floyd (yellow curves) of the wind speed at an altitude of 3 km show how an outer eyewall forms, contracts in the course of 51 hours, and replaces the former inner eyewall. Time increases downward and is indicated as date and time next to the axis for each profile. Red lines connect features across time. Image and data from the National Oceanic and Atmospheric Administration's Hurricane Research Division.

Timing and magnitude of these eyewall replacement cycles are crucial to impacts at landfall. In 1992, Hurricane Andrew completed an eyewall replacement, intensified rapidly as it crossed the Gulf Stream, and ripped into Miami-Dade County (*6*). By contrast, eyewall replacements and a less favorable environment reduced Hurricane Floyd of 1999 (see the figure) from a potentially catastrophic windstorm to a rainstorm that caused widespread flooding in the Carolinas. Modeling weakening during eyewall replacements is challenging, but the crucial forecast problem is rapid intensification or reintensification.

The accurate representation of individual bands of convective rainfall in the 1.67-km-resolution RAINEX simulations (*1*) suggests that hurricane modeling may have advanced to the point that sensitivity to initial conditions rather than model shortcomings is the limiting factor. Sensitivity to initial conditions may be overcome by running ensembles of forecasts starting from slightly different initial conditions (*7*). The ensemble mean outperforms individual members, and the ensemble spread provides a measure of forecast reliability.

Windstorm insurers employ catastrophe models based on Monte Carlo simulations of thousands of climatologically representative hurricanes (*8*). The calculated impact of these virtual hurricanes on the actual distribution of insured properties allows insurance companies to estimate underwriting risk on an annual basis. The very realistic RAINEX simulations suggest extension of this well-established technique to predict human and economic impacts of individual, real hurricanes as they approach the coast and pass onshore.

References and Notes

1. R. A. Houze Jr., S. S. Chen, B. F. Smull, W-C. Lee, M. M. Bell, *Science* **315**, 1235 (2007).
2. E. N. Lorenz, *J. Atmos. Sci.* **20**, 130 (1963).
3. Y. Liu, D-L Zhang, M. K. Yau, *Mon. Weather Rev.* **123**, 3073 (1997).
4. L. K. Shay, G. J. Goni, P. G. Black, *Mon. Weather Rev.* **125**, 1366 (2000).
5. M. L. Black, J. F. Gamache, F. D. Marks Jr., C. E. Samsury, H. E. Willoughby, *Mon. Weather Rev.* **130**, 2291 (2002).
6. H. E. Willoughby, P. G. Black, *Bull. Am. Meteor. Soc.* **77**, 543 (1996).
7. Z. Zhang, T. N. Krishnamurti, *Bull. Am. Meteor. Soc.* **78**, 2785 (1997).
8. P. J. Vickery, P. F. Skerlj, L. A. Twisdale, *J. Struct. Engr.* **126**, 1222 (2000).
9. This work was supported by grant NSF-ATM-0454501.

10.1126/science.1140041

Was There Really an Archean Phosphate Crisis?

Kurt O. Konhauser,[1]* Stefan V. Lalonde,[1] Larry Amskold,[1] Heinrich D. Holland[2]

It has been suggested that sedimenting particles of ferric oxyhydroxide may have stripped dissolved phosphate from the ocean's photic zone during the Archean (*1*), when massive amounts of iron were deposited in the form of banded iron formations (BIF). Hypothesized phosphate concentrations of only 10 to 25% of the present-day values would have led to a reduction in phytoplankton productivity and, therefore, to lower rates of oxygen production and organic carbon burial. This model is predicated on the observation that ferric oxyhydroxide particles, resulting from the oxidation of Fe(II) in some modern submarine hydrothermal systems, sorb phosphate with a distribution coefficient (K_D) value of about 0.06 μM^{-1} (*2*).

However, compared with the modern ocean, the Archean ocean had substantially higher concentrations of dissolved silica, at least as high as at saturation with cristobalite (0.67 mM at 40°C in seawater) and possibly even at saturation with amorphous silica (2.20 mM) (*3*); modern oceans average <0.10 mM (*4*). Silica strongly sorbs to ferric oxyhydroxides, and, at the proposed concentration of phosphate in the Archean ocean [ranging from 0.03 to 0.29 μM (*1*)], silica could effectively compete with phosphate for available sorption sites [on the basis of α-FeOOH adsorption constants (*5*)]. Furthermore, iron-silica coprecipitation diminishes the resulting particle's point of zero net charge (PZNC) (*6*), rendering it less reactive to dissolved anions.

We determined the significance of high silica concentrations on phosphate sorption in two ways: (i) by using preformed ferrihydrite particles to demonstrate the competitive adsorption between silica and phosphate at different pH values and (ii) by oxidizing Fe(II) to precipitate ferrihydrite, in the presence of silica and phosphate, for the determination of K_D values (*7*). In the first instance, maximum phosphate adsorption onto preformed ferrihydrite particles occurs at pH < 7 and in the absence of silica (Fig. 1A); silica outcompetes phosphate as silica concentration increases. Furthermore, ferrihydrite incorporating silica shows a consistent decrease in PZNC (Fig. 1B) and correspondingly adsorbs even less phosphate (stippled lines in Fig. 1A).

Coprecipitation experiments with an initial Fe(II) concentration of 0.2 mM revealed that the presence of silica reduced the phosphate content of the resulting particles (Fig. 1C). In the complete absence of silica, we calculated a K_D value of 0.075 ± 0.003 μM^{-1}, similar to the K_D value used by Bjerrum and Canfield (*1*) for particles formed at modern submarine hydrothermal vents [compare with (*2*)], whereas K_D values decreased to 0.011 ± 0.004 μM^{-1} and 0.002 ± 0.002 μM^{-1} for solutions near cristobalite and amorphous silica saturation, respectively. Additionally, we observed silica to exert an even greater effect at lower dissolved Fe concentrations [0.02 mM Fe (fig. S6)]. Consequently, our calculated K_D values are conservative at 0.2 mM Fe, especially considering that previous estimates of dissolved Fe concentrations for the Archean ocean are around 0.05 mM (*8*). Only at much higher dissolved Fe concentrations (e.g., ~2 mM), such as in some hydrothermal vent fluids, does the effect of silica on phosphate sorption become negligible (fig. S6).

With the use of the P:Fe ratio in BIF as a proxy for dissolved phosphate concentrations in the Archean ocean [as the authors of (*1*) used, with whom we compare our data], we calculated that average dissolved phosphate concentrations would have ranged from 0.14 ± 0.01 μM (no silica) to 5.25 ± 2.63 μM in an amorphous silica-saturated ocean. The latter value is of the same order of magnitude as modern oceans (2.3 μM) (*1*). Importantly, there would have been diagenetic remobilization of phosphate during burial (probably leading to lower P:Fe ratios in BIF). Thus, the actual dissolved phosphate concentrations could have been even higher. If the Archean ocean contained abundant dissolved silica, as is generally believed, sedimenting ferrihydrite particles would not have been a major sink for phosphate. It is unlikely that there was a phosphate crisis, and a related reduction in phytoplankton productivity, caused by BIF deposition in the Archean ocean.

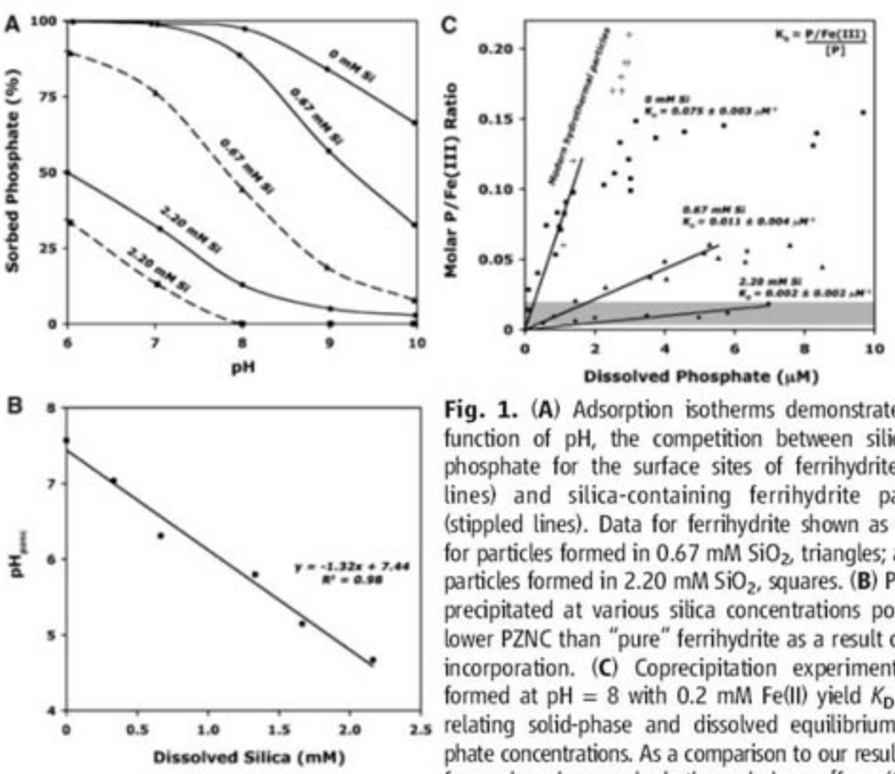

Fig. 1. (**A**) Adsorption isotherms demonstrate, as a function of pH, the competition between silica and phosphate for the surface sites of ferrihydrite (solid lines) and silica-containing ferrihydrite particles (stippled lines). Data for ferrihydrite shown as circles; for particles formed in 0.67 mM SiO_2, triangles; and for particles formed in 2.20 mM SiO_2, squares. (**B**) Particles precipitated at various silica concentrations possess a lower PZNC than "pure" ferrihydrite as a result of silica incorporation. (**C**) Coprecipitation experiments performed at pH = 8 with 0.2 mM Fe(II) yield K_D values relating solid-phase and dissolved equilibrium phosphate concentrations. As a comparison to our results, data for modern deep-sea hydrothermal plumes [from (*2*)], and previously used to estimate Archean ocean phosphate concentrations (*1*), are plotted (plus signs). Also shown are the range of P/Fe(III) values in BIF [gray box; compare with (*1*)]. It is apparent from the coprecipitation data that the particles incorporate decreasing amounts of phosphate with increasing dissolved silica concentrations, and consequently the data suggest higher dissolved phosphate concentrations during BIF deposition.

References and Notes

1. C. J. Bjerrum, D. E. Canfield, *Nature* **417**, 159 (2002).
2. R. A. Feely, J. H. Trefry, G. T. Lebon, C. R. German, *Geophys. Res. Lett.* **25**, 2253 (1998).
3. R. G. Maliva, A. H. Knoll, B. M. Simonson, *Geol. Soc. Am. Bull.* **117**, 835 (2005).
4. P. Tréguer *et al.*, *Science* **268**, 375 (1995).
5. L. Sigg, W. Stumm, *Colloids Surf.* **2**, 101 (1981).
6. U. Schwertmann, H. Fechter, *Clay Miner.* **17**, 471 (1982).
7. Materials and methods are available as supporting material on *Science* Online.
8. H. D. Holland, *The Chemical Evolution of the Atmosphere and Oceans* (Princeton Univ. Press, Princeton, NJ, 1984).

9. We thank A. Kappler, A. Knoll, S. Smith, and three anonymous reviewers for comments on this manuscript. This work was supported by Natural Sciences and Engineering Research Council Discovery grant 249565-02.

Supporting Online Material

www.sciencemag.org/cgi/content/full/315/5816/1234/DC1
Materials and Methods
Figs. S1 to S8
Tables S1 to S7
References

16 October 2006; accepted 19 December 2006
10.1126/science.1136328

[1]Department of Earth and Atmospheric Sciences, University of Alberta, Edmonton, Alberta T6G 2E3, Canada. [2]Department of Earth and Planetary Sciences, Harvard University, Cambridge, MA 02138, USA.

*To whom correspondence should be addressed. E-mail: kurtk@ualberta.ca

Hurricane Intensity and Eyewall Replacement

Robert A. Houze Jr.,[1]* Shuyi S. Chen,[2] Bradley F. Smull,[1] Wen-Chau Lee,[3] Michael M. Bell[3]

Observations made during the historic 2005 hurricane season document a case of "eyewall replacement." Clouds outside the hurricane eyewall coalesce to form a new eyewall at a greater radius from the storm center, and the old eyewall dies. The winds in the new eyewall are initially weaker than those in the original eyewall, but as the new eyewall contracts, the storm reintensifies. Understanding this replacement mechanism is vital to forecasting variations in hurricane intensity. Processes in the "moat" region between the new and old eyewall have been particularly unclear. Aircraft data now show that the moat becomes dynamically similar to the eye and thus is converted into a region inimical to survival of the inner eyewall. We suggest that targeting aircraft to key parts of the storm to gain crucial input to high-resolution numerical models can lead to improvements in forecasting hurricane intensity.

The tragedy of Hurricane Katrina in 2005 redoubled attention to the problem of tropical cyclone forecasting. Although forecasts of hurricane tracks and landfall location have improved in recent decades, forecasting of hurricane intensity (how strong the wind will be at landfall) has not (*1*). This comparative state of progress is not surprising, because a storm's track is primarily determined by the large-scale environment in which the tropical cyclone is embedded. Improvements in models that forecast surrounding large-scale wind patterns, combined with extra aircraft and satellite observations in the environments of storms, have thus led to improved track forecasts.

Changes of intensity (as measured by maximum surface wind strength) are more challenging to anticipate. Rapid changes of storm intensity are connected with the detailed spatial arrangement and unsteady pattern of smaller-scale cloud and precipitation features internal to the storm. These features are not resolved by large-scale models and are particularly difficult to observe because data must be obtained in the active central portion of the storm, where internal structural changes are taking place, while the storm is still over the ocean.

Eyewall replacement—a key process in hurricane intensity change. In a tropical cyclone, the radius of maximum wind is located in a circular region of heavily precipitating cloud called the "eyewall," which encircles the relatively calm "eye" of the storm. Outside the eyewall are lines of convective cloud that spiral in toward the eyewall and are called "rainbands." In the 1960s and 1970s, R. H. Simpson and J. S. Malkus hypothesized that cloud seeding could reduce hurricane intensity (*2*). The strategy was to use aircraft to seed rainbands located outside the original eyewall in such a way as to form a circular ring of deep clouds around the storm that would take over as a new eyewall and choke off the old eyewall. Once the inner eyewall weakened, the outer eyewall would contain the strongest winds in the storm, but because the new eyewall formed farther from the storm center, these winds would be weaker than in the original eyewall. If this change of storm intensity could be induced just before landfall, a storm moving ashore would produce less damage.

The cloud-seeding approach ultimately proved ineffective (*3*, *4*). Many strong, mature tropical cyclones exhibit a natural "eyewall replacement" process (*5*) in which a new (outer) eyewall takes over from the original (inner) eyewall, just as had been hypothesized—but with no cloud seeding taking place. Theoretical studies further show that the new eyewall's dynamics may cause it to contract over time (*6*). After an outer eyewall forms and envelops the inner eyewall, and the storm deintensifies, the new larger-diameter eyewall itself may shrink in radius, so that the storm reintensifies. This process may repeat itself. As additional new eyewalls form, the storm may undergo one or more large oscillations in intensity by natural processes alone. Therefore, the focus has changed: Instead of producing such changes artificially, by seeding, the goal is to forecast the intensity changes occurring as a result of natural eyewall replacement.

A field experiment revealing the process of eyewall replacement. The difficulty in forecasting when eyewall replacement will and will not occur was a key factor motivating the Hurricane Rainband and Intensity Change Experiment (RAINEX) in 2005 (*7*), in which an innovative set of aircraft measurements were obtained in Hurricanes Katrina, Ophelia, and Rita. The premise was that the variations in intensity occurring in conjunction with eyewall replacement involve interactions of the rainbands with each other, with the eyewall, and with the large-scale environment. The aircraft therefore focused on documenting detailed aspects of the specific rainbands and eyewalls that appear most likely to interact and affect intensity changes.

In carrying out this mission, RAINEX did three things differently from past hurricane observational efforts (*7*). First, RAINEX deployed the Naval Research Laboratory's (NRL) P-3 aircraft equipped with the National Center for Atmospheric Research (NCAR) ELDORA (Electra Doppler radar) (*8*), the highest quality meteorological airborne Doppler available, never before used in hurricanes. This research platform was flown in coordination with two Doppler-radar–equipped P-3 aircraft operated by the National Oceanic and Atmospheric Administration (NOAA) (*9*). Second, satellite communications and specialized interactive visualization technology were used to transmit, accumulate, and combine the data from aircraft radars, coastal radars, and satellite data onto a continuously updated master chart in the operations center with all the aircraft positions and tracks. This integrated map, which provided a wider and more comprehensive view of the detailed storm structure and situation than is possible from a single aircraft's radar, made it possible for a ground controller to optimally coordinate the flights of the three P-3 aircraft to observe those small-scale features most likely associated with intensity changes. Third, high-resolution (1.67 km) model forecasts of the investigated storms were made in real time to aid flight planning. These forecasts used input from larger-scale models (*7*). In the future, high-resolution forecasts of tropical cyclone intensity can potentially make use of the sort of detailed real-time ground-controlled aircraft observations obtained in RAINEX. Ground control can systematically target the measurements to small-scale features deemed most likely to affect intensity changes and assimilate these key observations back into the models.

Figure 1 shows a sequence of the high-resolution model forecasts of the structure of Hurricane Rita made during RAINEX. They show three stages of the storm's development, during a period when eyewall replacement occurred over the Gulf of Mexico. Comparison with radar data shows that the simulated structures and sequence of events were very similar to those captured by airborne observations of the actual storm. Figure 1A shows a closed annulus of heavy rain in the center of the panel. This was the original eyewall. To its west and east were spiral rainbands, intense cores of heavy rain aligned in curved bands angling in toward and becoming tangent to the eyewall. Figure 1B

[1]Department of Atmospheric Sciences, University of Washington, Seattle, WA 98195–1640, USA. [2]Rosenstiel School of Marine and Atmospheric Sciences, University of Miami, Miami, FL 33149, USA. [3]Earth Observing Laboratory, National Center for Atmospheric Research, Boulder, CO 80307, USA.

*To whom correspondence should be addressed. E-mail: houze@atmos.washington.edu

shows that 28 hours later, eyewall replacement had begun. The rainbands had organized into a coherent circular feature. A more weakly precipitating annular zone, which we call the moat, separated this new outer eyewall from the inner eyewall, which itself had begun to weaken. The process by which the second eyewall forms, although it happens frequently in nature, is not fully understood. One school of thought is that circular flow pattern around the center of the storm spawns small-scale disturbances called "vortex Rossby waves," which propagate radially outward from the original eyewall region (*10*). Depending on the exact structure of the hurricane vortex, the waves may act to concentrate angular momentum at a critical radius where their phase velocity matches the mean swirling flow and in this way coalesce to form a new outer eyewall. Another idea is that the large-scale humidity field surrounding the storm can affect the structure of the rainbands at a certain radius, which may lead to a second eyewall formation (*11*). Figure 1C shows that the inner eyewall had nearly vanished, while the outer eyewall, which was replacing it, was taking shape at a somewhat greater radius. The maximum winds in the storm had decreased from about 70 m s^{-1} to 52 m s^{-1}. Also notable is that the new eyewall had a smaller radius in Fig. 1C than in Fig. 1B, indicating that it had begun to contract, as expected from theory (*6*).

Aircraft radar data collected in Rita (Fig. 2) confirmed the double eyewall structure suggested by the model forecast. The NRL P-3 with ELDORA concentrated on the inner portion of the storm by flying in a circular fashion, repeatedly circumnavigating the inner core of the storm (Fig. 2A). Figure 2B shows the radar echo detected by ELDORA. Because the radar receives microwave radiation backscattered from precipitation particles in the path of the beam (*12*), the echo intensity pattern (color shading in Fig. 2B) indicates the precipitation pattern. The data clearly show two concentric eyewalls with a circular moat of weak echo between them. This pattern compares favorably to the simulated precipitation pattern (Fig. 1B), although the model timing was ~6 to 7 hours too fast.

The inner eyewall (Fig. 2B) was still fairly strong, although its southeast side had weakened, just as it did in the model forecast once the new eyewall surrounded it (Fig. 1B). A distinct wind maximum accompanied each eyewall (*7*). Because the Doppler radar scanned approximately orthogonal (±70°) to the track (*8*), the circular flight path gave a continuous view of the two eyewalls and their interactions. The cells of heavy precipitation in the outer eyewall seen in Fig. 2B are of a scale of detail not seen in hurricanes before the use of ELDORA in RAINEX. The cells produced by small-scale intense air motions tend to be elongated and distributed intermittently around the outer eyewall. Recent theoretical studies (e.g., *10*, *13*) have shown that as a new eyewall forms, small-scale air motion features generated in rainbands gather into an incipient eyewall. ELDORA indicates that this process was likely taking place in this young secondary eyewall.

The moat takes on the characteristics of a hurricane eye. Figure 2C shows the detailed wind field inferred by established methods (*14*, *15*) from ELDORA's measurement of precipitation particle motions (*12*). This cross section is a snapshot of the profound new information gained in this study. The moat region between the two eyewalls is occupied throughout its volume by downward air motion. An earlier study of aircraft radar data obtained on radial flight legs crossing a storm with two eyewalls had shown some indications of downward motion in the moat (*16*). However, because the aircraft with the ELDORA in Rita was ground-controlled to fly in a circle between the two eyewalls (Fig. 2A), we were able to show that the downward motion in the moat extended from upper to lower levels and all around the storm. Figure 2D is a composite of all the data collected during the ELDORA circumnavigation of Rita. It shows quantitatively how this pervasive downward motion determined the mean structure of the entire moat. The dynamics of the moat were transitioning to those of an eye.

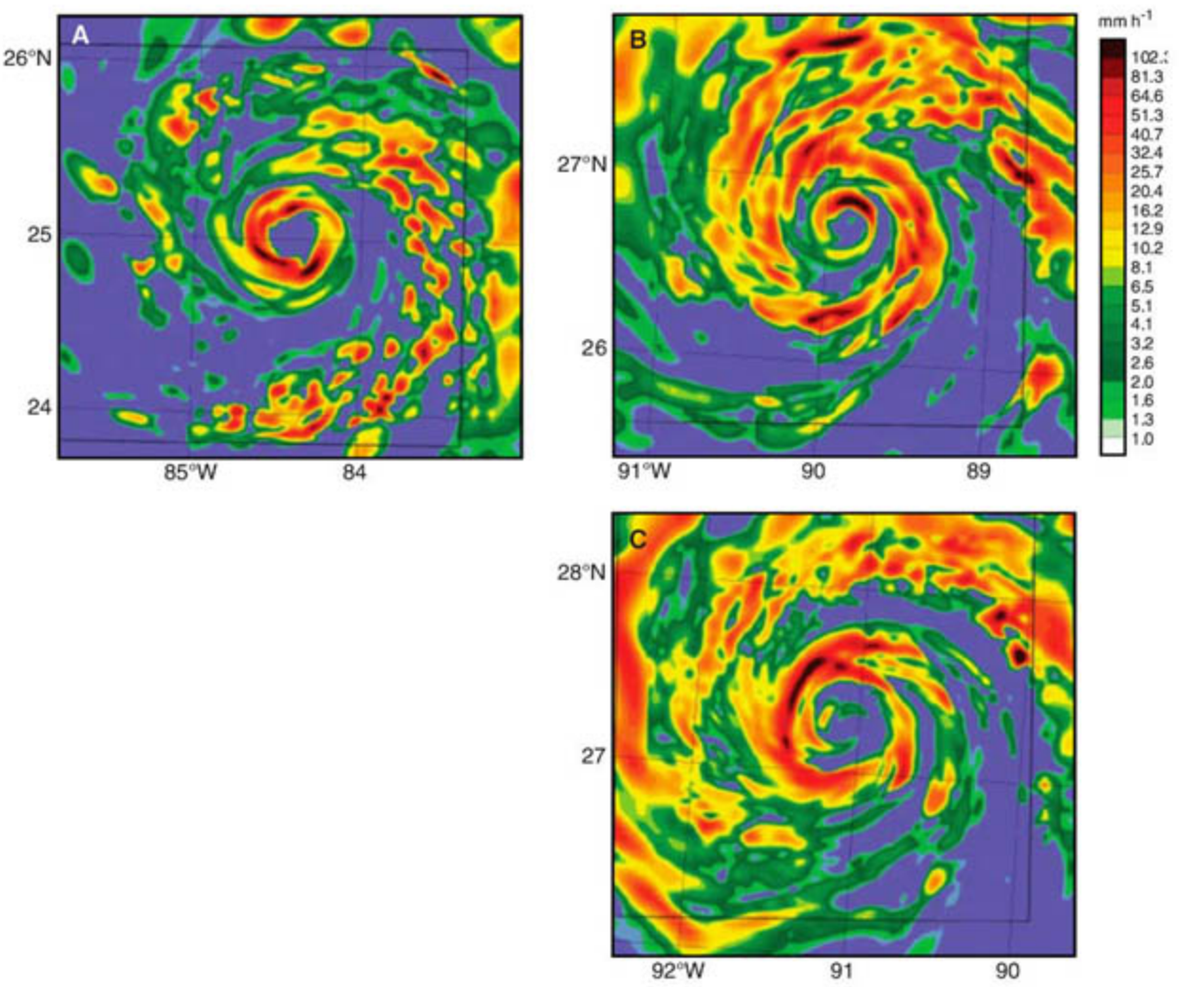

Fig. 1. Forecast of surface rainfall intensity in Hurricane Rita. (**A**) 0715 UTC 21 September, (**B**) 1115 UTC 22 September, (**C**) 1715 UTC 22 September. Colors show the rainfall rate (mm h^{-1}) at the sea surface generated by the University of Miami's high-resolution, vortex-following, coupled atmosphere-wave-ocean version of the fifth-generation Pennsylvania State University/NCAR nonhydrostatic mesoscale model (MM5) (*34*) operating at a horizontal resolution of 1.67 km. Initial fields at 0000 UTC 20 September 2005 and lateral boundary conditions are from the NOGAPS global numerical forecast model (*35*).

The eye is a region of singular dynamics determined by the spinning motion of the air in the eyewall, the buoyancy of the cloudy air in the eyewall, the large-scale environment of the storm, and the thermodynamic and turbulent character of the ocean surface. In the initial stages of a tropical cyclone, before a closed eyewall forms, convective clouds occur in ambient air, whose condition is characteristic of the large-scale atmospheric conditions in the region (*17*). Once formed, a circular eyewall effectively fences off a portion of the environment air. The trapped air is then modified by the near-field effect of the eyewall. Latent heat released in the surrounding eyewall cloud induces a circulation that draws low-level air out of the eye region (*18*), causing air farther aloft within the eye to subside. Consequently, the air in the eye is very dry (*19*) except for the layer of air in contact with the ocean. Temperature and moisture profiles obtained every 30 to 60 km by dropsondes (*20*) along the NRL aircraft track (Fig. 2A) show the dryness (relative humidity generally well below 100%) above 1000 m in the eye of Rita (Fig. 3A, green and red curves). Similar dryness seen above 1000 m in the moat (Fig. 3A, blue curve) together with the downward motion throughout the zone between the old and new eyewall (Fig. 2, C and D) suggests that the moat region was not a passive void between the two eyewalls. It was a dynamic entity that would take on the characteristics of an eye and join with the original eye, thus snuffing out the original eyewall.

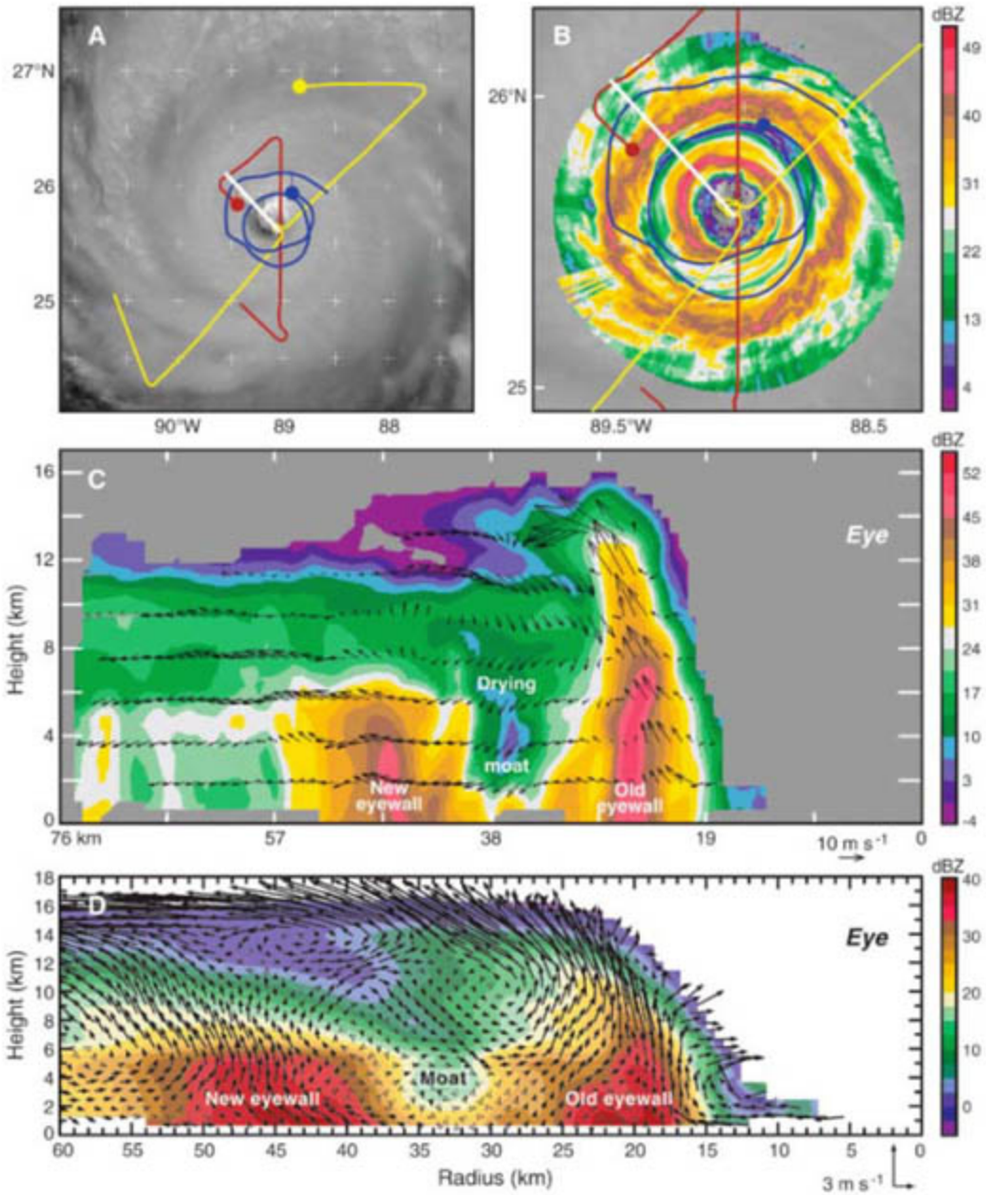

Fig. 2. Aircraft data collected in Hurricane Rita between 1800 and 1820 UTC 22 September 2005. (**A**) and (**B**) are plan views; (**C**) is a vertical cross section across the northwest side of the storm (along the white line in the plan views). Colored lines in (A) denote the flight tracks of the three RAINEX aircraft: yellow and red are the NOAA aircraft tracks; blue is the NRL aircraft, which was instrumented with ELDORA. The dots show aircraft locations as of 1830 UTC. The yellow track segment is for the 80 min preceding that time; the red and blue track segments are for the preceding 45 min. The yellow NOAA track was part of a wide pattern to determine the broad-scale structure of the cyclone vortex. The red NOAA track was part of an intermediate pattern, with shorter legs across the center of the storm to monitor the two eyewalls. The blue NRL track was the circumnavigation that obtained the key radar and sounding data referred to in this article. The color shades in (B) and (C) correspond to values of radar reflectivity (a measure of precipitation intensity). (**D**) depicts a comprehensive mean of dual-Doppler storm-relative winds derived from ELDORA data obtained during the period 1800 to 1820 UTC while the NRL aircraft that was flying in the moat circumnavigated the storm. Vectors show the component of air motions within the cross-sections [(C) and (D)].

Conceptual model of a hurricane undergoing eyewall replacement. Figure 4 conceptualizes our view of the eyewall replacement in Rita. The center portion consisting of the eye and the old eyewall reflects a conventional picture of eye dynamics. Immediately outside the original storm core, the new eyewall and moat mimic the old eyewall and eye, respectively. To describe the replacement, we first consider the conventional eye structure in the center of the diagram. The old eyewall circulation draws in near-surface air both from outside the eyewall and from within the eye itself (*6*). The air in the eye sinks to compensate for this transfer of air into the eyewall (*18*). Also contributing to the subsidence in the eye is turbulent mixing of angular momentum at the interface of the rapidly rotating eyewall and more quiescent eye region (*21*). The subsidence warms and dries the air within the eye, thus producing the cloud-free hole commonly characterizing the center of these storms in satellite imagery (Fig. 2A). Near the ocean surface the drying is counteracted by strong turbulent mixing, which transfers water vapor and sea spray from the warm and choppy sea surface upward and maintains high humidity in the lowest layer of the eye. The air at low levels within the inner eye draws energy from the sea more effectively because it is at low pressure (so that the moist enthalpy in equilibrium with the sea is elevated) and because strong winds whipping the moisture off the sea surface often extend well inward from the eyewall. The moisture in the lower layer is also maintained by air near the ocean surface that flows under rather than turning upward into the eyewall, and by a thin layer of moist air cascading down the inner edge of the eyewall. This cascade is produced by cloudy air mixing with the dry air at the inner edge of the eyewall (*18*). In simplest terms, the eye of the storm thus has a two-layer structure: moist at low levels, with dry descending air above. Capping the moist layer is a stable layer produced by the subsidence. In strong storms, the stable layer capping the lower moist mixed layer takes the form of an "inversion" (temperature increasing with height).

Our conceptual model (Fig. 4) depicts the moat during the replacement as taking on the dynamic behavior of a hurricane eye when

environmental air trapped in the zone between the old and new eyewalls is forced to sink, warming and drying in the process—just as the eye itself formed dynamically when air from the environment was surrounded by and responded to the original eyewall. Dropsondes obtained along the circular flight track in the moat (Fig. 2A) support the idea that the moat was undergoing just such a transition. Depicted dropsonde data was obtained in the eye of Rita at approximately the time the hurricane became the fourth strongest ever observed in the Atlantic basin (Fig. 3, green curves). The eye exhibited high humidity in the first 500 m above the ocean, capped by an extreme temperature inversion (temperature increasing upward to ~27°C at 2 km). Dropsondes in the eye on the next day (red curves) showed that as the storm weakened owing to the observed eyewall replacement process, the capping stable layer in the eye became less pronounced (*22*) and turbulent mixing at low levels was able to extend the moist layer up to about 1200 m. In the moat (blue curves), the humidity and temperature structure were essentially identical to those in the eye at the time of the replacement. Thus, both the airborne Doppler radar data (Fig. 2, C and D) and dropsondes (Fig. 3) obtained in Rita on 22 September show conditions within the moat taking on the characteristics of an eye.

Once the dynamics of Rita's moat region resembled those of an eye, the inner eyewall could only weaken with time. The bulk of the low-level inflow of high-energy air from the large-scale environment was robbed by the new outer eyewall (note that inflow toward the eye is absent at low levels between the new eyewall and old eyewall in Fig. 2, C and D). The old eyewall was ultimately destroyed by this lack of environmental inflow combined with active downward motion induced by the new eyewall, which evaporated the eyewall clouds and warmed the air surrounding the inner eyewall so that the old eyewall's buoyancy decreased. The progression of the eyewall replacement in Rita observed by radar (Fig. 2) was forecast accurately (Fig. 1). However, when the model resolution was degraded from 1.67 km to about 5 km, simulated eyewall replacement failed to occur, which indicates that the eyewall replacement dynamics are fundamentally small-scale and require high-resolution modeling to be accurately represented and forecast.

Even though Rita's second eyewall had enclosed the original eyewall by the time of Fig. 2, the inner eyewall remained strong for 12 hours (indicated by tall and intense inner-eyewall radar echoes, as in Fig. 2C). This slow demise of the inner eyewall is typical of hurricanes undergoing eyewall replacement (*5*). Because the inner eyewall was cut off from the large-scale environment, we conclude that the inner eyewall was drawing some energy from within the storm's inner core. As indicated in Fig. 4, the eyewall draws warm, moist air from the lower portion of the eye into its upward circulation (*18*). This air provides fuel to the old eyewall. The inner eyewall can apparently survive through this mechanism for several hours before finally expiring. Recent work (*23*, *24*) has suggested that when small-scale vortices form along the inner eyewall (*25*), the low-level eye air is more efficiently entrained into the eyewall. ELDORA data in Rita document the existence of a well-defined small-scale vortex on the inner edge of the inner eyewall at about the time of Fig. 2. We suspect it contributed to maintaining the intensity of the inner eyewall.

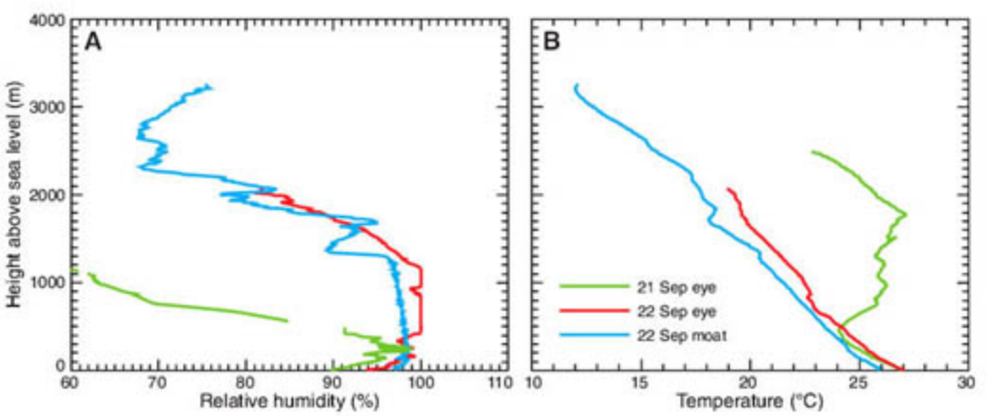

Fig. 3. Relative humidity (**A**) and temperature (**B**) profiles measured by dropsondes launched from aircraft in Hurricane Rita. The green curves show data obtained on 21 September (1601 UTC) in the eye of Rita, when the storm was reaching category 5 strength and was still intensifying. It reached its minimum observed pressure of 897 mb about 12 hours later. The red and blue curves show data obtained in Rita 24 hours later, during the eyewall replacement on 22 September 2005, when the central pressure had risen to 915 to 920 mb. The red curves (1619 UTC) show data obtained in the eye. The blue curves (1801 UTC) show the data from one of eight soundings obtained in the moat.

Possible new approaches to forecasting hurricane intensity changes. Eventually, Rita's inner eyewall died and was replaced by the outer eyewall. In conjunction with this eyewall replacement, Rita decreased from category 5 intensity (*26*, *27*) on 21 September, with maximum winds of 77 m s^{-1}, to category 3 or 4 on 22 September 2005, with maximum winds of 50 to 60 m s^{-1} (*28*). Figure 1 suggests that with a sufficiently high-resolution model, the eyewall replacement and accompanying intensity decrease can be forecast. In addition, the successful documentation of the eyewall replacement process in Rita during RAINEX by ground-controlled aircraft-targeting of the small-scale features internal to the tropical cyclone vortex could be a harbinger of improved forecasting of hurricane intensity. The adoption of real-time targeting of

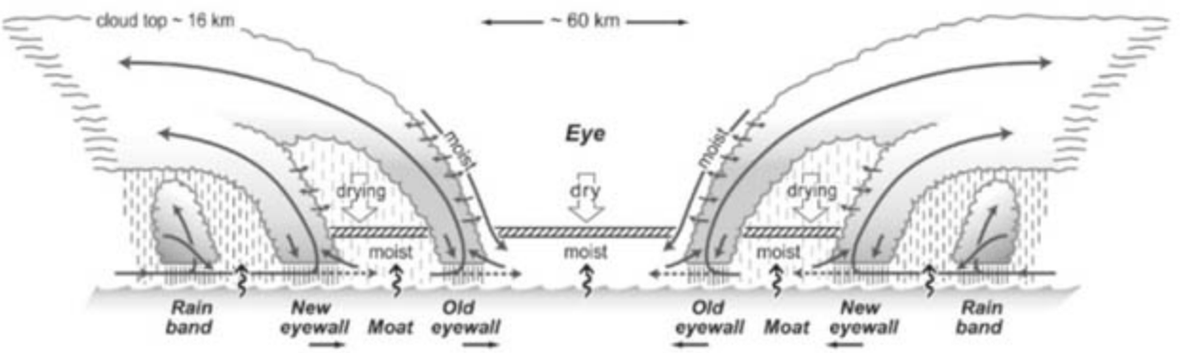

Fig. 4. Inner region of a hurricane undergoing eyewall replacement. The structure of the eye and innermost (original) eyewall are based primarily on (*18*) and (*21*). The structure of the rainbands is based on (*36*). The double-eyewall structure, including the moat separating the two interacting eyewalls, is based on RAINEX observations. Arrows at the bottom indicate that both eyewalls were contracting inward. The density of vertical lines below the clouds indicates relative precipitation intensity. Thin arrows show the direction of air motion relative to the storm. Dashed segments indicate partially interrupted flow. Small, wavy arrows at the sea surface indicate water vapor mixing upward from the ocean surface. The broad arrows indicate the downward motion induced by the heating in the eyewall and (possibly) momentum mixing across the inner edges of the eyewalls. The hatched zone shows the top of the near-surface moist layer, which is capped by the stabilizing and drying effect of subsiding air above. The moist layer is not to scale; its depth is exaggerated to show details of the airflow at low levels.

aircraft onto small-scale storm features likely to be associated with storm intensity change could provide timely input that would improve operational forecasts of hurricane intensity.

References and Notes

1. This well-known fact is statistically documented at (*29*).
2. R. H. Simpson, J. S. Malkus, *Sci. Am.* **211**, 27 (1964).
3. H. E. Willoughby, D. P. Jorgensen, R. A. Black, S. L. Rosenthal, *Bull. Am. Meteorol. Soc.* **66**, 505 (1985).
4. R. C. Sheets, in *Hurricane! Coping With Disaster*, R. Simpson, Ed. (American Geophysical Union, Washington, DC, 2003), chap. 3.
5. H. E. Willoughby, J. A. Clos, M. G. Shoreibah, *J. Atmos. Sci.* **39**, 395 (1982).
6. L. J. Shapiro, H. E. Willoughby, *J. Atmos. Sci.* **39**, 378 (1982).
7. R. A. Houze Jr. *et al.*, *Bull. Am. Meteorol. Soc.* **87**, 1503 (2006).
8. P. H. Hildebrand *et al.*, *Bull. Am. Meteorol. Soc.* **77**, 213 (1996).
9. S. Aberson *et al.*, *Bull. Am. Meteorol. Soc.* **87**, 1039 (2006).
10. M. T. Montgomery, R. J. Kallenbach, *Q. J. R. Meteorol. Soc.* **123**, 435 (1997).
11. D. Ortt, S. S. Chen, 27th Conference on Hurricanes and Tropical Meteorology, American Meteorological Society, 24 to 28 April 2006, Monterey, CA, preprint 12A.5 (2006) (available at http://ams.confex.com/ams/pdfpapers/108643.pdf).
12. Precipitation particles are liquid drops or ice particles heavy enough to be falling relative to Earth's surface. Most meteorological radars, including those deployed on the aircraft in RAINEX, detect precipitation but do not see smaller, non-falling cloud particles. Therefore, the intensity of the radar signal is related to precipitation intensity. The radar also detects the Doppler shift between emitted and received signals, which indicates the speed of movement of the precipitation particles along the beam of the radar. The wind speed and direction can be inferred from the Doppler velocities when the same precipitation particles are observed in more than one radar beam.
13. J. P. Kossin, W. H. Schubert, M. T. Montgomery, *J. Atmos. Sci.* **57**, 3890 (2000).
14. D. P. Jorgensen, T. Matejka, J. D. DuGranrut, *Meteorol. Atmos. Phys.* **59**, 83 (1996).
15. P. D. Reasor, M. T. Montgomery, F. D. Marks Jr., J. F. Gamache, *Mon. Weather Rev.* **128**, 1653 (2000).
16. P. Dodge, R. W. Burpee, F. D. Marks Jr., *Mon. Weather Rev.* **127**, 987 (1999).
17. E. A. Ritchie *et al.*, in *Hurricane! Coping With Disaster*, R. Simpson, Ed. (Amerian Geophysical Union, Washington, DC, 2003), chap. 12.
18. H. E. Willoughby, *Mon. Weather Rev.* **126**, 3053 (1998).
19. When air subsides, its relative humidity decreases because the air temperature increases adiabatically. Consequently, saturation vapor pressure rises while the water vapor content remains constant.
20. A dropsonde is a package of pressure, temperature, and humidity sensors that is dropped from an aircraft and tracked with a Global Positioning System receiver. The data obtained provide vertical profiles of temperature, humidity, and wind below the aircraft. For further information, see (*30*).
21. K. A. Emanuel, *J. Atmos. Sci.* **54**, 1014 (1997).
22. A temperature inversion is not required for a layer of air to be stable, i.e., resistant to vertical mixing. Stability exists in unsaturated air as long as the temperature decrease with height is >10°C/km.
23. J. Persing, M. T. Montgomery, *J. Atmos. Sci.* **60**, 2349 (2003).
24. M. T. Montgomery, M. M. Bell, S. D. Aberson, M. L. Black, *Bull. Am. Meteorol. Soc.* **87**, 1335 (2006).
25. F. D. Marks Jr., R. A. Houze Jr., *Bull. Am. Meteorol. Soc.* **65**, 569 (1984).
26. The hurricane-strength categories 1 to 5 represent, in ascending order, the degree of damage that can be done by the storm. For further details, see (*27*, *31*).
27. H. S. Saffir, in *Hurricane! Coping With Disaster*, R. Simpson, Ed. (American Geophysical Union, Washington, DC, 2003), chap. 7.
28. The range of the observed winds can be found at (*32*).
29. National Hurricane Center (NHC), www.nhc.noaa.gov/verification.
30. Earth Observing Laboratory, National Center for Atmospheric Research, www.eol.ucar.edu/rtf/facilities/dropsonde.
31. NHC, www.nhc.noaa.gov/aboutsshs.shtml.
32. NHC, www.nhc.noaa.gov/pdf/TCR-AL182005_Rita.pdf.
33. Navy Operational Global Atmospheric Prediction System (NOGAPS), www.nrlmry.navy.mil/nogaps_his.htm.
34. S. S. Chen, J. F. Price, W. Zhao, M. A. Donelan, E. J. Walsh, *Bull. Am. Meteorol. Soc.*, in press; available at http://orca.rsmas.miami.edu/~schen/publications/Chen.etal_InBox_CBLAST_final_8Sept06.pdf.
35. In RAINEX, the high-resolution MM5 was run with input from four different global models. The input from NOGAPS (*33*) gave the best result for Hurricane Rita. Also see (*7*).
36. G. M. Barnes, E. J. Zipser, D. Jorgensen, F. D. Marks Jr., *J. Atmos. Sci.* **40**, 2125 (1983).

37. Aircraft operations in RAINEX were under the direction of C. Newman (NRL aircraft) and J. MacFadden (NOAA aircraft). Lead airborne missions scientists for RAINEX included R. Rogers, M. Black (NOAA Hurricane Research Division), and D. Jorgensen (NOAA National Severe Storms Laboratory). Daily aircraft mission planning was led by J. Moore and G. Stossmeister (University Corporation for Atmospheric Research), and D. Nolan (University of Miami) contributed scientific guidance to the planning. Engineering support for ground control of flights was provided by C. Burghart and J. Scannel (NCAR), P. Chang (NOAA National Environmental Satellite, Data, and Information Service), J. Carswell (Remote Sensing Solutions, Inc.), and S. Brodzik (University of Washington). Engineering support for the radar and dropsonde measurements was directed by E. Loew, M. Strong, H.-Q. Cai, and E. Korn (NCAR). Real-time high-resolution model runs were carried out by W. Zhao (University of Miami). Forecasting for flight operations was done by J. Cangialosi and D. Ortt (University of Miami). G. Stossmeister and J. Meitín (University Corporation for Atmospheric Research) provided web support and data management for the project. B. Tully (University of Washington) coordinated the graphics. This research was supported by NSF grants ATM-0432623 and ATM-0432717.

27 September 2006; accepted 19 January 2007
10.1126/science.1135650

Chankillo: A 2300-Year-Old Solar Observatory in Coastal Peru

Ivan Ghezzi[1,2,3]* and Clive Ruggles[4]

The Thirteen Towers of Chankillo run north to south along a low ridge within a fourth-century B.C.E. ceremonial complex in north coastal Peru. From evident observing points within the adjacent buildings to the west and east, they formed an artificial toothed horizon that spanned—almost exactly—the annual rising and setting arcs of the Sun. The Chankillo towers thus provide evidence of early solar horizon observations and of the existence of sophisticated Sun cults, preceding the Sun pillars of Incaic Cusco by almost two millennia.

The identification of places from which astronomical observations were made in prehistory, together with evidence on the nature and context of those observations, can reveal much about the ways in which people before the advent of written records perceived, understood, and attempted to order and control the world they inhabited (*1*, *2*). Evidence of systematic observations of the changing position of the rising and setting Sun along the horizon (*3*), in particular, can provide information on the development, nature, and social operation of ancient calendars (*4*). Solar horizon calendars were certainly important among indigenous Americans, with one of the best-known modern examples being at the Hopi village of Walpi (*5*). In Mesoamerica before European contact, systematic studies of the orientations of sacred buildings and city plans strongly suggest the existence of horizon calendars in which special meaning was attributed to certain key dates. It has been argued that these dates included not only the solstices but also the dates of solar zenith passage (*6*) and dates counted off from both at intervals that were important in the intermeshing cycles of the Mesoamerican calendar round (*7*). In South America, accounts going back to the 16th century C.E. record various details of indigenous practices relating to Inca state-regulated Sun worship and related cosmological beliefs (*8*, *9*). Various schemes of landscape timekeeping have been suggested, which are supported by a combination of historical evidence and analyses of the spatial disposition of sacred architecture: in particular, the system of shrines placed along lines (*ceques*) conceived as radiating out from the central Sun temple, the Coricancha, in Cusco, Peru (*10*–*12*). "Sun pillars" are described by various chroniclers as having stood around the horizon from Cusco and been used to mark planting times and regulate seasonal observances (*13*), but all the Cusco pillars have vanished without trace and their precise location remains unknown. Here, we describe a much earlier structure in coastal Peru that seems to have been built to facilitate sunrise and sunset observations throughout the seasonal year.

The group of structures known as the Thirteen Towers is found within Chankillo, a ceremonial center in the Casma-Sechin River Basin of the coastal Peruvian desert (fig. S1). Seventeen ^{14}C dates fall between 2350 and 2000 calibrated years

[1]Instituto Nacional de Cultura, Avenida Javier Prado Este 2465, Lima 41, Peru. [2]Pontificia Universidad Catolica del Peru, Avenida Universitaria Cuadra 18, Lima 32, Peru. [3]Yale University, 51 Hillhouse Avenue, New Haven, CT 06511, USA. [4]School of Archaeology and Ancient History, University of Leicester, Leicester LE1 7RH, UK.

*To whom correspondence should be addressed. E-mail: ighezzi@yahoo.com

before the present (B.P.) (Fig. 1) and point to the beginning of occupation at the site in the fourth century B.C.E., during the late Early Horizon period (*14*). The site contains multiple standing structures and plazas distributed over ~4 km^2 of rock outcrops and sand ramps. It is oriented south of east (azimuth 118°). Its best-known feature is a 300-m-long hilltop structure built in a remote location and heavily fortified with massive walls, restricted gates, and parapets (fig. S2). This famous structure has been discussed often as a fort, a redoubt, or a ceremonial center (*15*). However, recent research supports an alternative interpretation as a fortified temple (*14*). A lesser-known part of the site is a ceremonial-civic area to the east, which contains buildings, plazas, and storage facilities. The Thirteen Towers form the most outstanding feature within this area: a row of 13 cuboidal constructions placed along the ridge of a low hill (Fig. 2B). The towers run north to south, although towers 11 to 13 are twisted around slightly toward the southwest. As seen from the buildings and plazas below this hill, on either side, the towers form an artificial toothed horizon with narrow gaps at regular intervals (Fig. 3).

The towers are relatively well preserved; their corners have mostly collapsed, but enough of the original architecture survives to allow a reconstruction. They were flat-topped and rectangular to rhomboidal in shape. Their size (75 to 125 m^2) and height (2 to 6 m) vary widely. Nonetheless, they are regularly spaced: The gaps between the towers vary from 4.7 to 5.1 m. Each tower has a pair of inset staircases leading up to the summit on the

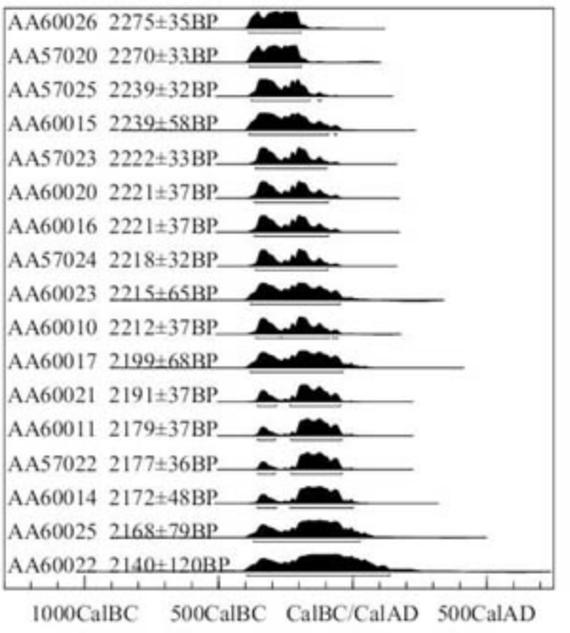

Fig. 1. Calibrated years B.P. date ranges (±SE) for samples from Chankillo, prepared by means of the program OxCal version 3.10 (*30*, *31*) with the use of Southern Hemisphere atmospheric data (*32*). For each sample, the first column represents the laboratory (NSF-Arizona Accelerator Mass Spectrometry Laboratory) identification number. The shaded area refers to the probability distribution of possible intersection points with the calibration curve, and the horizontal line below represents the 2-sigma calibrated age range. Five dates (AA57020 to AA57025) were sampled following dendrochronological principles from the outer sapwood rings preserved under bark in algarrobo (*Prosopis* sp.) lintels found still plugged into the architecture; these give a firm date for the construction of the site. The rest were obtained from the remains (including seed and fiber) of plants with short life spans. Thus, the "old wood" problem, especially troubling on the coastal desert of Peru, was minimized. CalBC, calibrated years B.C.E.; CalAD, calibrated years C.E.

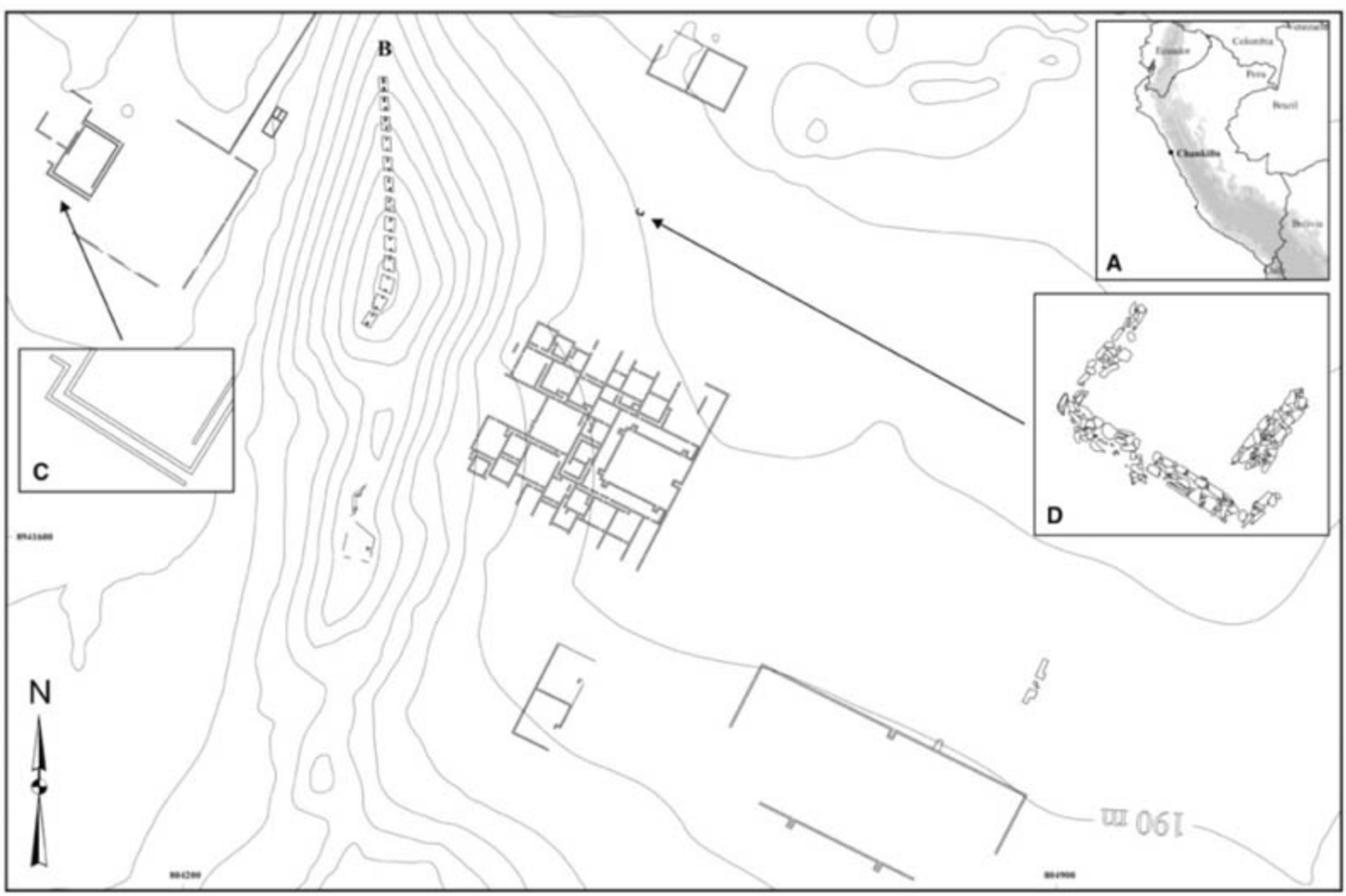

Fig. 2. Plan of the Thirteen Towers and adjacent buildings in Chankillo (see materials and methods). (**A**) Location within Peru. (**B**) The Thirteen Towers. (**C**) The external corridor and western observing point. (**D**) The eastern observing point.

north and south sides (fig. S3). Most of the northern staircases are centered along this side, although not all are aligned with the general orientation of the tower. Most of the southern staircases are offset toward the east. The staircases are narrow (1.3 to 1.5 m wide), but because the heights of the towers vary, they are of different lengths (1.3 to 5.2 m). Most of the tower summits are well preserved; no artifacts remain on these surfaces, though it is clear from the staircases that the summits were foci of activity.

A group of enclosures is found 200 m to the west of the towers (Fig. 2). The southernmost enclosure contains a building comprising two courtyards. The southeast courtyard is 53.6 m long and 36.5 m wide and is well preserved. Running along its southern side is a unique construction: a 40-m-long exterior corridor (Fig. 2C). The corridor, like the rest of the building, was carefully constructed, plastered, and painted white; however, it never led into the building. Instead, it connected a doorway on the northwest side, to which access was restricted by a blocking wall, with an opening on the southeast side that directly faced the towers 235 m away. The southeast opening, unlike every other doorway at Chankillo, did not have the typical barholds, or small niches where a pin was firmly tied into the stone masonry and presumably used to attach a wooden door (*16*). We infer that the purpose of the corridor was to orchestrate movement from its restricted entryway to a doorless opening directly facing the towers. Considering the original height of the corridor walls, estimated at roughly 2.2 m, only when the opening was reached would there have been an unobstructed view of the full row of towers. Archaeological excavations revealed offerings of pottery, shells, and lithic artifacts within 5 m of, and in stratigraphic association with, the floor level of the opening. No other offerings were found associated with 15 openings excavated elsewhere at the site (*16*). This suggests that ritualistic practices were involved in the process of passing through the corridor and standing at the end of it to observe the towers. Consequently, we designate this opening the "western observing point."

To the east of the towers (Fig. 2) is a large area (1.4 km^2) with several buildings, including an impressive complex of interconnected patios and rooms, corn beer (*chicha*) storage facilities, and a large plaza (0.16 km^2). In several places within the plaza, there were surface offerings of ceramic panpipes and thorny oyster (*Spondylus princeps*) shells, and middens near the plaza contained remains of serving vessels, more ceramic panpipes, and abundant maize remains. This whole area was probably a setting for large ceremonial feasts.

From several locations around this ceremonial area, the Thirteen Towers are the dominant feature of the landscape and could be used as solar horizon markers, but one building is of particular interest (Fig. 2D). It is a small, isolated building in the middle of a large, open space. Its position in relation to the Thirteen Towers is almost an exact mirror of the western observing point: The two lie almost exactly on an east-west line, are at the same elevation, and are at roughly the same distance from the towers. When viewed from inside this building, the spread of the towers forms an artificial horizon as well.

Only an incomplete outline of a rectangular room, 6 m wide, is preserved from this building. Like the corridor leading to the western observing point on the opposite side of the towers, this room had a doorway (in this case on the southeast side) that was restricted by a small blocking wall. We hypothesize that this doorway was the eastern observing point, but its exact position cannot be known with the same certainty as that of the western observing point.

We determined the locations of the two observing points, together with the corners of each tower, using hand-held differential Global Positioning System equipment. This enabled each point on the "false" horizon formed by the towers, as viewed from each observing point in turn, to be defined in terms of its azimuth, altitude, and (astronomical) declination (tables S1 and S2). Independent compass-clinometer determinations of azimuths and altitudes, calibrated by means of a direct observation of sunrise against the towers, provided consistency checks. By "altitude," we mean the vertical angle between a viewed point and the horizontal plane through the observer, with "elevation" being the height of a location above sea level (*17*).

Declinations of +23.75° and –23.75° correspond to the center of the Sun at the extreme positions of sunrise and sunset in 300 B.C.E., at the June and December solstices, respectively, with the Sun's disk extending between +23.5° and +24.0° (June) and between –24.0° and –23.5° (December) (*18*). Intermediate declinations correspond to sunrise and sunset on other dates.

Notably, as viewed from the two observing points, the spread of the towers along the horizon corresponds very closely to the range of movement of the rising and setting positions of the Sun over the year. This in itself argues strongly that the towers were used for solar observation. From the western observing point, the southern slopes of Cerro Mucho Malo, at a distance of 3 km, meet the nearer horizon (formed by the nearby hill on which the towers are constructed) just to the left of the northernmost tower (tower 1), providing a 13th "gap" of similar width to those between each pair of adjacent towers down the line (Fig. 4).

From the eastern observing point, the southernmost tower (tower 13) would not have been visible at all, and the top of tower 12 would only just have been visible (it is only partially visible now in its ruinous condition). From here, the December solstice Sun would have been seen to set behind the left side of the southernmost visible tower (tower 12), whereas the June solstice Sun set directly to the right of the northernmost tower (tower 1) (Fig. 5). In either case, once the Sun had begun to move appreciably away from either of its extreme rising positions a few days after each solstice, the various towers and gaps would have provided a means to track the progress of the Sun up and down the horizon to within an accuracy of two or three days.

If we accept that the towers were used as foresights for solar observations, then does their disposition suggest anything about the way the ancient calendar year might have been broken down? The flat tops of the towers originally formed their own smooth, false horizon, with their varying heights compensating to some extent for the slope of the hill on which they were built. This false horizon was broken at intervals

Fig. 3. The Thirteen Towers of Chankillo, as viewed from the fortified temple. Tower 1 is the leftmost tower in the image.

by deep, narrow cuts formed by the gaps between the towers. When viewed from the western observing point, the Sun rose for just one or two days in each gap. One possibility, then, is that critical sunrises were observed in the gaps. However, the regularity of the gaps argues against this, suggesting instead that the year was divided into regular intervals. The sunrises in the gaps between the central towers (towers 3 to 11) were all separated by time intervals of (or close to) 10 days, implying that a 10-day interval may have been a feature of the solar calendar. However, the time intervals are longer between the outer towers in the line, where the sunrise moves along more slowly. Furthermore, the situation is different from the eastern observing point, because no gaps would have been visible between the southernmost towers in the line as far as tower 10 (and possibly tower 9), and the remaining gaps correspond to time intervals between sunsets of 11 or 12 days (table S2).

From the eastern observing point, the December solstice Sun set into the left side of the leftmost visible tower, whereas the June solstice Sun set into the right side of the rightmost tower. From the western observing point, the December solstice Sun rose up from the top of the rightmost tower, whereas the June solstice Sun rose a little way up the slopes of Cerro Mucho Malo. There is an evident symmetry here also, suggesting that this natural hill was perceived as the leftmost "tower" in this profile. Midwinter would have been the one time of year when the Sun was seen to emerge from a natural hill rather than from a human construction.

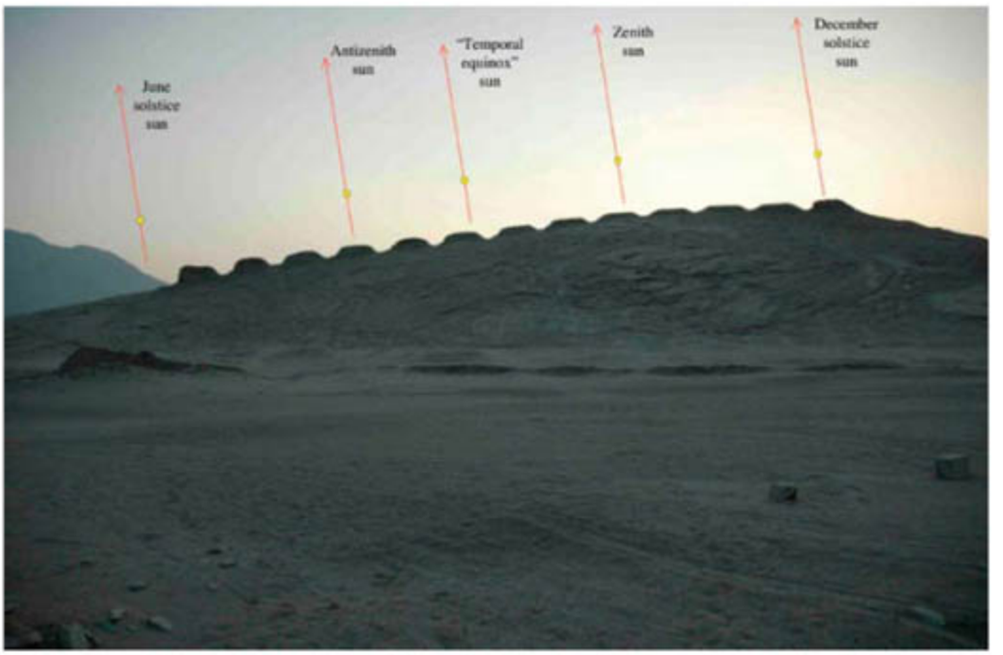

Fig. 4. The Thirteen Towers as viewed from the western observing point, annotated with the positions of sunrise at the solstices, equinoxes, and the dates of zenith and antizenith passage in ~300 B.C.E. Tower 1 is the leftmost tower in the image.

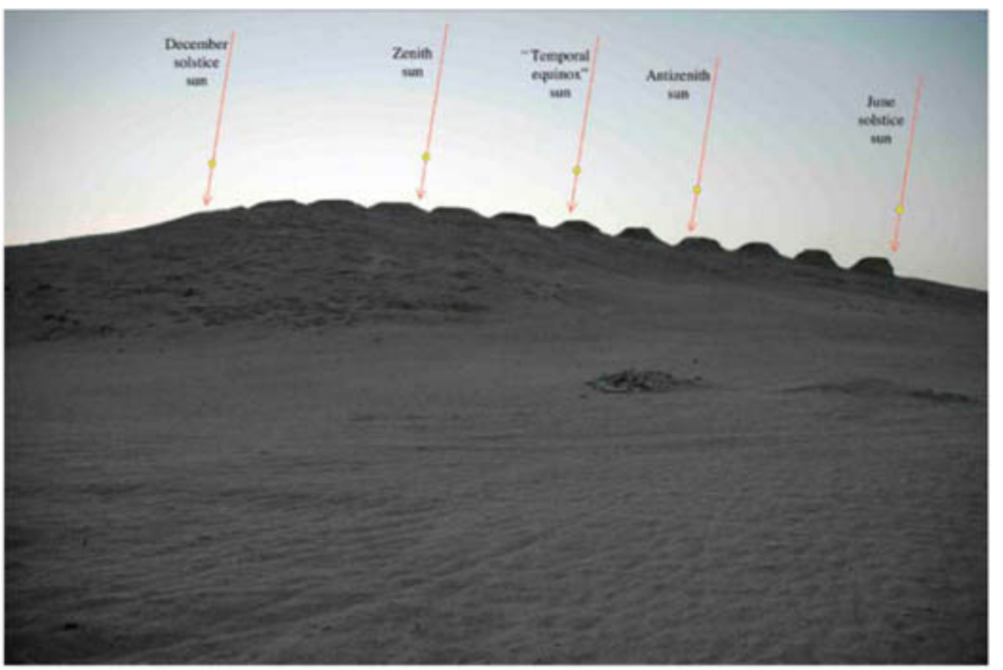

Fig. 5. The Thirteen Towers as viewed from the eastern observing point, annotated with the positions of sunset at the solstices, equinoxes, and the dates of zenith and antizenith passage in ~300 B.C.E. Tower 1 is the rightmost tower in the image.

Equinoctial sunrise (declination 0.0°) occurred in the central gap directly between towers 6 and 7. If Cerro Mucho Malo is included, so that there are 13 gaps, then this gap is the central one. In the other direction, equinoctial sunset occurred just to the right of this same gap, which as seen from the east is the central gap within the 12 visible towers. However, the applicability of the concept of the equinox outside a Western conceptual framework is highly questionable (*19*). At Chankillo, there is clear evidence that a mechanism existed to help count off the days, which might suggest that the mid-days between the solstices (the "temporal equinoxes" or "Thom equinoxes") are more likely to have been important. However, in 300 B.C.E., the Sun's declination on these days was between +0.6° and +1.0°, and there is no evidence that these days were specially marked.

A variety of evidence suggests that the date of solar zenith passage was important to early cultures in the American tropics in general and in the Andes in particular (*20*). It has also been suggested that the dates of solar antizenith passage might have been of importance in Incaic Cusco (*21*), although this idea has been debated (*22*). However, there is nothing in the pattern of disposition of the towers to suggest that it was deliberately preconceived in relation to sunrise or sunset on these dates. Only zenith passage sunset falls close to (and even then, not exactly within) a gap between two towers.

Astronomical "explanations" can be fitted notoriously easily to preexisting alignments. Repeated instances of solar and lunar alignments can provide strong evidence of intentionality, as among many local groups of later prehistoric tombs and temples in Britain, Ireland, and mainland Europe (*23*, *24*). However, at a unique site, there is always a danger of supporting a circular argument if the judgment of what might have been important to people in the past is made solely on the basis of the alignment evidence itself. Fortuitous stellar alignments are particularly likely, given the number of stars in the sky and the fact that their positions change steadily over the centuries owing to precession. The Chankillo towers, on the other hand, just span (to within a couple of degrees) the solar rising and setting arcs as seen from two observing points, each clearly defined by a distinctive structure with no other apparent purpose. Thus, we are not selecting putative astronomical targets from innumerable possibilities but seeing direct indications of all four solstitial rising and setting points: astronomical "targets" whose broad importance across cultures is self-evident and widely attested.

It is uncontroversial to postulate direct observations of the annual movement of the rising or setting Sun along the horizon for the purposes of regulating seasonal events such as religious festivals or for maintaining a seasonal calendar. Nonetheless, it is not simple to evaluate the nature of the observations made and the social and ritualistic context within which they operated and derived their relevance. This point is well illustrated by recent debates concerning the function of the so-called E-group structures in the Mayan heartlands of the Peten in Guatemala (*25*–*27*). In the case of the Thirteen Towers and nearby plazas, we can infer that they provided a setting for people participating in public rituals and feasts directly linked to the observation and interpretation of the seasonal passage of the Sun. By contrast, entry to the observing points themselves appears to have been highly restricted. Individuals with the status to access them and conduct ceremonies would have had the power to regulate time, ideology, and the rituals that bound this society together. Additionally, the excavations at Chankillo have uncovered ceramic warrior figurines holding a great variety of offensive (and defensive) weapons (*14*) (fig. S5). The warriors depicted wear signs of distinction, such as headdresses, shirts, and especially neck, chest, and nose ornaments. The artistic representation of these warriors, holding specialized weapons and wearing the symbols of their high status, indicates the possible rise of a class of war leaders and the centralization of power and authority in the hands of a few. Thus, Sun worship and related cosmological beliefs at Chankillo could have helped to legitimize the authority of an elite class, just as they did within the Inca empire two millennia later. And this, in turn, implies that the towers were not a simple instrument for solar observation but the monumental expression of existing—and therefore by implication even older—knowledge.

There is increasing evidence that the Sun cult, which, as the official cult of the Inca empire, regulated calendrical ceremonies and supported the established social hierarchy, had precursors. For example, historically attested sunrise ceremonies at a sanctuary on the Island of the Sun in Lake Titicaca (*28*), surrounding a crag regarded as the origin place of the Sun, almost certainly had pre-Incaic roots (*29*). Given the similarity between the solar observation device at Chankillo and the Cusco pillars documented some two millennia later (*12*), it seems likely that similar practices were common within many of the great states that developed in the Andes before, as well as including, the Inca empire.

References and Notes

1. C. L. N. Ruggles, in *Archaeology: The Key Concepts*, A. C. Renfrew, P. G. Bahn, Eds. (Routledge, New York, 2005), pp. 11–16.
2. C. L. N. Ruggles, *Ancient Astronomy: An Encyclopedia of Cosmologies and Myth* (ABC-CLIO, Santa Barbara, CA, 2005).
3. A. F. Aveni, *Skywatchers* (Univ. of Texas Press, Austin, 2001), pp. 55–67.
4. Not all accurate sky-based seasonal calendars rely on horizon observations of the Sun: One exception is the traditional calendar of the Borana of Ethiopia and Kenya [M. Bassi, *Curr. Anthropol.* **29**, 619 (1988)], which is luni-stellar.
5. S. C. McCluskey, *J. Hist. Astron.* **8**, 174 (1977).
6. A. F. Aveni, H. Hartung, *Trans. Am. Phil. Soc.* **76**, 1 (1986).
7. I. Šprajc, *Orientaciones Astronómicas en la Arquitectura Prehispánica del Centro de México* (Instituto Nacional de Antropología e Historia, México Distrito Federal (D.F.), 2001).
8. M. S. Ziółkowski, R. M. Sadowski, Eds., *Time and Calendars in the Inca Empire* (British Archaeological Reports International Series, Oxford, 1989), vol. 479.
9. B. S. Bauer, D. S. P. Dearborn, *Astronomy and Empire in the Ancient Andes* (Univ. of Texas Press, Austin, 1995).
10. R. T. Zuidema, *The Ceque System of Cuzco: The Social Organization of the Capital of the Inca* (Brill, Leiden, Netherlands, 1964).
11. A. F. Aveni, *Stairways to the Stars* (Wiley, New York, 1997), pp. 147–176.
12. B. S. Bauer, *The Sacred Landscape of the Inca: The Cusco Ceque System* (Univ. of Texas Press, Austin, 1998).
13. B. S. Bauer, D. S. P. Dearborn, *Astronomy and Empire in the Ancient Andes* (Univ. of Texas Press, Austin, 1995), pp. 67–100.
14. I. Ghezzi, in *Andean Archaeology III: North and South*, W. Isbell, H. Silverman, Eds. (Springer, New York, 2006), pp. 67–84.
15. J. R. Topic, T. L. Topic, in *Arqueología, Antropología e Historia en los Andes: Homenaje a María Rostworowski*, R. Varon, J. Flores, Eds. (Instituto de Estudios Peruanos, Lima, 1997), pp. 567–590.
16. I. Ghezzi, *Proyecto Arqueológico Chankillo: Informe de la Temporada 2003* (Instituto Nacional de Cultura, Lima, 2004).
17. C. L. N. Ruggles, *Astronomy in Prehistoric Britain and Ireland* (Yale Univ. Press, New Haven, CT, 1999), pp. ix.
18. C. L. N. Ruggles, *Astronomy in Prehistoric Britain and Ireland* (Yale Univ. Press, New Haven, CT, 1999), pp. 18, 24, and 57.
19. C. L. N. Ruggles, *J. Hist. Astron.* **28** (suppl. 22), S45 (1997).
20. A. F. Aveni, *Skywatchers* (Univ. of Texas Press, Austin, 2001), pp. 40–46 and 265–269.
21. R. T. Zuidema, in *Archaeoastronomy in the Americas*, R. A. Williamson, Ed. (Ballena, Los Altos, CA, 1981), pp. 319–342.
22. B. S. Bauer, D. S. P. Dearborn, *Astronomy and Empire in the Ancient Andes* (Univ. of Texas Press, Austin, 1995), pp. 94–98.
23. C. L. N. Ruggles, *Astronomy in Prehistoric Britain and Ireland* (Yale Univ. Press, New Haven, CT, 1999), pp. 91–111.
24. M. A. Hoskin, *Tombs, Temples and Their Orientations* (Ocarina Books, Bognor Regis, UK, 2001).
25. A. F. Aveni, H. Hartung, in *World Archaeastronomy*, A. F. Aveni, Ed. (Cambridge Univ. Press, Cambridge, 1989), pp. 441–461.
26. A. F. Aveni, A. S. Dowd, B. Vining, *Latin Am. Antiq.* **14**, 159 (2003).
27. G. R. Aylesworth, *Archaeoastronomy* **18**, 34 (2004).
28. B. S. Bauer, C. Stanish, *Ritual and Pilgrimage in the Ancient Andes: The Islands of the Sun and the Moon* (Univ. of Texas Press, Austin, 2001).
29. D. S. P. Dearborn, M. T. Seddon, B. S. Bauer, *Latin Am. Antiq.* **9**, 240 (1998).
30. C. Bronk Ramsey, *Radiocarbon* **37**, 425 (1995).
31. C. Bronk Ramsey, *Radiocarbon* **43**, 355 (2001).
32. F. G. McCormac *et al.*, *Radiocarbon* **46**, 1087 (2004).

33. We thank the numerous archaeologists and volunteers who participated in the Chankillo project, and especially J. L. Pino. We also thank Yale University, the Pontificia Universidad Católica del Peru, NSF, the Wenner-Gren Foundation, the Field Museum, the Schwerin Foundation, and Earthwatch Institute for support, as well as the Asociación Cultural Peruano Británica in Lima, Peru, for logistical and financial support. R. Towner and K. Anchukaitis were instrumental in securing five samples for dendrochronological dating. The warrior figurines were restored by Futuro Anterior. NSF funded all Accelerator Mass Spectrometry radiocarbon dates. I.G. is director of archaeology at the Instituto Nacional de Cultura.

Supporting Online Material

www.sciencemag.org/cgi/content/full/315/5816/1239/DC1
Materials and Methods
SOM Text
Figs. S1 to S5
Tables S1 to S4
References and Notes

17 October 2006; accepted 21 December 2006
10.1126/science.1136415

Human Neuroblasts Migrate to the Olfactory Bulb via a Lateral Ventricular Extension

Maurice A. Curtis,[1,2] Monica Kam,[1] Ulf Nannmark,[3] Michelle F. Anderson,[2] Mathilda Zetterstrom Axell,[2] Carsten Wikkelso,[2] Stig Holtås,[4] Willeke M. C. van Roon-Mom,[1] Thomas Björk-Eriksson,[5] Claes Nordborg,[6] Jonas Frisén,[7] Michael Dragunow,[8] Richard L. M. Faull,[1]* Peter S. Eriksson[2]*

The rostral migratory stream (RMS) is the main pathway by which newly born subventricular zone cells reach the olfactory bulb (OB) in rodents. However, the RMS in the adult human brain has been elusive. We demonstrate the presence of a human RMS, which is unexpectedly organized around a lateral ventricular extension reaching the OB, and illustrate the neuroblasts in it. The RMS ensheathing the lateral olfactory ventricular extension, as seen by magnetic resonance imaging, cell-specific markers, and electron microscopy, contains progenitor cells with migratory characteristics and cells that incorporate 5-bromo-2′-deoxyuridine and become mature neurons in the OB.

In the rodent brain, the RMS contains progenitor cells that migrate from the subventricular zone (SVZ), adjacent to the lateral ventricle, out to the OB. The RMS takes a course rostral to the striatum, and then the cells migrate forward in the olfactory tract to the OB. The human forebrain follows the basic structural organization of the mammalian brain but is extensively developed compared with that of rodents. The human OB, and hence the olfactory interneuron replacement

system, is comparatively smaller than that in rodents and is anatomically organized differently; therefore, the RMS has remained elusive in the human brain.

Many species possess an open tube between the lateral ventricle and olfactory ventricle, and this allows the free flow of cerebrospinal fluid (CSF) as well as a continuous SVZ between the two regions (*1*, *2*). This structure has not been previously shown in the human brain.

In the present study, we provide a characterization of the human ventriculo-olfactory neurogenic system (VONS) containing the SVZ, the RMS, the olfactory tract, and the OB. We demonstrate that the human RMS is organized around a lateral ventricular extension reaching the OB.

The anatomical location of the RMS in the human brain. Analysis of proliferating cell nuclear antigen (PCNA)–stained sagittal human forebrain sections (counterstained with Nissl) showed the presence of an RMS-like pathway. Proliferating cells were observed from the SVZ adjacent to the lateral ventricle overlying the caudate nucleus (CN) to the olfactory tract in the base of the forebrain (Fig. 1, A and B). A cleft in the floor of the anterior horn of the lateral ventricle contained large numbers of PCNA-positive cells that were continuous with the PCNA-positive cells in the SVZ that overlie the CN. The stream of cells first takes a caudal and ventral track along the undersurface of the CN, caudal to the genu of the corpus callosum and the frontal cortical white matter of the gyrus rectus (Fig. 1, A to D). When the descending limb reaches the ventral CN, the stream takes a rostral turn to form the rostral limb of the RMS that passes ventrally and rostrally to enter the anterior olfactory cortex (AOC), which gives rise to the olfactory tract that leads to the OB (Fig. 1A). Near the SVZ, more than 20 serial sagittal sections extending mediolaterally over 2.1 mm had PCNA-positive cells evident in the descending limb; at the level of the rostral limb, proliferating cells only extended mediolaterally over 0.6 mm. Thus, the overall mediolateral extent of the RMS is 2.7 mm from the SVZ to the olfactory tract, and the total length of the RMS pathway from the SVZ to the start of the olfactory tract is about 17 mm. High-magnification photomicrographs revealed the specific nuclear localization of the PCNA protein at the funnel where the RMS begins (Fig. 1E), in the decending limb (Fig. 1F), and in the rostral limb (Fig. 1G).

Serial coronal PCNA-stained sections revealed that the RMS takes a path from medial, by the SVZ, to lateral, beneath the CN; close to the SVZ the RMS is very wide in the coronal plane (Fig. 2, A and B). Coronal sections taken from the AOC region revealed two small oval bundles of PCNA-positive cells; the more dorsal bundle represented the descending limb of the RMS, and the more ventral bundle, the rostral limb of the RMS (Fig. 2C). Total cell counts throughout the entire lengths of the descending limb and the rostral limb of the RMS conducted on three cases showed that the RMS comprised 108,300 ± 13,310 cells (mean ± SD). Over 90% of the PCNA-positive cells were present in the descending limb and under 10% in the rostral limb, suggesting differentiation and dispersal along the stream (Fig. 2C). In the core of the olfactory tract, PCNA labeling formed a flat band. PCNA-labeled cells were present in the olfactory tract throughout its extension from the caudal region near the AOC (Fig. 2D) to the rostral extent, where the olfactory tract enters the OB.

Cell death is not the fate of most of the RMS progenitor cells. To examine whether PCNA was being expressed in the RMS cells because of DNA repair or apoptosis and not proliferation (*3*), we performed terminal deoxynucleotidyl transferase–mediated deoxyuridine triphosphate nick end labeling (TUNEL) to detect DNA fragmentation. No TUNEL was present in the descending limb of the RMS despite the presence of many TUNEL-positive cells in the adjacent CN (fig. S1).

Progenitors in the RMS have migratory proteins and a migratory morphology. Immunostaining for polysialylated–neural cell adhesion molecule (PSA-NCAM), which is expressed by migrating cells in the rodent RMS (*4*, *5*), was investigated in the SVZ near the cleft, the descending and rostral limbs of the RMS, the olfactory tract core and periphery, and the OB. In each region examined, PSA-NCAM–positive

[1]Department of Anatomy with Radiology, Faculty of Medical and Health Sciences, University of Auckland, Private Bag 92019, Auckland, New Zealand. [2]Center for Brain Repair and Rehabilitation, Institute of Neuroscience and Physiology, Sahlgrenska Academy, Medicinaregatan 11, Box 432, SE 405 30 Göteborg, Sweden. [3]Institute of Biomedicine at Sahlgrenska Academy, Medicinaregatan 11, Box 432, SE 405 30 Göteborg, Sweden. [4]Department of Radiology, Bruna Stråket 11 plan 2, Sahlgrenska University Hospital, SE 413 45 Göteborg, Sweden. [5]Department of Oncology, Sahlgrenska University Hospital, 413 45 Göteborg, Sweden. [6]Department of Pathology, Sahlgrenska University Hospital, 413 45 Göteborg, Sweden. [7]Department of Cell and Molecular Biology, Medical Nobel Institute, Karolinska Institute, SE-171 77 Stockholm, Sweden. [8]Department of Pharmacology, Faculty of Medical and Health Sciences, University of Auckland, Private Bag 92019, Auckland, New Zealand.

*To whom correspondence should be addressed. E-mail: per@neuro.gu.se (P.S.E.); rlm.faull@auckland.ac.nz (R.L.M.F.)

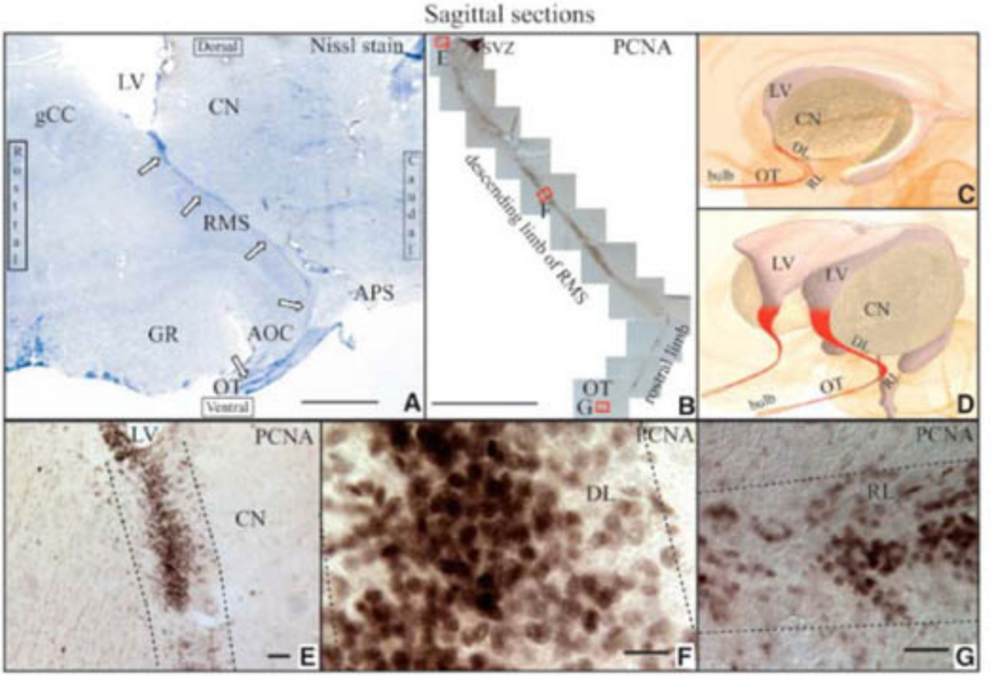

Fig. 1. The human RMS takes a caudal path en route from the SVZ to the olfactory cortex. (**A**) Nissl staining of human serial sagittal human forebrain sections reveals the intense stained cells that delineate the path of the RMS behind the frontal cortex white matter of the gyrus rectus (GR) and in front of the CN and anterior perforated substance (APS); arrows indicate the pathway. LV indicates lateral ventricle; gCC, genu of the corpus callosum; and OT, olfactory tract. Scale bar indicates 5 mm. (**B**) A montage of PCNA labeling of the human RMS shows the presence of numerous proliferating cells in both descending and rostral limbs of the RMS. Scale bar, 5 mm. (**C**) Schematic diagram demonstrating the pathway of the RMS as viewed laterally. (**D**) Diagram demonstrating the RMS from a frontal-oblique angle where the wide dorsal descending limb (DL) of the RMS descends and narrows to form the rostral limb (RL), which enters and courses rostrally in the OT toward the OB. (**E**) High-magnification photomicrograph of the PCNA-positive cells in the funnel part of the RMS. The area the photo was taken from is highlighted with a red box in (B). Scale bar, 50 μm. (**F**) Photomicrograph of the PCNA-positive cells in the DL of the RMS. The area the photo was taken from is highlighted with a red box in (B). Scale bar, 15 μm. (**G**) Photomicrograph of the PCNA-positive cells in the funnel part of the RMS. The area the photo was taken from is highlighted with a red box in (B). Scale bar, 30 μm.

cells were present. In the SVZ, the cell bodies faced the ependymal layer, and the processes were oriented away from the ependymal layer. The cell bodies were about 10 to 15 μm in diameter, and the length of the processes was half the width of the SVZ (Fig. 3, A to D). The gap region showed substantial background labeling and some small fiber staining (Fig. 3A). In the descending limb and the rostral limb of the RMS, there were also numerous bipolar and elongated PSA-NCAM–positive cells (Fig. 3, E to G). The olfactory tract core and periphery were also abundant in PSA-NCAM–positive cells that had a morphology and a staining pattern similar to those seen in the descending limb (Fig. 3, H and I). PSA-NCAM–positive cells in the OB were more randomly oriented, had fewer processes, and were larger than the cells in the olfactory tract core, indicating possible early stages of maturation (Fig. 3I). The descending limb had the largest number of PSA-NCAM–positive cells (the most PCNA cells were also present) within the RMS; the cell body labeling was mainly confined to a discrete bundle of bipolar cells (which showed leading and trailing processes) between the white matter of the gyrus rectus and the CN (Fig. 3E). In addition, small numbers of scattered PSA-NCAM–positive cells were seen just outside the main bundle, coursing into the surrounding white matter. In the rostral limb of the RMS, the morphology of the PSA-NCAM cells was similar to the morphology of those in the descending limb (Fig. 3, E and F). βIII-tubulin, an immature neuronal marker, was examined in the SVZ, the descending limb, and the olfactory tract. Fiber staining was observed in the SVZ beneath the gap region and close to the SVZ, as well as in the descending limb of the RMS (Fig. 4, A to C). In the descending limb, the fibers were particularly long and discretely located in the same place that PCNA immunoreactivity was located (Fig. 3, B and C). We performed double labeling and laser scanning confocal microscopy for PSA-NCAM and βIII-tubulin, which demonstrated that in the SVZ PSA-NCAM and βIII-tubulin are colocalized on the same bipolar cells (Fig. 4, D to F). Double-labeled PSA-NCAM– and βIII-tubulin–positive cells were seen in the olfactory tract (Fig. 4, G to J), as well as in the OB.

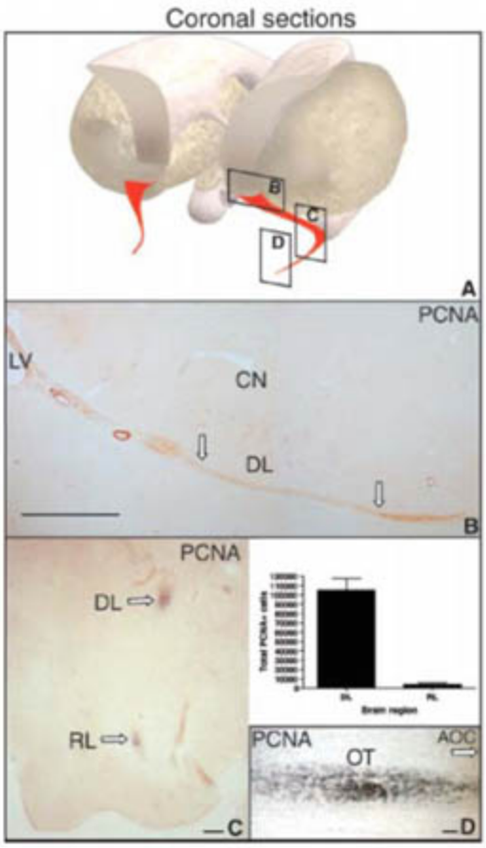

Fig. 2. The dorsal RMS is a broad band of proliferating cells, but ventrally there are fewer cells in the RMS. (**A**) Schematic diagram showing the orientation and location in the RMS of photomicrographs (B) to (D). (**B**) PCNA labeling in a montage of coronal serial forebrain sections showing the DL (arrows) as it courses laterally from the SVZ, then ventral to the CN. Scale bar, 1 mm. (**C**) PCNA labeling in a coronal section of the ventral forebrain showing a cross section of the DL (arrow) and the RL (arrow) of the RMS. The graph shows the total number of PCNA-positive cells in the RL compared with that of the DL of the RMS ($n = 3$). Scale bar, 200 μm. Error bars indicate SEM. (**D**) A longitudinal section of the OT very close to the AOC, showing large numbers of PCNA-positive cells. Scale bar, 100 μm.

Ultrastructural studies verify that the human SVZ contains cells with migratory-like morphology. In the adult mouse brain, where neuronal migration from the SVZ is common, ultrastructural and immunolabeling studies demonstrated that migrating neuronal precursors in the SVZ express PSA-NCAM (Doetsch classification, type A cells) (*6*, *7*). We sought to determine whether the human SVZ had similar migratory, type A cells. Electron microscopy (EM) revealed different types of cells that could be identified on the basis of their nuclear morphology and overall shape (Fig. 4K). Type A cells had an elongated cell body and a smooth contour. Their nuclei contained lax chromatin with one or two small nucleoli. They were located between the myelin layer and the ependymal layer. Positioned at the interface of the SVZ and myelin layer were the type B1 cells. These cells contained irregular nuclei with frequent invaginations and clumped chromatin [see (*8*) for a detailed analysis of type A, B, and C cells in the human SVZ]. We also detected an astrocytic ribbon in the SVZ of the adult human brain that contained dividing astrocytes (fig. S2), confirming previous work (*4*).

Progenitor cells become neurons in the OB. We used human OB from patients that had been administered 5-bromo-2′-deoxyuridine (BrdU) for the purpose of tracing the development of laryngeal and pharyngeal carcinomas. BrdU is a thymidine analog and labels cells in the S phase of the cell cycle (*9*, *10*). We double-labeled the OB with neuronal nuclei (NeuN), a mature neuronal marker, and an antibody against BrdU. Laser-scanning confocal z-series analysis revealed the colocalization of BrdU and NeuN in the same cells in the periglomerular layer (Fig. 4L), confirming previous work (*11*).

The human RMS is organized around a tubular extension of the lateral ventricle that reaches the OB. We performed gross dissection of the OB that revealed that the rostral OB region contains a hollow ventricle (Fig. 5, A and B). At the light microscope level, the wall of the olfactory ventricle was a scant layer of cells, although some of the cells were aligned in an ependymal-like layer (Fig. 5C). Ultrastructural analysis also revealed a loose cell structure in the wall of the olfactory ventricle; cells in the wall of the ventricle were nonciliated. The core of the olfactory tract also contained a hollow tube with predominantly acellular walls and associated blood vessels (Fig. 5D). Immunohistochemistry for PCNA at various anatomical planes of the descending limb of the RMS also revealed the RMS to be organized around a hollow tubelike structure (Fig. 5E).

By using magnetic resonance imaging (MRI) scans, we observed a central high signal consistent with fluid in the center of the OB. Surrounding the central core there was low-signal (black) OB tissue that was in the shape of the OB overlying the cribriform plate (Fig. 5, F to H). The visualized (with MRI) olfactory ventricle measured about 7 mm in length (Fig. 5, F and G), with a transverse diameter of about 1.5 mm (Fig. 5H).

Ultrastructural studies reveal progenitors at all levels of the RMS that have migratory morphology. Next, we wanted to determine the cell types present in the human VONS compared with the rodent brain, focusing on the OB, the olfactory tract, and the AOC with light microscopy (LM) and transmission electron microscopy (TEM). Figure 6A shows the location of samples for TEM and LM examination. In the OB on the ventral side, there were numerous large glomerular structures that had a prominent nerve fiber with multiple smaller branches and abundant synapses (Fig. 6, B and C). In the core region of the OB, caudal to the olfactory ventricle, a large number of progenitor-like cells were observed that had round nuclei and widespread euchromatin. These cells tended to be clustered in comparison with the mature cells in the OB that had irregularly shaped nuclei and predominantly heterochromatin (Fig. 6, D to G). The olfactory tract also contained numerous round progenitor cells that often appeared in groups (Fig. 6H). LM and TEM examination of longitudinal olfactory tract sections revealed groups of cells with elongated nuclei that were always oriented in the long axis of the olfactory tract (Fig. 6, I to K). In longitudinal sections, the cells often overlapped each other (Fig. 6I), and the leading end of the cells was usually prominent and for the most part free of organelles (Fig. 6J). EM of the longitudinally cut

tract revealed that progenitor cells had a pointed, narrow leading process that contained a few mitochondria, whereas the trailing area of the cell was densely packed with cell organelles and was much wider than the leading process (Fig. 6K). In the AOC, progenitor cells were present in a single layer (Fig. 6L). Collectively, progenitor cells in the RMS share some ultrastructural features with cells undergoing chain migration in the rodent RMS

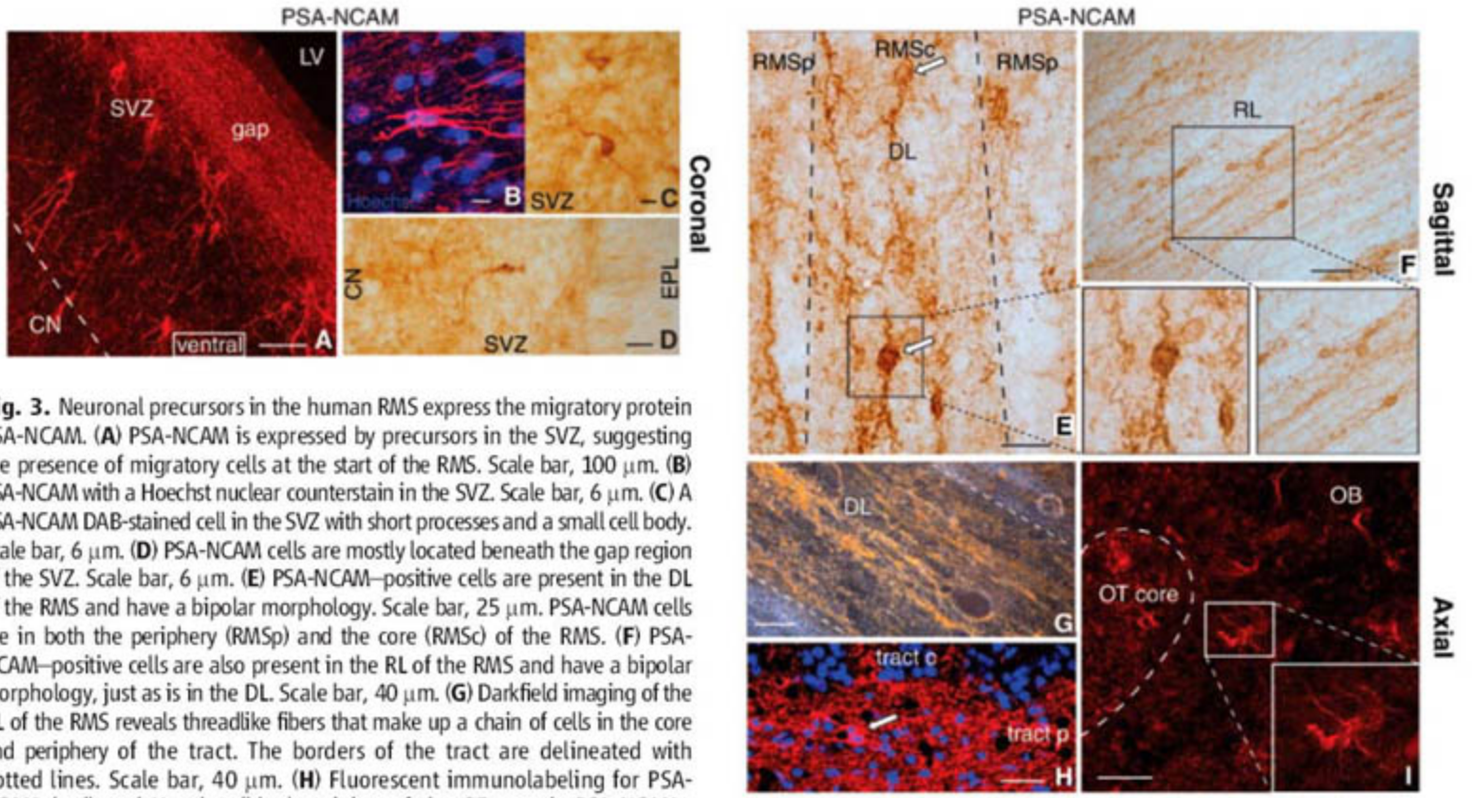

Fig. 3. Neuronal precursors in the human RMS express the migratory protein PSA-NCAM. (**A**) PSA-NCAM is expressed by precursors in the SVZ, suggesting the presence of migratory cells at the start of the RMS. Scale bar, 100 μm. (**B**) PSA-NCAM with a Hoechst nuclear counterstain in the SVZ. Scale bar, 6 μm. (**C**) A PSA-NCAM DAB-stained cell in the SVZ with short processes and a small cell body. Scale bar, 6 μm. (**D**) PSA-NCAM cells are mostly located beneath the gap region of the SVZ. Scale bar, 6 μm. (**E**) PSA-NCAM–positive cells are present in the DL of the RMS and have a bipolar morphology. Scale bar, 25 μm. PSA-NCAM cells are in both the periphery (RMSp) and the core (RMSc) of the RMS. (**F**) PSA-NCAM–positive cells are also present in the RL of the RMS and have a bipolar morphology, just as is in the DL. Scale bar, 40 μm. (**G**) Darkfield imaging of the DL of the RMS reveals threadlike fibers that make up a chain of cells in the core and periphery of the tract. The borders of the tract are delineated with dotted lines. Scale bar, 40 μm. (**H**) Fluorescent immunolabeling for PSA-NCAM (red) and Hoechst (blue) staining of the OT reveals PSA-NCAM–positive cells in the OT periphery (tract p, arrow). Scale bar, 25 μm. (**I**) The OT core and the OB have many PSA-NCAM–positive cells; in the bulb, the cells are more randomly oriented and larger than in the tract, suggesting early stages of maturation (high-magnification inset). Scale bar, 40 μm.

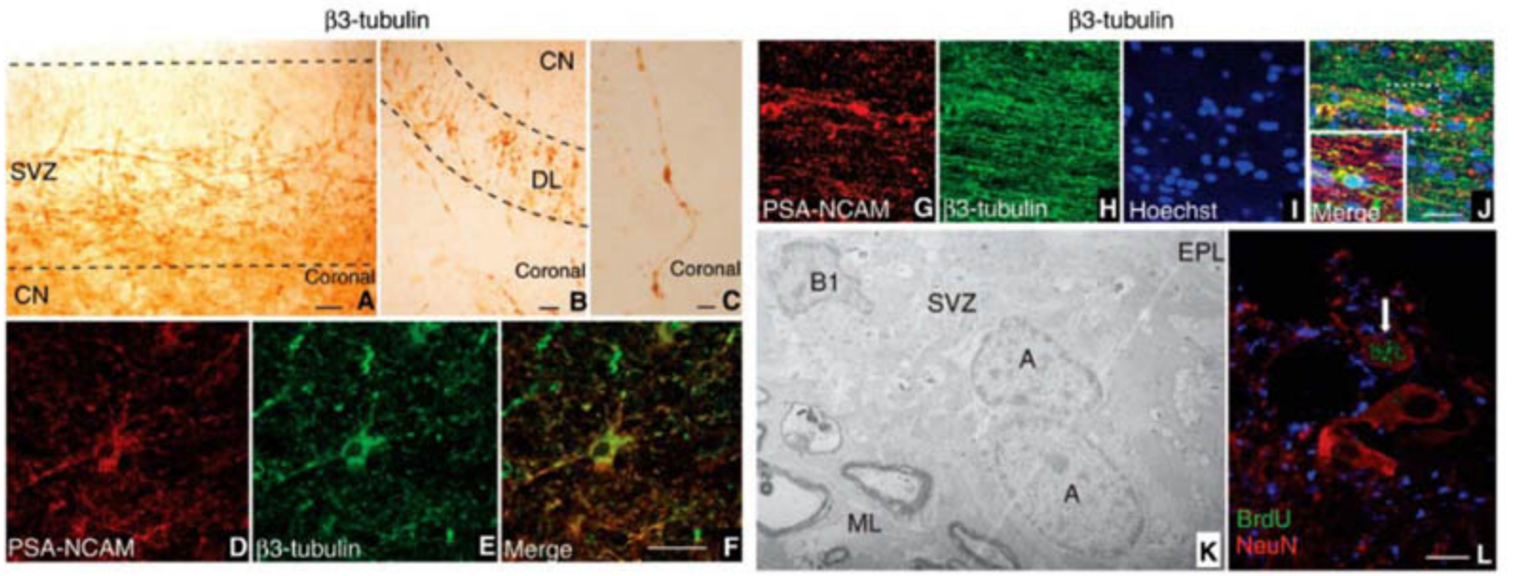

Fig. 4. Immature neurons that express both βIII-tubulin and PSA-NCAM are present in the RMS, and some mature in the olfactory bulb and express NeuN. (**A**) The immature neuronol marker βIII-tubulin forms a meshwork in the SVZ beneath the gap region. Scale bar, 20 μm. (**B**) The DL of the RMS has a bundle of βIII-tubulin fibers that follow the same path as the PSA-NCAM–positive cells. Scale bar, 20 μm. (**C**) High magnification of a βIII-tubulin–positive cell that reveals a cell body and two long processes that are oriented along the long axis of the DL of the RMS. Scale bar, 10 μm. (**D**) PSA-NCAM and (**E**) βIII-tubulin are colocalized in the same cell in the SVZ, as evidenced by the merged picture in (**F**). Scale bar, 20 μm. In the OT, (**G**) PSA-NCAM, (**H**) βIII-tubulin, and (**I**) Hoechst are colocalized (**J**) in the same cell in the periphery of the tract. Scale bar, 25 μm. (**K**) The rodent SVZ is enriched in type A cells that have an ultrastructure corresponding to the PSA-NCAM–positive cells that migrate in the RMS. This is an electron photomicrograph of cells in the human SVZ. Type A cells had an elongated cell body and smooth contour. Their nuclei contained lax chromatin with one or two small nucleoli. They were located between the myelin layer (ML) and ependymal layer (EPL). Positioned at the interface of the SVZ and myelin layer were type B1 cells. These cells contained irregular nuclei with frequent invaginations and clumped chromatin. (**L**) A cell expressing the mature neuronal marker NeuN (red) and the thymidine analog BrdU (green), indicating that adult-born neurons exist in the OB. Scale bar, 10 μm.

(*7*). Furthermore, immuno-TEM revealed that the cells with a migratory-like morphology were also positive for PSA-NCAM (fig. S3). There was an electron-dense cell membrane as a result of the PSA-NCAM contrasting; furthermore, there were many contrasted processes showing immunopositivity for PSA-NCAM (fig. S3). In the AOC, the progenitor cells were plentiful and tightly packed together with myelinated nerve fibers and mature cells.

Pax6, Olig 2, and DCX gene expression is consistent with differentiation along the VONS. Next, we investigated the differential gene expression pattern in different parts of the olfactory system. We performed reverse transcription polymerase chain reaction (RT-PCR) on fresh human brain homogenates from the AOC, the olfactory tract, and the OB. We chose to examine messenger RNA (mRNA) for three factors that regulate differentiation of olfactory neurons: Pax6, which induces differentiation; Olig2, which inhibits differentiation; and double cortin (DCX), which promotes cell migration (Fig. 6, M and N). Glyceraldehyde-3-phosphate dehydrogenase (GAPDH) was used as an internal control (*12*–*14*). As expected, Pax6 was highly expressed in the OB and weakly expressed in the AOC and the olfactory tract (Fig. 6M). This is consistent with previous studies showing the importance of Pax6 for the fate specification of progenitor cells into periglomerular neurons in the OB (*12*). In contrast, expression of Olig2, a transcription factor thought to inhibit olfactory neuron differentiation, was much higher in the olfactory tract compared with in the OB (Fig. 6M). RT-PCR for DCX revealed extensive expression in each region of the VONS examined, although the expression was higher in the OB than in the olfactory tract and the AOC (Fig. 6M). In the rodent brain, DCX is expressed throughout the olfactory system by progenitor cells that are migrating from the SVZ toward the OB (*15*). Therefore, it is not surprising that we see DCX mRNA evenly abundant in all regions of the VONS in the human brain. To confirm the PCR results, we immunostained various parts of the VONS with antibodies to Pax6, Olig2, and DCX (fig. S4).

Our work demonstrates a remarkable similarity between human and rodent olfactory systems. However, because of the pronounced enlargement of the frontal cortex in the human forebrain, most of the rostral CN, SVZ, and frontal cortex are located at levels rostral to the olfactory tubercle. The RMS in the human brain must, therefore, take a caudal path before entering the olfactory tract. In fact, forward rotation of the rodent forebrain by about 75° shows the RMS to be situated in an orientation comparable to that of the human; the larger frontal cortex and relatively smaller OB in the human accounts for this geometric difference between the human and the rodent RMS. Because the human RMS is relatively small and takes a caudal path before entering the olfactory tract (Fig. 1C), rigorous serial sagittal sectioning of whole forebrains was required to see the long axis of it (for example, Fig. 1A versus Fig. 2C). Previous attempts to find a human RMS (*16*) were probably unsuccessful because of the use of coronal sections in these studies. Our group has the access to large numbers of normal, well-preserved, perfused, whole human brains that was necessary for this extensive analysis of the VONS.

The VONS contains an extension of the lateral ventricle, the ventriculo-olfactory extension (VOE), that appears to be fluid-filled and is connected via a patent duct to the OB in the ventral forebrain. Thus, it appears that the human brain contains a continuous SVZ organized around the VOE that connects the lateral and the olfactory ventricles. The organization of the RMS around the VOE could support the notion that the migration of neuroblasts may be influenced by CSF circulation, as recently suggested (*17*).

Progenitor cells in the human VONS express PSA-NCAM and DCX, two proteins important for cell migration in the rodent RMS (*18*–*20*). These cells have many ultrastructural characteristics that have previously been used as reliable indicators of neuroblast migration in the rodent RMS (*17*, *21*). The close association of the progenitor cells to one another suggests that the progenitors may migrate in chains, as in rodents; alternatively, the progenitors may use the extracellular matrix surrounding the VOE (*21*). On the basis of the morphological characteristics of cells within the human VONS, the expression of migratory proteins, the orientation of the leading processes in the direction of migration, and the emergence of new neurons in the OB, we conclude that the cells within the human VONS probably undergo directed migration toward the OB. Studies in higher mammals have established that insults to the brain can induce neurogenesis via the recruitment of progenitor cells from the RMS (*22*). Our study

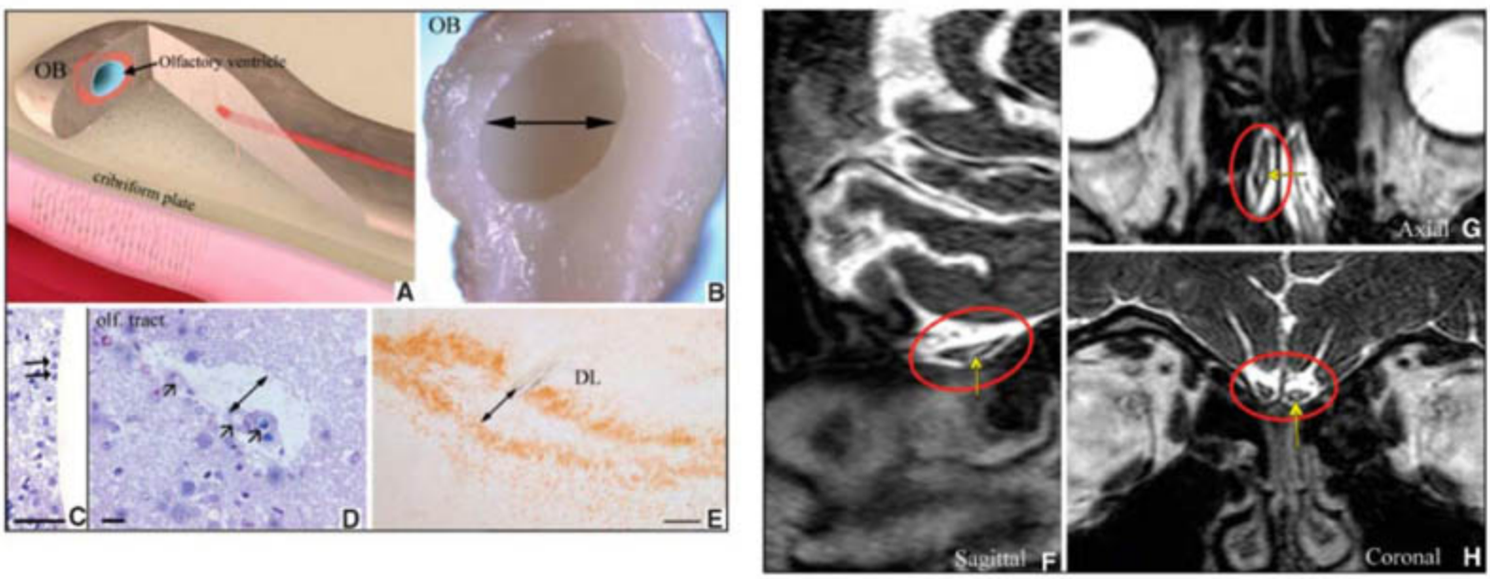

Fig. 5. The OB contains a hollow CSF-filled ventricle. (**A**) Diagram showing the hollow OB and part of the human olfactory sytem. (**B**) Dissections of the human OB reveal a hollow OB. The double arrow indicates the width of the olfactory ventricle. (**C**) LM of thin Richardson-stained sections showing unciliated, loosely packed cells in the olfactory ventricle wall (arrows). Scale bar, 100 μm. (**D**) Cross sections of the OT core reveal a hollow tube (double arrow). Blood vessels are indicated by single arrows. Scale bar, 10 μm. (**E**) A coronal, PCNA-stained section reveals a tubelike structure (double arrow) in the DL of the human RMS. Scale bar, 50 μm. (**F**) Sagittal, high-resolution heavily T2-weighted MR images of the rostral part of the human forebrain reveal that the elongated olfactory ventricle is in fact fluid-filled (arrow and red ring around the OB). (**G**) Axial MR image demonstrates fluid in the OB ventricle (red ring around the OB and arrow pointing to the central fluid compartment). (**H**) Coronal MR image shows two small fluid-filled compartments, one in each OB (red ring around the OB and arrow indicating the central fluid compartment).

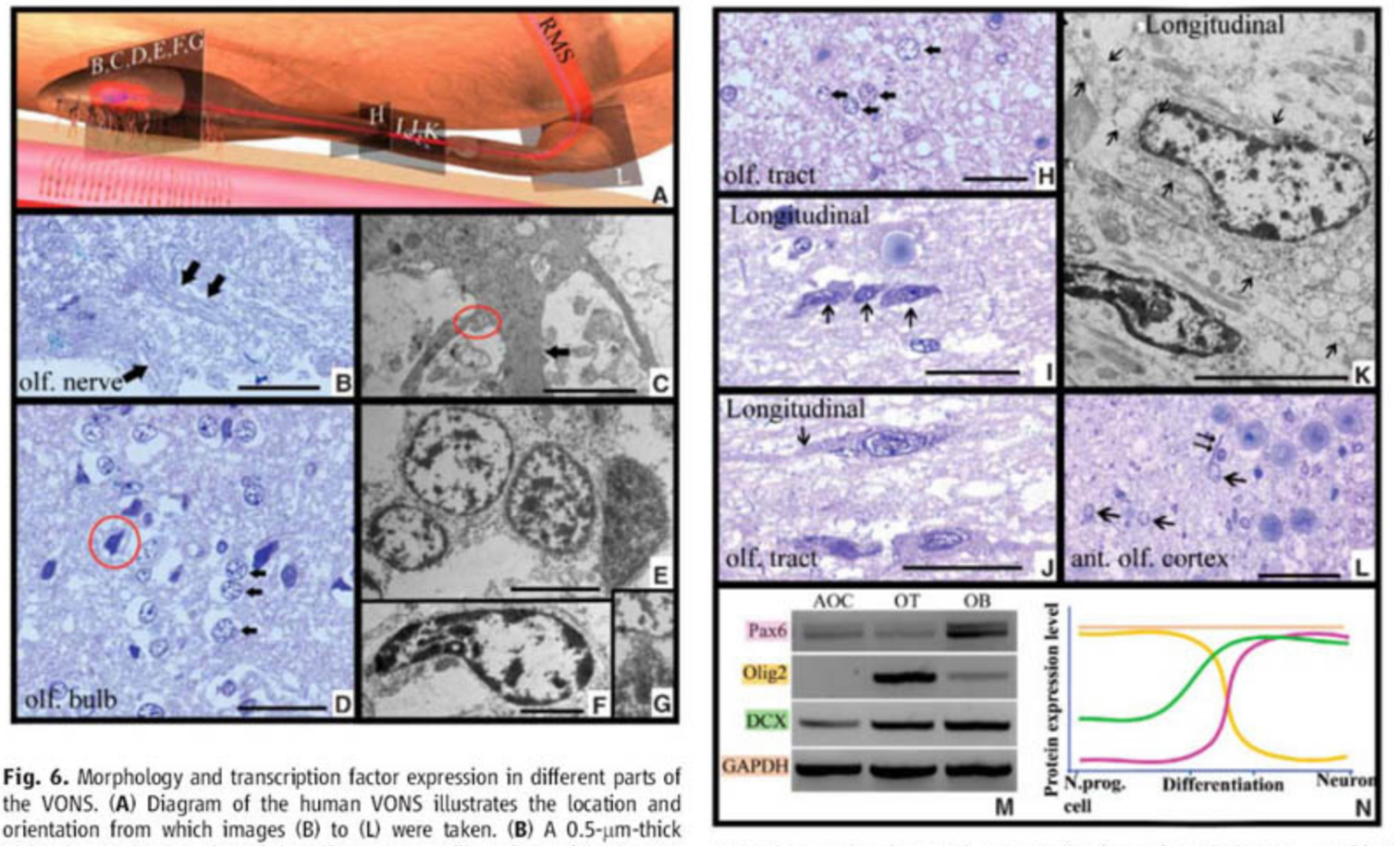

Fig. 6. Morphology and transcription factor expression in different parts of the VONS. (**A**) Diagram of the human VONS illustrates the location and orientation from which images (B) to (L) were taken. (**B**) A 0.5-μm-thick Richardson-stained section of the olfactory nerve fibers (arrows) in the OB. Scale bar, 100 μm. (**C**) Fibers of an olfactory nerve close to the surface of the OB (arrow) and a synapse with another nerve fiber (red ring). Scale bar, 2 μm. (**D**) The central region of the OB core contains progenitors (arrows) and more mature cells with irregularly shaped and densely stained nuclei (red ring). Scale bar, 100 μm. (**E**) Progenitor cells (three cells to the left) with aligned euchromatin and a mature cell (right) with heterochromatin and an irregular nucleus. Scale bar, 5 μm. (**F**) A mature cell with dense chromatin and an irregular nucleus, features of type B2 astrocytic cells. Scale bar, 2 μm. (**G**) The interface between an active (young) cell and an inactive (old/heterochromatin) cell is made clear by the nuclear density. (**H**) The OT contains round progenitor cells (arrows) that appear to be clustered together. Scale bar, 25 μm. (**I**) Progenitor cells with migratory features: elongated cell bodies and nuclei close to each other, with the leading process of one progenitor overlapping another progenitor (arrows). Scale bar, 25 μm. (**J**) A long leading process on a progenitor cell in the OT (arrow). The nucleus is elongated in the direction of the tract. Scale bar, 25 μm. (**K**) The ultrastructure of an elongated progenitor cell. The cells have an oval-shaped nucleus (in this plane), and cytoplasmic organelles are mostly located in the thickened trailing component of the cell (arrows indicate the cell membrane). Scale bar, 5 μm. (**L**) The AOC has many nerve fibers (parallel pair of arrows). The progenitor cells are present in one layer (single arrows). Scale bar, 100 μm. (**M**) Pax6 mRNA is highly expressed in the OB but not in the AOC or the OT. Olig2 is highly expressed in the OT and weakly expressed in the OB. DCX mRNA is expressed in AOC, OT, and OB. The housekeeping gene GAPDH is expressed equally in each region examined. (**N**) Scheme illustrating the relative abundance of Pax 6, Olig2, and DCX during the differentiation of progenitor cells.

provides a foundation for this possibility in the adult human brain.

The olfactory system has evolved as an important survival system to detect signs of danger such as smoke or contaminated food. The addition of new neurons in the human OB in adulthood may contribute to plasticity in this system. In rodents, the turnover of neurons in the adult OB is regulated by experience and modulates the circuitry in response to external stimuli. Some indications on the functional role of adult OB neurogenesis in humans may be gained from pathological conditions. Progenitor proliferation in the SVZ and neuroblast migration is reduced both in animal models and in patients with Parkinson's disease (*23*, *24*). Reduced OB neurogenesis in rodents results in impaired odor discrimination (*25*), a common and early sign of Parkinson's disease in humans. The presence, but also the function, of adult neurogenesis may be conserved from lower mammals to humans.

References and Notes

1. Brain Atlas of the Domestic Rabbit, www.brainmuseum.org/Specimens/lagomorpha/domesticrabbit/sections/thumbnail.html.
2. A. S. Rae, *Clin. Neuropathol.* **13**, 17 (1994).
3. G. Tomasevic, F. Kamme, T. Wieloch, *Mol. Brain Res.* **60**, 168 (1998).
4. A. Bedard, M. Levesque, P. J. Bernier, A. Parent, *Eur. J. Neurosci.* **16**, 1917 (2002).
5. L. Bonfanti, *Prog. Neurobiol.* **80**, 129 (2006).
6. F. Doetsch, J. M. Garcia-Verdugo, A. Alvarez-Buylla, *J. Neurosci.* **17**, 5046 (1997).
7. C. Lois, J. M. Garcia-Verdugo, A. Alvarez-Buylla, *Science* **271**, 978 (1996).
8. M. A. Curtis, H. J. Waldvogel, B. Synek, R. L. Faull, *J. Chem. Neuroanat.* **30**, 55 (2005).
9. F. Dolbeare, *Histochem. J.* **27**, 339 (1995).
10. F. Dolbeare, *Histochem. J.* **28**, 531 (1996).
11. A. Bernard, A. Parent, *Dev. Brain Res.* **19**, 159 (2004).
12. M. A. Hack *et al.*, *Nat. Neurosci.* **8**, 865 (2005).
13. M. Kohwi, N. Osumi, J. L. Rubenstein, A. Alvarez-Buylla, *J. Neurosci.* **25**, 6997 (2005).
14. A. Lee *et al.*, *Ann. Neurol.* **53**, 668 (2003).
15. J. P. Brown *et al.*, *J. Comp. Neurol.* **467**, 1 (2003).
16. N. Sanai *et al.*, *Nature* **427**, 740 (2004).
17. K. Sawamoto *et al.*, *Science* **311**, 629 (2006); published online 11 January 2006 (10.1126/science.1119133).
18. G. Chazal, P. Durbec, A. Jankovski, G. Rougon, H. Cremer, *J. Neurosci.* **20**, 1446 (2000).
19. H. Koizumi *et al.*, *Nat. Neurosci.* **9**, 779 (2006).
20. P. J. Ocbina, M. L. Dizon, L. Shin, F. G. Szele, *Mol. Cell. Neurosci.* **33**, 126 (2006).
21. B. T. Schaar, S. K. McConnell, *Proc. Natl. Acad. Sci. U.S.A.* **102**, 13652 (2005).
22. A. Arvidsson *et al.*, *Nat. Med.* **8**, 963 (2002).
23. G. U. Höglinger *et al.*, *Nat. Neurosci.* **7**, 726 (2004).
24. N. Freundlieb *et al.*, *J. Neurosci.* **26**, 2321 (2006).
25. P. M. Lledo, M. Alonso, M. S. Grubb, *Nat. Rev. Neurosci.* **7**, 179 (2006).

26. We thank J. F. Westin for assistance with the illustrations; G. Rougon for donation of the PSA-NCAM antibody; the Neurological Foundation of New Zealand for their support of M.A.C. as a Wrightson Postdoctoral Fellow and M.K. as a Miller Postgraduate Scholar; Swedish Medical Research

Council (project nos. 12X-1253 and K2002X-72X-10358-10A); Swedish Cancer Research Foundation (project no. 3911); Torsten och Ragnar Söderbergs Foundation; King Gustaf V:s and Drottning Victorias Foundation; Axel Linders Foundation; the Regional Developmental Board and the Chamber of Commerce and Industry in Western Sweden; Sahlgrenska Academy; the Neurological Foundation of New Zealand; the Health Research Council of New Zealand; the National Research Centre for Growth and Development, New Zealand; A.-M. Alborn, and J. Lind for the technical support; and J. Faijerson, M. Komitova, and G. Kuhn for scientific and technical advice.

Supporting Online Material
www.sciencemag.org/cgi/content/full/1136281/DC1
Materials and Methods
Figs. S1 to S5
Table S1

13 October 2006; accepted 24 January 2007
Published online 15 February 2007;
10.1126/science1136281
Include this information when citing this paper.

Predictions of the Properties of Water from First Principles

Robert Bukowski,[1] Krzysztof Szalewicz,[1] Gerrit C. Groenenboom,[2] Ad van der Avoird[2]

A force field for water has been developed entirely from first principles, without any fitting to experimental data. It contains both pairwise and many-body interactions. This force field predicts the properties of the water dimer and of liquid water in excellent agreement with experiments, a previously elusive objective. Precise knowledge of the intermolecular interactions in water will facilitate a better understanding of this ubiquitous substance.

Water has been extensively studied on account of its ubiquity and importance for so many aspects of human activity. The deceptively simple water molecule forms one of the most complex liquids and solids, and investigations continue to focus on all forms of pure water, including small clusters [e.g., (*1*, *2*)], bulk liquid [e.g., (*3*–*6*)], and a multitude of ice polymorphs. Similarly numerous are theoretical analyses of water, all of which require knowledge of the intermolecular potential (the derivatives of this potential give the force field that governs the dynamics). Most such investigations use empirical pair potentials fitted to reproduce certain measured bulk properties in Monte Carlo (MC) or molecular dynamics (MD) simulations of water. These "effective" potentials account for the important many-body interactions in water by (nonphysical) deformations of the true pair potential. The well-known result is that such potentials poorly describe the water dimer, give very inaccurate second virial coefficients, and fail to reproduce experimental spectra of small water clusters. Therefore, studies of molecular-scale properties of water with empirical potentials, such as the molecular jump mechanism of water reorientation (*7*), may suffer from an inadequate representation of the force field. Another known drawback of empirical potentials is that the quality of their predictions deteriorates quickly beyond the range of thermodynamic parameters used in the fitting procedure. Moreover, there does not appear to be any systematic method to improve the predictive accuracy of these potentials.

Another way of obtaining the force fields—which does not require prior knowledge of any experimental data—is by quantum mechanical ab initio calculations. Such an approach can provide the most reliable foundation for an understanding of water and other substances. However, the accuracy of ab initio force fields is limited by unavoidable approximations in the level of theory and incompleteness of basis sets.

A first-principles approach can proceed either "on the fly" (i.e., by computing the electronic energy for each configuration of the N molecules present in a simulation of bulk water, where N at least equals 32) or by computing the interaction energy as a sum of relatively simple analytic many-body potentials (pair, three-body, etc.) fitted beforehand to ab initio data. The former approach can be realized only with the fastest electronic structure methods such as density functional theory (DFT). Although for some time the published results suggested that this approach reproduced the properties of liquid water very well, recent work has shown that this agreement was due to fortuitous choices of the DFT functionals (*8*). Even for the same functional, different values of some parameters in the simulations may lead to markedly different predictions [e.g., the results in (*9*) and (*10*)]. Moreover, the current DFT approaches cannot describe the dispersion component of the intermolecular interaction energy, which is nonnegligible in water.

The many-body expansion of the potential requires ab initio calculations on dimers, trimers, and larger clusters. If the many-body expansion converges sufficiently rapidly, such calculations can be restricted to only a few small clusters and can make use of accurate electronic structure methods. In practice, the interaction energy must already be well reproduced at the three-body level, because calculations of the complete four-body potential for water would be too time-consuming. An important advantage of using the many-body expansion approach is that it can be systematically improved by extending the level of theory, using larger basis sets, calculating more grid points, and improving the form of the fitting function. A large number of ab initio water dimer potentials have been published [e.g., (*11*–*16*)]. However, so far no first-principles approach has simultaneously reproduced the experimental results for both the water dimer and the condensed phases of water. Here we present substantial progress toward this goal.

We developed a pair potential for water on the basis of the coupled cluster method with single, double, and noniterative triple excitations [CCSD(T)], generally regarded as the most accurate of practically applicable electronic structure methods. We have used the same set of 2510 carefully selected grid points as in the SAPT-5s potential developed previously by our group (*12*). The H_2O monomer was assumed to be rigid in the averaged ground-state vibrational geometry, as in (*12*). For each grid point, we first computed the interaction energies with the use of second-order perturbation theory based on the Møller-Plesset partitioning of the Hamiltonian (MP2). The MP2 energies were computed in augmented triple- and quadruple-zeta quality basis sets supplemented by midbond functions. The energies were then extrapolated to the complete basis set (CBS) limit by means of the well-established extrapolation formula that assumes a convergence rate proportional to the inverse third power of the cardinal number of the basis set. The CCSD(T) contribution beyond the MP2 level was computed in the triple-zeta quality basis set and added to the extrapolated MP2 values. We also performed single-point calculations in a quintuple-zeta quality basis. The basis set convergence patterns indicate that the uncertainty of the computed interaction energies is about 0.07 kcal/mol. For comparison, the uncertainty of the SAPT-5s potential was 0.3 kcal/mol. The accuracy of the current calculations is virtually the same as that of the most extensive published ab initio work [e.g., (*17*)]. However, the cited calculations have been performed only for a few selected geometries of the dimer, whereas we have obtained the complete six-dimensional potential surface.

[1]Department of Physics and Astronomy, University of Delaware, Newark, DE 19716, USA. [2]Theoretical Chemistry, Institute for Molecules and Materials, Radboud University Nijmegen, Toernooiveld 1, 6525 ED Nijmegen, Netherlands.

We fitted the computed interaction energies by an analytic potential function. The form of this function is analogous to that used for the SAPT-5s potential (*12*), except for an added "polarization" term to streamline molecular simulations. This term also fits the induction energy more accurately than did the site-site expansion used in SAPT-5s. A single polarizable center, almost identical to that used in the SAPT three-body potential of (*18*, *19*), was placed 0.1946906 Å away from the oxygen atom toward the hydrogens and had an isotropic polarizability of 9.922 $bohr^3$. During the fit of the asymptotic coefficients of the potential [in a manner analogous to (*12*)], the contribution of the polarization term was subtracted from the long-range interaction energies. The root-mean-square deviation (RMSD) of the fit for the points with negative energies was 0.09 kcal/mol. The analytic polarizable potential produced by this fit is hereafter termed CC-pol. The functional form of CC-pol represents a good compromise between the accuracy of reproducing the computed points and the simplicity needed for molecular simulations.

The CC-pol potential was used in nearly exact quantum mechanical calculations to predict the spectrum of the water dimer. The intermolecular vibrations of this dimer are strongly anharmonic, and its ro-vibrational levels are split by quantum mechanical tunneling between eight equivalent equilibrium geometries (*20*). The largest splitting $a(K)$ is due to the acceptor switching tunneling; smaller splittings i_1 and i_2 originate from the donor-acceptor interchange tunneling. The vibration-rotation-tunneling (VRT) levels for states with overall rotation quantum numbers J and K equal to 0, 1, and 2 were computed by an approach described in (*21*) that is similar to a coupled-channel scattering method, well converged with respect to the number of channels included. It has been shown (*22*) by calculations with various water potentials from the literature that the VRT levels of the water dimer are extremely sensitive to such details as the shape of the anharmonic potential wells and the barriers between these wells.

The CC-pol dimer levels agree very well with the levels deduced from the measured spectra, both for the ground state and for the excited intermolecular vibrations (Fig. 1). The only substantial error occurs for the interchange splitting $a(0) + a(1)$, which is 19% too large. This observable is particularly sensitive to monomer flexibility effects that decrease its value (*23*). Thus, rigid-monomer potentials such as CC-pol should overestimate this splitting.

The CC-pol prediction of the dimer spectra is markedly better than those of the earlier ab initio potentials: ASP-W, ASP-S, SAPT-5s, TTM2.1, and SDFT-5s (Table 1). The empirical TIP4P and MCY-KW potentials fail completely, even though the latter is polarizable and was partly fitted to ab initio data. The agreement of the CC-pol spectra with experiment represents an improvement over the predictions of the VRT(ASP-W)III potential, containing parameters fitted to these spectra. Only SAPT-5st, which was tuned to reproduce the measured splitting $a(0) + a(1)$, and VRT(MCY-5f) give somewhat better agreement with the measured dimer levels. The VRT(MCY-5f) potential is 12-dimensional (i.e., it includes flexible monomers), and all of its parameters were optimized to fit the H_2O dimer spectra. It has not yet been tested in simulations of liquid water (see below).

The second virial coefficient computed from CC-pol agrees very well with the compilation of experimental results by Harvey and Lemmon (*24*) (Fig. 2). For temperatures lower than 500 K, it proves even more accurate than SAPT-5s, which was sufficiently accurate to guide the experimental determination (*24*).

The CC-pol potential was also applied together with the SAPT three-body potential from (*18*, *19*) in NVE (constant number of particles,

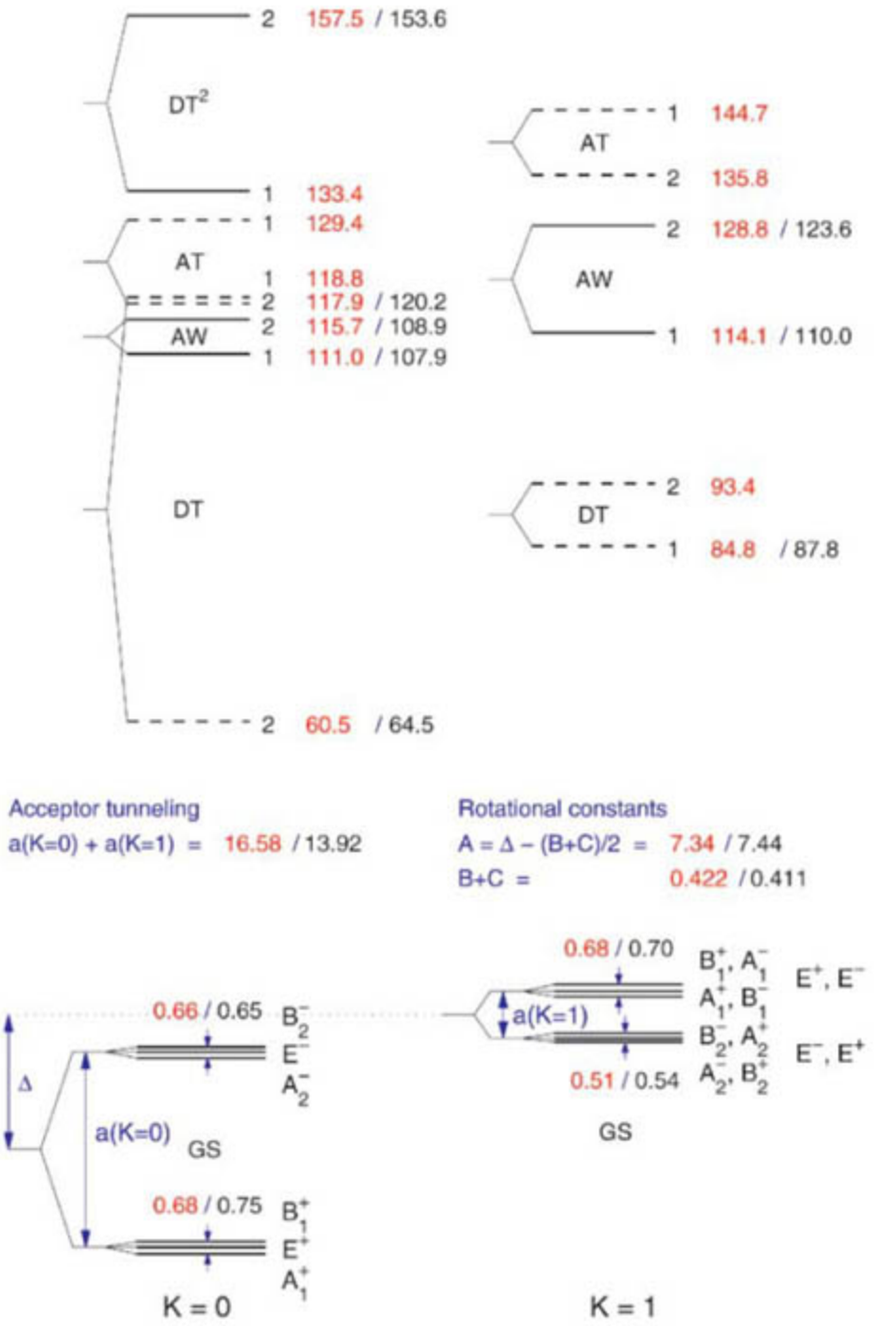

Fig. 1. VRT levels of the H_2O dimer (in cm^{-1}) from converged calculations with the CC-pol ab initio potential (first number, in red), in comparison with experimental data (*31*, *32*) (second number, in black). Virtually all the measured levels have been shown except for some data for the ground state nearly redundant with those presented. The symbols $A_i^{\pm}$ and $B_i^{\pm}$ are standard spectroscopic notations for VRT states [see (*21*)]. Abbreviations for modes: GS, ground state; DT, donor torsion; AW, acceptor wag; AT, acceptor twist; DT^2, donor torsion overtone. The individual GS splittings $a(K)$ for $K = 0$ and $K = 1$ could not be measured, so their sum is used in the comparison. The excited levels are drawn at a smaller energy scale than the GS levels and the small splittings are omitted, that is, the origins 1 and 2 (the averages of the $A_1^{\pm}$, $B_1^{\pm}$ and $A_2^{\pm}$, $B_2^{\pm}$ levels, respectively) are shown.

volume, and energy) MD simulations of liquid water in ambient conditions. The three-body potential used was fitted to ab initio calculations for the water trimer. It is the only such potential that includes three-body exchange terms in addition to polarization effects. The four- and higher-body effects were computed with the polarization model included in CC-pol (applying proper subtractions to avoid double counting of two- and three-body induction effects). Up to 512 molecules were used and the velocities were scaled during the equilibration to achieve the ambient temperature. Most calculations were performed with 256 molecules in a box size of 19.71 Å, corresponding to a density of 1 g/cm^3. The time step was 1 fs and the simulation time was 30 ps, including a 10-ps equilibration period. The radial atom-atom distribution functions g_{XY} obtained in these simulations are shown in Fig. 3. The simulations with only the pair potential result in g_{XY} values quite different from the measured ones, thus revealing the crucial role of pair-nonadditive forces in water. Including the many-body nonadditive potential with the pair-only CC-pol potential (CC-pol+NB curves) strongly improves agreement with experiment. In particular, the positions of the minima and maxima on the g_{OO} curve, which are measured most accurately, are in near-perfect agreement. The g_{OH} and g_{HH} functions from CC-pol+NB calculations reproduce the experiment equally well. The CC-pol+NB(ind) model—which represents both the pair and many-body polarization effects just by the simple polarization term in CC-pol—also gives g_{XY} functions that agree very well with experiment. This observation is encouraging because many-body effects beyond the polarization model are very difficult to compute. We note that the agreement is likely as good as possible considering the neglected quantum and monomer-flexibility effects. In particular, there are indications (*10*) that the latter make the first minimum in g_{OO} deeper, which would improve the agreement with experiment, although quantum effects (*25*) may partly cancel this trend.

The g_{XY} functions obtained from CC-pol reproduce the experimental data virtually as well as the empirical potentials fitted to bulk water observables. We computed RMSDs from experiment for three characteristic points on each curve: first maximum, first minimum, and second maximum. This quantity amounts to 0.13 for CC-pol and 0.15 for TIP4P (*26*).

The empirical potentials fitted to spectral data were recently used in simulations of liquid water with the many-body effects described only by a simple classical polarization model (*27*). The empirical VRT(ASP-W)III potential performed rather well. Thus, among all published potentials, VRT(ASP-W)III provides the best overall (i.e., for both clusters and liquid water) agreement with experiment. Although VRT(ASP-W)III gave radial distribution functions in good agreement with experiment, overall the CC-pol potential compares more favorably. The RMSD for the three characteristic points on the three g_{XY} VRT(ASP-W)III curves is 0.21. In particular, the first peak on the VRT(ASP-W)III g_{OO} curve is about 19% too low, whereas it is within 5% of experiment in the CC-pol simulation. The 12-dimensional VRT(MCY-5f) potential has not been used in simulations so far. Its rigid form with added polarization effects, VRT(MCY-5r/pol), performed poorly in simulations, producing pair distribution curves similar to those given by the two-body-only CC-pol (i.e., the dotted curves in Fig. 3). Also, SAPT-5st performed rather poorly in liquid water simulations, similarly to SAPT-5s.

We also computed the internal energy, the self-diffusion coefficient, and the coordination number of liquid water. The internal energy for the CC-pol+NB model is –10.89 kcal/mol, compared to the experimental value of –9.92 ± 0.3 kcal/mol [see (*28*)]. Our value is in still better agreement with experiment if the correction for quantum effects, equal to 0.86 kcal/mol (*25*), is added. The classical and quantum values for the TIP4P potential are –9.81 and –8.95 kcal/mol, respectively (*25*). For the diffusion coefficient, a value of 2.4×10^{-5} cm^2/s was obtained, in perfect agreement with experiment (*29*). This agreement is partly fortuitous, as quantum effects may increase the theoretical value by about 50% (*25*). The TIP4P potential gives the classical and quantum diffusion coefficients of 3.6×10^{-5} cm^2/s and 5.5×10^{-5} cm^2/s, respectively (*25*). The so-called coordination number was determined by integrating the function g_{OO} up to the first minimum. The result for the CC-pol+NB model is 5.6, whereas the experimental curve (*30*) gives 4.8. We have not calculated the number of hydrogen bonds for the CC-pol models, but such numbers are known for the SAPT-5s models (*18, 19*). We found that the number of hydrogen bonds is well correlated with the coordination number because hydrogen bonds lead to a more structured liquid and narrower g_{OO} peaks. For example, for the SAPT-5s+3B, SAPT-5s+NB, and SAPT-5s models, the numbers of hydrogen bonds are 3.31, 3.34, and 2.77, whereas the coordination numbers are 7.9, 8.6, and 11.3, respectively. Because the relation between the number of hydrogen bonds and the coordination number was found to be approximately linear, we

Table 1. Root-mean-square relative percentage errors in various properties of H_2O dimer from calculations with different potentials, compared with experimental data from (*31, 32*) and references therein. The following properties are used in this analysis: ground-state rotational constants A and $B + C$, ground state tunneling splittings $a(0) + a(1)$ (acceptor switch), i_1 and i_2 (donor acceptor interchange), and frequencies of the intermolecular vibrations DT, AW, AT, and DT^2 for $K = 0$ (see Fig. 1). For more information on these properties, see (*21*).

Potential	Rotational constants	Tunneling splittings	Vibrational frequencies
MCY-KW*	9.1	87	37
TIP4P†	14	81	23
ASP-W‡	7.4	325	17
ASP-S‡	5.2	110	15
TTM2.1§	16	72	12
VRT(ASP-W)III‖	6.6	38	7.1
SAPT-5s¶	4.9	26	7.8
SDFT-5s#	2.9	35	6.6
CC-pol	2.1	12	4.4
VRT(MCY-5f)**	3.8	11	1.7
SAPT-5st††	1.7	2.3	5.8

*From energy levels calculated in (*22*) with potential of (*33*). †From energy levels calculated in present work with potential of (*26*). ‡From energy levels calculated in (*22*) with potential of (*11*). §From energy levels calculated in present work using the potential of (*15*) with monomer geometries fixed in the equilibrium position. ‖From energy levels calculated in (*31, 32, 34*) using ASP-W potential form with parameters fitted to spectral data, except for rotational constants calculated in present work. ¶From energy levels calculated in (*21*) with potential of (*12*), excited levels calculated in present work. #From energy levels calculated in (*16*) and in present work with potential of (*16*). **From energy levels calculated in (*31, 32, 35*) using an extended MCY potential form with all parameters fitted to spectral data. ††From energy levels calculated in (*21*) with potential of (*12*) tuned to reproduce the measured interchange splitting $a(0) + a(1)$.

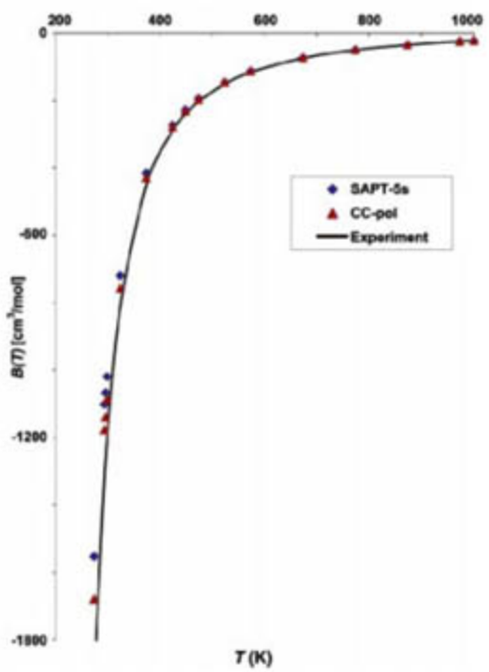

Fig. 2. Comparison of theoretical and experimental second virial coefficients. Theoretical data were computed including quantum effects to infinite order. Experimental data are from (*24*).

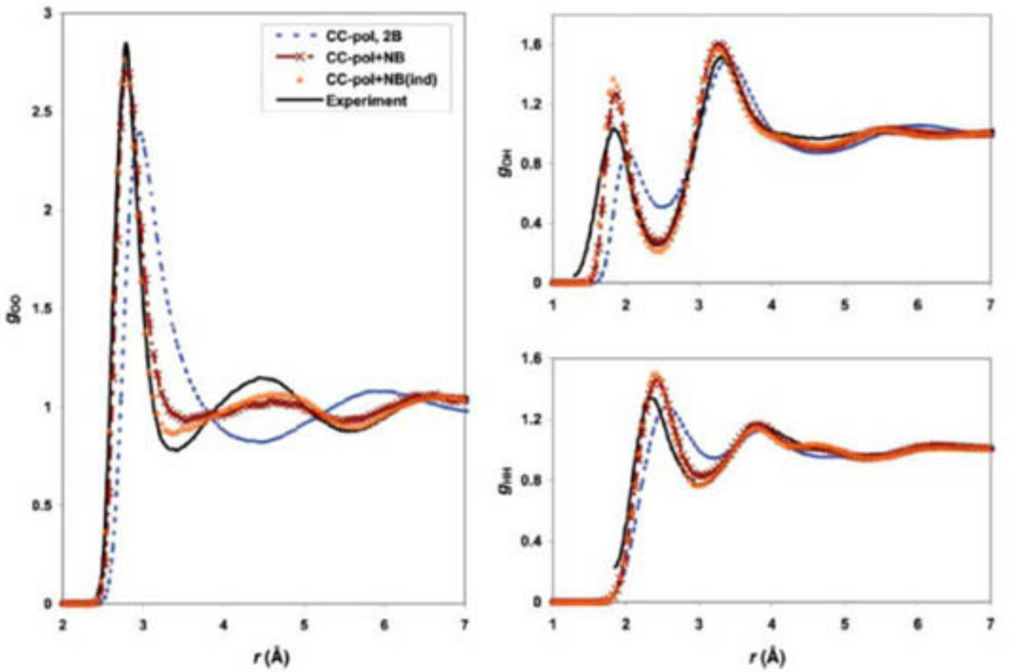

Fig. 3. Atom-atom radial distribution functions from MD simulations based on the CC-pol potential. See text for explanations of acronyms. The experimental curves are from (*30*).

could extrapolate this dependence to obtain 3.8 hydrogen bonds for the CC-pol+NB model. Thus, this model supports the standard picture of water, wherein each molecule is on average almost tetrahedrally coordinated, rather than the lower coordination geometry proposed in (*3*, *5*). With the use of only the CC-pol pair potential, the simulations gave a very large coordination number, 11.9 (the extrapolated number of hydrogen bonds equal to 2.7). Hence, the many-body interactions play an important role in determining the structure of liquid water, particularly in predicting tetrahedral coordination.

The ab initio water pair potential developed in this work recovers well a diverse range of experimental data from water dimer to liquid water. It predicts dimer spectra and second virial coefficients that not only agree well with existing experimental data, but also can be considered to complement experiments in spectral or temperature ranges inaccessible to measurement. When the CC-pol potential together with an earlier representation of three-body forces (*18*, *19*) was used in simulations of liquid water, the predictions agreed well with the neutron and x-ray diffraction data. These predictions, made entirely from first principles, are of comparable accuracy to results of simulations with empirical potentials fitted to liquid water experimental data.

We believe that the ab initio force field presented here will find numerous applications in predicting the properties of water. It can be used, for example, to resolve the current controversies about the coordination of water molecules in the liquid (*3*–*6*). The analysis of the temporal structures in MD simulations should provide the ultimate picture of liquid water. The force field can also be used to investigate the numerous polymorphic forms of ice. Important applications can be made in extreme regimes where empirical potentials fail completely, such as supercritical, overcooled, or confined water.

Further improvements in the first-principles predictions for water should take account of the monomer flexibility and of quantum effects in the liquid simulations. For the former case, the first step has recently been attained (*23*). Quantum effects in molecular simulations can be accounted for by either path-integral MC or centroid MD (*25*) methods.

References and Notes

1. K. Liu, J. Cruzan, R. Saykally, *Science* **271**, 929 (1996).
2. J. K. Gregory, D. C. Clary, K. Liu, M. G. Brown, R. Saykally, *Science* **275**, 814 (1997).
3. Ph. Wernet *et al.*, *Science* **304**, 995 (2004); published online 1 April 2004 (10.1126/science.1096205).
4. J. D. Smith *et al.*, *Science* **306**, 851 (2004).
5. A. Nilsson *et al.*, *Science* **308**, 793a (2005).
6. J. D. Smith *et al.*, *Science* **308**, 793b (2005).
7. D. Laage, J. T. Hynes, *Science* **311**, 832 (2006); published online 25 January 2006 (10.1126/science.1122154).
8. J. VandeVondele *et al.*, *J. Chem. Phys.* **122**, 014515 (2005).
9. M. Sharma, Y. Wu, R. Car, *Int. J. Quantum Chem.* **95**, 821 (2003).
10. M. Allesch, E. Schwegler, F. Gygi, G. Galli, *J. Chem. Phys.* **120**, 5192 (2004).
11. C. Millot, A. J. Stone, *Mol. Phys.* **77**, 439 (1992).
12. E. M. Mas *et al.*, *J. Chem. Phys.* **113**, 6687 (2000).
13. C. J. Burnham, S. S. Xantheas, *J. Chem. Phys.* **116**, 1500 (2002).
14. C. J. Burnham, S. S. Xantheas, *J. Chem. Phys.* **116**, 5115 (2002).
15. G. S. Fanourgakis, S. S. Xantheas, *J. Phys. Chem. A* **110**, 4100 (2006).
16. R. Bukowski, K. Szalewicz, G. C. Groenenboom, A. van der Avoird, *J. Chem. Phys.* **125**, 044301 (2006).
17. G. S. Tschumper *et al.*, *J. Chem. Phys.* **116**, 690 (2002).
18. E. M. Mas, R. Bukowski, K. Szalewicz, *J. Chem. Phys.* **118**, 4386 (2003).
19. E. M. Mas, R. Bukowski, K. Szalewicz, *J. Chem. Phys.* **118**, 4404 (2003).
20. R. S. Fellers, C. Leforestier, L. B. Braly, M. G. Brown, R. J. Saykally, *Science* **284**, 945 (1999).
21. G. C. Groenenboom *et al.*, *J. Chem. Phys.* **113**, 6702 (2000).
22. R. S. Fellers, L. B. Braly, R. J. Saykally, C. Leforestier, *J. Chem. Phys.* **110**, 6306 (1999).
23. K. Szalewicz, G. Murdachaew, R. Bukowski, O. Akin-Ojo, C. Leforestier, in *Lecture Series on Computer and Computational Science: ICCMSE 2006*, G. Maroulis, T. Simos, Eds. (Brill Academic, Leiden, Netherlands, 2006), vol. 6, pp. 482–491.
24. A. H. Harvey, E. W. Lemmon, *J. Phys. Chem. Ref. Data* **33**, 369 (2004).
25. L. Hernández de la Peña, P. G. Kusalik, *J. Chem. Phys.* **121**, 5992 (2004).
26. W. L. Jorgensen, J. Chandrasekhar, J. D. Madura, R. W. Impey, M. L. Klein, *J. Chem. Phys.* **79**, 926 (1983).
27. N. Goldman, C. Leforestier, R. J. Saykally, *Philos. Trans. R. Soc. London Ser. A* **363**, 493 (2005).
28. W. L. Jorgensen, *J. Chem. Phys.* **77**, 4156 (1982).
29. R. Mills, *J. Phys. Chem.* **77**, 685 (1973).
30. A. K. Soper, *Chem. Phys.* **258**, 121 (2000).
31. F. N. Keutsch, N. Goldman, H. A. Harker, C. Leforestier, R. J. Saykally, *Mol. Phys.* **101**, 3477 (2003).
32. F. N. Keutsch *et al.*, *J. Chem. Phys.* **119**, 8927 (2003).
33. S. Kuwajima, A. Warshel, *J. Phys. Chem.* **94**, 460 (1990).
34. N. Goldman *et al.*, *J. Chem. Phys.* **116**, 10148 (2002).
35. C. Leforestier, F. Gatti, R. Fellers, R. Saykally, *J. Chem. Phys.* **117**, 8710 (2002).

36. We thank C. Leforestier for many discussions of the water dimer spectra. Supported by NSF grants CHE-0239611 and CHE-0555979.

16 October 2006; accepted 26 January 2007
10.1126/science.1136371

The Focusing of Electron Flow and a Veselago Lens in Graphene *p-n* Junctions

Vadim V. Cheianov,[1*] Vladimir Fal'ko,[1] B. L. Altshuler[2,3]

The focusing of electric current by a single *p-n* junction in graphene is theoretically predicted. Precise focusing may be achieved by fine-tuning the densities of carriers on the *n*- and *p*-sides of the junction to equal values. This finding may be useful for the engineering of electronic lenses and focused beam splitters using gate-controlled *n-p-n* junctions in graphene-based transistors.

There are many similarities between optics and electronics. Rays in geometrical optics are analogous to classical trajectories of electrons, whereas electron de Broglie waves can interfere. The electron microscope is one example of the technological implementation of this similarity. The analogy with optics may also hold considerable potential for semiconductor elec-

tronics. In optics, transparent interfaces between materials are used in lenses and prisms to manipulate light beams. So far, interfaces have played a rather different role in semiconductors, where the central place was, for a long time, occupied by the *p-n* junction (PNJ). As a result of a depletion region near the contact between two semiconductors with different types of charge carriers (and a large energy gap), conventional PNJs are not suitable for precision manipulation of electron beams, which, if realized, may lead to a new functionality in microelectronics. From this perspective, a lot of promise is offered by the recently discovered (*1*) two-dimensional (2D) gapless semiconductor, graphene (*2*). Fine-tuning of the carrier density in graphene by means of electrical gates (*3*–*5*) or doping of the underlying substrate (*6*) was demonstrated, thus paving the way toward controllable ballistic PNJs. On the one hand, the PNJ in graphene is highly transparent for the charge carriers (*7*, *8*). On the other, the transmission of electrons through the *p-n* interface may resemble optical refraction (*9*) at the surface of metamaterials with negative refractive index (*10*–*12*): The straight interface is able to focus electric current, whereas a ballistic stripe of *p*-type graphene separating two *n*-type regions acts as a lens.

A feature of the band structure of graphene [monolayer of graphite (*2*, *13*)] is that its valence band (π) and conduction band (π^*) touch each other. In the absence of doping, the Fermi level in graphene is at the energy that belongs to both bands and corresponds to the Bloch states in the corners of the hexagonal Brillouin zone of this 2D honeycomb crystal. For the states with a small quasi-momentum $\hbar\mathbf{k}$ counted from the corresponding corner of the Brillouin zone, the dispersion $\varepsilon(\mathbf{k})$ and group velocity $\mathbf{V} = d\varepsilon/d(\hbar\mathbf{k})$ of electrons are given by $\varepsilon_c(\mathbf{k}) = \hbar vk$, $\mathbf{V}_c = v\mathbf{k}/k$ in conduction band and $\varepsilon_v(\mathbf{k}) = -\hbar vk$, $\mathbf{V}_v = -v\mathbf{k}/k$ in valence band ($\hbar$ is Planck's constant, $h/2\pi$). Figure 1 illustrates such a dispersion for electrons in *n*-type graphene (on the left) and *p*-type graphene (on the right). In a split-gate structure (Fig. 1), voltages $\pm U$ applied to the two gates shift the degeneracy point of the electron dispersion cones down by $\hbar vk_c$ on the left and up by $\hbar vk_v$ on the right, thus forming a PNJ separating the *n*-region with the density of electrons $\rho_e = k_c^2/\pi$ and the *p*-region with the density of holes $\rho_h = k_v^2/\pi$. Here, $k_{c(v)}$ is the radius of the Fermi circle in the conduction (valence) band.

The transmission of charge through the PNJ bears resemblance to the refraction of light by left-handed metamaterials (*10*–*12*) with refractive index equal to −1. As a wave enters such a material, the relative direction of its group velocity **V** and the wave vector **k** of the wave reverses from parallel (in vacuum) to antiparallel. Therefore, upon refraction, the sign of the tangential velocity component of the propagating wave inverts, and the normal component remains the same. As a result, rays that diverge in vacuum become convergent after entering the metamaterial (*9*). For electrons in the PNJ, the Fermi momentum $k_{c(v)}$ plays the same role as the refractive index in geometrical optics, with the sign determined by the type of band—positive for the conduction band and negative for the valence band.

Indeed, let us consider, in Figs. 2A and 3A, a de Broglie wave of an electron approaching the PNJ from the *n*-side with the velocity $\mathbf{V} = (v\cos\theta_c, v\sin\theta_c)$ and the wave vector $\mathbf{k} = (k_c\cos\theta_c, k_c\sin\theta_c)$. At the interface, this wave is partly reflected to the state with the wave vector $\mathbf{k}' = (-k_c\cos\theta_c, k_c\sin\theta_c)$ and partly transmitted to the valence band state with the velocity $\mathbf{V} = (v\cos\theta_v, v\sin\theta_v)$ and the wave vector $\mathbf{k} = (-k_v\cos\theta_v, -k_v\sin\theta_v)$ on the *p*-side. For a sharp PNJ, the probability of the transmission is $\cos^2\theta_c/\cos^2(\frac{1}{2}\theta_c + \frac{1}{2}\theta_v)$ (*7*, *8*). Because the component of the electron momentum along a straight interface should be conserved, $k_c\sin\theta_c = -k_v\sin\theta_v$, which determines Snell's law for transmitted electrons.

$$\frac{\sin\theta_c}{\sin\theta_v} = -\frac{k_v}{k_c} = n \qquad (1)$$

The negative sign of *n* in Eq. 1 implies that the PNJ transforms a divergent flow of electrons emitted by a source on the *n*-side into a convergent flow on the *p*-side. This results in focusing (Fig. 2A) for a symmetric junction, $\rho_h = \rho_e$ corresponding to $n = -1$. Under the latter condition, electrons injected at $(-a,0)$ in the *n*-region at the Fermi energy meet again in a symmetric spot at $(a,0)$.

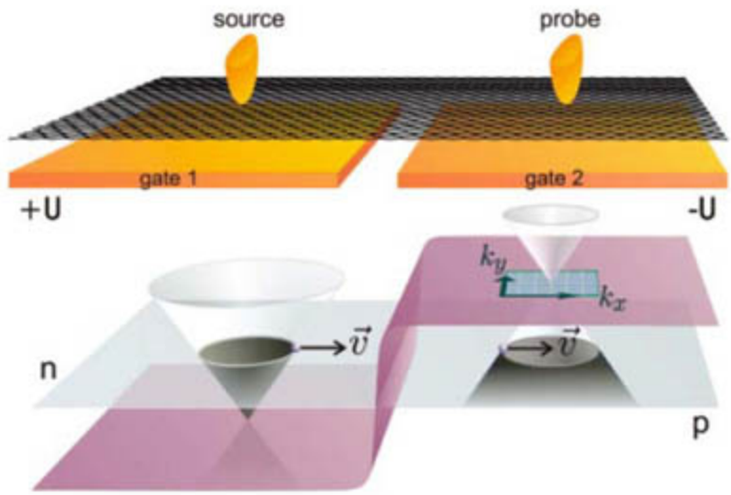

Fig. 1. Graphene *p-n* junction (PNJ). Monolayer of graphite is placed over the split gate, which is used to create *n*- (**left**) and *p*-doped (**right**) regions. The energy diagram shows the position of the Fermi level with respect to the touching point of the valence and the conduction bands.

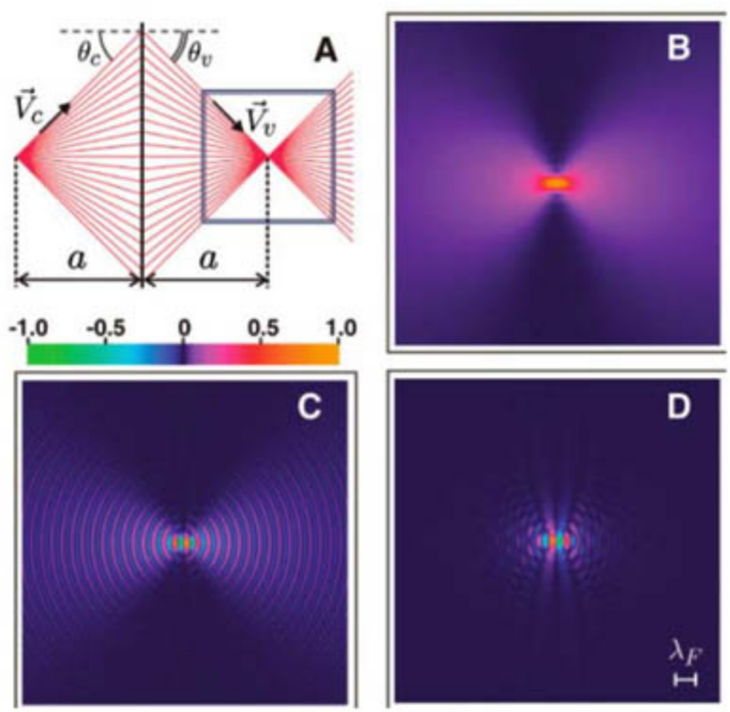

Fig. 2. Focusing of electrons by symmetric PNJ, $\rho_h = \rho_e$. (**A**) Classical trajectories of electrons diverging from a source at distance *a* from the junction become convergent after refraction. (**B**) Interference-induced pattern in the charge current near the focal image of the source-contact. (**C** and **D**) "Quantum mirage" in graphene. LDOS oscillations around the image of a perturbation applied on the other side of PNJ, created by (C) a small island of bilayer and (D) potential of a remote Coulomb charge.

[1]Physics Department, Lancaster University, Lancaster LA1 4YB, UK. [2]Physics Department, Columbia University, 538 West 120th Street, New York, NY 10027, USA. [3]NEC-Laboratories America, 4 Independence Way, Princeton, NJ 085540, USA.

*To whom correspondence should be addressed. E-mail: v.cheianov@lancaster.ac.uk

In an asymmetric junction (Fig. 3A) for, e.g., $n = -0.82$, which corresponds to $\rho_h/\rho_e = 0.67$, a sharp focus transforms into a pair of caustics that coalesce in a cusp—a singularity in the density of classical trajectories. Similar singularities in ray and wave optics were investigated and classified (*14*) with general catastrophe theory (*15*). Ballistic trajectories of electrons in the p-region of an asymmetric PNJ are rays $y = a\tan\theta_e + x\tan\theta_v$, where θ_v is related to θ_e by Eq. 1. The condition for a singularity, $\partial y/\partial\theta_e = 0$, determines the form of caustics $y_{caust}(x)$ as well as the position x_{cusp} of the cusp.

$$y_{caust}(x) = \pm\sqrt{\frac{(x^{2/3} - x_{cusp}^{2/3})^3}{n^2 - 1}},\ x_{cusp} = |n|a \quad (2)$$

To detect focusing by a single flat interface in graphene, one can use a small electric contact as a source of electrons while another local probe located on the p-side plays the role of a detector. Electric conductance between the two contacts would reflect the probability for a carrier to get from the source to the probe. When the concentration of carriers is low, their de Broglie wavelength is big enough to envisage contacts smaller than the wavelength. To study electron transmission in a phase-coherent system between contacts of such a small size, the above-described classical picture should be complemented with the analysis of quantum interference pattern of electron de Broglie waves. Figures 2B and 3B show the result of full quantum mechanical calculations of the current of electrons emitted at $(-a,0)$ and detected by a point contact near the focal point in the symmetric PNJ (Fig. 2B) and in the vicinity of a cusp (Eq. 2) that appears when the symmetry $\rho_h = \rho_e$ is lifted off (Fig. 3B). The calculation was performed by applying the Kubo formula to the single-particle Dirac-like Hamiltonian (*2*, *7*, *8*) of electrons in graphene. It is assumed that the sample is ballistic, that is, that both the elastic and inelastic mean free path of electrons is larger than the typical size of the structure. Around, but not too close to the focus ($k_v r >> 1$), the analytically calculated current is $j \sim (x-a)^2/r^3$ [$r = \sqrt{(x-a)^2 + y^2}$ stands for the distance from the probe to the focus]. The anisotropy of the current distribution is caused by the dependence of the transmission coefficient on the incidence angle and is smeared at shorter distances $k_v r < 1$. The current map calculated in the vicinity of the cusp for $\rho_h \neq \rho_e$ shows characteristic patterns described by the canonical diffraction function for this type of wave catastrophe (*14*). The maximum of the current would be when the probe is at the tip of the cusp, $(|n|a,0)$. The width y_* of the bright spot near the cusp (Fig. 3B) or the focus (Fig. 2A) in the y direction can be estimated as $y_* k_v \sim \max[1,(\frac{1}{2}ak_e|n^{-1} - n|)^{1/4}]$. For a junction with $|n| > 1$ ($\rho_h > \rho_e$), the pattern near the cusp is mirror-reflected as compared with that shown in Fig. 3B for $|n| < 1$.

It has been discovered (*16*) in the scanning tunneling microscopy (STM) studies of elliptically shaped corals on the surface of copper that the presence of an impurity at one focus of the ellipse is reflected by the STM map in the vicinity of the other focus. Therefore, oscillations of the local density of states of electrons formed around a static local perturbation (*17*) can be replicated through focusing by a carefully engineered fence of atoms. Similarly, focusing of electrons by a sharp PNJ in graphene could create a "mirage" that mimics the effect of a perturbation on the opposite side of the n-p interface. Consider, for example, a small island of a bilayer (*5*, *18*), which locally distinguishes between two sublattices (A and B) of the honeycomb lattice for electrons in the surrounding sheet [due to Bernal stacking of two adjacent monolayers (*19*, *20*)]. It induces a change in the local electron density of states (LDOS), which is different on sublattices A and B. The long-range oscillations of the alternating LDOS can be detected, with STM, as a difference of $\delta j_{A\text{-}B} \sim j^{(0)}_{A\text{-}B}\sin(2kr)/r$ between the tunneling current from the STM tip to the A and B sites. Figure 2C shows the results (obtained with the Green's

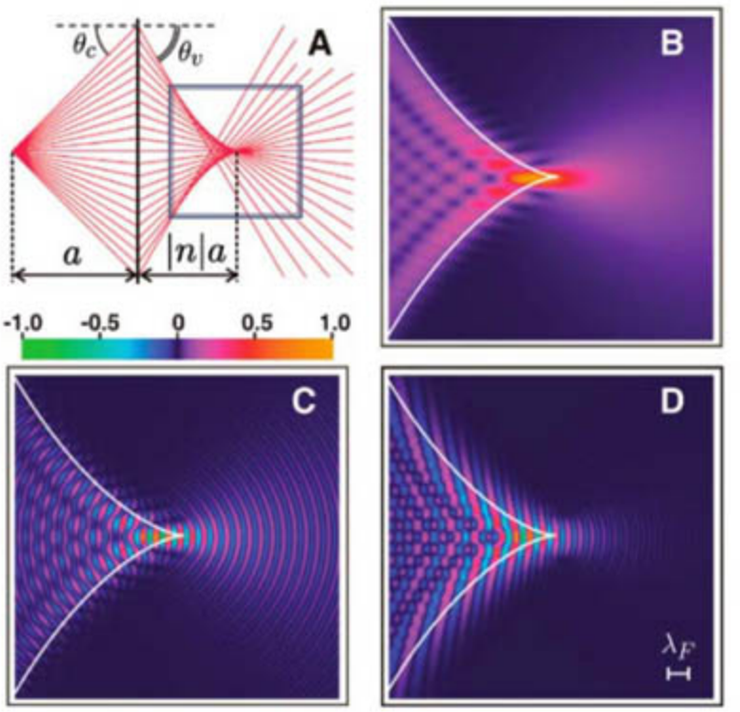

Fig. 3. Wave singularities in an asymmetric PNJ, $\rho_h/\rho_e = 0.67$. (**A**) Formation of caustics by refracted waves. (**B**) Characteristic interference pattern for the current near the cusp. (**C** and **D**) LDOS oscillations (in the region between caustics) created by (C) a small island of bilayer and (D) a remote Coulomb charge on the other side of PNJ.

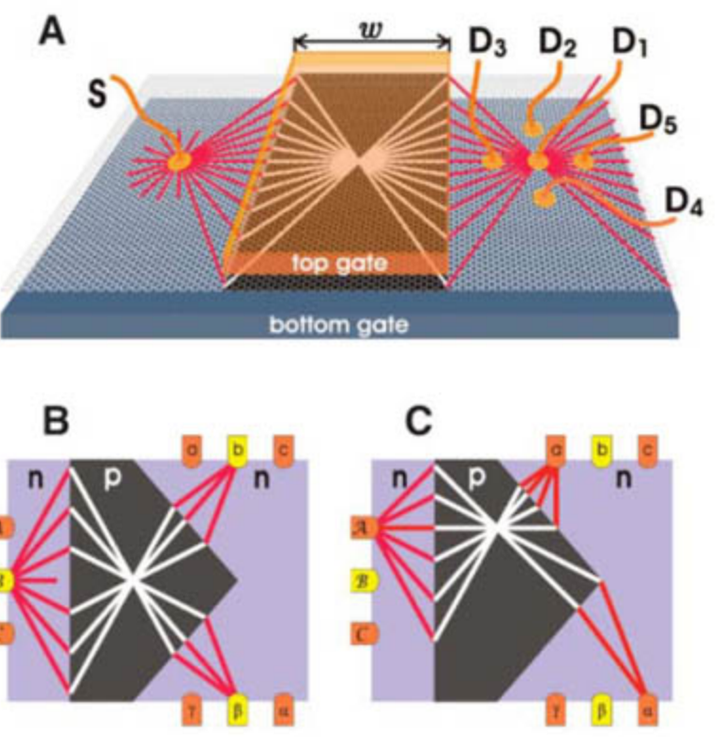

Fig. 4. (**A**) Electron Veselago lens and (**B** and **C**) prism-shaped focusing beam splitter in the ballistic n-p-n junction in graphene-based transistor.

functions technique) of a quantum-mechanical analysis of oscillations of $\delta j_{A\text{-}B}$ around the mirage image of a bilayer island formed on the other side of symmetric PNJ in the monolayer sheet. To compare Fig. 2D shows the calculated mirage image of a spike of electrostatic potential (smooth at the scale of the lattice constant in graphene), which induces LDOS oscillations equal on the two sublattices. The difference between these two images is caused by the lack of backscattering off A-B symmetric scatterers specific to graphene (*21*).

Unlike the ideal left-handed metamaterial (*10*), focusing in the PNJ is not perfect. In symmetric junctions, it occurs only for electrons exactly at the Fermi level, and it is spread into caustics for electrons excited to higher energies. Therefore, the sharpness of electron focusing decreases with temperature. If the focused electron flow is detected by a contact of size $d >> \lambda_F$, a pronounced signal in the focus will persist up to $T \sim \hbar v\, k_e d/a$. For example, in a ballistic structure with $a \sim 1$ μm, $d \sim 0.1$ μm, and $\rho_e = \rho_p \sim 3 \times 10^{12}$ cm^{-2}, focusing may persist up to the nitrogen temperature. The interference effects shown in Figs. 2 and 3 are washed out at a much smaller temperature scale, $T \sim \hbar v/a$.

Focusing of electrons by a sharp *p-n* junction in graphene can be used to turn the *n-p-n* junction into a Veselago lens for electrons. In such a device (Fig. 4A), the density of charge carriers in the *p*-region (with width w) can be controlled by the top gate. If the densities in the *n*- and *p*-regions are equal ($\rho_h = \rho_e$), charge carriers injected into graphene from the contact S shown in Fig. 4A would meet again in the focus at the distance $2w$ from the source (contact D_3 in Fig. 4A). Varying the gate voltage over the *p*-region changes the ratio $n^2 = \rho_h/\rho_e$. This enables one to transform the focus into a cusp displaced by about $2(|n| - 1)w$ along the x axis and, thus, to shift the strong coupling from the pair of leads SD_3 to either SD_1 (for $\rho_h < \rho_e$) or SD_5 (for $\rho_h > \rho_e$). Fig. 4, B and C, illustrate another graphene-based device in which a prism-shaped top-gate may be used as a focusing beam splitter. For example, electrons emitted from contact B (Fig. 4B) are distributed between the contacts b and β, whereas the signal sent from contact A (Fig. 4C) is replicated into the pair of contacts a and α. Graphene has recently been brought into contact with a superconducting metal, and the Josephson proximity effect through graphene has been observed (*22*). Consequently, a beam splitter (Fig. 4, B and C) can be used to experiment with Einstein-Podolsky-Rosen (*23*) pairs of particles.

References and Notes

1. K. Novoselov *et al.*, *Science* **306**, 666 (2004).
2. R. Saito, G. Dresselhaus, M. S. Dresselhaus, *Physical Properties of Carbon Nanotubes* (Imperial College Press, London, 1998).
3. K. Novoselov *et al.*, *Nature* **438**, 197 (2005).
4. Y. Zhang, Y.-W. Tan, H. L. Stormer, P. Kim, *Nature* **438**, 201 (2005).
5. K. Novoselov *et al.*, *Nat. Phys.* **2**, 177 (2006).
6. T. Ohta, A. Bostwick, T. Seyller, K. Horn, E. Rotenberg, *Science* **313**, 951 (2006).
7. V. V. Cheianov, V. I. Fal'ko, *Phys. Rev. B* **74**, 041403 (2006).
8. M. Katsnelson, K. Novoselov, A. Geim, *Nat. Phys.* **2**, 620 (2006).
9. V. G. Veselago, *Sov. Phys. Usp.* **10**, 509 (1968).
10. J. B. Pendry, *Phys. Rev. Lett.* **85**, 3966 (2000).
11. J. B. Pendry, *Nature* **423**, 22 (2003).
12. D. R. Smith, J. B. Pendry, M. Wiltshire, *Science* **305**, 788 (2004).
13. M. S. Dresselhaus, G. Dresselhaus, *Adv. Phys.* **51**, 1 (2002).
14. M. Berry, *Adv. Phys.* **25**, 1 (1976).
15. V. I. Arnold, *Singularities of Caustics and Wave Fronts*; Mathematics and Its Applications Series, Vol. 62 (Kluwer, Dordrecht, 1990).
16. H. C. Manoharan, C. P. Lutz, D. M. Eigler, *Nature* **403**, 512 (2000).
17. J. Friedel, *Philos. Mag.* **43**, 153 (1952).
18. E. McCann, V. I. Fal'ko, *Phys. Rev. Lett.* **96**, 086805 (2006).
19. J. D. Bernal, *Proc. Phys. Soc. London A* **106**, 749 (1924).
20. S. Hembacher *et al.*, *Phys. Rev. Lett.* **94**, 056101 (2005).
21. V. V. Cheianov, V. I. Fal'ko, *Phys. Rev. Lett.* **97**, 226801 (2006).
22. H. B. Heersche, P. Jarillo-Herrero, J. B. Oostinga, L. Vandersypen, A. F. Morpurgo, http://arxiv.org/ftp/cond-mat/papers/0612/0612121.pdf.
23. A. Einstein, B. Podolsky, N. Rosen, *Phys. Rev.* **47**, 777 (1935).

24. This project started during the Max Planck Institute für Physik Komplexer Systeme workshop "Dynamics and Relaxation in Complex Quantum and Classical Systems and Nanostructures" and was funded by the Engineering and Physical Sciences Research Council, Lancaster Portfolio Partnership grant EP/C511743.

27 November 2006; accepted 31 January 2007
10.1126/science.1138020

Halwaxiids and the Early Evolution of the Lophotrochozoans

Simon Conway Morris[1]* and Jean-Bernard Caron[2]*

Halkieriids and wiwaxiids are cosmopolitan sclerite-bearing metazoans from the Lower and Middle Cambrian. Although they have similar scleritomes, their phylogenetic position is contested. A new scleritomous fossil from the Burgess Shale has the prominent anterior shell of the halkieriids but also bears wiwaxiid-like sclerites. This new fossil defines the monophyletic halwaxiids and indicates that they have a key place in early lophotrochozoan history.

Burgess Shale–type faunas house numerous taxa that are phylogenetically controversial and open to widely different interpretations. One approach is to incorporate these taxa into the stem groups of major phyla (*1*), but this often presupposes homologies of disparate structures and typically depends on an attenuated fossil record. Alternative views regard such taxa as either belonging to extant phyla (*2*, *3*) or representing extinct phyla (*4*). These differences have major evolutionary implications. For example, the assignment of taxa to either extant or extinct phyla implies that body plans arose by macroevolutionary mechanisms. This is consistent with body plans having a seemingly abrupt appearance and potentially with claims of a protracted (albeit cryptic) history (*5*). In contrast, hypotheses based on the construction of stem groups generally imply microevolutionary processes. The component taxa would be initiated in the latest Neoproterozoic, with body plans emerging by functional transitions that were connected to feeding, locomotion, and defense (*6*, *7*). This view is consistent with an explosive diversification of metazoans (*8*, *9*).

Numerous Cambrian groups have multiplated skeletons (or scleritomes) (*10*). Typically, the scleritomes of these groups occur as disarticulated fossils, notably in the small shelly assemblages. Burgess Shale–type faunas, however, yield articulated material such as the halkieriids, which are probably related to the siphogonuchitids [known only from disassociated sclerites (*10*)], and wiwaxiids. However, the wider relationships of these groups, the members of which are similar to armored slugs, are uncertain. One hypothesis interprets the halkieriids as stem-group lophotrochozoans, closely linking them to the origin of annelids and brachiopods (*11*).

The evolutionary route to the annelids was hypothesized to be via the related wiwaxiids (*12*), and the peculiar halkieriid arrangement of a prominent anterior and posterior shell presaged the bivalved brachiopods (*11*). More recently, the micrinids and tannuolinids, known only as isolated shells, have been interpreted as key intermediates (*13*) between the halkieriids and brachiopods. Alternative hypotheses have assigned the halkieriids to the crown-group mollusks (*3*), questioned the relevance of the micrinids and tannuolinids (*14*), and rejected the wiwaxiids as stem-group annelids (*15*). One substantial contribution to this debate is the identification of *Odontogriphus* and *Wiwaxia* as stem-group mollusks (*16*). Despite these conflicting hypotheses, the Cambrian fossil record, in principle, will be central to unravel-

[1]Department of Earth Sciences, University of Cambridge, Cambridge CB2 3EQ, UK. [2]Department of Natural History, Royal Ontario Museum, Toronto, M5S 2C6, Canada.

*To whom correspondence should be addressed. E-mail: sc113@esc.cam.ac.uk (S.C.M.); jcaron@rom.ca (J.B.C.)

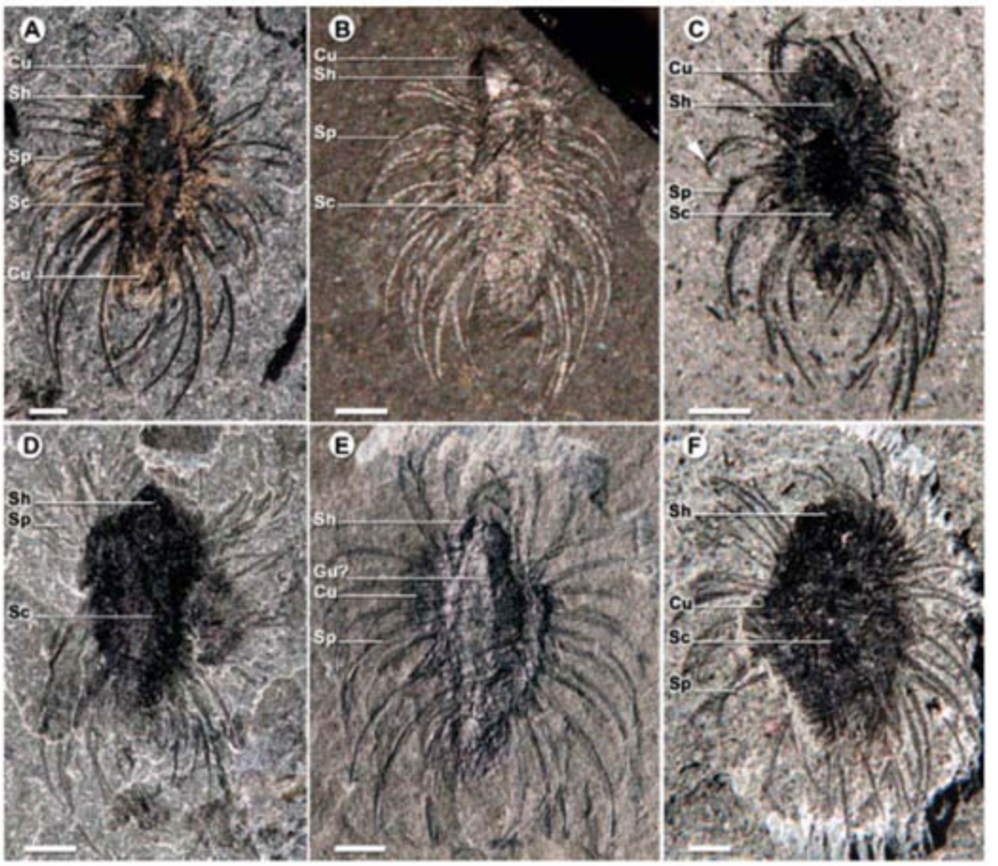

Fig. 1. *O. reburrus* from the Middle Cambrian Burgess Shale. (A to D) Dorsal view. (**A**) Holotype, ROM 57197; (**B**) ROM 57837; (**C**) ROM 57835; (**D**) ROM 57839. White arrow in (C) indicates a bended spine. (E to F) Ventral view. (**E**) ROM 57836; (**F**) ROM 57838. Only the doublure of the shell is visible in (E). Images were obtained by light microphotography on uncoated material. Scale bars, 1 mm. Cu, cultrate; Gu, gut; Sc, dorsal sclerites; Sh, shell; Sp, dorso-lateral spines.

ing many aspects of early lophotrochozoan evolution, even though substantial lacunae remain, not least those concerning the origins of the nemerteans and sipunculans.

Here we describe a new taxon [scleritomorph C in (*17*), *Orthrozanclus reburrus* (*18*), based on 11 specimens recovered from the Burgess Shale] that shares characters with both the halkieriids and wiwaxiids (Figs. 1 to 3). Like other Burgess Shale fossils (*19*), they are exceptionally preserved, although their small size and degree of having been crushed result in fine details sometimes being difficult to discern. Some specimens also have abundant diagenetic pyrite (Figs. 1A and 2, A, D, and E). Including their spinose sclerites, the specimens are 6 to 10.3 mm long. The central zone of the dorsal body is strongly convex but is flanked by flatter margins. The ventral side was evidently soft-bodied and tapered to a broad termination. The scleritome consists of three zones or sets of sclerites and at least one shell (Fig. 1). One set extends around the entire body. At the anterior end, two types of sclerites project forward: Most are blade-like and slightly recurved abaxially (Fig. 2A), but much more elongate spines are also interspersed. This anterior array of sclerites then extends posteriorly to form a lateral component of symmetrical sclerites (Fig. 1E), whereas, at the posterior end, the array comprises abaxially recurved sclerites (Fig. 1A). The prominent second set of sclerites consists of about 16 to 20 elongate, recurved spines on either side of the body, which are inserted abaxial to the lateral sclerites (Fig. 1). Distal to the body, these sclerites may lie at slightly different levels in the sediment and overlap. This disposition suggests that, although these sclerites arose from a narrow zone, their arrangement may not have been as a single row. These sclerites taper quite strongly but individually appear to have an expanded base (Fig. 2, F and H). Externally, they may bear one or two ridges. Pyritized material indicates that they probably had an internal cavity (Fig. 2, D and E). In cases of heavy pyritization, these sclerites reveal a circular cross section, which may be the original configuration in life. A few sclerites are kinked, which is suggestive of a nonmineralized composition (Fig. 1C). The third set of sclerites covers the convex central region and, as a result of crushing, is the least well preserved (Figs. 1 and 2, F and G). These small sclerites appear to have formed a posteriorly imbricated array.

In addition to the sclerites, the anterior bears a prominent convex shell (Fig. 1). In outline, it is roughly triangular, with an anterior umbo, an arched posterior margin, and a medial ridge expanding posteriorly (Fig. 2, B, C, and F). Finely spaced growth lines indicate accretionary growth (Fig. 2, C and F). The shell also bears coarser ridges (Fig. 2, A to C and F); they may represent either the internal surface of the shell or more probably metamerism, traces of which are also discernible more posteriorly. In the ventral view, the shell is largely obscured by soft tissue, but the anterior margin is fairly acute and bears a prominent doublure (Fig. 1E). A relatively prominent strand (that begins close to the margin of the anterior shell and can be traced indistinctly toward the posterior) may represent the gut.

In life, this animal was evidently benthic (Fig. 3), and it is assumed to have moved on a muscular foot. Feeding habits are conjectural, but the convex central region of the organism may have housed a voluminous sediment-filled gut. The scleritome, especially the elongate spines, was presumably protective and/or sensory in function. The shape of the spines suggests that they extended outward and then upward. Given their relative position in the scleritome, the spines are less likely to have provided any snowshoe-like support on the surface of flocculent sediment. The function of the anterior shell is conjectural, but, as hypothesized in the halkieriids (*11*), it could have provided a platform for the attachment of muscles associated with a feeding apparatus. *Orthrozanclus* combines features of both wiwaxiids and halkieriids. The smaller size and partial crushing in *Orthrozanclus* make precise comparisons with the wiwaxiid scleritome (*20*) somewhat tentative, but both were evidently unmineralized, and the overall arrangement is similar. There are convincing equivalents to both the cultrate (lateral) sclerites (including those that extend around the anterior) and the larger spines in *Wiwaxia*. The dorsal sets of spines are equivalent as well, but, in *Orthrozanclus*, the sclerites are smaller and do not seem to have any obvious segmental pattern. The most substantial difference appears to be the absence of siculate (ventro-lateral) sclerites in *Orthrozanclus*. The halkieriid scleritome is also comparable, in particular with marked similarities between the cultrate sclerites. The sclerites of halkieriids are, however, mineralized. Nevertheless, unlike *Wiwaxia* (*21*), both *Orthrozanclus* and the halkieriids have prominent shells. The shells of the halkieriids are best known in articulated material in which they consist of a prominent anterior and posterior shell, the former being notably more convex (*11*). Although *Orthrozanclus* seems to lack a posterior shell, its anterior shell is similar in shape to that of the halkieriids. In contrast, the direction of growth, as inferred from the location of the umbonal region, is reversed, presumably to allow the arched posterior margin to match the convex dorsal region. The shell of *Orthrozanclus* is also similar to a number of isolated small shelly fossils, notably *Ocruranus* (as well as *Eohalobia*) from the

Lower Cambrian of China (*10*, *22*) that are also likely to be halkieriid (*22*, *23*).

Orthrozanclus may also shed light on the Burgess Shale taxon *Oikozetetes* (*24*). This taxon was described on the basis of two shell morphs (A and B), which were suggested to derive from a halkieriid-like animal. The shell of morph B is similar to that of *Orthrozanclus*, apart from lacking the medial ridge (*25*).

The sclerites of halkieriids and wiwaxiids are similar in terms of mode of construction and external ornamentation (*26*), and members of both groups have a tripartite scleritome (*11*). Wiwaxiids, however, have unmineralized sclerites (*12*, *20*) and lack shells (*21*). In combining key features of halkieriids and wiwaxiids, *Orthrozanclus* provides evidence for the monophyletic halwaxiids (*18*). The importance of this group to the understanding of the early evolution of lophotrochozoans depends, however, on a number of critical assumptions, especially concerning the origin of mollusks. The discovery that seriality in monoplacophorans and polyplacophorans, long thought to be amongst the most primitive of mollusks, may be highly derived could undermine long-held assumptions about the nature of the ancestral mollusk (*27*). Indeed, this question may be most readily answered on the basis of fossil material. In this context, the best candidate appears to be the *Kimberella-Odontogriphus* clade (*16*), but, although the dorsal zone presumably had the potential to biomineralize, it remains difficult to establish convincing homologies between any molluskan shell or spicule array and the halwaxiid shell or sclerite field, respectively. It is also clear that shoehorning the halkieriids into the crown-group mollusks (*3*) fails on account of inappropriate comparisons of sclerite structure and unconvincing homologies with younger multiplacophorans (*28*).

Further discussion of the phylogenetic position of the halwaxiids, and hence their role in early mollusk evolution, depends crucially on the assumed polarity of the three component taxa (Fig. 4). Taking *Odontogriphus* as a stem-group mollusk would suggest that the acquisition of a shell in *Orthrozanclus* and the biomineralization of sclerites in halkieriids were later events. This scheme, however, makes it difficult to accommodate the stratigraphically older siphogonuchitids, which have a simpler scleritome (*10*, *29*) and a shell composed of fused sclerites (*23*). An alternative phylogeny is to take *Kimberella* and *Odontogriphus* as stem-group lophotrochozoans, with the halwaxiids forming a distinct clade with a polarity opposite to the first scheme. Accordingly, we hypothesize that mollusks had already diverged before the evolution of the halwaxiids. This

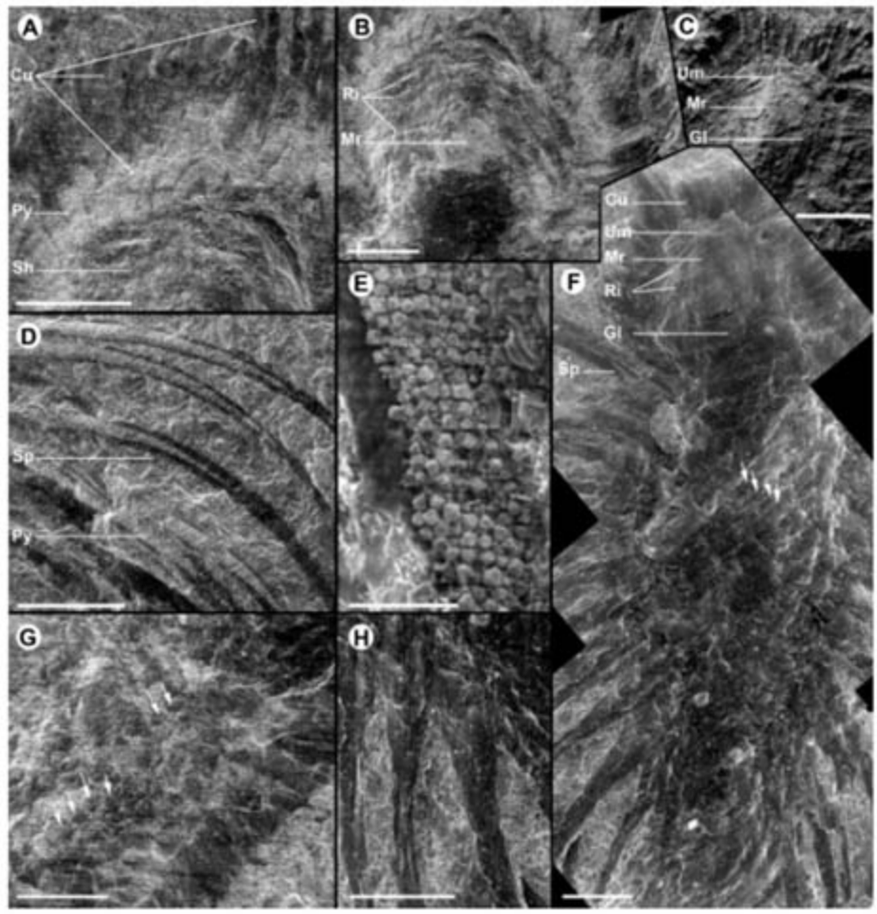

Fig. 2. *O. reburrus* from the Middle Cambrian Burgess Shale. (**A**) Close-up view of the anterior cultrates. (**B** and **C**) Close-up views of the shell. (**D**) Pyritized spines. (**E**) Close-up view of (D) showing octahedra. (**F**) Entire individual. A composite of three images is shown. (**G**) Detail of the dorsal sclerites. White arrows in (F) and (G) point to dorsal sclerites. (**H**) Close-up view of the posterior spines from (F). In (A), (B), and [(D) to (H)], images were obtained by environmental scanning electron microscopy on uncoated material. In (C), image was obtained by light microphotography; specimen was coated with ammonium chloride. Scale bars, 0.5 mm except (E), 0.05 mm. Gl, growth lines; Mr, medial ridge; Py, pyrite; Ri, ridge; Um, umbo.

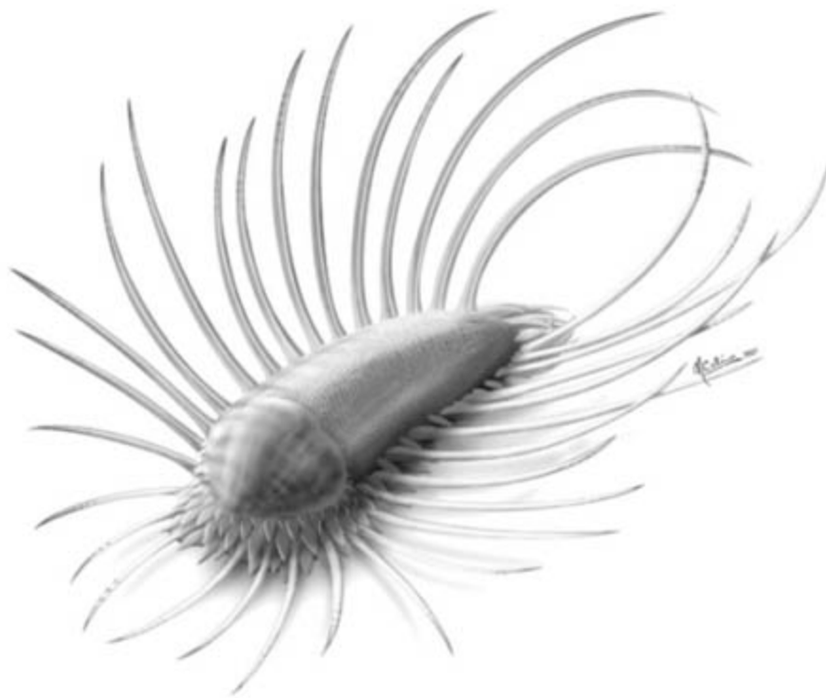

Fig. 3. Reconstruction of *O. reburrus* by M. Collins. The precise arrangement of the anteriormost region remains somewhat conjectural.

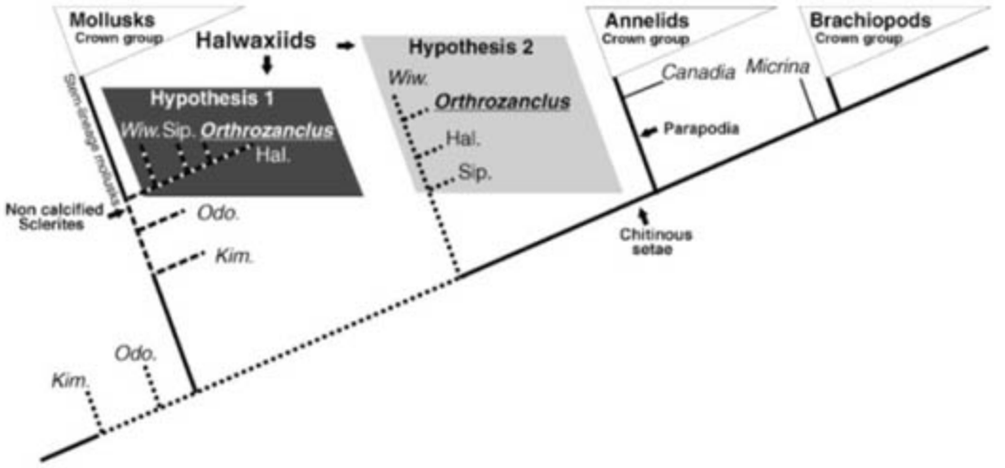

Fig. 4. An outline of lophotrochozoan phylogeny showing the two most plausible positions of the halwaxiid *O. reburrus*, depending on the assumed polarity of sclerite acquisition and biomineralization in the associated taxa *Kimberella* (*Kim.*), halkieriids (Hal.), *Odontogriphus* (*Odo.*), siphogonuchitids (Sip.), and *Wiwaxia* (*Wiw.*). Dashed lines indicate alternative interpretations of the phylogeny (see the SOM). The first hypothesis (hypothesis 1) accepts *Odontogriphus* (and probably *Kimberella*) as stem-group mollusks (*16*), with the halwaxiids as a sister group of mollusks. In this latter clade, chitinous sclerites are first acquired (in *Wiwaxia*), followed by their biomineralization in the siphogonuchitids. Members of this latter group, however, are stratigraphically older and appear to have a simpler scleritome (*10*). Halkieriids would then reacquire a more complex scleritome [similar to that of *Wiwaxia* (*11*)] and shells. In the sister group represented by *Orthrozanclus*, the sclerites demineralize, and the posterior shell is probably lost (or highly reduced). The second hypothesis (hypothesis 2) treats the halwaxiids as monophyletic, with the further implication that *Odontogriphus* (and probably *Kimberella*) are stem-group lophotrochozoans. In hypothesis 2, the earliest halwaxiids are the siphogonuchitids with a mineralized scleritome of two types of sclerite (*10*) and with a shell composed of fused sclerites (*23*). Shells are then acquired, along with a third type of sclerite, in the halkieriids. Demineralization of sclerites occurs in *Orthrozanclus*, and (finally) complete shell loss occurs in *Wiwaxia*. A cladistic analysis gives some support for hypothesis 1, but the best tree is not robust (see the SOM).

scheme is more congruent with respect to the siphogonuchitids. It also suggests that biomineralization was achieved independently in the earliest mollusks and halwaxiids, with the latter group later demineralizing its sclerites and subsequently losing the shells. A cladistic analysis (with the use of Phylogenetic Analysis Using Parsimony software) gives some support for hypothesis 1 over hypothesis 2 (Fig. 4), but the bootstrap values are generally very low and the most parsimonious tree is far from robust [see the Supporting Online Material (SOM)]. In addition, when discussing the origin of major body plans, it is likely that the genetic and morphological gaps in the Cambrian were much smaller than the present disparity of phyla would suggest.

References and Notes

1. G. E. Budd, S. Jensen, *Biol. Rev.* **75**, 253 (2000).
2. J. W. Durham, *J. Paleontol.* **48**, 750 (1974).
3. J. Vinther, C. Nielsen, *Zool. Scr.* **34**, 81 (2005).
4. S. J. Gould, *Wonderful Life: The Burgess Shale and the Nature of History* (Norton, New York, 1989).
5. J. E. Blair, S. B. Hedges, *Mol. Biol. Evol.* **22**, 2275 (2005).
6. G. E. Budd, *Lethaia* **31**, 197 (1998).
7. D.-G. Shu, S. Conway Morris, J. Han, Z.-F. Zhang, J.-N. Liu, *Nature* **430**, 422 (2004).
8. S. Aris-Brosou, Z. Yang, *Mol. Biol. Evol.* **20**, 1947 (2003).
9. A. Rokas, D. Krüger, S. B. Carroll, *Science* **310**, 1933 (2005).
10. Y. Qian, S. Bengtson, *Fossils Strata* **24**, 1 (1989).
11. S. Conway Morris, J. S. Peel, *Philos. Trans. R. Soc. London Ser. B* **347**, 305 (1995).
12. N. J. Butterfield, *Paleobiology* **16**, 287 (1990).
13. A. Williams, L. E. Holmer, *Palaeontology* **45**, 845 (2002).
14. G. Li, S. Xiao, *J. Paleontol.* **78**, 900 (2004).
15. D. Eibye-Jacobsen, *Lethaia* **37**, 317 (2004).
16. J. B. Caron, A. H. Scheltema, C. Schander, D. Rudkin, *Nature* **442**, 159 (2006).
17. J. B. Caron, D. A. Jackson, *Palaios* **21**, 451 (2006).
18. Systematic section is as follows: Superphylum Lophotrochozoa. Stem-group Halwaxida, defined as cataphract metazoans with three principal zones of sclerites and usually at least one shell. Component genera include *Australohalkieria*, *Drepanochites*, *Eohalobia*, *Halkieria*, *Lomasulcachites*, *Ninella*, *Ocruranus*, *Oikozetetes*, *Orthrozanclus*, *Sinosachites*, *Siphogonuchites* (*Lopochites* and *Maikhanella* may be junior synonyms), *Thambetolepis*, and *Wiwaxia*. This list is likely to be incomplete and possibly also includes synonyms, not in the least because most taxa are only known from disarticulated material. Family Orthrozanclidae Conway Morris and Caron fam. nov. Component genus is *Orthrozanclus* and possibly *Oikozetetes*. Genus *Orthrozanclus* Conway Morris and Caron gen. nov. *Orthrozanclus reburrus* sp. nov. Etymology: Generic name is compound, based on sickle-like (Greek *zanclon*) sclerites and oblique reference to ancestral nature (Greek *orthros*, or "dawn"); specific name refers to hairy (Latin *reburrus*) appearance. Holotype: Royal Ontario Museum (ROM) 57197. Other material: ROM 57833 to 57840, National Museum of Natural History (USNM) 213695 and 213696. Stratigraphy and locality: Burgess Shale Formation, Walcott Quarry Member, Middle Cambrian. All specimens are from the Greater Phyllopod Bed, Fossil Ridge, near Mount Field, British Columbia, Canada (*17*). Diagnosis: Cataphract metazoan, scleritome of individual sclerites, and at least one shell. Sclerites form at least three zones: small dorsal sclerites, prominent dorso-lateral spines, and lateral (cultrate), including elongate, anterior spines. Anterior shell convex, anterior umbo, arched posterior margin, ventrally anterior doublure.
19. Sclerites show similar preservation to co-occurring wiwaxiids, which are known to be unmineralized and probably were originally chitinous (*12*). The shell shows prominent relief and clear growth lines and was almost certainly composed of calcium carbonate, although it is now demineralized.
20. S. Conway Morris, *Philos. Trans. R. Soc. London Ser. B* **307**, 507 (1985).
21. In one disarticulated specimen of *Wiwaxia* [figures 46 and 47, A to D, in (*11*)], there is a shell-like structure, but this is unlike those in either *Orthrozanclus* or *Oikozetetes* and appears to be an occurrence known only in this case. It may be a fortuitous association.
22. H. Siegmund, *Lethaia* **30**, 285 (1997).
23. S. Bengtson, *Lethaia* **25**, 401 (1992).
24. S. Conway Morris, *Neues Jahrb. Geol. Palaeontol. Abh.* **195**, 319 (1995).
25. The holotype of *Oikozetetes seilacherii* was based on morph A (*24*), so synonymy with *Orthrozanclus* is not appropriate. Although earlier tentatively placed in the Halkieriidae (*24*), these two genera are almost certainly closely related (*18*). The relationships, however, between these two taxa are difficult to resolve on present evidence, in particular because *Orthrozanclus* only shows one definite shell. Morph B could be another species of *Orthrozanclus* or, alternatively, *Oikozetetes* may be correctly identified. In contrast to the interpretation of (*24*) and consistent with the evidence presented here, it is more likely that morph A represented the posterior shell (and so is possibly equivalent to the tentatively identified and much smaller posterior shell in *Orthrozanclus*), and, correspondingly, morph B would be equivalent to the anterior shell.
26. P. A. Jell, *Alcheringa* **5**, 85 (1981).
27. G. Giribet *et al.*, *Proc. Natl. Acad. Sci. U.S.A.* **103**, 7723 (2006).
28. S. Conway Morris, *Philos. Trans. R. Soc. London Ser. B* **361**, 1069 (2006).
29. S. Bengtson, in *Evolving Form and Function: Fossils and Development*, D. E. G. Briggs, Ed. (Peabody Museum of Natural History, Yale University, New Haven, CT, 2005), pp. 101–124.

30. We thank V. Brown for technical support in Cambridge; D. Evans, C. Schander, A. Scheltema, and D. Zanatta for assistance and comments on the cladistic analysis; M. Collins for drafting the reconstruction; and three anonymous referees for constructive criticism. This work is supported by the Royal Society, Cowper-Reed Fund, St. John's College, Parks Canada, and the Royal Ontario Museum. Collections were made under the direction of D. Collins. This is Royal Ontario Museum Burgess Shale Research Project #10.

Supporting Online Material

www.sciencemag.org/cgi/content/full/315/5816/1255/DC1
Analysis S1

6 November 2006; accepted 16 January 2007
10.1126/science.1137187

Rethinking Organic Aerosols: Semivolatile Emissions and Photochemical Aging

Allen L. Robinson,[1]* Neil M. Donahue,[1]* Manish K. Shrivastava,[1] Emily A. Weitkamp,[1] Amy M. Sage,[1] Andrew P. Grieshop,[1] Timothy E. Lane,[1] Jeffrey R. Pierce,[1] Spyros N. Pandis[1,2]

Most primary organic-particulate emissions are semivolatile; thus, they partially evaporate with atmospheric dilution, creating substantial amounts of low-volatility gas-phase material. Laboratory experiments show that photo-oxidation of diesel emissions rapidly generates organic aerosol, greatly exceeding the contribution from known secondary organic-aerosol precursors. We attribute this unexplained secondary organic-aerosol production to the oxidation of low-volatility gas-phase species. Accounting for partitioning and photochemical processing of primary emissions creates a more regionally distributed aerosol and brings model predictions into better agreement with observations. Controlling organic particulate-matter concentrations will require substantial changes in the approaches that are currently used to measure and regulate emissions.

Airborne particles pose serious health risks and have a controlling influence on Earth's climate. Organic aerosol (OA) is a major component of fine-particle mass throughout the atmosphere (*1*). OA comprises primary organic aerosol (POA, particle mass directly emitted from sources such as motor vehicles and forest fires) and secondary organic aerosol (SOA, particle mass formed in the atmosphere from the oxidation of gas-phase precursors) (*1*). The relative contribution of POA and SOA to the overall OA budget remains controversial. Research using individual organic compounds to estimate POA (*2*, *3*), organic-to-elemental C ratios to estimate SOA (*4*, *5*), and atmospheric chemistry models (*6*, *7*) indicates that POA dominates the urban OA budget. However, recent field measurements indicate SOA dominance, even in heavily urbanized areas, that cannot be explained by the oxidation of known SOA precursors (*8*–*10*). The persistent discrepancies between measured OA concentrations and predictions of atmospheric chemistry models underscore the substantial uncertainty regarding the sources of OA (*6*, *11*, *12*).

Combining laboratory, field, and modeling results, we propose two major amendments to the current OA conceptual framework: (i) accounting for gas-particle partitioning of POA and (ii) explicitly representing gas-phase oxidation of all low-volatility vapors in current SOA-production mechanisms. This replaces the current static representation of POA emissions with a far more dynamic picture in which low-volatility material evaporates, oxidizes, and recondenses over time. This paper presents experimental results supporting this revised framework, first showing that primary emissions indeed evaporate substantially upon dilution to ambient conditions and then showing that photo-oxidation of those vapors in a smog chamber produces SOA far exceeding that from traditional precursors. Finally, we implement these amendments in a chemical transport model to illustrate their implications for our understanding of OA in the atmosphere.

Sources emit thousands of organic compounds, ranging from CH_4 to species with 30-or-more C atoms (*13*–*15*). The amount of POA depends on the gas-particle partitioning of this complex mixture (*16*, *17*). However, emission inventories and models treat POA as nonvolatile, implicitly assuming that standard emissions tests represent the full range of atmospheric conditions. This is wrong (*17*). To illustrate the semivolatile character of POA, Fig. 1 presents a compilation of diesel exhaust data measured at different levels of dilution, extending from conventional emissions sampling to typical atmospheric conditions. The POA emission factor (EF) decreases with increasing dilution because of the evaporation of semivolatile organic compounds (SVOCs) (*17*). This evaporation causes POA concentrations to decrease considerably more than does dispersion alone. Furthermore, the data follow well-established partitioning theory (*17*, *18*), indicating that POA levels also vary with temperature. This dynamic picture complicates the definition of POA and underscores the need for our first amendment to the current OA conceptual framework: explicit treatment of gas-particle partitioning of primary emissions.

Partitioning depends on the volatility distribution of the emissions. Figure 1B shows the

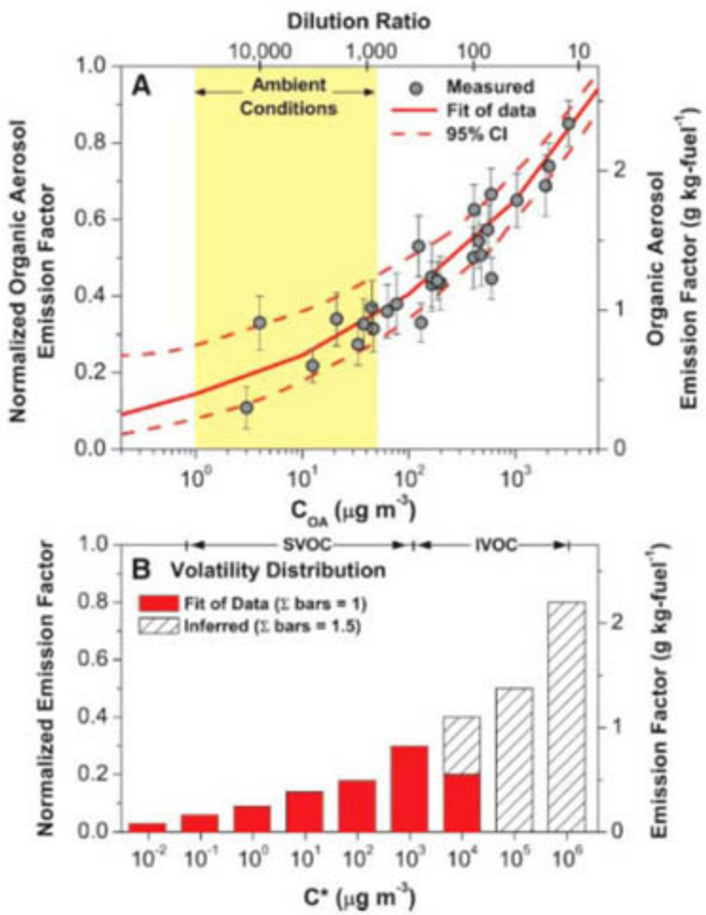

Fig. 1. Partitioning data and volatility distribution of diesel POA measured at 300 K. The circles in (**A**) indicate POA EF data from previously published dilution-sampler measurements (*21*) and new results obtained at higher levels of dilution. The data are plotted as a function of OA concentration (C_{OA}), following the principles of partitioning theory (*17*, *18*). The values are normalized by the traditional POA EF, measured by means of a quartz filter at low levels of dilution. The results show substantial evaporation of POA with decreasing C_{OA} and that only a quarter of the traditionally defined POA exists in the particle phase at atmospherically relevant C_{OA}. The curve shows a fit based on absorptive partitioning (*19*), along with a 95% confidence interval (CI). The red bars in (**B**) are the volatility distribution determined by this fit (*19*), plotted in terms of C* (related to effective saturation vapor pressure). These bars reveal the volatility distribution of traditionally defined nonvolatile POA emissions and therefore sum to one (Σ bars = 1) (*19*). The hatched bars show an assumed volatility distribution of additional IVOC emissions estimated from other data (*13*–*15*, *19*) that indicate that IVOCs contribute one to three times the POA emissions (here, we assume 1.5 times) (*19*). Secondary axes show un-normalized fuel-based EFs and levels of dilution for our experiments.

[1]Center for Atmospheric Particle Studies, Carnegie Mellon University, Pittsburgh, PA 15213, USA. [2]Department of Chemical Engineering, University of Patras, Patra 26500, Greece.

*To whom correspondence should be addressed. E-mail: alr@andrew.cmu.edu (A.L.R.); nmd@andrew.cmu.edu (N.M.D.)

volatility distribution for diesel exhaust at 300 K. It is presented in terms of lumped species that span a volatility basis set of effective saturation concentrations (C*), allowing a physically meaningful treatment of partitioning for all organics (*18*). Conceptually, a volatility distribution can be constructed from speciated emissions data by lumping species with similar saturation vapor pressures. However, this is not possible because less than 10% of the condensed and semivolatile mass has been speciated (*13*–*15*). We determined the distribution in Fig. 1B by fitting isothermal dilution data with absorptive partitioning theory (*19*), as done in well-established analyses of SOA data (*20*).

The distribution shown in Fig. 1B comprises emissions of all organics less volatile than approximately a C_{12} *n*-alkane, covering the range of material that can change phase between the high-temperature conditions at the end of the exhaust pipe and the cool, highly dilute ambient atmosphere. Based on partitioning at typical atmospheric conditions, this distribution includes "nonvolatile" ($C^* < 0.1\ \mu g\ m^{-3}$), "semivolatile" (SVOC; $0.1\ \mu g\ m^{-3} < C^* < 1000\ \mu g\ m^{-3}$), and "intermediate-volatility" (IVOC; $1000\ \mu g\ m^{-3} < C^* < 100{,}000\ \mu g\ m^{-3}$) organic compounds. Even more volatile species dominate the overall emissions of reduced organic C (*13*–*15*); however, these species are largely accounted for in models, either as part of ozone chemistry mechanisms or as traditional SOA precursors.

The red bars in Fig. 1B show the volatility distribution of the traditionally defined POA emissions that are currently treated as nonvolatile in models and inventories. The majority of these emissions have a $C^* > 100\ \mu g\ m^{-3}$ and therefore exist largely in the gas phase at typical atmospheric conditions. Some of the emissions are misclassified as POA because dilution-sampler measurements are typically conducted at unrealistically high concentrations, which biases gas-particle partitioning relative to much more dilute atmospheric conditions (*17*, *21*).

Most of the emissions shown in Fig. 1B are vapors in the atmosphere, but given their low volatility, they may be important SOA precursors. The first several generations of oxidation typically produce compounds with lowered vapor pressures (*19*, *22*). Low-volatility vapors should also produce SOA much more efficiently than the traditional high-volatility SOA precursors (such as monoterpenes and light aromatics) that are thought to dominate ambient SOA production (*6*, *7*, *23*). Figure 1B indicates that the aggregate emissions of low-volatility vapors are substantial compared with the POA emissions. However, these vapors are largely uncharacterized, instead appearing as an unresolved complex mixture of presumably branched aliphatic and cyclic hydrocarbons (*13*, *14*).

To investigate this hypothesis, diluted diesel exhaust was exposed to ultraviolet (UV) light inside our environmental chamber at initial aerosol loadings near typical ambient conditions (*19*). The evolution of both the gas and the particle phase was monitored. Typical results are shown in Fig. 2. UV illumination initiated photochemistry, which caused an initial burst of SOA formation, followed by steady production through the remainder of the experiment. After 3 hours of aging, SOA has almost doubled the initial aerosol mass. Approximately half of the trimethylbenzene was oxidized over the course of the experiment, indicating roughly one generation of processing and $\sim 2 \times 10^6$ molecules cm^{-3} of OH, which is typical of a summer day (*24*).

We examined the potential contribution of traditional-SOA precursors empirically by spiking the chamber with additional aromatics. Adding enough toluene to roughly double the potential SOA production from the measured aromatics caused only a slight inflection in the aerosol-mass time series. Oxidation of traditional precursors can thus explain only a small fraction of the SOA formed in the chamber.

We also calculated the traditional SOA production using measured precursor consumption and published SOA yield curves (*19*). Our model accounts for 58 SOA precursors, but ~90% of the calculated SOA production is from the measured decay of light aromatics, such as toluene. Initial concentrations of these species were at most a few parts per billion by volume. The calculation is complicated by losses of particles and vapor to the wall of the environmental chamber (*19*). Our maximum estimate of the contribution of SOA from the oxidation of known precursors is shown in Fig. 2A. It indicates that traditional SOA contributes at most 15% of the new aerosol, we hypothesize that the majority of the substantial unexplained SOA production is due to the oxidation of low-volatility gas-phase species—our second amendment to the current OA conceptual framework.

SVOC and IVOC vapors constitute a potentially large source of SOA. Their mass emission

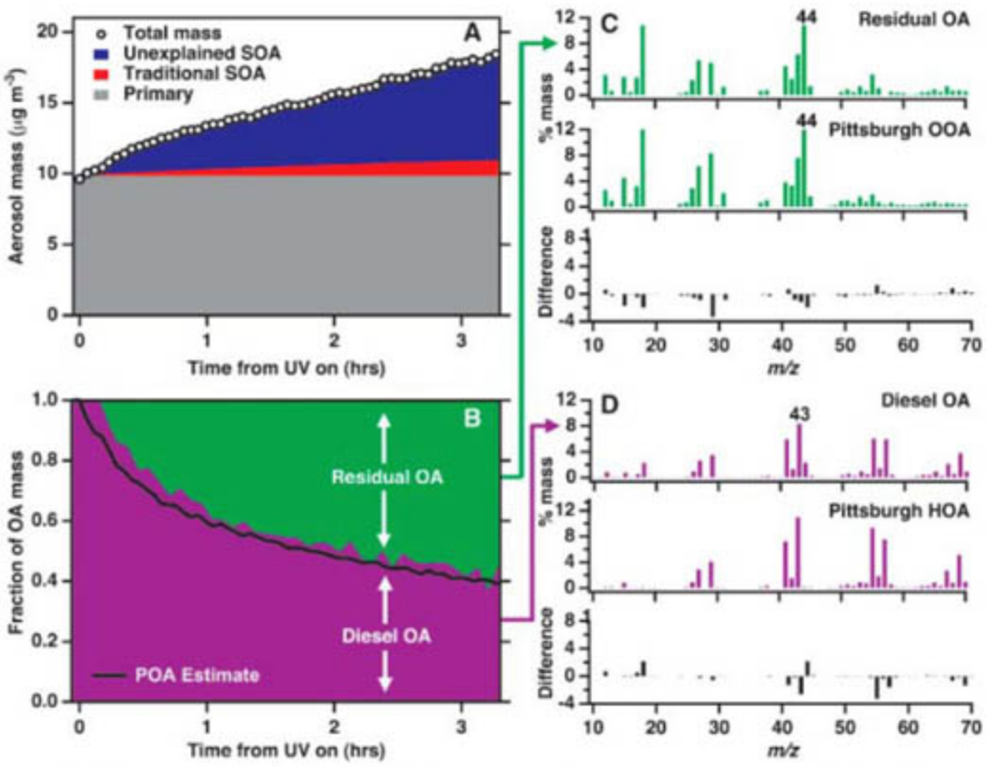

Fig. 2. Results from the photochemical oxidation of diesel exhaust in an environmental chamber. (**A**) The wall-loss–corrected aerosol mass, measured with a scanning mobility particle sizer, assuming a density of 1 g cm^{-3}. The wall-loss correction is based on measured loss of the particle number, accounting for the effects of coagulation, and it assumes that semivolatile vapors are in equilibrium with both the suspended aerosol and the material deposited on the wall during the experiment (*19*). The gray area indicates the primary aerosol (POA + other species). The red area shows the upper-bound estimate of the contribution of known SOA precursors to the suspended aerosol mass (*19*). We attribute the blue area to SOA formed from SVOC and/or IVOC oxidation. AMS results are shown in (**B**) to (**D**). The AMS OA spectrum can be described by two components: the initial diesel spectrum (diesel OA) and an oxidized residual spectrum (residual OA). The relative contribution of these two components to the overall OA spectrum is shown in (B). The spectra of these two components are compared to reference spectra obtained from factor analysis of ambient AMS data in (C) and (D). The spectrum of the diesel OA component is quite similar to the hydrocarbonlike OA (HOA) factor (*8*, *9*). By the end of the experiment, the spectrum of the oxidized residual OA component is quite similar to that of the OOA factor (*8*, *9*). The solid line in (B) indicates the fractional contribution of POA to the suspended OA, based on the initial particle mass and the wall-loss rate and analogous to the results shown in (A). The excellent agreement between this line and the relative contribution of the two AMS components indicates that these two independent approaches yield the same estimate of SOA. *m/z*, mass/charge ratio.

rate is several times that of condensed-phase compounds (Fig. 1B) (*19*); therefore, SOA produced from the oxidation of these vapors will probably exceed the POA emissions. These vapors also oxidize on atmospherically relevant time scales. Large saturated organics have OH rate constants on the order of 3×10^{-11} cm^3 per molecule s^{-1} (*25*) and therefore will undergo one generation of oxidation every 4 hours at typical summertime OH levels. Winter OH levels are three to five times lower (*26*), resulting in slower but still significant processing over multiday time scales associated with regional transport. Finally, the total non-CH_4 hydrocarbon burden in urban environments can exceed 1000 μg m^{-3} (*27*), as compared to typical OA concentrations of less than 10 μg m^{-3}. Therefore, even at only a few percent of the total hydrocarbon budget, SVOC and IVOC vapors could be an important source of ambient OA.

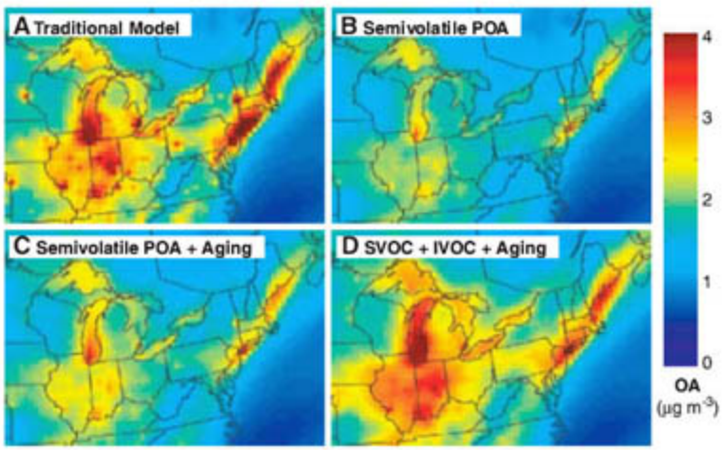

Fig. 3. Maps of predicted ground-level OA concentrations for four PMCAMx simulations: (**A**) a traditional model with nonvolatile POA emissions and (**B** to **D**) three simulations that account for the partitioning of primary emissions—one assuming nonreactive emissions and two considering photochemical aging. In (B), the red bars in Fig. 1B are used to represent the volatility distribution of all POA emissions, and the emissions are allowed to partition but not react; this results in substantial evaporation of the POA (*19*). In (C) and (D), gas-phase primary emissions are also aged by OH (*19*). (C) shows the same emissions scenario as (B), whereas (D) includes additional IVOC emissions by applying the entire volatility distribution shown in Fig. 1B to the existing POA emissions (*19*). The explicit representation of photochemical aging of IVOC and SVOC vapors used in (C) and (D) substantially increases the amount of anthropogenic SOA. In the traditional model, the oxidation of low-volatility vapors contributes only 25% of anthropogenic SOA, as compared to 85% in the revised model shown in (D). The balance of the anthropogenic SOA is from the oxidation of aromatics, which contributes essentially the same amount of SOA on an absolute basis in all simulations. The maps present averages over an 8-day period in July 2001 and show only a subset of the modeling domain (*19*).

The particle composition during our chamber experiments was characterized with an Aerodyne aerosol mass spectrometer (AMS). The measured OA mass spectra can be described as a combination of two components (*19*): (i) diesel OA, whose spectrum is the same as that of the fresh primary emissions (Fig. 2D), and (ii) an oxidized residual that becomes progressively more oxidized during the experiment. By the end of the experiment, the oxidized residual is quite similar to the oxygenated OA (OOA) factor that often dominates ambient OA levels in Pittsburgh, Pennsylvania, and elsewhere (*8*, *9*). This oxidized residual does not look like the mass spectra of SOA formed from aromatics (*28*), confirming that traditional precursors are a minor source of SOA in these experiments. Figure 2B shows that the relative contribution of these two mass-spectrum components evolves over time. This evolution matches the independent estimate of the primary-secondary split, based on the measured wall loss. Therefore, the relative contribution of the oxidized residual spectrum provides a good estimate of SOA, supporting the conclusion drawn from ambient AMS data that SOA dominates the ambient OA burden (*8*, *9*).

To investigate the implications of our two major amendments, we used a three-dimensional chemical transport model, PMCAMx, to simulate pollutant concentrations across the eastern half of the United States (*19*). The model was modified to account for the volatility distribution and gas-particle partitioning of POA and to more explicitly represent SOA production from the oxidation of IVOC and/or SVOC vapors by means of a framework that is consistent with our experimental data (*19*).

Figure 3 presents maps of ground-level OA concentrations from four simulations. The traditional model with nonvolatile POA (Fig. 3A) predicts high POA concentrations (>3 μg m^{-3}) in heavily urbanized areas and substantial urban-to-regional concentration gradients. Allowing the primary emissions to partition but not react (Fig. 3B) dramatically reduces the POA levels throughout the modeling domain, indicating that the majority of the traditional POA emissions are actually evaporated at ambient OA levels (Fig. 1A). Photochemical aging of the SVOC and IVOC vapors creates a considerable amount of regional SOA (Fig. 3, C and D). If one accounts only for partitioning and aging of the existing POA emissions (Fig. 3C), the predicted OA levels are lower than the traditional model. Therefore, even with aging, evaporation of traditional POA reduces OA concentrations. The most comprehensive simulation (Fig. 3D) adds additional IVOC emissions to the model. This creates large amounts of regional SOA. The net result is that regional (but not urban) OA levels exceed the traditional model.

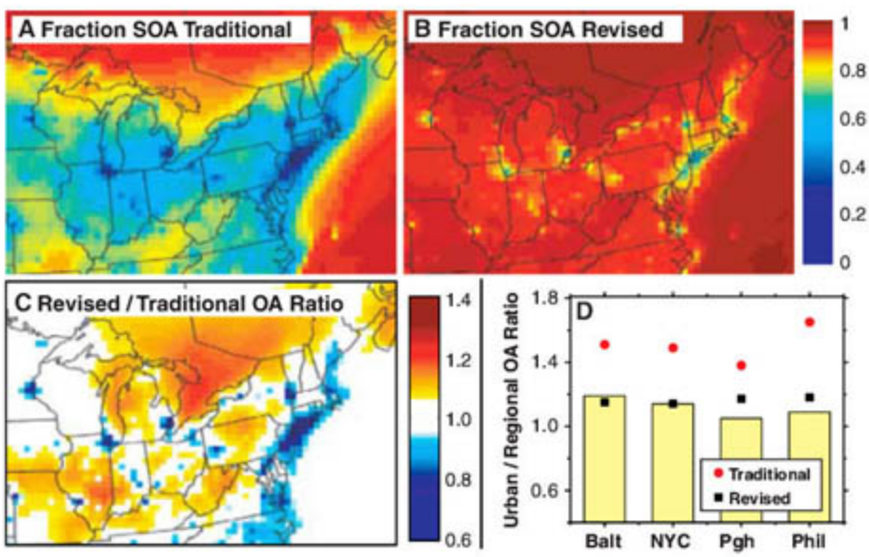

Fig. 4. Predicted changes in the POA/SOA split and total OA between the current framework and the revised model (results shown in Fig. 3, A and D). (**A**) and (**B**) show the ratio of SOA to total OA for the two cases, respectively. (**C**) shows the ratio of the OA predictions for the two cases. (**D**) compares average measured urban-to-regional OA ratios to model predictions for four large cities. The measured ratios (yellow bars) are based on data from the U.S. EPA Speciation Trends Network. The regional concentrations are estimated with the use of a site located upwind of the city. The predicted ratios are based on the average OA concentrations for the grid cells in which the monitoring stations are located. For all cities, the base-case model significantly overpredicts the urban-to-regional ratio, whereas the revised model shows much better agreement. Balt, Baltimore, Maryland; NYC, New York City, New York; Pgh, Pittsburgh, Pennsylvania; Phil, Philadelphia, Pennsylvania.

The effects of our amendments on both the POA/SOA split and the total OA burden are shown in Fig. 4. The traditional model predicts substantial contributions from POA, whereas the revised model predicts that ambient OA is dominated by SOA during the summer. Such a shift is consistent with recent field measurements indicating dominant contributions from SOA (*8*–*10*) while remaining consistent with POA estimates based on low-volatility tracers. In terms of the overall OA budget, the revised model decreases predicted OA in urban areas by as much as 50% and increases it in many rural areas by 15 to 30% (Fig. 4C), reducing the large urban-to-regional gradients predicted by the traditional model and resulting in considerably better agreement with measured urban-to-regional OA ratios (Fig. 4D).

This work has several implications for our understanding of OA. The semivolatile character of primary emissions requires that instead of measuring fixed POA EFs, we must measure the volatility distribution of the emissions. Models and inventories must account for these distributions and their evolution with photochemical age. Regulations and control technologies may also need to be revised to control SVOC and IVOC emissions because of their importance as SOA precursors. The results also imply that, except for people living close to sources, the majority of the population (even in urban areas) is exposed mostly to SOA. Ultimately, a relatively local urban emissions problem is transformed into a regional source of oxidized and presumably hydrophilic OA. The health consequences and climate effects of this oxidized material are almost certainly dramatically different from those of primary emissions.

References and Notes

1. M. Kanakidou *et al.*, *Atmos. Chem. Phys.* **5**, 1053 (2005).
2. J. J. Schauer, W. F. Rogge, L. M. Hildemann, M. A. Mazurek, G. R. Cass, *Atmos. Environ.* **30**, 3837 (1996).
3. M. Zheng, G. R. Cass, J. J. Schauer, E. S. Edgerton, *Environ. Sci. Technol.* **36**, 2361 (2002).
4. B. J. Turpin, J. J. Huntzicker, *Atmos. Environ.* **29**, 3527 (1995).
5. J. C. Cabada *et al.*, *Aerosol Sci. Technol.* **38**, 140 (2004).
6. S. Vutukuru, R. J. Griffin, D. Dabdub, *J. Geophys. Res.* **111**, D10S12 (2006).
7. B. K. Pun *et al.*, *Environ. Sci. Technol.* **37**, 3647 (2003).
8. Q. Zhang, D. R. Worsnop, M. R. Canagaratna, J. L. Jimenez, *Atmos. Chem. Phys.* **5**, 3289 (2005).
9. R. Volkamer *et al.*, *Geophys. Res. Lett.* **33**, L17811 (2006).
10. J. A. de Gouw *et al.*, *J. Geophys. Res.* **110**, D16305 (2005).
11. D. Johnson *et al.*, *Atmos. Chem. Phys.* **6**, 403 (2006).
12. C. L. Heald *et al.*, *Geophys. Res. Lett.* **32**, L18809 (2005).
13. J. J. Schauer, M. J. Kleeman, G. R. Cass, B. R. T. Simoneit, *Environ. Sci. Technol.* **36**, 1169 (2002).
14. J. J. Schauer, M. J. Kleeman, G. R. Cass, B. R. T. Simoneit, *Environ. Sci. Technol.* **33**, 1578 (1999).
15. J. J. Schauer, M. J. Kleeman, G. R. Cass, B. R. T. Simoneit, *Environ. Sci. Technol.* **35**, 1716 (2001).
16. L. M. Hildemann, G. R. Cass, G. R. Markowski, *Aerosol Sci. Technol.* **10**, 193 (1989).
17. M. K. Shrivastava, E. M. Lipsky, C. O. Stanier, A. L. Robinson, *Environ. Sci. Technol.* **40**, 2671 (2006).
18. N. M. Donahue, A. L. Robinson, C. O. Stanier, S. N. Pandis, *Environ. Sci. Technol.* **40**, 2635 (2006).
19. Materials and methods are available as supporting material on *Science* Online.
20. J. R. Odum *et al.*, *Environ. Sci. Technol.* **30**, 2580 (1996).
21. E. M. Lipsky, A. L. Robinson, *Environ. Sci. Technol.* **40**, 155 (2006).
22. Y. B. Lim, P. J. Ziemann, *Environ. Sci. Technol.* **39**, 9229 (2005).
23. B. Y. Koo, A. S. Ansari, S. N. Pandis, *Atmos. Environ.* **37**, 4757 (2003).
24. D. E. Heard, M. J. Pilling, *Chem. Rev.* **103**, 5163 (2003).
25. R. Atkinson, J. Arey, *Chem. Rev.* **103**, 4605 (2003).
26. W. J. Bloss *et al.*, *Faraday Discuss. Chem. Soc.* **130**, 425 (2005).
27. M. Y. Chung, C. Maris, U. Krischke, R. Meller, S. E. Paulson, *Atmos. Environ.* **37** (suppl. 2), S159 (2003).
28. R. Bahreini *et al.*, *Environ. Sci. Technol.* **39**, 5674 (2005).

29. This research has been funded by the U.S. Environmental Protection Agency (EPA) through grants RD-83108101 and R832162. It has not been subjected to the agency's required peer and policy review and therefore does not necessarily reflect the views of the agency; no official endorsement should be inferred. The Proton Transfer Reaction-Mass Spectrometer and AMS were acquired with support from NSF (grant ATM-0420842).

Supporting Online Material

www.sciencemag.org/cgi/content/full/315/5816/1259/DC1
Materials and Methods
Table S1
References

26 July 2006; accepted 17 January 2007
10.1126/science.1133061

Anti-Hebbian Long-Term Potentiation in the Hippocampal Feedback Inhibitory Circuit

Karri P. Lamsa,[1] Joost H. Heeroma,[1] Peter Somogyi,[2] Dmitri A. Rusakov,[1] Dimitri M. Kullmann[1]*

Long-term potentiation (LTP), which approximates Hebb's postulate of associative learning, typically requires depolarization-dependent glutamate receptors of the NMDA (*N*-methyl-D-aspartate) subtype. However, in some neurons, LTP depends instead on calcium-permeable AMPA-type receptors. This is paradoxical because intracellular polyamines block such receptors during depolarization. We report that LTP at synapses on hippocampal interneurons mediating feedback inhibition is "anti-Hebbian": It is induced by presynaptic activity but prevented by postsynaptic depolarization. Anti-Hebbian LTP may occur in interneurons that are silent during periods of intense pyramidal cell firing, such as sharp waves, and lead to their altered activation during theta activity.

Associative *N*-methyl-D-aspartate receptor (NMDAR)–dependent LTP is induced by coincident activity in afferent pathways sufficient to depolarize postsynaptic neurons (*1*). However, the voltage dependence of Ca^{2+}-permeable α-amino-3-hydroxy-5-methyl-4-isoxazolepropionic acid receptors (CP-AMPARs) is opposite to that of NMDARs (*2*, *3*). Because CP-AMPARs are blocked by cytoplasmic polyamines upon depolarization (*4*, *5*), maximal Ca^{2+} influx occurs when the membrane potential is relatively negative. LTP dependent on CP-AMPARs occurs in interneurons of the spinal cord and amygdala (*6*, *7*), but its postsynaptic voltage dependence has not been explored. In hippocampal interneurons, CP-AMPARs have been implicated in long-term depression (*8*–*10*), and contribute to synaptic Ca^{2+} transients, especially in the stratum oriens/alveus (*11*). Many interneurons in the oriens/alveus also show NMDAR-independent LTP (*12*). We therefore looked for associative LTP in these cells, while recording with the gramicidin perforated patch technique to preserve intracellular polyamines (*13*).

Stimulation of pyramidal cell axon collaterals in the alveus evoked monosynaptic excitatory postsynaptic potentials (EPSPs) subthreshold for evoking action potentials. After recording a baseline, we paired high-frequency burst (HFB) stimulation (five pulses at 100 Hz, repeated 20 times) with stimulation of a second, suprathreshold, alveus pathway. "In-phase" associative pairing (phase difference $\Delta\Phi = 0°$) failed to elicit associative LTP in either pathway ($n = 7$; Fig. 1, A and B). In a further set of experiments, we alternately stimulated two weak pathways, and then delivered HFBs to both pathways antiphase ($\Delta\Phi = 180°$). This evoked a persistent increase in EPSP initial slope in one or both pathways in all cells ($n = 7$; Fig. 1, C and D). LTP was elicited even when HFB stimuli were delivered to only one weak pathway ($n = 7$; Fig. 1, E and F). Thus, LTP at excitatory synapses on interneurons in the oriens/alveus is prevented by associative pairing, in direct contrast to NMDAR-dependent LTP (*1*).

Can direct manipulation of the postsynaptic membrane potential similarly gate LTP induction? We delivered HFBs to one pathway

[1]Institute of Neurology, University College London, Queen Square, London WC1N 3BG, UK. [2]Anatomical Neuropharmacology Unit, Medical Research Council, Oxford University, Mansfield Road, Oxford OXI 3HT, UK.

*To whom correspondence should be addressed. E-mail: d.kullmann@ion.ucl.ac.uk

coinciding with the trough (somatic voltage: −90 mV) of an imposed 4-Hz sinusoidal somatic membrane potential oscillation. HFBs were then delivered to the other pathway coinciding with the depolarizing phase. In 8 out of 11 cells, pairing with hyperpolarization, but not with depolarization, resulted in LTP (Fig. 2, A and B). One cell showed the opposite behavior, and the other two showed no effect of either pairing (fig. S1). Single alveus stimuli in phase with maximum hyperpolarization (100 times) also induced LTP (n = 10; Fig. 2C), but pairing with depolarization was ineffective (Fig. 2D). Thus, even low-frequency stimulation can trigger LTP if interneurons are hyperpolarized.

Because the induction requirements for LTP in most interneurons in the oriens/alveus are diametrically opposite to Hebb's postulate (*14*, *15*), we refer to it as "anti-Hebbian." We tested the same LTP induction protocols in interneurons in the stratum radiatum. Hebbian LTP could be elicited in about half of these cells, many of which mediate feedforward inhibition (*16*), whereas pairing either HFB or low-frequency stimuli with hyperpolarization was uniformly unsuccessful (figs. S1 and S2). Anti-Hebbian LTP is thus characteristic of excitatory synapses made by local pyramidal cells on interneurons in the oriens/alveus but not of Schaffer collateral synapses on interneurons in the stratum radiatum.

Can differences in synaptic glutamate receptors explain whether Hebbian, anti-Hebbian, or no LTP is elicited? When interneurons in the oriens/alveus were recorded in whole-cell voltage clamp [with γ-aminobutyric acid (GABA) receptors blocked, and with spermine included in the pipette solution], synaptic AMPARs activated by alveus stimulation were generally strongly rectifying (Fig. 2E), consistent with expression of CP-AMPARs (*11*). Furthermore, only small NMDAR-mediated synaptic currents were detected at a positive holding potential, consistent with low synaptic expression of the NR1 subunit (*17*).

We tested interneurons in the oriens/alveus, recorded in perforated patch mode, with a further anti-Hebbian protocol High-frequency stimulation of one alveus pathway (100 Hz, 100 pulses, delivered twice) paired with hyperpolarization, with NMDARs blocked, elicited LTP in 25 out of 31 cells (Figs. 3A and 4C). We repatched 11 of these cells in whole-cell voltage-clamp mode and found pronounced synaptic AMPAR rectification in every cell where anti-Hebbian LTP was evoked. The rectification index did not differ detectably between control and potentiated pathways (Fig. 3B), yielding no evidence for an LTP-related change in the permeability of synaptic AMPARs to Ca^{2+} (*18*).

In contrast, repatched interneurons in the stratum radiatum generally showed nonrectifying AMPARs and a large NMDAR-mediated component of Schaffer collateral-evoked synaptic currents (fig. S2) (*9*). The anti-Hebbian LTP induction protocol was successful in only 2 out of 20 cells in the stratum radiatum. AMPARs at Schaffer collateral synapses on 11 cells (none of which showed anti-Hebbian LTP) were nonrectifying (fig. S3).

Anti-Hebbian LTP thus typically occurs at synapses on interneurons in the oriens/alveus equipped with rectifying CP-AMPARs. Are these a uniform subgroup? Seven interneurons were regular-spiking oriens-lacunosum moleculare (O-LM) cells (Fig. 3C, fig. S4), which mediate feedback inhibition of the apical dendrites of pyramidal neurons (*19*). Twelve other interneurons had horizontal dendrites and electrophysiological properties typical of O-LM cells, but axon visualization was incomplete (fig. S5). Anti-Hebbian LTP, however, also occurred in 17 out of 24 fast-spiking interneurons in the strata oriens or pyramidale, including one anatomically confirmed axo-axonic and two basket cells, which are innervated by CA1 pyramidal cells and target their perisomatic area. Seven other cells could not be classified.

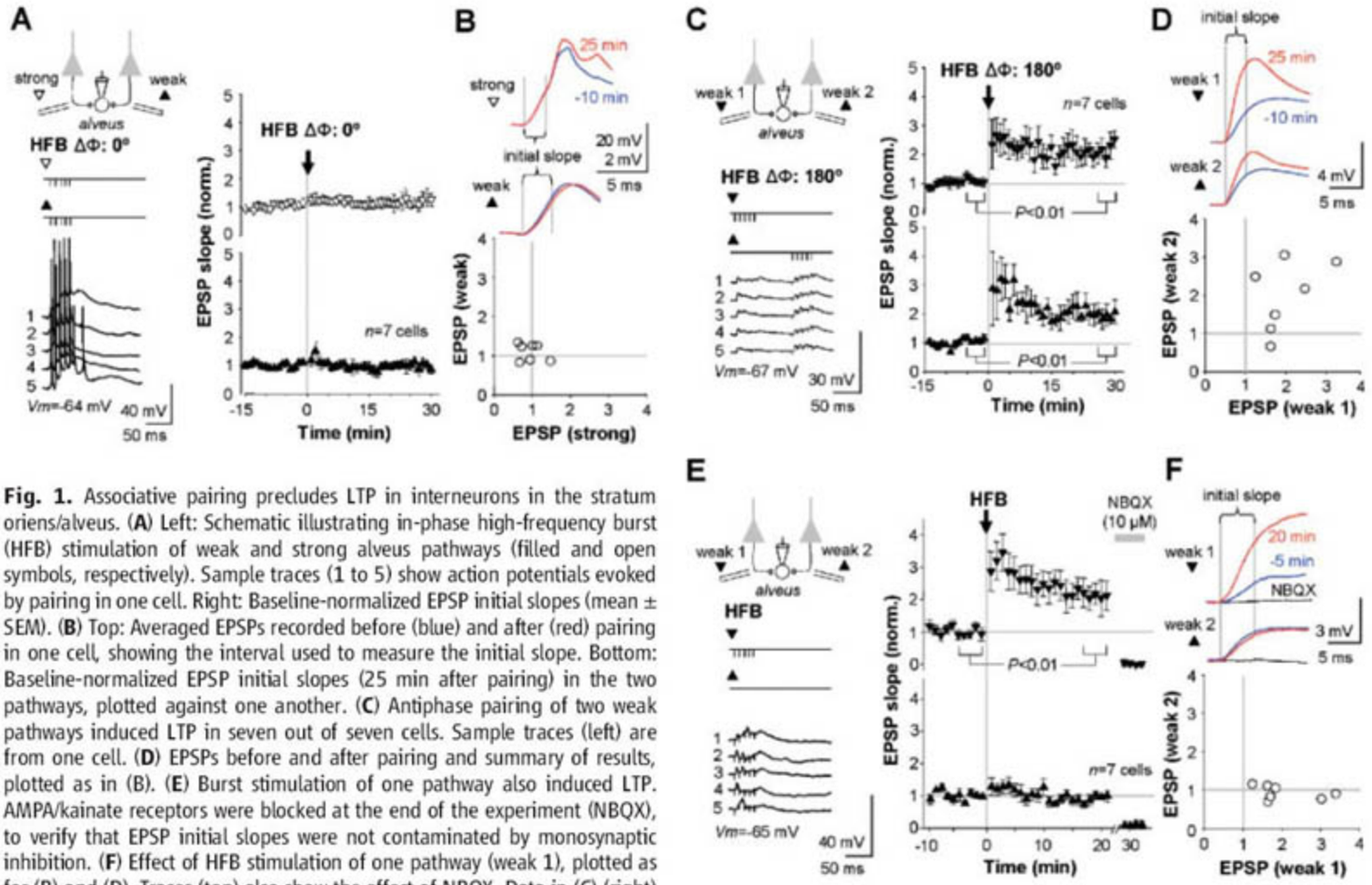

Fig. 1. Associative pairing precludes LTP in interneurons in the stratum oriens/alveus. (**A**) Left: Schematic illustrating in-phase high-frequency burst (HFB) stimulation of weak and strong alveus pathways (filled and open symbols, respectively). Sample traces (1 to 5) show action potentials evoked by pairing in one cell. Right: Baseline-normalized EPSP initial slopes (mean ± SEM). (**B**) Top: Averaged EPSPs recorded before (blue) and after (red) pairing in one cell, showing the interval used to measure the initial slope. Bottom: Baseline-normalized EPSP initial slopes (25 min after pairing) in the two pathways, plotted against one another. (**C**) Antiphase pairing of two weak pathways induced LTP in seven out of seven cells. Sample traces (left) are from one cell. (**D**) EPSPs before and after pairing and summary of results, plotted as in (B). (**E**) Burst stimulation of one pathway also induced LTP. AMPA/kainate receptors were blocked at the end of the experiment (NBQX), to verify that EPSP initial slopes were not contaminated by monosynaptic inhibition. (**F**) Effect of HFB stimulation of one pathway (weak 1), plotted as for (B) and (D). Traces (top) also show the effect of NBQX. Data in (C) (right) and (E) (right) are shown as the mean ± SEM. *Vm*, membrane potential.

Anti-Hebbian LTP is, however, rare at Schaffer collateral synapses on interneurons in the stratum radiatum, which generally mediate feedforward inhibition and express nonrectifying receptors (Fig. 3, D and E). Synaptic responses evoked by stratum radiatum stimulation in fast-spiking interneurons in the stratum pyramidale, however, had strongly rectifying AMPARs and a small NMDA component, and the Hebbian LTP induction protocol was uniformly unsuccessful ($n = 4$; fig. S6).

Does rectification of CP-AMPARs fully explain the anti-Hebbian nature of LTP in interneurons in the oriens/alveus? We first verified that AMPA/kainate receptors are necessary for induction, by pairing HFS with postsynaptic hyperpolarization while AMPA/kainate receptors were blocked with 2,3-dihydroxy-6-nitro-7-sulfamoyl-benzo[f]quinoxaline (NBQX, 5 μM): After washout of the antagonist, EPSPs in the tetanized and control pathways recovered to the same extent ($n = 7$; Fig. 3F). We then explored systematically the voltage dependence of LTP. In five cells in the oriens/alveus where anti-Hebbian LTP was evoked in one alveus pathway, subsequent pairing of the other pathway with depolarization only evoked short-lived post-tetanic potentiation (Fig. 4A). In six other cells, pairing the second pathway with hyperpolarization elicited robust LTP in all cases (Fig. 4, B and C). We then adapted this experimental design to explore the effect of manipulating the rectification properties of CP-AMPARs. Having demonstrated anti-Hebbian LTP in one pathway, we repatched the interneuron in whole-cell mode either with or without spermine in the pipette solution. Following a short baseline recording (≤7 min from patch rupture), we then paired HFS of the second pathway either with depolarization (+20 mV) or with hyperpolarization (−90 mV). When spermine was omitted, pairing with depolarization evoked LTP in five out of five cells (Fig. 4D), consistent with Ca^{2+} influx via CP-AMPARs rendered nonrectifying by removal of polyamines (*4*). In contrast, HFS paired with depolarization failed to elicit LTP in five cells that were repatched with a spermine-containing pipette (Fig. 4E). In five other interneurons repatched with a spermine-containing solution, pairing HFS of the second pathway with hyperpolarization to −90 mV evoked LTP (Fig. 4F).

Polyamine-mediated rectification of AMPARs (and/or kainate receptors) thus explains the voltage dependence of LTP induction in these interneurons and reconciles our results with previous reports that a Hebbian protocol induces LTP in interneurons in the oriens/alveus when recorded with a polyamine-free whole-cell pipette solution (*12*). Also consistent with these reports, blockade of group I metabotropic glutamate receptors prevented LTP induction in interneurons with horizontal dendrites in the oriens/alveus (fig. S7). Finally, we looked for evidence that anti-Hebbian LTP is accompanied by an increase in glutamate-release probability (*12*), by applying extracellular polyamines, which also block CP-AMPARs in a use-dependent manner (*20*). After inducing anti-Hebbian LTP in one pathway, bath perfusion of *N*-(4-hydroxyphenylpropanoyl)-spermine (5 to 10 μM) caused a progressive decrease in EPSP initial slope, which was significantly faster in the paired than in the control pathway ($n = 7$; fig. S8). Given that anti-Hebbian LTP did not alter AMPAR rectification (Fig. 3B), this result is consistent with presynaptic expression.

Anti-Hebbian LTP may play distinct roles in neurons that show characteristic phase relationships in different network states (*21*, *22*). During sharp-wave ripples, O-LM cells are typically silent, while many of their input pyramidal neu-

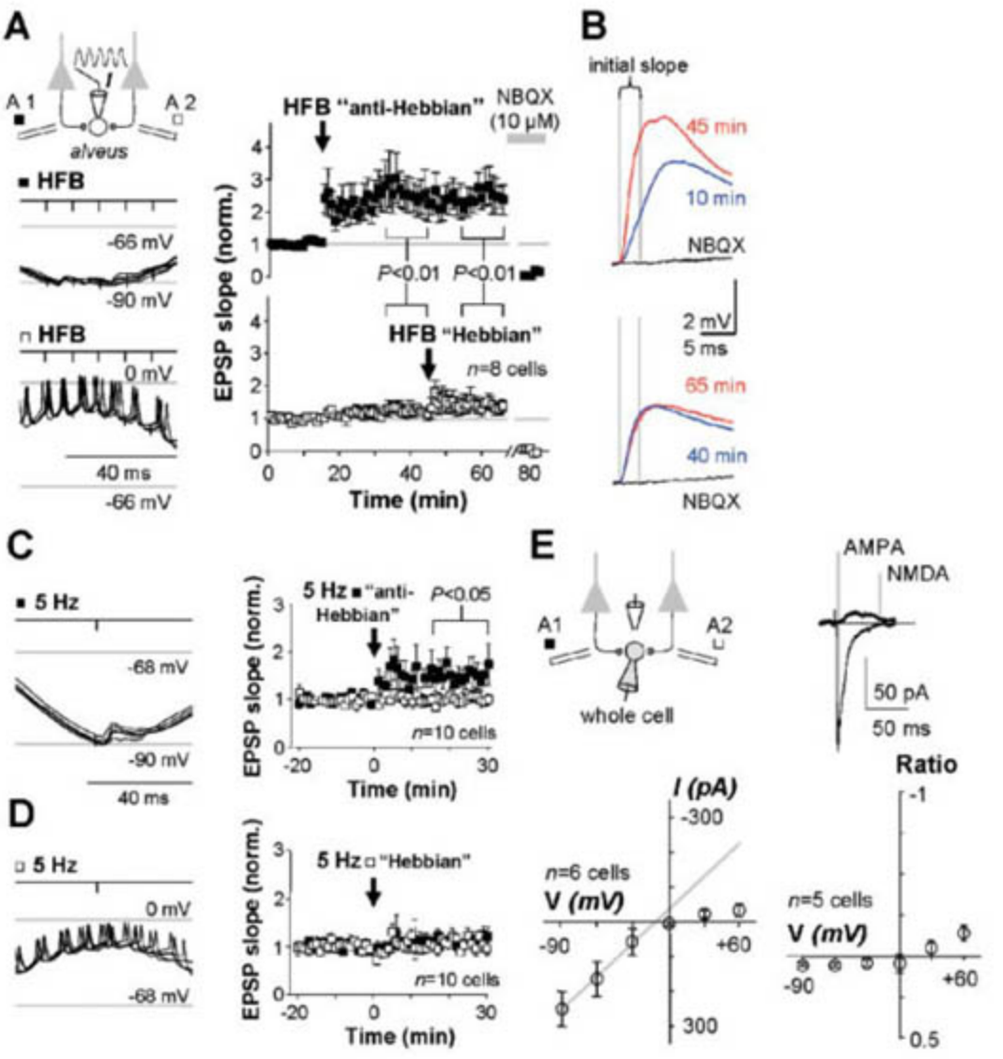

Fig. 2. Postsynaptic membrane potential gates anti-Hebbian LTP induction. (**A**) LTP was evoked by pairing presynaptic stimulation with the hyperpolarizing but not the depolarizing phase of an imposed sinusoidal membrane potential oscillation. Left: Schematic and sample membrane potential traces during pairing in one cell (five sweeps superimposed for each pairing protocol). Right: Baseline-normalized EPSP initial slopes in eight cells showing LTP after anti-Hebbian pairing of HFB stimulation of one pathway with hyperpolarization. Subsequent Hebbian pairing of the other pathway with depolarization was ineffective. AMPA/kainate receptors were blocked at the end of the experiment (NBQX). Data are shown as the mean ± SEM. (**B**) Averaged EPSPs in one cell taken at the times indicated and after NBQX addition. Top: Anti-Hebbian pairing. Bottom: Hebbian pairing. (**C**) LTP was induced by pairing single stimuli at 5 Hz with hyperpolarization. Left: Sample traces during pairing. Right: Averages of all cells tested. Data are shown as the mean ± SEM. (**D**) Pairing with depolarization failed to induce LTP. Left: Sample traces during pairing. Right: Averages of all cells tested. Data are shown as the mean ± SEM. (**E**) Repatched interneurons recorded in whole-cell voltage-clamp mode show rectifying AMPARs and a negligible NMDAR-mediated component (GABA receptors blocked). Traces: Averaged EPSCs at +60 and −60 mV, showing the times at which the two components were measured. Bottom: current-voltage (*I-V*) relation of AMPAR-mediated EPSCs in six repatched interneurons (left). *I-V* relation for the NMDAR-mediated component, normalized by the AMPA EPSC at −60 mV (right).

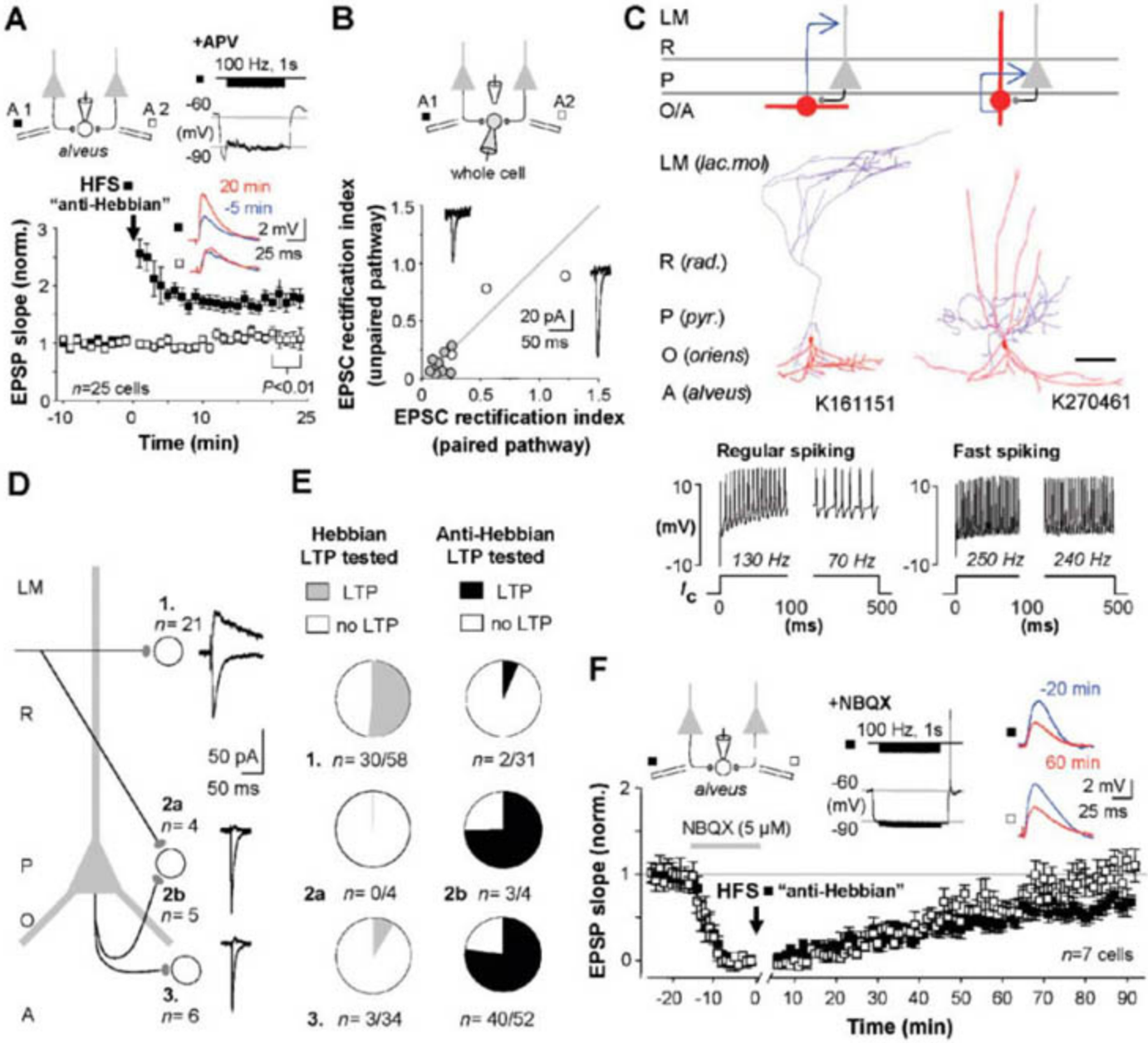

Fig. 3. Anti-Hebbian LTP occurs in interneurons with rectifying AMPARs in the feedback circuit. (**A**) High-frequency stimulation (HFS) paired with hyperpolarization evoked LTP in 25 out of 31 interneurons in the oriens/alveus [NMDARs blocked with 100 μM D,L-2-amino-5-phosphonovalerate (APV)]. Insets: Averaged EPSPs before and after LTP induction, and membrane potential during pairing, in one interneuron. Data are shown as the mean ± SEM. (**B**) Repatched interneurons recorded in whole-cell voltage-clamp mode revealed strongly rectifying synaptic AMPARs (rectification index < 0.3). Gray and open symbols show cells that did and did not exhibit LTP, respectively. Insets: Averaged EPSCs at −60 and +60 mV in one cell that showed anti-Hebbian LTP. (**C**) O-LM cells were the commonest identified interneuron type exhibiting anti-Hebbian LTP (left: schematic, with dendritic and axonal arborizations for one cell shown in red and blue, respectively). Three fast spiking perisomatic-projecting neurons were also identified, including a basket cell (right). Scale bar: 200 μm. Firing patterns in response to current injection (I_c) are shown below. (**D**) Typical layer- and pathway-specific properties of EPSCs in experiments where NMDARs were not blocked (*n*, number of repatched interneurons). Interneurons were recorded in the stratum radiatum (1), stratum pyramidale (2), and stratum oriens/alveus (3). (**E**) Success rates for eliciting Hebbian or anti-Hebbian LTP at synapses made by axons illustrated in (D). (**F**) Anti-Hebbian LTP requires activation of AMPA/kainate receptors. HFS stimulation of one pathway (filled symbols) was paired with hyperpolarization in NBQX (5 μM) (inset). After wash-out, EPSPs in both pathways recovered at the same rate. Inset: Averaged EPSPs before pairing (blue) and after recovery (red) in the two pathways in one experiment. Data are shown as the mean ± SEM.

rons fire at high frequency (*21*), possibly satisfying the induction conditions for anti-Hebbian LTP. Binding of pyramidal neurons to a spatial map may occur during periods of high-frequency firing (*23*), similar to sharp-wave ripples. In contrast, during theta activity, which is associated with exploratory behavior (*24*), O-LM cells fire in phase with pyramidal cells (*21*) and may contribute to this oscillation through phase-locked dendritic inhibition (*25*). Anti-Hebbian LTP induced during ripples may therefore result in a long-term alteration of pyramidal cell excitation of O-LM cells, which persists during theta activity, and may therefore contribute to spatial memory formation, the early stages of which have been shown to withstand NMDAR blockade (*26*).

References and notes

1. T. V. Bliss, G. L. Collingridge, *Nature* **361**, 31 (1993).
2. P. Jonas, C. Racca, B. Sakmann, P. H. Seeburg, H. Monyer, *Neuron* **12**, 1281 (1994).

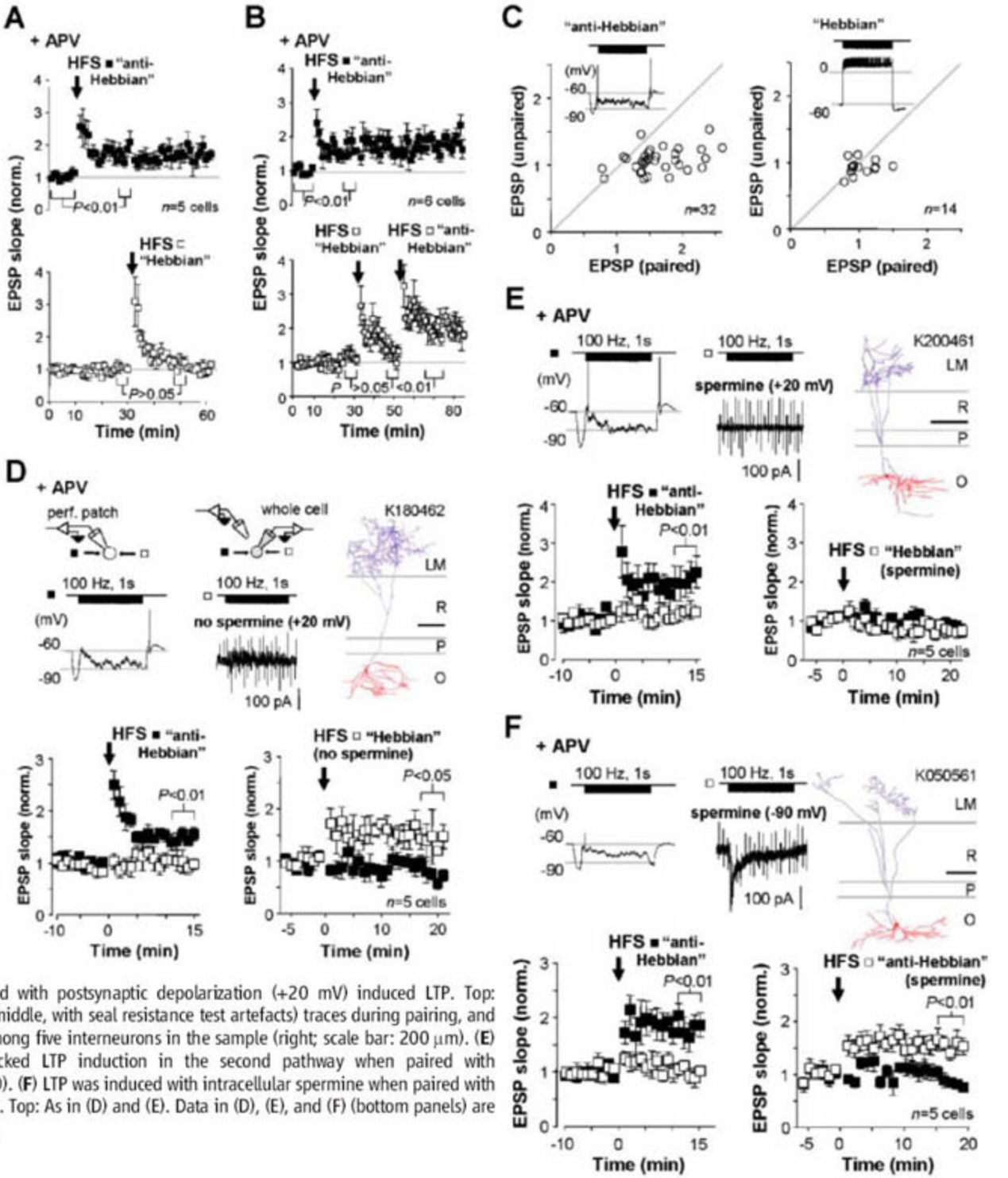

Fig. 4. Intracellular polyamines determine the voltage dependence of anti-Hebbian LTP. (**A**) Postsynaptic depolarization prevents LTP induction. Data from cells recorded in perforated patch mode, showing LTP induced by pairing high-frequency stimulation (HFS) of one pathway with hyperpolarization (top, "anti-Hebbian"), and failure to induce LTP by pairing the other pathway with depolarization (bottom, "Hebbian"). NMDARs were blocked throughout. Data are the mean ± SEM. (**B**) In six other cells, the second pathway was subsequently paired with hyperpolarization, yielding anti-Hebbian LTP in all cases. Data are the mean ± SEM. (**C**) Baseline-normalized EPSP slopes plotted against one another 20 min after anti-Hebbian (left) and Hebbian (right) pairing. Insets: Sample membrane potential traces during pairing. (**D**) Anti-Hebbian LTP was first induced in one pathway (left, filled symbols). The interneuron was then repatched in whole-cell mode with a polyamine-free pipette solution. HFS delivered to the second pathway (right, open symbols) paired with postsynaptic depolarization (+20 mV) induced LTP. Top: Voltage (left) and current (middle, with seal resistance test artefacts) traces during pairing, and one O-LM cell identified among five interneurons in the sample (right; scale bar: 200 μm). (**E**) Intracellular spermine blocked LTP induction in the second pathway when paired with depolarization. Top: As in (D). (**F**) LTP was induced with intracellular spermine when paired with hyperpolarization (–90 mV). Top: As in (D) and (E). Data in (D), (E), and (F) (bottom panels) are shown as the mean ± SEM.

3. M. S. Washburn, M. Numberger, S. Zhang, R. Dingledine, *J. Neurosci.* **17**, 9393 (1997).
4. S. D. Donevan, M. A. Rogawski, *Proc. Natl. Acad. Sci. U.S.A.* **92**, 9298 (1995).
5. D. Bowie, M. L. Mayer, *Neuron* **15**, 453 (1995).
6. J. G. Gu, C. Albuquerque, C. J. Lee, A. B. MacDermott, *Nature* **381**, 793 (1996).
7. N. K. Mahanty, P. Sah, *Nature* **394**, 683 (1998).
8. F. Laezza, J. J. Doherty, R. Dingledine, *Science* **285**, 1411 (1999).
9. S. Lei, C. J. McBain, *Neuron* **33**, 921 (2002).
10. F. Laezza, R. Dingledine, *J. Neurophysiol.* **92**, 3575 (2004).
11. L. Topolnik, P. Congar, J. C. Lacaille, *J. Neurosci.* **25**, 990 (2005).
12. Y. Perez, F. Morin, J. C. Lacaille, *Proc. Natl. Acad. Sci. U.S.A.* **98**, 9401 (2001).
13. Materials and methods are available as supporting material on *Science* Online.
14. D. O. Hebb, *The Organization of Behavior* (Wiley, New York, 1949).
15. G. Bi, M. Poo, *Annu. Rev. Neurosci.* **24**, 139 (2001).
16. K. Lamsa, J. H. Heeroma, D. M. Kullmann, *Nat. Neurosci.* **8**, 916 (2005).
17. G. Nyiri, F. A. Stephenson, T. F. Freund, P. Somogyi, *Neuroscience* **119**, 347 (2003).
18. K. Plant *et al.*, *Nat. Neurosci.* **9**, 602 (2006).
19. J. M. Blasco-Ibanez, T. F. Freund, *Eur. J. Neurosci.* **7**, 2170 (1995).
20. Z. F. Mainen, Z. Jia, J. Roder, R. Malinow, *Nat. Neurosci.* **1**, 579 (1998).
21. T. Klausberger *et al.*, *Nature* **421**, 844 (2003).
22. T. Klausberger *et al.*, *Nat. Neurosci.* **7**, 41 (2004).
23. G. Dragoi, K. D. Harris, G. Buzsaki, *Neuron* **39**, 843 (2003).
24. G. Buzsaki, *Neuron* **33**, 325 (2002).
25. M. J. Gillies *et al.*, *J. Physiol.* **543**, 779 (2002).
26. C. Kentros *et al.*, *Science* **280**, 2121 (1998).

27. Animal procedures followed the Animals (Scientific Procedures) Act 1986. Supported by the Wellcome Trust, the Academy of Finland, and the Medical Research Council. We are grateful to M. C. Walker and K. Volynski for comments, and to J. D. B. Roberts for help with histological processing.

Supporting Online Material

www.sciencemag.org/cgi/content/full/315/5816/1262/DC1
Materials and Methods
Figs. S1 to S8
References

13 November 2006; accepted 1 February 2007
10.1126/science.1137450

Nucleus Accumbens D2/3 Receptors Predict Trait Impulsivity and Cocaine Reinforcement

Jeffrey W. Dalley,[1,2]* Tim D. Fryer,[1,3] Laurent Brichard,[1]† Emma S. J. Robinson,[1]‡ David E. H. Theobald,[1,2] Kristjan Lääne,[1,2] Yolanda Peña,[1]§ Emily R. Murphy,[1,2] Yasmene Shah,[4] Katrin Probst,[1,3] Irina Abakumova,[1,3] Franklin I. Aigbirhio,[1,3] Hugh K. Richards,[1,5] Young Hong,[1,3] Jean-Claude Baron,[1,6] Barry J. Everitt,[1,2] Trevor W. Robbins[1,2]

Stimulant addiction is often linked to excessive risk taking, sensation seeking, and impulsivity, but in ways that are poorly understood. We report here that a form of impulsivity in rats predicts high rates of intravenous cocaine self-administration and is associated with changes in dopamine (DA) function before drug exposure. Using positron emission tomography, we demonstrated that D2/3 receptor availability is significantly reduced in the nucleus accumbens of impulsive rats that were never exposed to cocaine and that such effects are independent of DA release. These data demonstrate that trait impulsivity predicts cocaine reinforcement and that D2 receptor dysfunction in abstinent cocaine addicts may, in part, be determined by premorbid influences.

Accumulating evidence suggests that certain personality traits, including sensation (or novelty) seeking, impulsivity, and antisocial conduct disorder, may predispose humans to drug abuse and addiction (*1*–*4*). However, from studies of human drug addicts alone, it is difficult to determine whether comorbid impulsivity and cognitive dysfunction (*5*, *6*) pre-date the onset of drug use or emerge as a consequence of chronic drug use. Current hypotheses suggest that long-term drug use impairs inhibitory control functions mediated by the prefrontal cortex and the associated limbic brain circuitry, leading to a loss of inhibition or to impulsivity (*7*, *8*). However, there is little evidence to date that chronic exposure to cocaine and other psychostimulant drugs leads to long-term increases in impulsive behavior in animals (*9*–*11*).

The view that individual differences in drug abuse reflect distinct behavioral and physiological traits is richly supported by studies in animals (*12*–*17*). Rats that are selected for high novelty-induced locomotor activity more readily acquire intravenous amphetamine and cocaine self-administration at lower doses than do rats that show reduced levels of activity (*12*, *13*). In addition, rats that are impulsive on a delay-of-reward task, choosing a small immediate reward over a large but delayed reward, show an increased propensity to self-administer cocaine, as compared to low-impulsive rats (*18*). Finally, the existence of trait variables related to drug-abuse vulnerability is encouraged by studies in nonhuman primates in which cocaine is more readily self-administered by subordinate, rather than dominant, monkeys (*19*).

A key neural substrate underlying individual differences in drug vulnerability is thought to involve the brain dopamine (DA) systems, in particular the mesolimbic and mesocortical DA pathways innervating the nucleus accumbens and prefrontal cortex (*19*–*22*). Positron emission tomography (PET) studies in nonhuman primates have indicated a role for DA D2 receptors in determining individual differences in intravenous cocaine self-administration (*19*, *20*). Specifically, low D2 receptor availability in the striatum inversely predicts subsequent levels of intravenous cocaine self-administration in rhesus monkeys (*20*), a result apparently similar to that seen in studies of human cocaine abusers (*23*).

However, it is not clear how individual differences in D2 receptor availability relate to a specific behavioral endophenotype or behavioral process that confers vulnerability to drug addiction. In addition, there have been few, if any, studies where DA release in vivo has been combined with PET estimates of D2 receptor availability. This is important because D2 receptor availability is influenced by both receptor density and competing DA release (*24*, *25*). Thus, there is a need to conduct analogous PET studies in animals to investigate the predictive relationship between D2 receptor availability and trait behavioral markers of drug-abuse vulnerability.

We investigated the relevance of a spontaneously occurring form of impulsivity in outbred Lister hooded (LH) rats to intravenous cocaine self-administration and to underlying changes in striatal DA function, as measured by microPET and in vivo microdialysis (*26*). We defined impulsivity as high levels of anticipatory responses made before the presentation of a

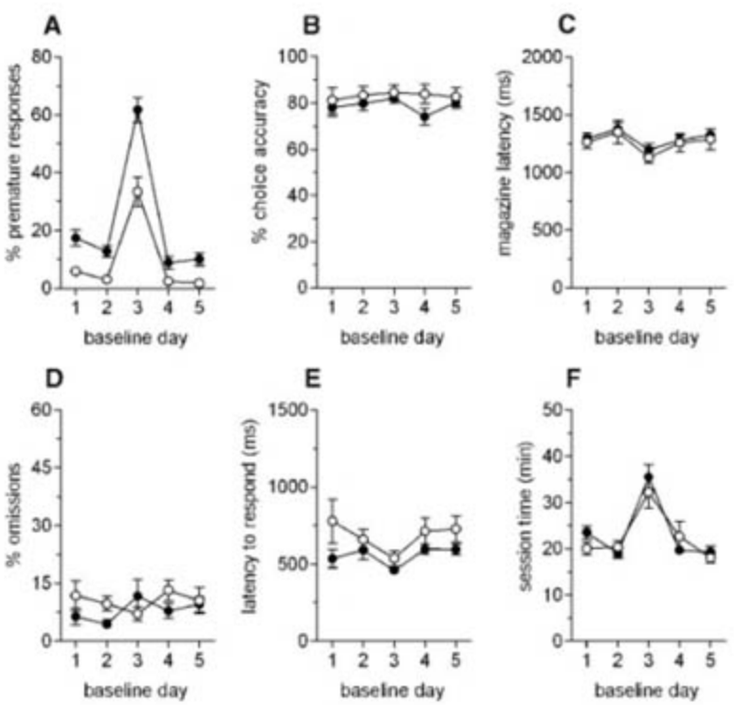

Fig. 1. Behavioral attributes of trait impulsivity on the 5-CSRT task. (**A**) Impulsive rats exhibit high levels of premature responding on days when visual targets are presented either 5 s after trial initiation (days 1, 2, 4, and 5) or 7 s after trial initiation (day 3), as compared to non-impulsive rats. Two-way analysis of variance (ANOVA) of premature responses revealed a significant main effect of day [$F(4,40) = 144.9$, $P < 0.01$] and a significant main effect of group [$F(1,10) = 26.1$, $P < 0.01$]. However, there were no significant effects on other measures of task performance, including (**B**) attentional accuracy [$F(1,10) = 1.17$, $P = 0.306$], (**C**) latency to collect food reward [$F < 1$, not significant (ns)], (**D**) omissions ($F < 1$, ns), (**E**) latency to respond correctly [$F(1,10) = 3.0$, $P = 0.113$], and (**F**) the time required to complete both standard and challenge (long-ITI) sessions ($F < 1$, ns). Black circles, high-impulsive rats; white circles, non-impulsive rats.

[1]Behavioral and Clinical Neuroscience Institute, University of Cambridge, Downing Street, Cambridge CB2 3EB, UK. [2]Department of Experimental Psychology, University of Cambridge, Downing Street, Cambridge CB2 3EB, UK. [3]Wolfson Brain Imaging Centre, Department of Clinical Neurosciences, University of Cambridge, Addenbrooke's Hospital, Cambridge CB2 2QQ, UK. [4]Sir Peter Mansfield Magnetic Resonance Centre, School of Physics and Astronomy, University of Nottingham, Nottingham NG7 2RD, UK. [5]Neurosurgery Unit, Department of Clinical Neurosciences, University of Cambridge, Addenbrooke's Hospital, Cambridge CB2 2QQ, UK. [6]Neurology Unit, Department of Clinical Neurosciences, University of Cambridge, Addenbrooke's Hospital, Cambridge CB2 2QQ, UK.

*To whom correspondence should be addressed. E-mail: jwd20@cam.ac.uk

†Present address: Laboratoire d'Imagerie Moléculaire et Fonctionnelle: de la Physiologie à la Thérapie, ERT CNRS/Université Victor Segalen Bordeaux 2, Bordeaux, France.

‡Present address: Department of Pharmacology, University of Bristol, Bristol BS8 1TD, UK.

§Present address: Departament de Psiquiatria i de Medicina Legal, Universita Autònoma de Barcelona, Barcelona, Spain.

food-predictive, brief light stimulus in a five-choice serial reaction time (5-CSRT) task of sustained visual attention (*27*). Typically, 5-CSRT task impulsivity occurs in ~7% of male LH rats and, once identified, is a stable trait that persists throughout adulthood.

We first investigated the behavioral specificity of trait impulsivity on the 5-CSRT task and the correspondence of this trait to the high-responder (HR) drug-vulnerable phenotype described previously in rats by Piazza and colleagues (*12*). Trait impulsivity on the 5-CSRT task was characterized by a near-twofold increase in premature responding under both standard test conditions and when the intertrial interval (ITI) was increased to 7 s (Fig. 1A). In contrast to the HR rat, in our study trait impulsivity on the 5-CSRT task was inversely related to the level of locomotor activity measured in a novel environment [correlation coefficient (r) = 0.49, P = 0.02] (fig. S1).

Twelve cocaine-naïve adult male rats were then used to investigate DA D2/3 receptor availability in the ventral and dorsolateral striatum by means of micro-PET and the selective high-affinity DA D2/3 receptor antagonist [^{18}F] fallypride (*28*). Six non-impulsive rats and six high-impulsive rats were prepared previously with an intravenous catheter. The ventral striatum was included as a region of interest (ROI), because the primary reinforcing and psychostimulant effects of drugs of abuse depend on the functional integrity of DA afferents to this region (*29*–*31*). In contrast, DA neurotransmission in the dorsolateral striatum mediates the persistent or compulsive forms of drug-seeking behavior (*32*), which is consistent with a role for this region in stimulus-response habit-based learning mechanisms (*33*, *34*).

We found significantly reduced D2/3 receptor availability in the ventral striatum (P = 0.037) but not the dorsolateral striatum of high-impulsive rats as compared to non-impulsive rats (Fig. 2), and we also found a significant inverse correlation between D2/3 receptor availability in the ventral striatum and impulsivity (r = 0.58, P = 0.048) (fig. S2). An example of the quality of the data fit obtained with the simplified reference tissue model (*35*) is shown in fig. S3.

We also investigated the possibility that reduced [^{18}F]fallypride binding potential in the ventral striatum was due to excessive release of DA in the nucleus accumbens. We postulated that enhanced DA release may have displaced [^{18}F]fallypride from D2/3 receptors in this region, leading to an apparent reduction in D2/3 receptor availability. DA release and metabolism [inferred from levels of 3,4-dihydroxyphenylacetic acid and homovanillic acid (4-hydroxy-3-methoxyphenylacetic acid)] in the nucleus accumbens were not significantly different between impulsive rats and non-impulsive rats. There was also no significant difference in levels of the 5-hydroxytryptamine metabolite 5-hydroxyindoleacetic acid in this brain region (table S1). Thus, the most likely explanation for the significant reduction in D2/3 receptor availability in trait-impulsive rats was a decrease in the number of D2/3 receptors.

We next investigated the consequences of trait impulsivity for the acquisition and maintenance of intravenous cocaine self-administration.

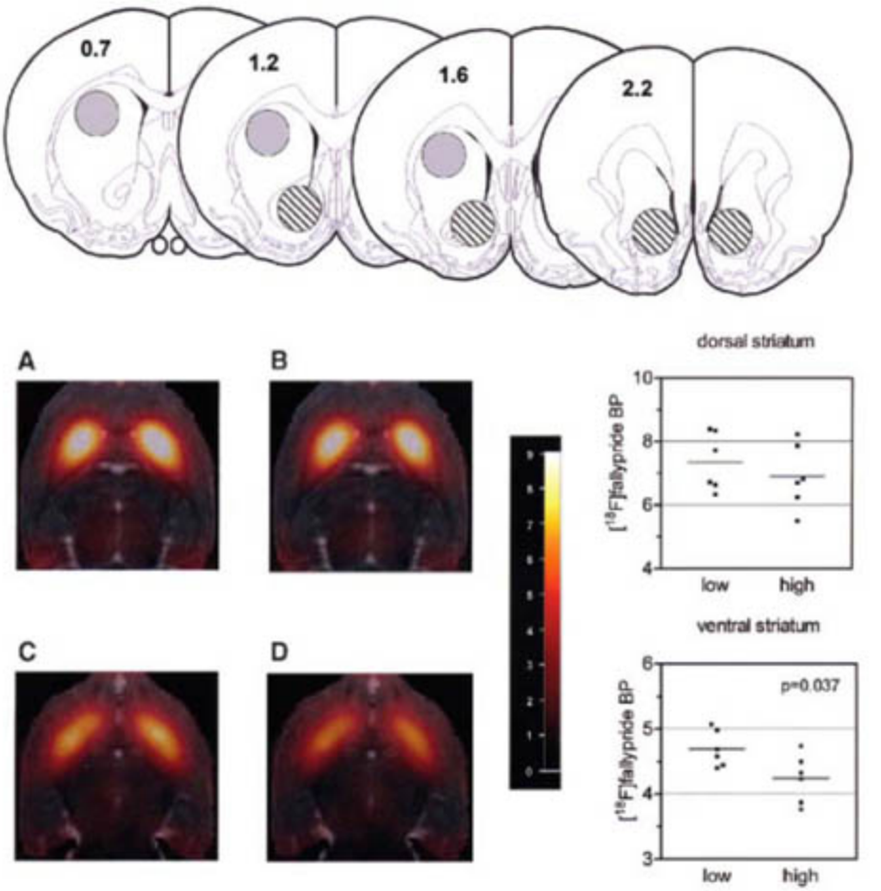

Fig. 2. Reduced binding potential (BP) of the selective D2/3 receptor antagonist [^{18}F]fallypride in the ventral striatum of drug-naïve trait-impulsive rats (n = 6 rats) as compared to drug-naïve non-impulsive rats (n = 6). (**Top**) ROIs are shown in the schematic coronal sections of the rat forebrain [adapted from (*46*)]. Dorsal and ventral striatal ROIs are depicted by the shaded and striped circles, respectively. Anterior-posterior coordinates (in millimeters) relative to bregma are shown on each coronal section. The ROIs have diameters of 2 mm in the transverse plane. BP values are averages of left and right striata. (**A** to **D**) Horizontal MR coregistered PET images of [^{18}F]fallypride binding in the dorsal (upper panels) and ventral (lower panels) striatum of a non-impulsive rat [(A) and (C)] and a high-impulsive rat [(B) and (D)]. The images are 4.5 mm [(A) and (B)] and 7.0 mm [(C) and (D)] below the dorsal brain surface (BP threshold = 9).

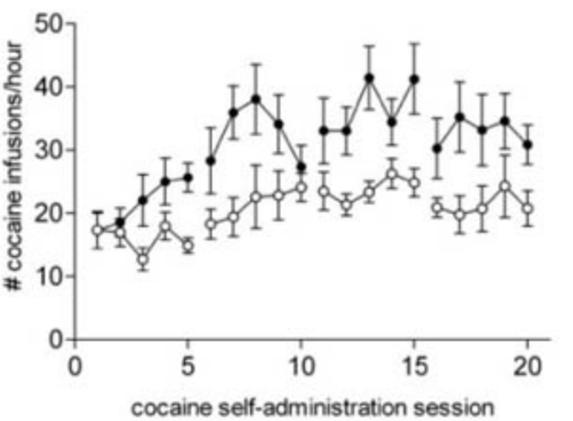

Fig. 3. Differential escalation of intravenous cocaine self-administration in high-impulsive rats (n = 8) as compared to non-impulsive rats (n = 8). On the first 5 days, access to cocaine was restricted to 5 hours and a maximum of 50 infusions. After a withdrawal period of 9 days, access to cocaine was increased on each of the following 5 days to 8 hours and a maximum of 150 infusions. This pattern of intermittent cocaine self-administration was repeated on two further occasions. Impulsive rats showed a differential increase in their rate of cocaine self-administration after extended access to cocaine [session: $F(19,133) = 2.04$, $P = 0.01$; group: $F(1,14) = 32.82$, $P < 0.001$; session × group: $F(19,133) = 1.92$, $P = 0.017$]. Subsequent pairwise comparisons revealed significant differences ($P < 0.05$) between the first session and sessions 10, 13, 14, and 15 for the non-impulsive group and between the first session and all sessions but nos. 2, 3, 4, 10, and 16 for the high-impulsive group. Black circles, high-impulsive rats; white circles, non-impulsive rats.

Intravenously catheterized rats that were screened previously for impulsivity on the 5-CSRT task, as well as their non-impulsive controls, were trained to acquire intravenous cocaine self-administration under a continuous-reinforcement schedule (fig. S4). Impulsive rats exhibited a clear increase in their rate of intravenous cocaine self-administration as compared to non-impulsive rats (Fig. 3), as well as a vertical shift in the cocaine dose-response curve (fig. S5).

In a final experiment, we investigated the effects of repeated intermittent withdrawal of cocaine on pretrained performance of the 5-CSRT task (Fig. 4). Our objective was to determine whether high rates of cocaine self-administration exhibited by trait-impulsive rats resulted in differential impairments in sustained visual attention, as compared to non-impulsive rats. We found that prolonged exposure of trait-impulsive rats to cocaine decreased levels of premature responding on the 5-CSRT task when the animals were tested in withdrawal (Fig. 4), but that it had no effect on other measures of performance, including attentional accuracy, omissions, and response latencies. Thus, one clear consequence of long-access cocaine exposure and subsequent cocaine withdrawal in trait-impulsive rats was a selective normalization of premature responding on the 5-CSRT task, relative to non-impulsive rats.

We have shown that individual differences in impulsive behavior on a five-choice task of sustained visual attention strongly predict individual variation in the rate of intravenous cocaine self-administration. Specifically, rats exhibiting trait impulsivity on the 5-CSRT task (*27*) showed a greater tendency for escalation of intravenous cocaine self-administration than did their non-impulsive counterparts. We also found unequivocal evidence for a significant inverse relationship between D2/3 receptor availability in the ventral striatum and trait impulsivity that could not be explained by abnormalities in presynaptic DA release and function in this region. These results expand on previous findings in abstinent human cocaine addicts (*23*, *36*) by demonstrating that decreased D2 receptor availability in the striatum may be a predisposing neurobiological trait and not only a consequence of chronic cocaine exposure. They also add to the finding that D2 receptor availability in the striatum inversely predicts rates of intravenous cocaine self-administration in previously cocaine-naïve rhesus monkeys (*20*), by defining the characteristics of a drug-vulnerable phenotype in terms of a specific behavioral construct, as well as by underlying abnormalities in D2 receptor function in the striatum. Thus, the present data demonstrate that trait impulsiveness is a drug-vulnerable phenotype and highlight a potential overlapping involvement of D2-like DA receptors, which have been previously implicated in genetic studies of both impulsivity and vulnerability to drug-abuse disorders (*37*, *38*).

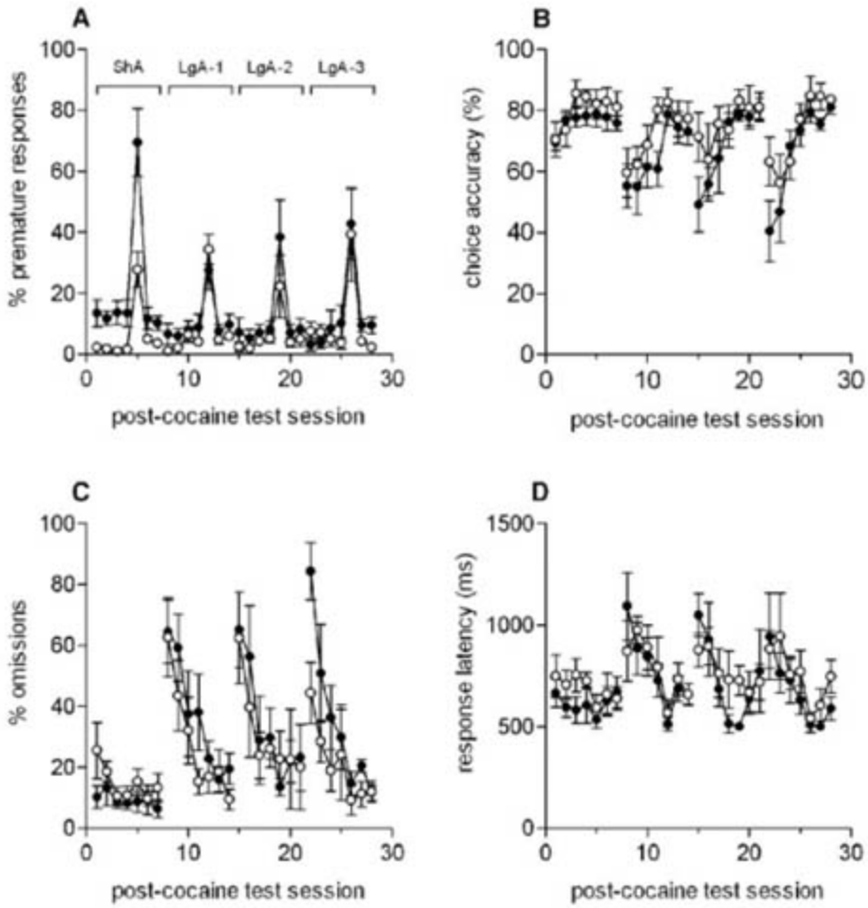

Fig. 4. Effects of intermittent intravenous cocaine self-administration in high-impulsive rats (n = 8) and non-impulsive rats (n = 8) on sustained visual attention on the 5-CSRT task. (**A**) Rats were withdrawn from intravenous cocaine self-administration on four occasions and tested 24 hours later for 7 consecutive days on the 5-CSRT task. ShA, tested after short access to cocaine over 5 days, when rats received 50 cocaine infusions over 5 hours; LgA-1, tested after long access to cocaine, when the daily number of cocaine infusions increased to 150 and the session duration to 8 hours; LgA-2, tested after a second long-access exposure to cocaine; LgA-3, tested after a third long-access exposure to cocaine. ANOVA of premature responses revealed significant group × cycle [$F(3,42) = 7.86$, $P = 0.023$] and group × cycle × session [$F(18,252) = 4.29$, $P < 0.001$] interactions. Subsequent analyses revealed that premature responding was higher in high-impulsive rats as compared to non-impulsive rats during the ShA cycle [group: $F(1,14) = 20.58$, $P < 0.001$] but not during subsequent LgA-1 [$F(1,14) = 0.62$, $P = 0.44$], LgA-2 [$F(1,14) = 3.82$, $P = 0.071$], and LgA-3 [$F(1,14) = 0.51$, $P = 0.49$] cycles. There were no significant differences between non-impulsive and high-impulsive rats with respect to (**B**) attentional accuracy, (**C**) omissions, and (**D**) correct response latency ($F < 1.44$, $P > 0.24$ for all comparisons). Black circles, high-impulsive rats; white circles, non-impulsive rats.

Trait impulsivity on the 5-CSRT task is negatively correlated with novelty-induced locomotor activity and so is unlikely to be equivalent to the HR drug-vulnerable phenotype (*12*). In contrast to HR rats (*12*, *13*), the high-impulsive rats in the present study did not acquire cocaine self-administration faster than the low-impulsive rats. Although impulsive female rats screened by means of a food-motivated delayed-discounting task acquired cocaine self-administration more rapidly than did low-impulsive rats (*18*), the high-impulsive rats acquired the delayed-discounting task more readily, suggesting that a more fundamental difference in instrumental learning may underpin the difference in the initiation of drug-taking behavior. HR rats also self-administer high doses of stimulants (*12*, *13*), and so it is conceivable that this phenotype overlaps with the present high-impulsive animals to some extent. However, our findings specifically link trait impulsivity, rather than hyperactivity, to the maintenance and escalation of cocaine self-administration and to reduced D2/3 receptor binding in the nucleus accumbens.

Mutant mice lacking D2-like receptors show high rates of intravenous cocaine self-administration when high doses of cocaine are made available (*39*). Thus, D2 receptors may play a role in regulatory processes that normally act to limit excessive rates of cocaine self-administration. The decreased D2/3 receptor availability in the nucleus accumbens of high-impulsive rats may therefore contribute to increased cocaine self-administration. This finding may have broad relevance to a number of abused drugs in humans, including nicotine and opiates, where high consumption rates have also been

linked to reduced D2 receptor function, specifically because of the presence of the D2 *Taq* I A1 allele (*40*, *41*), which has previously been shown by PET to be associated with reduced D2 receptor density in the striatum (*42*).

Our results are consistent with the hypothesis that dysfunctional DA neurotransmission at D2-like receptors in the nucleus accumbens confers susceptibility to increased cocaine self-administration in high-impulsive rats. Recent findings in rhesus monkeys trained to self-administer cocaine support this view (*19*, *20*), but there has been little evidence to date that D2 receptor dysregulation that is present either as a trait marker or induced by chronic cocaine exposure is restricted to the nucleus accumbens. Indeed, analogous PET studies in monkeys (*19*, *20*, *43*) and abstinent human cocaine addicts (*23*) report generalized reductions in D2 receptor availability throughout the striatum. In contrast, as in the present study, D2 receptor density and D2 mRNA content were found to be significantly reduced in the nucleus accumbens but not in the dorsal striatum or medial prefrontal cortex of HR rats (*44*).

The contrast between specific reductions in D2 receptor availability in the nucleus accumbens in rats before cocaine self-administration, as compared to the more divergent effects in the striatum after chronic exposure to cocaine self-administration, suggests the hypothesis that the ventral striatal changes confer susceptibility to cocaine taking, which subsequently affects DA neurotransmission in the dorsal striatum, with corresponding effects on the number of D2 receptors in that region (*20*, *23*, *43*). Thus, the development of psychostimulant drug addiction may represent a progression from initial impulsivity mediated by the nucleus accumbens to the development of compulsive habitual responding mediated by the dorsal striatum (*32*, *45*).

References and Notes

1. N. Chakroun, J. Doron, J. Swendsen, *Encephale* **30**, 564 (2004).
2. S. Dawe, N. J. Loxton, *Neurosci. Biobehav. Rev.* **28**, 343 (2004).
3. K. J. Sher, B. D. Bartholow, M. D. Wood, *J. Consult. Clin. Psychol.* **68**, 818 (2000).
4. J. B. Adams *et al.*, *Am. J. Drug Alcohol Abuse* **29**, 691 (2003).
5. K. I. Bolla, R. Rothman, J. L. Cadet, *J. Neuropsychiatry Clin. Neurosci.* **11**, 361 (1999).
6. R. Hester, H. Garavan, *J. Neurosci.* **24**, 11017 (2004).
7. J. D. Jentsch, J. R. Taylor, *Psychopharmacology* **146**, 373 (1999).
8. M. Lyvers, *Exp. Clin. Psychopharmacol.* **8**, 225 (2000).
9. T. A. Paine, H. C. Dringenberg, M. C. Olmstead, *Behav. Brain Res.* **147**, 135 (2003).
10. J. W. Dalley *et al.*, *Psychopharmacology* **182**, 579 (2005).
11. J. W. Dalley *et al.*, *Neuropsychopharmacology* **30**, 525 (2005).
12. P. V. Piazza, J. M. Deminiere, M. Le Moal, H. Simon, *Science* **245**, 1511 (1989).
13. J. R. Mantsch, A. Ho, S. D. Schlussman, M. J. Kreek, *Psychopharmacology* **157**, 31 (2001).
14. E. B. Larson, M. E. Carroll, *Pharmacol. Biochem. Behav.* **82**, 590 (2005).
15. A. D. Morgan, N. K. Dess, M. E. Carroll, *Psychopharmacology* **178**, 41 (2005).
16. B. A. Gosnell, *Psychopharmacology* **149**, 286 (2000).
17. E. L. van der Kam, B. A. Ellenbroek, A. R. Cools, *Neuropharmacology* **48**, 685 (2005).
18. J. L. Perry, E. B. Larson, J. P. German, G. J. Madden, M. E. Carroll, *Psychopharmacology* **178**, 193 (2005).
19. D. Morgan *et al.*, *Nat. Neurosci.* **5**, 169 (2002).
20. M. A. Nader *et al.*, *Nat. Neurosci.* **9**, 1050 (2006).
21. P. V. Piazza *et al.*, *Brain Res.* **567**, 169 (1991).
22. M. Tonissaar, L. Herm, A. Rinken, J. Harro, *Neurosci. Lett.* **403**, 119 (2006).
23. N. D. Volkow *et al.*, *Synapse* **14**, 169 (1993).
24. R. H. Mach *et al.*, *Pharmacol. Biochem. Behav.* **57**, 477 (1997).
25. M. Laruelle *et al.*, *Neuropsychopharmacology* **17**, 162 (1997).
26. Materials and methods are available as supporting material on *Science* Online.
27. T. W. Robbins, *Psychopharmacology* **163**, 362 (2002).
28. J. Mukherjee *et al.*, *Nucl. Med. Biol.* **26**, 519 (1999).
29. D. C. Roberts, M. E. Corcoran, H. C. Fibiger, *Pharmacol. Biochem. Behav.* **6**, 615 (1977).
30. S. B. Caine, G. F. Koob, *J. Exp. Anal. Behav.* **61**, 213 (1994).
31. H. O. Pettit, A. Ettenberg, F. E. Bloom, G. F. Koob, *Psychopharmacology* **84**, 167 (1984).
32. L. J. Vanderschuren, P. Di Ciano, B. J. Everitt, *J. Neurosci.* **25**, 8665 (2005).
33. M. G. Packard, B. J. Knowlton, *Annu. Rev. Neurosci.* **25**, 563 (2002).
34. H. H. Yin, B. J. Knowlton, B. W. Balleine, *Eur. J. Neurosci.* **19**, 181 (2004).
35. R. N. Gunn, A. A. Lammertsma, S. P. Hume, V. J. Cunningham, *Neuroimage* **6**, 279 (1997).
36. D. Martinez *et al.*, *Neuropsychopharmacology* **29**, 1190 (2004).
37. G. R. Uhl, *Ann. N. Y. Acad. Sci.* **1025**, 1 (2004).
38. A. M. Persico, G. Bird, F. H. Gabbay, G. R. Uhl, *Biol. Psychiatry* **40**, 776 (1996).
39. S. B. Caine *et al.*, *J. Neurosci.* **22**, 2977 (2002).
40. D. E. Comings, K. Blum, *Prog. Brain Res.* **126**, 325 (2000).
41. M. Shahmoradgoli Najafabadi *et al.*, *Am. J. Med. Genet. Neuropsychiatr. Genet.* **134**, 39 (2005).
42. T. Pohjalainen *et al.*, *Mol. Psychiatry* **3**, 256 (1998).
43. M. A. Nader *et al.*, *Neuropsychopharmacology* **27**, 35 (2002).
44. M. S. Hooks *et al.*, *J. Neurosci.* **14**, 6144 (1994).
45. B. J. Everitt, T. W. Robbins, *Nat. Neurosci.* **8**, 1481 (2005).
46. G. Paxinos, C. Watson, in *The Rat Brain in Stereotaxic Coordinates* (Academic Press, San Diego, CA, ed. 4, 1998), p. xxvi.

47. This research was supported by a joint award from the U.K. Medical Research Council (MRC) and the Wellcome Trust and by an MRC Pathfinder grant (G0401068) to J.W.D., B.J.E., and T.W.R. D.E.H.T. was supported by the Wellcome Trust. Y.P. was supported by a predoctoral Formación Investigadora scholarship from Generalitat de Catalunya. E.S.J.R. holds a Research Councils UK Academic Fellowship supported by the British Pharmacological Society Integrative Pharmacology Fund. E.R.M. was supported by a Gates Cambridge scholarship. We thank Merck, Sharp, & Dohme for originally donating the micro-PET scanner to Cambridge University.

Supporting Online Material

www.sciencemag.org/cgi/content/full/315/5816/1267/DC1
Materials and Methods
Figs. S1 to S5
Table S1
References

1 November 2006; accepted 1 February 2007
10.1126/science.1137073

Reconstitution of DNA Segregation Driven by Assembly of a Prokaryotic Actin Homolog

Ethan C. Garner,[1,2,3] Christopher S. Campbell,[1,2,3] Douglas B. Weibel,[3,4] R. Dyche Mullins[1,2,3]*

Multiple unrelated polymer systems have evolved to partition DNA molecules between daughter cells at division. To better understand polymer-driven DNA segregation, we reconstituted the three-component segregation system of the R1 plasmid from purified components. We found that the ParR/*parC* complex can construct a simple bipolar spindle by binding the ends of ParM filaments, inhibiting dynamic instability, and acting as a ratchet permitting incorporation of new monomers and riding on the elongating filament ends. Under steady-state conditions, the dynamic instability of unattached ParM filaments provides the energy required to drive DNA segregation.

To ensure fidelity of gene transmission, DNA molecules must be evenly distributed among daughter cells before division. Eukaryotes harness the polymerization of tubulin to drive alignment and segregation of chromosomes (*1*); chromosome segregation in some eubacteria requires assembly of actin-like filaments (*2*, *3*); and some extrachromosomal DNA elements have evolved their own polymer-based DNA segregation machinery (*4*, *5*). Plasmid R1 is a large (100 kb), low–copy number plasmid with segregation machinery encoded by the *par* operon (*6*, *7*). This operon is composed of three elements: *parC*, *parR*, and *parM* (*6*). *parM* encodes an actin-like protein that assembles into dynamically unstable filaments (*8*). *parR* encodes a protein that binds cooperatively to sequence repeats within *parC*, forming a complex that binds ParM filaments (*9*). It has been proposed that products of the *par* operon assemble into a bipolar spindle-like structure whose elongation drives plasmid segregation (*9*), but it is not yet

[1]Cellular and Molecular Pharmacology, University of California, San Francisco, CA 94158, USA. [2]UCSF/UCB Nanomedicine Development Center, San Francisco, CA 94158, USA. [3]Physiology Course, Marine Biological Laboratory, Woods Hole, MA 02543, USA. [4]Department of Biochemistry, University of Wisconsin, Madison, WI 53706, USA.

*To whom correspondence should be addressed. E-mail: dyche@mullinslab.ucsf.edu

known how these components assemble and how they convert the free energy of ParM polymerization into useful work.

By atomic structure, ParM is similar to actin (*10*), but by filament assembly dynamics, ParM is distinguished from actin by three important properties: (i) rapid, rather than slow, spontaneous nucleation; (ii) symmetrical, bidirectional elongation rather than polarized growth; and (iii) dynamic instability [the tendency to switch spontaneously (*11*) between phases of steady elongation and rapid shortening] rather than steady-state treadmilling (*8*). In vitro, the combination of these kinetic parameters results in a steady-state population of short (~1.5 μm) and unstable (lifetime ~20 s) ParM filaments (*8*).

To understand how ParR and *parC* harness filament assembly to segregate DNA, we purified all three components and tested their ability to self-assemble in vitro. We expressed and purified ParM and ParR proteins from *Escherichia coli* (fig. S1). We attached fluorescent (Cy3-labeled) DNA containing the *parC* sequence to 350-nm spherical beads. We then mixed the *parC*-coupled microspheres with ParR, added fluorescently labeled (Alexa 488) ParM, and induced filament assembly by adding adenosine triphosphate (ATP).

ParM filaments formed small radial arrays surrounding isolated *parC* beads (Fig. 1A), reminiscent of microtubule asters formed around isolated centrosomes (*12*). Aster formation required ATP, ParR (fig. S2A), and DNA containing the *parC* sequence (fig. S2B). Asters were dynamic, with filaments growing and shrinking from the surface of the bead, and grew to a maximum radius of 3 μm (Fig. 1B and movie S1), similar to the maximum lengths of individual ParM filaments in solution (*8*). In the presence of the nonhydrolyzable ATP analog adenylyl-imidodiphosphate (AMP-PNP), astral ParM projections grew much longer (Fig. 1C, fig. S3, and movie S2), indicating that the dynamic instability of ParM limited filament length even when one end of the filament was bound to the ParR/*parC* complex.

In addition to dynamic asters, ParM filaments also formed long, stable bundles connecting pairs of *parC* beads (Fig. 1, D to G), similar to bipolar structures previously observed in vivo (*7*). The bundles and attached beads moved as a single unit with fluid flow, indicating that ParM filaments were tightly attached to the ParR/*parC* complex. By electron microscopy (EM) we observed *parC* beads connected by ParM bundles of varying thickness. We traced individual filaments from one *parC* bead to the other (Fig. 1E), indicating that both ends of the ParM filament interacted with the ParR/*parC* complex. In time-lapse movies, the bivalently attached ParM bundles elongated at a constant rate, pushing *parC* beads in opposite directions (Fig. 1, D and F, and movies S3 and S4) over long distances (>120 μm). Thus ParM, ParR, and *parC* are sufficient to form a bipolar, DNA-segregating spindle. In addition,

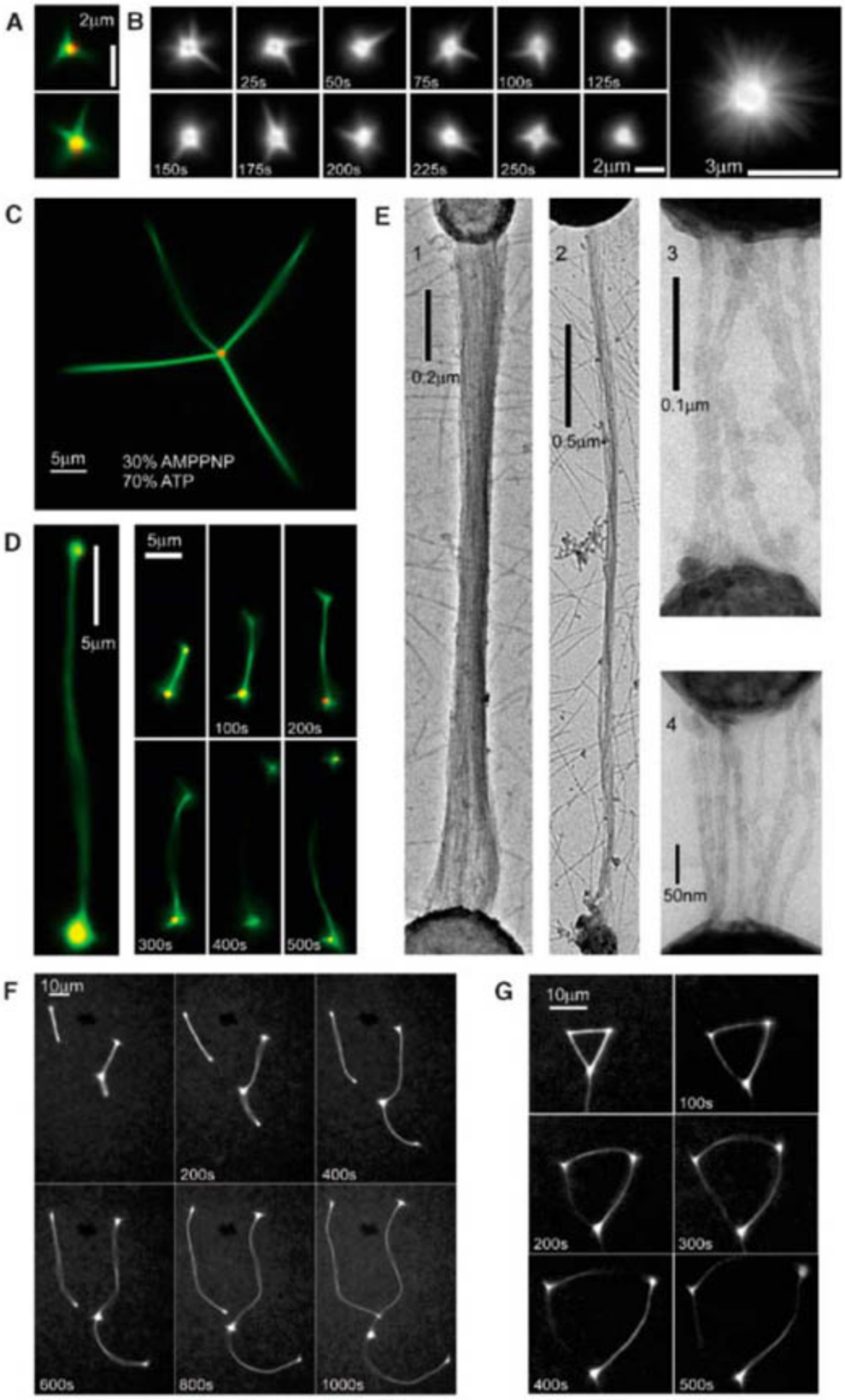

Fig. 1. In vitro reconstitution of the R1 plasmid spindle. (**A**) Individual ParR/*parC*-coated beads with radiating fluorescently labeled ParM asters (red, Cy3-labeled DNA; green, Alexa 488–labeled ParM). (**B**) Left: Time-lapse sequence of an Alexa 488–labeled ParM aster. Right: Maximum intensity projection of the time-lapse sequence, illustrating fall-off in fluorescence at 3 μm. (**C**) Inhibition of ParM dynamic instability with AMP-PNP produces substantially larger asters. (**D**) Two-color images and time-lapse sequence of bipolar ParM spindles segregating ParR/*parC*-coated beads. (**E**) Individual ParM filaments run from bead to bead, as shown by EM of negatively stained R1 spindles. (**F**) Time-lapse series of bipolar spindle elongation. (**G**) Elongation of a multipolar ParM structure.

multiple *parC* beads often interacted to form multipolar linear chains and polygons of ParM bundles (Fig. 1G and movies S5 and S6), structures that also expanded equilaterally as each bundle elongated at the same rate.

The fact that we observed long, stable ParM filaments only between pairs of *parC* beads argues that both ends of each filament are stabilized against catastrophic disassembly by interaction with the ParR/*parC* complex. This is supported by the observation of a "search-and-capture" (*13*) process of spindle formation: When two unconnected ParM asters come into proximity, they stabilize a filament bundle whose elongation pushes the asters apart (Fig. 2A, fig. S4, and movies S7 and S8). We tested whether bipolar attachment was required for stabilization by using laser irradiation to cut through ParM spindles. After cutting, both severed ends of the bundle depolymerized back to the *parC* beads (Fig. 2B, fig. S5, and movies S9 and S10). This requirement for bipolar stabilization of ParM spindles provides an explanation for the apparent plasmid counting observed in vivo, where ParM spindles occur only in cells containing two or more plasmids (*9*).

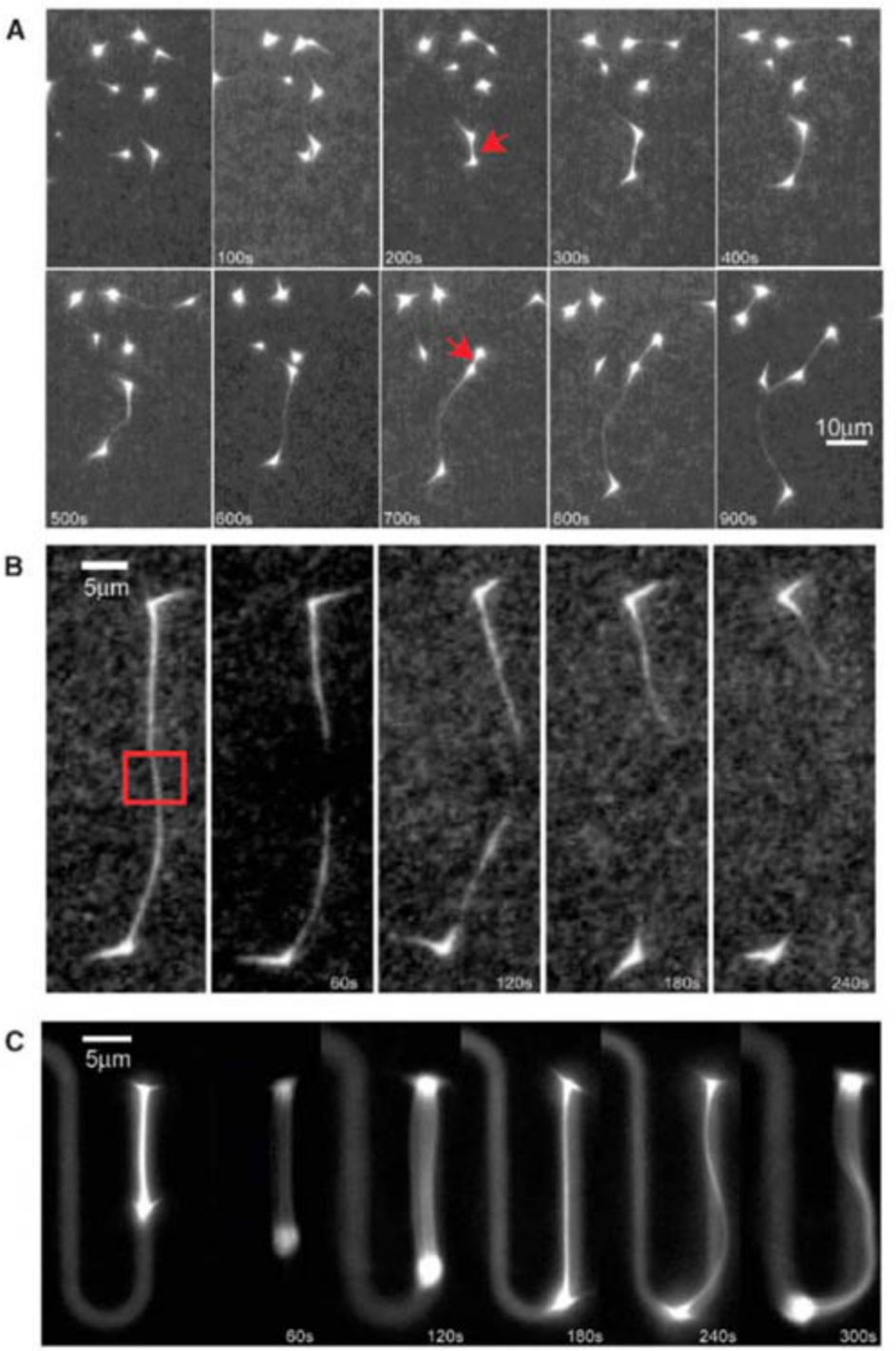

Fig. 2. ParM filaments are stabilized when bound at each end by the ParR/*parC* complex. (**A**) ParM spindles form by "search and capture." Sequence shows isolated ParM asters forming bipolar spindles that subsequently push the beads apart. Red arrows indicate capture events. (**B**) ParM filament bundles are stabilized a both ends by interaction with ParR/*parC* beads. Cutting a ParM spindle by laser irradiation (red box) results in depolymerization of severed ends. (**C**) The R1 spindle finds the long axis of a channel. Time-lapse sequence shows R1 spindles confined within a microfabricated channel.

To determine whether the R1 spindle was sufficient to find the long axis of a bacterium-sized space, we assembled spindles in microfabricated channels of various shapes. Spindles always aligned with the long axis of the channel and pushed *parC* beads in opposite directions (Fig. 2C and movie S11), demonstrating that orientation of R1 spindles can occur without cellular landmarks. Spindles elongated freely until they encountered resistance. Elongation stalled at the ends of the channels and slowed at bends. Thus, the R1 spindle could find the long axis of a rod-shaped cell by a simple Brownian ratchet-type mechanism.

We next used photobleaching and speckle microscopy to determine where new ParM monomers incorporated into the R1 spindle. We first used low-intensity laser irradiation to photobleach pairs of reference marks onto elongating spindles (Fig. 3A, fig. S6, and movie S12). In all cases (n = 6), the distance between the two bleached marks did not change with time, whereas the distance between each mark and the nearest *parC* bead increased at a constant rate (Fig. 3B). We never observed recovery of fluorescence within a bleached zone, which suggests that no polymerization took place in the middle of the ParM bundle and that individual filaments did not slide past each other. Speckle microscopy (*14*) of elongating spindles indicated that monomers incorporated exclusively at the surface of *parC* beads (Fig. 3C and movies S13 and S14).

Interaction with the ParR/*parC* complex did not affect the rate of ParM filament growth. From the photobleaching and speckling experiments, we determined that filaments within a spindle elongate at a rate of 11.6 ± 1.7 monomers s^{-1} (n = 5 ends). From the elongation rate and steady-state monomer concentration of 2.3 μM (*15*), we calculate a rate constant for elongation of bead-attached ParM filaments of 5 $\mu M^{-1} s^{-1}$, identical to the rate constant for elongation of free ParM filaments (*8*).

In ParM mutants defective in ATP hydrolysis, the critical concentration for assembly is 0.6 μM (*8*). This is the free monomer concentration above which ATP ParM filaments elongate and below which they shorten. The critical concentration of adenosine diphosphate (ADP) ParM filaments is greater by a factor of more than 200 (>120 μM), and this nucleotide-dependent increase is the basis for dynamic instability of ParM filaments. At steady state, in the presence of ATP, the rate of filament nucleation is balanced by the rate of filament catastrophe, and the combination of growing and shrinking filaments produces a steady-

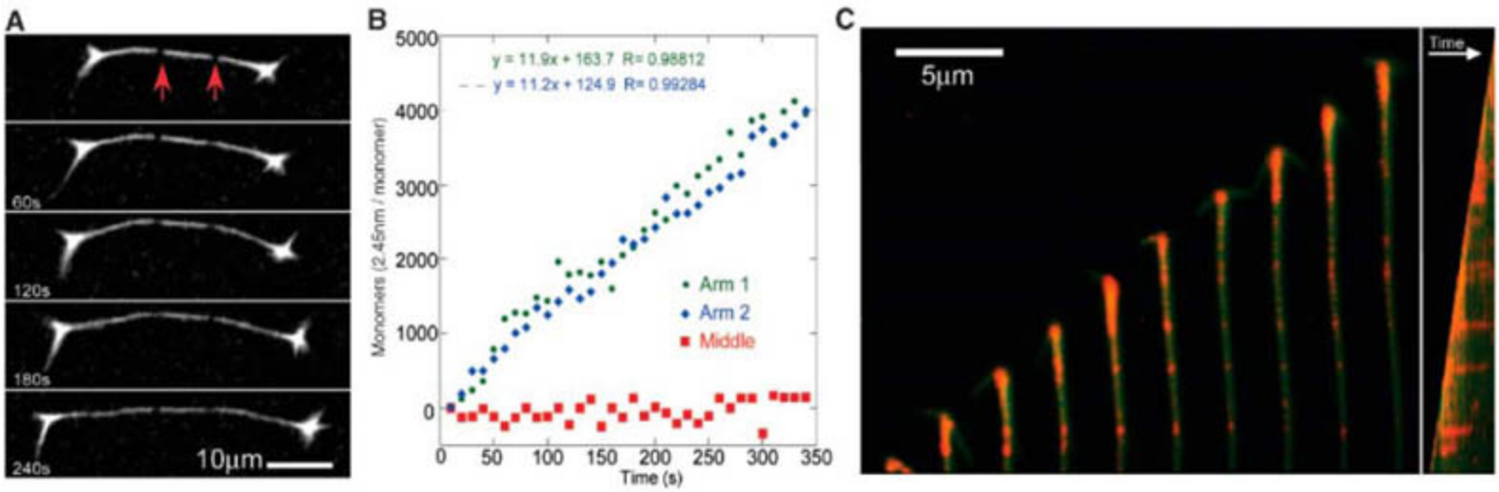

Fig. 3. R1 spindles elongate by insertion of ParM monomers at the ParR/*parC* complex. (**A**) Photobleaching (indicated by red arrows) of ParM spindles reveals symmetrical, bipolar elongation at the bead surface. (**B**) ParM spindles elongate at each end at the same rate as free filament ends. The distance between the two photobleached stripes or distance between the stripe and the bead in (A) was measured on a per-frame basis, and the change in distance was plotted against time. (**C**) By speckle microscopy, all new ParM monomers add to the spindle at the ParR/*parC* interface. Green, Alexa 488–ParM; red, rhodamine-ParM doped at 1:1000 to produce fluorescent speckles. Left: Time-lapse sequence of an elongating spindle end (80 s per frame). Right: Kymograph of the time-lapse sequence.

Fig. 4. Dynamic instability of free ParM filaments provides the energy for R1 spindle elongation. (**A**) The ParR/*parC* complex stabilizes ParM filaments down to the ParM-ATP critical concentration. Spindle assembly reactions were performed at the indicated concentrations of Alexa 488–labeled ParM. (**B**) By abolishing the difference in critical concentration between free and ParR/*parC*-bound ParM filaments, AMP-PNP eliminates sustained polymerization on ParR/*parC* beads. (**C**) Small amounts of ATP added into AMP-PNP restore sustained polymerization on ParR/*parC* beads. (**D**) Hydrolysis-dependent ParM tail elongation occurs specifically at filament ends bound to ParR/*parC* complexes and not at free filament ends. Assembly reactions as in (C) were initiated with Alexa 488–ParM (green); at indicated times, the reactions were spiked with Cy3-ParM (red). Results were visualized after 50 min. Two examples of each time point are shown. (**E**) Rates of ParM tail elongation scale with the fraction of hydrolyzable nucleotide. Reactions as in (C) were performed at various ATP/AMP-PNP ratios. The rate of tail elongation was plotted against the percent of ATP within the nucleotide mixture.

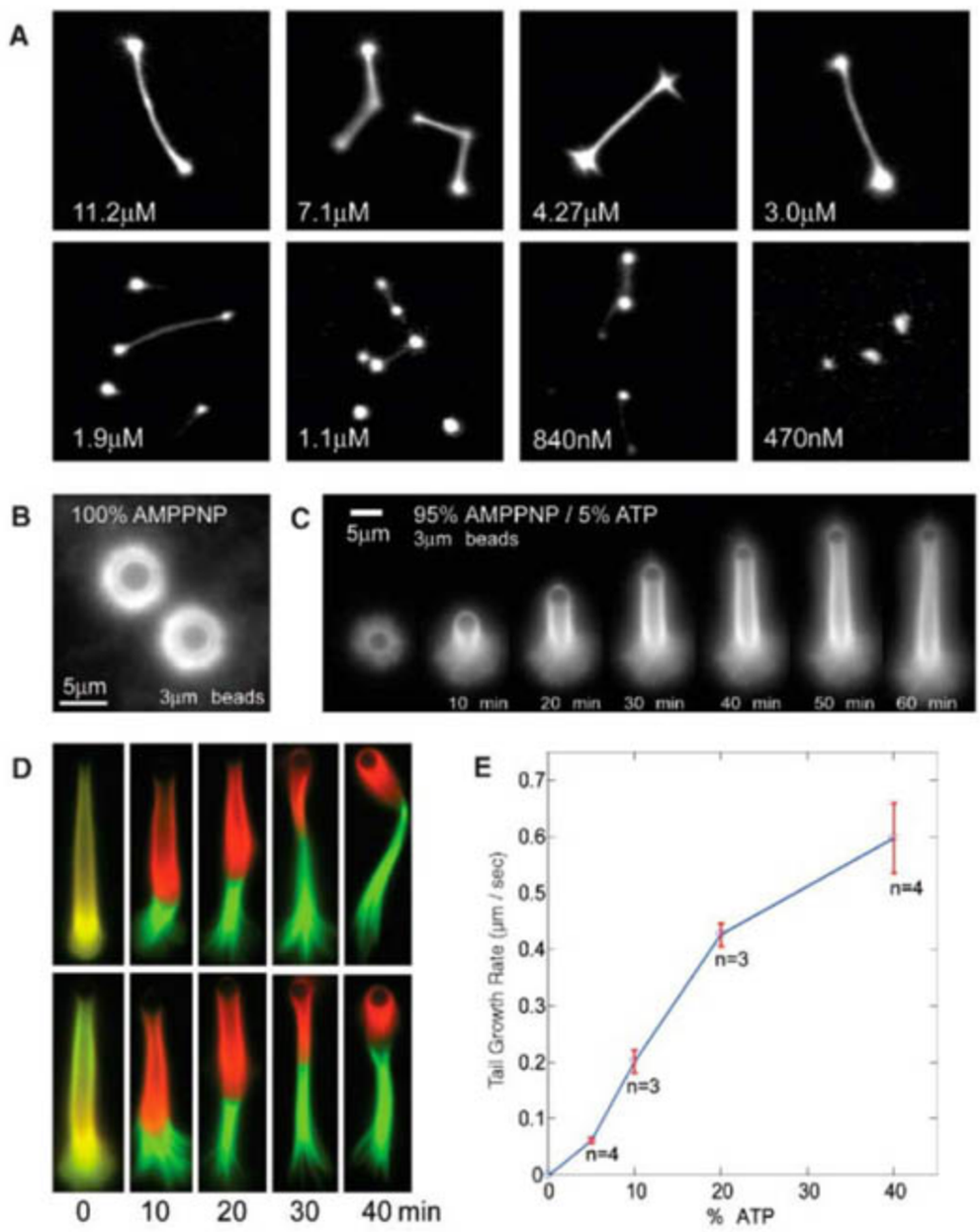

state monomer concentration of 2.3 μM. Beneath 2.3 μM, no filaments are detectable by fluorescence microscopy, fluorescence resonance energy transfer (FRET), or high-speed pelleting (*8*).

To determine how binding to the ParR/*parC* complex affects the critical concentration of ParM filaments, we investigated the concentration dependence of R1 spindle formation. At concentrations above 2.3 μM, ParM formed numerous dense and stable spindles connecting pairs of *parC* beads (Fig. 4A). Below 2.3 μM, ParM formed spindles between beads, but their frequency and lifetime decreased with decreasing ParM concentration. Below 0.6 μM, ParM failed to form any detectable spindles, even between *parC* beads in close contact. Thus, interaction with the ParR/*parC* complex stabilized ParM filaments down to, but not beneath, the ATP critical concentration of 0.6 μM, presumably because the ParR/*parC* complex simply inhibits dynamic instability.

One consequence of our results is that the energy to segregate *parC* beads must be supplied by dynamic instability of unattached ParM filaments. For polymerization to perform useful work, the monomer-polymer balance at the load must be kept away from equilibrium (*16*). We found that ParM filaments in the spindle are stabilized to the ATP critical concentration (0.6 μM) (Fig. 4A) yet elongate at a rate determined by the steady-state monomer concentration of 2.3 μM (Fig. 3B), a concentration that is maintained by dynamic instability of unattached ParM filaments (*8*).

To demonstrate this directly, we varied the energy difference between attached and unattached filaments by adding different ratios of ATP and AMP-PNP to our reconstituted DNA segregation system. In 100% AMP-PNP, the ParR/*parC*-attached and unattached filaments had the same critical concentration (0.6 μM), and the system quickly reached equilibrium (~2 min) with *parC* beads surrounded by a small, nondynamic shell of ParM filaments (Fig. 4B). Reestablishing an energy difference by adding small amounts of ATP produced sustained ParM polymerization at the bead surface. In 5% ATP and 95% AMP-PNP, slow-growing, stable, monopolar tails assembled on the surface of large *parC* beads, propelling them through the medium at a constant rate for up to 2 hours (Fig. 4C and movies S15 and S16). By using two colors of labeled ParM, added at different times (Fig. 4D), we found that filament elongation occurred exclusively on ParR/*parC* associated ends and not on free ends. Hence, the unattached filament ends are at steady state, whereas ParR/*parC*-associated ends elongate in a hydrolysis-dependent manner. The elongation rate of stabilized tails increased with the proportion of hydrolyzable ATP (Fig. 4E), demonstrating that the energy difference driving bead motility was proportional to the amount of hydrolysis-capable monomer that could be stabilized by the ParR/*parC* complex.

In response to evolutionary pressure, the R1 plasmid has evolved a self-contained, three-component system to ensure its segregation. All key functions of the R1 spindle require dynamic instability of ParM filaments. Dynamic instability enables unbound filaments to turn over without disassembly factors (*8*). Filaments stabilized at one end by ParR/*parC* can search for additional plasmids (fig. S8 and movie S17); filaments bound at both ends are stabilized against dynamic instability, forming a productive spindle. Finally, the dynamic instability of unbound filaments provides the excess monomer to drive elongation of the stabilized filaments within the spindle.

References and Notes

1. S. Inoue, H. Sato, *J. Gen. Physiol.* **50** (suppl.), 259 (1967).
2. Z. Gitai, N. A. Dye, A. Reisenauer, M. Wachi, L. Shapiro, *Cell* **120**, 329 (2005).
3. T. Kruse *et al.*, *Genes Dev.* **20**, 113 (2006).
4. K. Gerdes, J. Moller-Jensen, R. Bugge Jensen, *Mol. Microbiol.* **37**, 455 (2000).
5. G. E. Lim, A. I. Derman, J. Pogliano, *Proc. Natl. Acad. Sci. U.S.A.* **102**, 17658 (2005).
6. K. Gerdes, S. Molin, *J. Mol. Biol.* **190**, 269 (1986).
7. J. Moller-Jensen, R. B. Jensen, J. Lowe, K. Gerdes, *EMBO J.* **21**, 3119 (2002).
8. E. C. Garner, C. S. Campbell, R. D. Mullins, *Science* **306**, 1021 (2004).
9. J. Moller-Jensen *et al.*, *Mol. Cell* **12**, 1477 (2003).
10. F. van den Ent, J. Moller-Jensen, L. A. Amos, K. Gerdes, J. Lowe, *EMBO J.* **21**, 6935 (2002).
11. T. Mitchison, M. Kirschner, *Nature* **312**, 237 (1984).
12. M. Moritz *et al.*, *J. Cell Biol.* **130**, 1149 (1995).
13. T. E. Holy, S. Leibler, *Proc. Natl. Acad. Sci. U.S.A.* **91**, 5682 (1994).
14. C. M. Waterman-Storer, A. Desai, J. C. Bulinski, E. D. Salmon, *Curr. Biol.* **8**, 1227 (1998).
15. See supporting material on *Science* Online.
16. J. A. Theriot, *Traffic* **1**, 19 (2000).

17. We thank O. Akin and M. Quinlan for assistance with bead motility assays, Q. Justman and A. Murray for helpful discussions, and S. Layer for continued advice and inspiration. Supported by NIH grants RO1GM61010 and R01GM675287, the Sandler Family Supporting Foundation, and the UCSF/UCB Nanomedicine Development Center (R.D.M.).

Supporting Online Material

www.sciencemag.org/cgi/content/full/315/5816/1270/DC1
Materials and Methods
SOM Text
Figs. S1 to S8
Movies S1 to S17

7 December 2006; accepted 30 January 2007
10.1126/science.1138527

Multiple Functions of the IKK-Related Kinase IKKε in Interferon-Mediated Antiviral Immunity

Benjamin R. tenOever,[1] Sze-Ling Ng,[1] Mark A. Chua,[2,3] Sarah M. McWhirter,[1] Adolfo García-Sastre,[2,4] Tom Maniatis[1]*

IKKε is an IKK (inhibitor of nuclear factor κB kinase)–related kinase implicated in virus induction of interferon-β (IFNβ). We report that, although mice lacking IKKε produce normal amounts of IFNβ, they are hypersusceptible to viral infection because of a defect in the IFN signaling pathway. Specifically, a subset of type I IFN-stimulated genes are not activated in the absence of IKKε because the interferon-stimulated gene factor 3 complex (ISGF3) does not bind to promoter elements of the affected genes. We demonstrate that IKKε is activated by IFNβ and that IKKε directly phosphorylates signal transducer and activator of transcription 1 (STAT1), a component of ISGF3. We conclude that IKKε plays a critical role in the IFN-inducible antiviral transcriptional response.

Activation of innate immunity by virus infection begins with type I IFNα and IFNβ gene expression followed by induction of the Janus kinase–signal transducer and activator of transcription (JAK-STAT) pathway, leading to the expression of a large family of IFN-stimulated genes (ISGs) (*1*). The initial response is triggered by pattern recognition receptors that bind to virus-specific molecular signatures and activate latent kinase complexes such as the stress-activated protein kinases (c-Jun N-terminal kinase and p38), the IKK complex (IKKα/IKKβ/IKKγ), and the IKK-related kinases TANK-binding kinase 1 (TBK1) and IKKε [also called IKKi (*2*)] (*3*). These kinases coordinate the assembly of the IFNβ enhanceosome, a multisubunit complex composed of the transcription factors ATF2 (activating transcription factor 2)/cJun, NFκB, and interferon regulatory factors 3 and 7 (IRF3 and IRF7) (*3*). IFNβ induces dimerization of the type I IFN receptor and activates the associated kinases tyrosine kinase 2 (TYK2) and JAK1 (*1*), leading to the tyrosine phosphoryl-

[1]Department of Molecular and Cellular Biology, Harvard University, 7 Divinity Avenue, Cambridge, MA 02138, USA. [2]Department of Microbiology, Mount Sinai School of Medicine, One Gustave L. Levy Place, Box 1124, New York, NY 10029, USA. [3]Microbiology Graduate School Training Program, Mount Sinai School of Medicine, One Gustave L. Levy Place, Box 1124, New York, NY 10029, USA. [4]Emerging Pathogens Institute, Mount Sinai School of Medicine, One Gustave L. Levy Place, Box 1124, New York, NY 10029, USA.

*To whom correspondence should be addressed. E-mail: maniatis@mcb.harvard.edu

ation of STAT1 and STAT2 and STAT association with IRF9 to form the ISGF3 complex. This complex binds to ISREs (interferon-stimulated response elements) in the promoters of a large group of ISGs, resulting in their transcriptional activation (*4*).

Initial characterization of the kinases responsible for IFNβ transcription suggested that the virus-inducible expression of IKKε functions in a redundant role to its ubiquitous counterpart, TBK1, in the activation of IRF3 and IRF7 ex vivo (*5*–*8*). To investigate the function of IKKε in vivo, we generated mice deficient in IKKε (fig. S1A). Disruption of *Ikbke*$^{-/-}$ (the gene encoding IKKε) resulted in a complete loss of the kinase in both mice and embryonic fibroblasts (EFs) (fig. S1B). To determine whether IKKε is required to protect against virus infection in vivo, we infected wild-type (WT) and *Ikbke*$^{-/-}$ mice with increasing doses of influenza A/WSN/33 virus (WSN). Although inoculations of more than 7×10^3 plaque-forming units (pfu) resulted in 100% mortality of both cohorts, *Ikbke*$^{-/-}$ mice displayed an increased susceptibility to WSN at lower titers (Fig. 1A). After inoculation with 700 pfu, both WT and *Ikbke*$^{-/-}$ mice displayed greater than 10% body weight loss, although unlike WT controls *Ikbke*$^{-/-}$ mice continued to decline below 80% of their original body mass before succumbing to the infection (Fig. 1B).

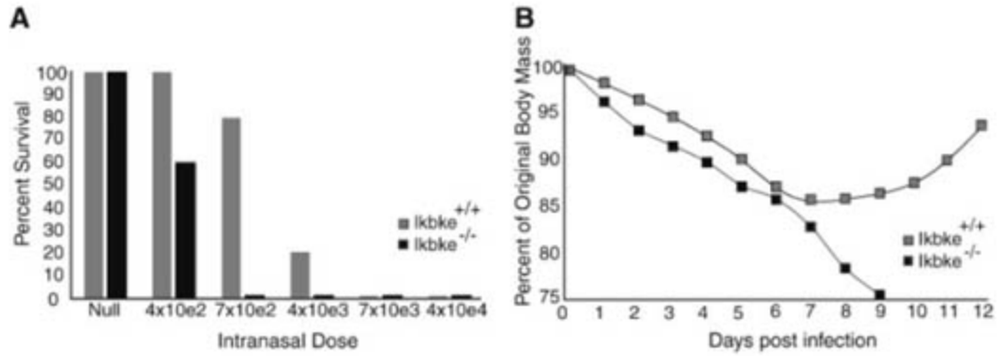

Fig. 1. IKKε knockout mice are hypersusceptible to influenza virus infection. (**A**) Mice were administered increasing amounts of WSN intranasally and observed over a 7-day period (n = 5 mice per cohort per dose). (**B**) Cohorts of mice were administered 7×10^2 pfu intranasally and weighed daily (n = 20 mice per cohort per dose). Values represent average scores of overall weight loss compared with initial body mass.

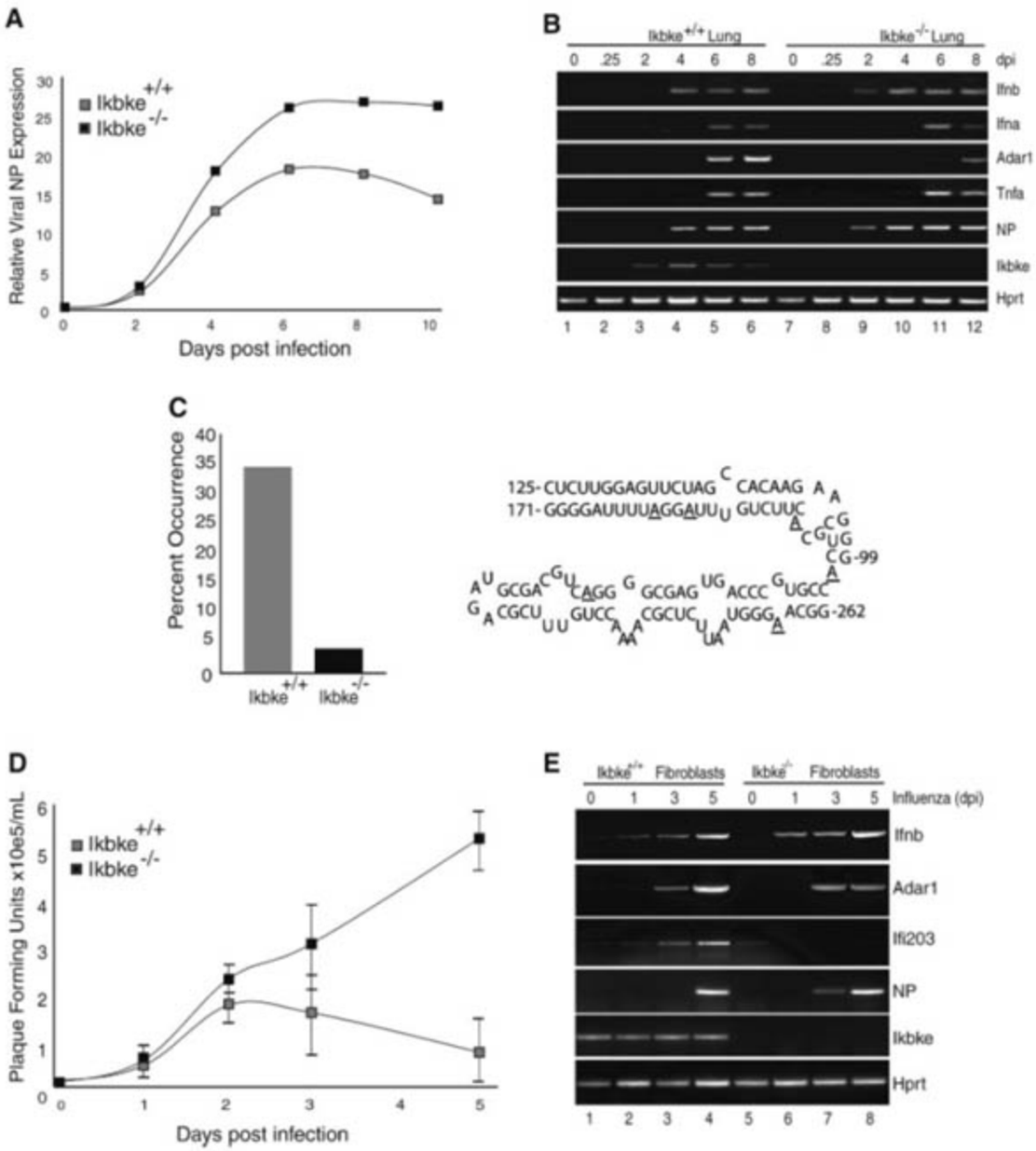

Fig. 2. IKKε is required for the normal host response to infection. (**A**) Viral expression from infected mice (7×10^2 pfu) was determined by Q-PCR from pooled lung samples. Values determined as ratios of viral nucleocapsid protein (NP) relative to *Hprt*. (**B**) Lung transcriptional profiles of IFNβ (*Ifnb*), IFNα (*Ifna*), *Adar1*, tumor necrosis factor α (*Tnfa*), NP, *Ikbke*, and *Hprt* as determined by RT-PCR. (**C**) ADAR1 activity as measured by influenza matrix (M) RNA sequencing. M was reverse transcribed from pooled lung samples (8 dpi) and sequenced for A to G substitutions (n = 96 transcripts per cohort). Underlined adenosines represent positions of base transitions. (**D**) Viral titers of primary EFs infected with WSN (multiplicity of infection = 0.01) as determined by plaque assay. Values represent the mean average of triplicate experiments. Error bars indicate standard error of the mean. (**E**) EF transcriptional profiles of *Ifnb*, *Adar1*, IFN-activated gene 203 (*Ifi203*), NP, *Ikbke*, and *Hprt* by RT-PCR.

Quantitative polymerase chain reaction (Q-PCR) for virus nucleocapsid mRNA and virus plaque assays from lung tissue indicated that *Ikbke*$^{-/-}$ mice had an elevated viral load compared with that of their control littermates (Fig. 2A and fig. S2A). Histopathology of lungs at seven days post infection (dpi) revealed that infected *Ikbke*$^{-/-}$ mice exhibited an inflammatory infiltrate consisting of lymphocytes, macrophages, and neutrophils (fig. S2B). However, reverse transcription PCR (RT-PCR) and enzyme-linked immunosorbent assay (ELISA) analyses of lung and serum, respectively, revealed no obvious deficiency in virus-induced cytokines, such as IFN α, β, and γ, RANTES, and IL2, or in the amounts of virus-specific antibodies (Fig. 2B and figs. S3 and S4A). By contrast, array (Affymetrix, Santa Clara, CA) analysis of RNA from pooled primary lung samples revealed a subset of ISGs, including *Ifit3*, *Ifi203*, and the double-stranded RNA (dsRNA)–activated adenosine deaminase gene (*Adar1*), that were poorly induced in the absence of IKKε as corroborated by RT-PCR analyses (Fig. 2B and fig. S4B). To determine whether the resulting loss of ADAR1 has functional consequences, we amplified and sequenced a stem loop structure present in WSN matrix (M) mRNA from infected lung tissue. ADAR1 binds double-stranded RNA (dsRNA) and deaminates adenosine residues, thus converting adenine to guanine and thereby mutagenizing viral RNA (*9*). Analysis of over 95 individual clones from each cohort revealed that greater than 30% of the viral M mRNA bears at least one or more A-to-G transitions in control mice, compared with less than 5% in *Ikbke*$^{-/-}$ mice (Fig. 2C). We conclude that IKKε is required for the induction of a subset of ISGs such as ADAR1, which displays antiviral activity in vivo.

To determine whether the in vivo phenotype of *Ikbke*$^{-/-}$ mice could be recapitulated ex vivo, we compared the rates of influenza virus replication in primary EFs from WT and *Ikbke*$^{-/-}$ mice. Comparable replication rates were observed at 2 dpi, although the titer continued to increase in *Ikbke*$^{-/-}$ cells relative to WT cells thereafter (Fig. 2D). RT-PCR analyses from the WT and *Ikbke*$^{-/-}$ samples showed comparable induction of IFNβ but revealed a decrease in the expression of a subset of ISGs (Fig. 2E). A low amount of virus-inducible ADAR1 mRNA was observed in *Ikbke*$^{-/-}$ EFs; however, the induction of other ISGs such as IFI203 was completely blocked. Thus, it appears that IKKε controls the optimal expression of a subset of ISGs required to control viral load both in vivo and ex vivo.

Certain ISGs are inducible by both virus infection and IFN treatment, whereas others are inducible only by IFN directly (*10*). To determine whether the IKKε-dependent ISGs are defective in IFN signaling, we treated WT and *Ikbke*$^{-/-}$ EFs with recombinant IFNβ (rIFNβ). About 30% of the IFN-inducible ISGs were poorly induced in *Ikbke*$^{-/-}$ EFs (Fig. 3A). This result was confirmed by RT-PCR analyses (Fig. 3B). Although the amount of IFN induction of several ISG genes, such as *Adar1*, *Ifit3*, and *Ifi203*, decreased in the absence of IKKε, others, such as *Irf7*, *Prkra* (RNA-activated protein kinase), and *Stat1*, were unaffected. Alignment of the DNA sequences of IKKε-dependent ISREs identified a consensus sequence similar to previously characterized ISGF3 binding sites (*4*, *11*) (fig. S5A). Electrophoretic mobility shift assays (EMSAs) using these ISREs identified an IFN-inducible DNA-protein complex that failed to bind to IKKε-dependent promoters in extracts from IFN-treated *Ikbke*$^{-/-}$ cells (Fig. 3C). This complex was shown to be ISGF3, because IRF9, STAT1, and STAT2 antibodies all disrupted DNA-protein complex formation (Fig. 3D). Ex-

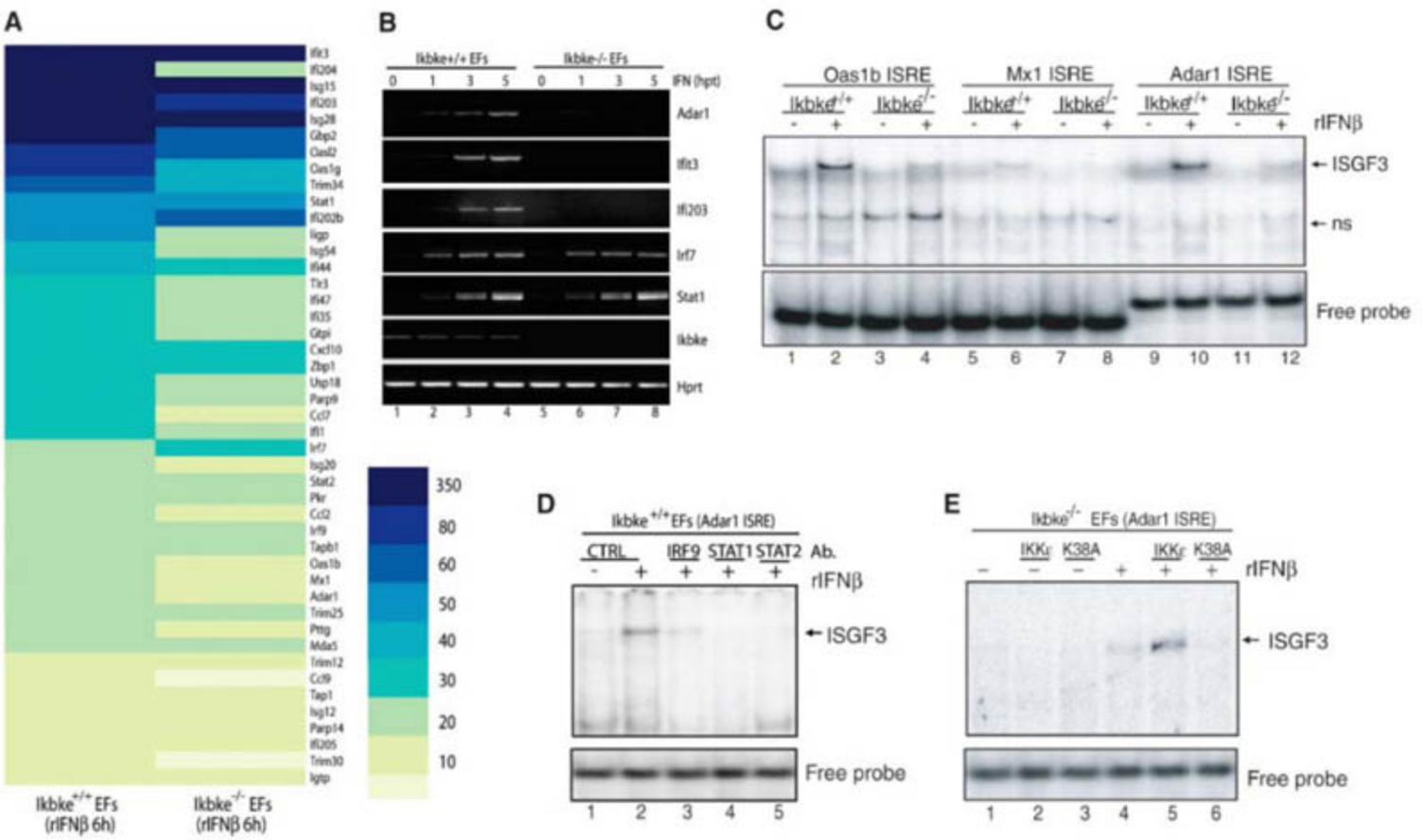

Fig. 3. The type I IFN response is defective in *Ikbke*$^{-/-}$ EFs. (**A**) Gene expression profile in primary EFs treated with rIFNβ (0.1 U/ml) for 6 hours. The heat map depicts the average mean induction of ISGs from triplicate Affymetrix samples. (**B**) Transcript quantities of *Adar1*, IFN-induced protein with tetratricopeptide repeats 3 (*Ifit3*), *Ifi203*, IRF7 (*Irf7*), *Stat1*, *Ikbke*, and *Hprt* as determined by RT-PCR from rIFNβ-treated EFs. hpt, hours posttreatment. (**C**) Cell extracts from rIFNβ-stimulated EFs were analyzed by EMSA with ISRE elements derived from the 2′-5′ oligoadenylate synthetase 1B (*Oas1b*), myxovirus resistance 1 (*Mx1*), and *Adar1* genes. The ns band denotes nonspecific binding. (**D**) Protein composition of ISGF3 was analyzed by antibody (Ab.) competition assays with IRF9, STAT1, and STAT2 antibodies. CTRL, control. (**E**) *Ikbke*$^{-/-}$ EFs were transfected with vector, IKKε, or K38A. Transfections were untreated or treated with rIFNβ and analyzed by EMSA on an *Adar1* ISRE.

pression of IKKε but not a dominant negative mutant of IKKε [Lys^{38}→Ala^{38} (K38A)] rescued IFNβ induction of ISGF3 binding in *Ikbke*$^{-/-}$ cells (Fig. 3E). Thus, ISGF3 binding to IKKε-dependent promoters requires IKKε kinase activity. To determine whether IKKε can be activated by IFN treatment, we transfected EFs, which express minute quantities of IKKε, with WT IKKε or the K38A mutant and treated the EFs with rIFNβ. Because Thr^{501} (T501) of IKKε has been implicated in virus-induced activation (*12*), we used a phosphospecific T501 antibody to observe a rapid induction of IKKε phosphorylation in IFN-treated cells (Fig. 4A). TBK1, which is not activated by IFN treatment, does not contain this T501 residue. On the basis of the amino acid sequence of the phosphorylation site in IKKε and previous studies that implicate p38 kinase in IFN- and virus-inducible phosphorylation, we speculate that IKKε activation may be mediated through p38 kinase signaling (*13*).

The *Ikbke*$^{-/-}$ phenotype is similar to that of *Stat1*$^{-/-}$ mice, which also displays an increased susceptibility to influenza virus infection both in vivo and ex vivo. However, in contrast to *Ikbke*$^{-/-}$ cells, where 30% of ISGs fail to be induced by IFN, no ISGs are induced in *Stat1*$^{-/-}$ cells (*14*, *15*). This suggests that STAT1 signaling is not completely compromised in the absence of IKKε. This observation is consistent with EMSA and chromatin immunoprecipitation (ChIP) analyses of IKKε-independent ISREs showing normal binding to ISGF3 in *Ikbke*$^{-/-}$ cells treated with IFNβ (Fig. 4, B and C). In addition, bone marrow–derived macrophages from *Ikbke*$^{-/-}$ mice display normal induction of IFNγ-stimulated genes (fig. S5B).

As critical components of ISGF3, STAT1 and STAT2 are potential targets for IKKε. We therefore investigated the status of these two transcription factors in response to IFN in *Ikbke*$^{-/-}$ mice. Initially, we carried out Western blot experiments with primary lung extracts from mice infected with different viruses. The quantities of both STAT1 and STAT2 increased normally in response to infection; however, discrete breakdown products of STAT1 were observed in WT mice but not in *Ikbke*$^{-/-}$ mice (fig. S6, A and B). In primary EFs, the amount of STAT1 in *Ikbke*$^{-/-}$ IFNβ-treated cells exceeded that of WT cells (fig. S6C). In considering these results together, we suggest that STAT1 appears to be subject to IKKε-dependent processing and/or degradation, an event that has been ascribed to STAT1 previously (*16*). This explanation also suggests the possibility that STAT1 may be a target of IKKε.

To determine whether IKKε acts directly on STAT1, we carried out in vitro phosphorylation studies with recombinant IKKε. Mass spectrometry analyses revealed that IKKε phosphorylates Ser^{708} (S708), S744, and S747 (fig. S7A). To determine the function of these serine residues, we created STAT1 mutants and transfected them into *Stat1*$^{-/-}$ EFs. Transfected cells were treated with IFN and assayed for ISGF3 binding (Fig. 4, D and E). The substitution of S708 with alanine (S708A) dramatically decreased ISGF3 binding to the IKKε-dependent Adar1 ISRE but not to the IKKε-independent Irf7 ISRE, as determined by both ChIP and EMSA experiments. In contrast, the binding of ISGF3 to both ISREs was unaffected by a C-terminal deletion of STAT1 that removed serine residues 744 and 747 (ΔS744/747).

Examination of the three-dimensional structure of STAT1 predicts that phosphorylation of S708 would favor the formation of STAT1-STAT2 heterodimers, rather than STAT1 homodimers (*17*). Heterodimer formation is necessary for the assembly of ISGF3 because STAT2 is thought to tether STAT1 and IRF9 to the ISRE (*18*). ISGF3 binds to adjacent GAAA repeats recognized by STAT1 and IRF9, respectively, on complementary major and minor grooves. STAT2 in turn, contacts both proteins while making additional contacts with sequences upstream from the GAAA repeats (fig. S7B) (*4*, *11*, *17*, *19*). Computational analyses of the DNA sequences of IKKε-dependent and -independent ISREs identify a purine-rich region upstream of the IKKε-independent ISREs. This purine tract could serve as an additional STAT2 binding site, permitting specific contacts with DNA. In the absence of this purine-rich sequence, ISGF3 binding may require a more stable STAT1-STAT2-IRF9 interaction, which in turn may require the phosphorylation of STAT1 S708 by IKKε. Although the structural consequences of this phosphorylation

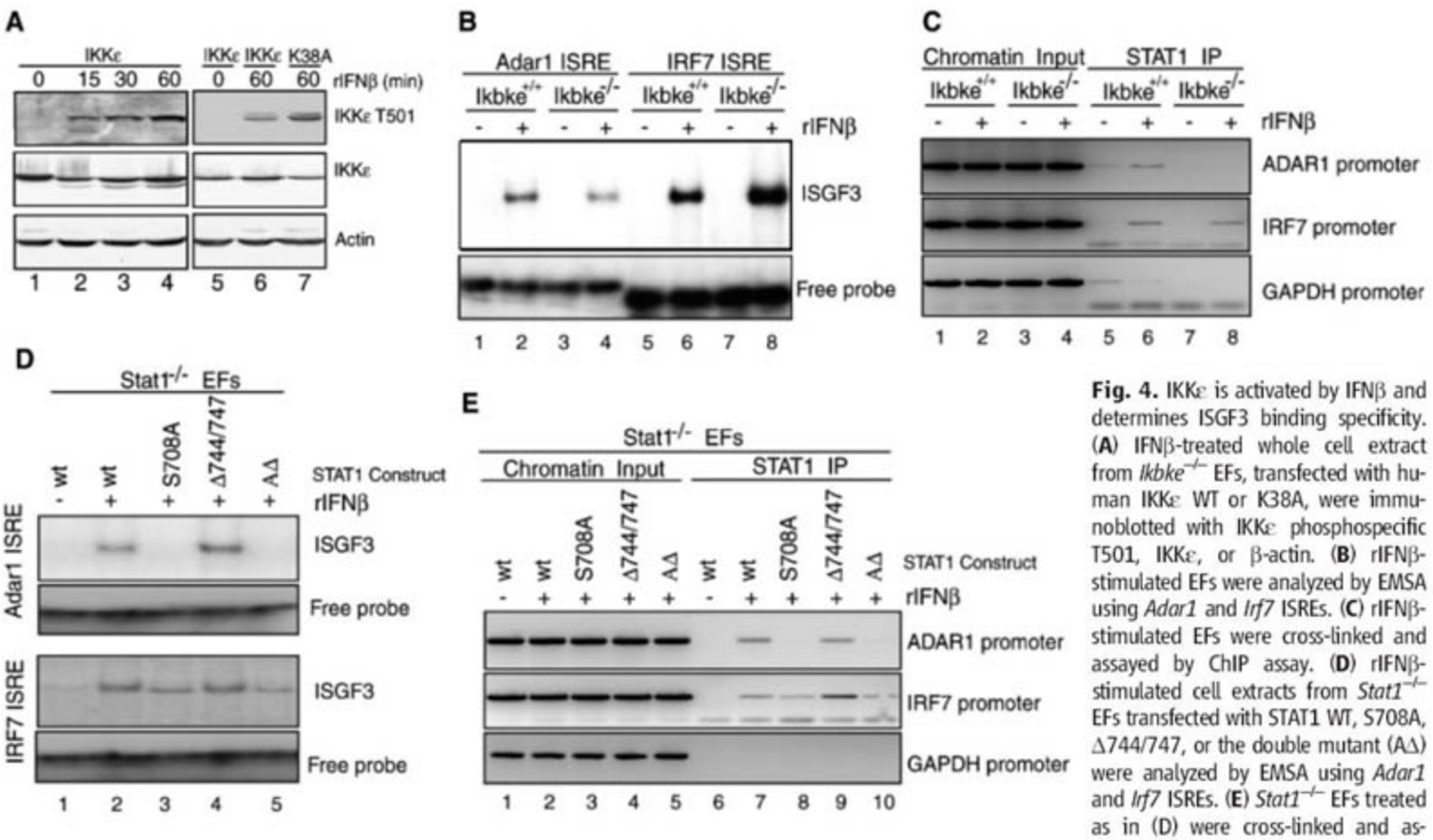

Fig. 4. IKKε is activated by IFNβ and determines ISGF3 binding specificity. (**A**) IFNβ-treated whole cell extract from *Ikbke*$^{-/-}$ EFs, transfected with human IKKε WT or K38A, were immunoblotted with IKKε phosphospecific T501, IKKε, or β-actin. (**B**) rIFNβ-stimulated EFs were analyzed by EMSA using *Adar1* and *Irf7* ISREs. (**C**) rIFNβ-stimulated EFs were cross-linked and assayed by ChIP assay. (**D**) rIFNβ-stimulated cell extracts from *Stat1*$^{-/-}$ EFs transfected with STAT1 WT, S708A, Δ744/747, or the double mutant (AΔ) were analyzed by EMSA using *Adar1* and *Irf7* ISREs. (**E**) *Stat1*$^{-/-}$ EFs treated as in (D) were cross-linked and assayed by ChIP assay.

remain to be determined, the function of IKKε in type I IFN signaling is to guide the transcriptional machinery to a subset of ISGs required for a direct antiviral response. By contrast, the IKKε-independent genes may function primarily in regulating the IFN signaling machinery, which is required for the integration of innate and adaptive immune systems. These results emphasize the importance of the interplay between local and systemwide antiviral mechanisms. Even when the systemwide antiviral response is intact, defects in the local response lead to an increase in viral load, ultimately overwhelming the immune defenses.

References and Notes

1. A. Garcia-Sastre, C. A. Biron, *Science* **312**, 879 (2006).
2. T. Shimada *et al.*, *Int. Immunol.* **11**, 1357 (1999).
3. S. M. McWhirter *et al.*, *Cell* **122**, 645 (2005).
4. X. Y. Fu *et al.*, *Proc. Natl. Acad. Sci. U.S.A.* **87**, 8555 (1990).
5. K. A. Fitzgerald *et al.*, *Nat. Immunol.* **4**, 491 (2003).
6. S. Sharma *et al.*, *Science* **300**, 1148 (2003); published online 17 April 2003 (10.1126/science.1081315).
7. H. Hemmi *et al.*, *J. Exp. Med.* **199**, 1641 (2004).
8. A. K. Perry *et al.*, *J. Exp. Med.* **199**, 1651 (2004).
9. C. X. George *et al.*, *J. Biol. Chem.* **280**, 15020 (2005).
10. M. G. Wathelet *et al.*, *Mol. Cell* **1**, 507 (1998).
11. D. E. Levy *et al.*, *Genes Dev.* **2**, 383 (1988).
12. S. E. Sweeney, G. S. Firestein, *Ann. Rheum. Dis.* **65** (suppl.), A98 (2006).
13. L. C. Platanias, *Nat. Rev. Immunol.* **5**, 375 (2005).
14. A. Garcia-Sastre *et al.*, *Virology* **252**, 324 (1998).
15. J. E. Durbin *et al.*, *Cell* **84**, 443 (1996).
16. T. K. Kim, T. Maniatis, *Science* **273**, 1717 (1996).
17. X. Chen *et al.*, *Cell* **93**, 827 (1998).
18. S. A. Qureshi *et al.*, *Proc. Natl. Acad. Sci. U.S.A.* **92**, 3829 (1995).
19. X. Mao *et al.*, *Mol. Cell* **17**, 761 (2005).

20. This work was supported by NIH grants to T.M. and A.G.-S. [RO1AI46954, PO1AI058113, and CIVIA, a National Institute for Allergy and Infectious Diseases (NIAID)–supported Center for Investigating Viral Immunity and Antagonism, U19AI62623]. B.R.t.O. is supported by a Canadian Institute of Health Research fellowship. S.L.N. is supported by an NSF and Soros fellowship. M.A.C. is supported by an NIAID predoctoral fellowship (F31 AI056678). We thank R. Cádagan for technical support, N. Silverman and K. Fitzgerald for manuscript reviews, B. Chang for recombinant STAT1ΔC, J. Zhang for microarray assistance, D. Panne for molecular modeling, and D. Hamilton for hematoxylin and eosin evaluation. Affymetrix data are available on National Center for Biotechnology Information's Geo database at accession number GSE6837.

Supporting Online Material

www.sciencemag.org/cgi/content/full/315/5816/1274/DC1
Materials and Methods
Figs. S1 to S7

20 October 2006; accepted 30 January 2007
10.1126/science.1136567

LRP6 Mutation in a Family with Early Coronary Disease and Metabolic Risk Factors

Arya Mani,[1]* Jayaram Radhakrishnan,[1] He Wang,[2] Alaleh Mani,[3] Mohammad-Ali Mani,[4] Carol Nelson-Williams,[1] Khary S. Carew,[1] Shrikant Mane,[1] Hossein Najmabadi,[5] Dan Wu,[2] Richard P. Lifton[1]*

Coronary artery disease (CAD) is the leading cause of death worldwide and is commonly caused by a constellation of risk factors called the metabolic syndrome. We characterized a family with autosomal dominant early CAD, features of the metabolic syndrome (hyperlipidemia, hypertension, and diabetes), and osteoporosis. These traits showed genetic linkage to a short segment of chromosome 12p, in which we identified a missense mutation in *LRP6*, which encodes a co-receptor in the Wnt signaling pathway. The mutation, which substitutes cysteine for arginine at a highly conserved residue of an epidermal growth factor–like domain, impairs Wnt signaling in vitro. These results link a single gene defect in Wnt signaling to CAD and multiple cardiovascular risk factors.

Coronary artery disease (CAD) due to atherosclerosis results in myocardial infarction (MI) and is the leading cause of death worldwide (*1*). Epidemiologic studies and clinical intervention trials have established the key roles of specific risk factors for CAD, including smoking, hypertension, high low-density lipoprotein (LDL) cholesterol, high triglycerides, low high-density lipoprotein (HDL) cholesterol, and diabetes mellitus (*2*–*4*). Surprisingly, many of these risk factors cluster with one another more often than expected by chance (*5*, *6*). This metabolic syndrome is recognized to be a common cause of CAD; however, the molecular mechanisms that unify their association have been obscure.

The marked increase in risk of early cardiovascular mortality to a second monozygotic twin when the first has died from early CAD provides evidence for a strong genetic effect and supports investigation of families with early disease (*7*). Such studies have the capacity to identify genes and pathways whose altered function impart large effects on CAD outcome; these may provide insight into basic mechanisms that are also involved in common forms of disease and that may be manipulated for health benefit.

From a screen of patients and families with CAD, we identified one extreme outlier kindred with an extraordinary prevalence of early CAD. Kindred CAD-100 is of Iranian ancestry, ascertained via Subject II-7 (table S1), who presented with MI at age 48. CAD risk factors included hypertension, hyperlipidemia, and diabetes mellitus; he had never smoked and his body mass index (BMI) was 24. Evaluation revealed critical stenosis of all three major coronary arteries, which led to coronary artery bypass grafting. His course was complicated by progressive atherosclerosis of the grafts and internal carotid arteries. At age 62, he suffered a low-impact hip fracture and was found to have very low bone mineral density of unknown cause (z score of −3.4 at the femoral neck of his intact hip). He died from a stroke at age 72.

Among 58 blood relatives of the index case, 28 were diagnosed with early CAD (MI, angina, or sudden cardiac death) at or before age 50 (men) or 55 (women) (Fig. 1). Of these, 23 have died from CAD (mean age of death, 52 years). In contrast, kindred members without early CAD died at a mean age of 81. This familial clustering is noteworthy given that early CAD and early CAD death are uncommon in the general population (*8*, *9*).

Detailed clinical data were obtained for all available kindred members, including 13 affected with early CAD, 5 free of early CAD at or beyond the age threshold of 50 years (men) and 55 (women), and 9 younger asymptomatic members (CAD phenotype unknown; mean age 35 years) (table S1). Cardiac risk factors before or at presentation among affected subjects were surprisingly homogeneous, including high fasting LDL cholesterol in all (mean 176.4 mg/dl, nl < 130 mg/dl), high fasting triglycerides in 90% (mean 240 mg/dl, nl < 150 mg/dl), marked hypertension in all (mean 175/103 mm Hg, nl < 140/90, typically diagnosed after age 40), and type II diabetes mellitus in 77% (fasting blood glucose > 126 mg/dl; typically diagnosed after hypertension and hyperlipidemia). Despite high triglycerides, HDL levels were normal in all, and only one had a history of smoking. Nearly all of the affected subjects met criteria of the NIH National Cholesterol Education Program for metabolic syndrome based on the presence of diabetes, high triglycerides, and hypertension (*10*). Although obesity is strongly associated with metabolic syndrome and each of these risk factors,

[1]Departments of Internal Medicine, Genetics and Molecular Biophysics, and Biochemistry, Howard Hughes Medical Institute and Yale University School of Medicine, New Haven, CT 06510, USA. [2]Department of Pharmacology, Yale University School of Medicine, New Haven, CT 06510, USA. [3]Department of Material Science, Amir Kabir University of Technology, Tehran 15875/4413, Iran. [4]Department of Human Sciences, Azad University of Tehran, Tehran 13185/786, Iran. [5]Genetics Research Center, The Social Welfare and Rehabilitation Sciences University, Tehran 19875/383, Iran.

*To whom correspondence should be addressed. E-mail: arya.mani@yale.edu (A.M.); richard.lifton@yale.edu (R.P.L.)

it is noteworthy that obesity is absent among affected subjects (mean BMI 24.6, none greater than 26). In contrast to these affected subjects, the five unaffected family members all had normal levels of blood pressure (mean 116/81 mm Hg), LDL cholesterol (mean 97.8 mg/dl), and triglycerides (mean 60.75 mg/dl), and type 2 diabetes mellitus was absent. Finally, among younger subjects with CAD phenotype unknown, all nine had high LDL levels and seven had high triglyceride levels, whereas hypertension and glucose intolerance were less frequent (table S1).

The marked clustering of early CAD and risk factors in this kindred suggests a strong genetic component. Among sibships in which all subjects are beyond the age threshold for onset of CAD, the offspring of single affected parents yielded 17 affected and 15 unaffected subjects, and male-to-male transmission is present; in addition, the union of two affected first cousins yielded six affected and one unaffected offspring. Similarly, LDL levels are strongly bimodal in the kindred, with all members having either high levels (157 to 195 mg/dl) or low levels (92 to 105 mg/dl), and these levels cosegregate with early CAD. This extreme familial clustering and segregation of phenotypes within the kindred is unlikely to be explained by chance or multifactorial determination and provides strong evidence that early CAD is transmitted as a highly penetrant autosomal dominant trait.

Nineteen family members were available for genetic studies, including seven with early

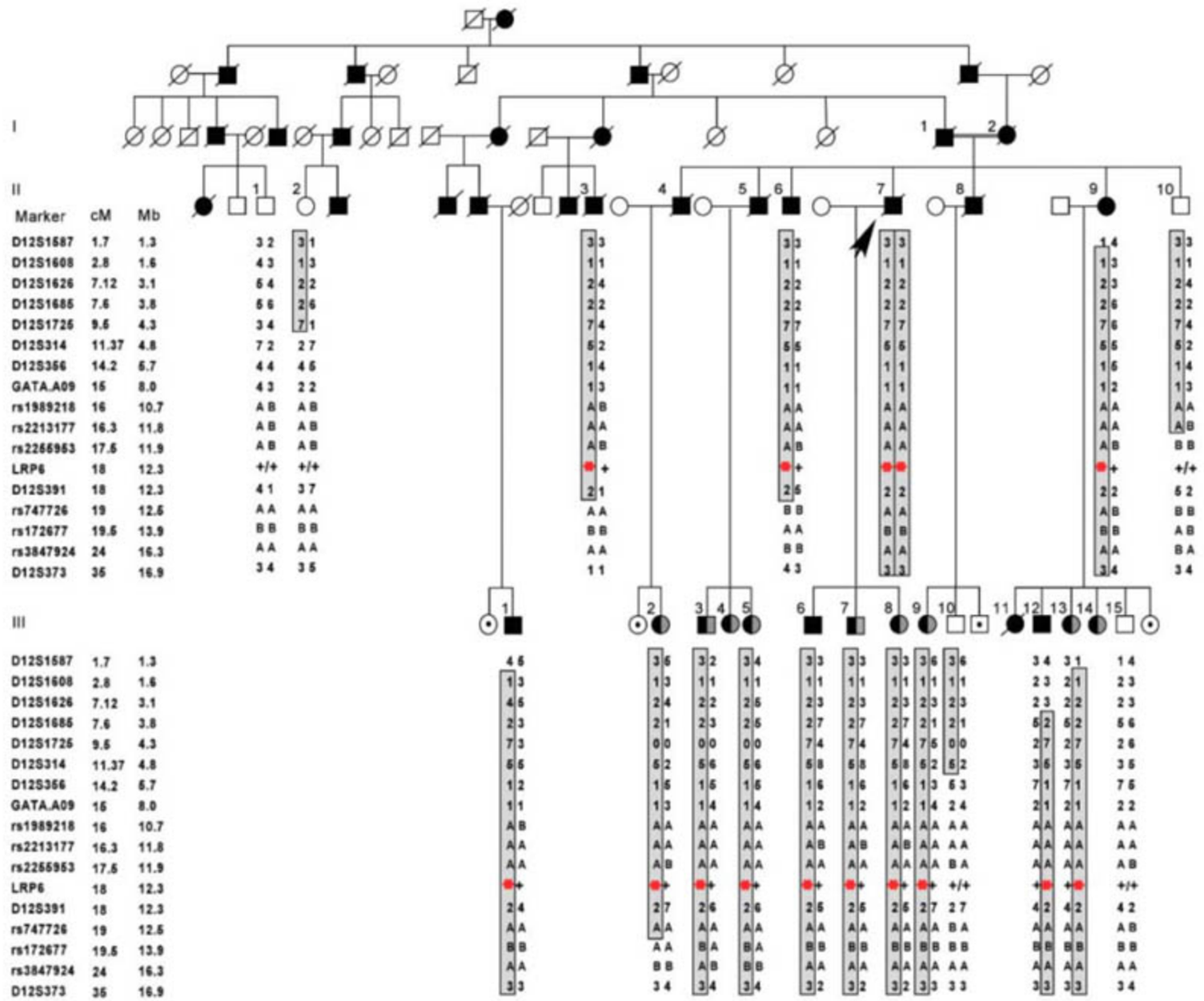

Fig. 1. Relationships of members of kindred CAD-100 are shown. The index case is indicated by the arrow. Numbered individuals correspond to those in table S1. Individuals with early CAD are indicated by black symbols; individuals without CAD who are beyond age 50 (men) or 55 (women) are shown as unfilled symbols; and individuals who are without symptomatic CAD, are below these ages, and have high LDL levels (range 157 to 192) are shown as half-black, half-gray symbols. Individuals who were not studied are indicated by symbols with dots. Circles represent females; squares represent males. Symbols with a slash through them indicate deceased subjects. Genotypes of informative microsatellite and SNP markers are shown in their chromosomal order below the symbol for each individual and their distance in centimorgans and megabases from 12pter is indicated. Segments of the haplotype seen in the index case which segregate with CAD and/or high LDL levels are indicated by shaded boxes. The presence of the wild-type *LRP6 or* $LRP6_{R611C}$ mutation is indicated by a plus sign or a red asterisk, respectively. Subjects III-6, III-7, and III-8 are offspring of a homozygous mutation carrier and hence obligate mutation carriers; subjects III-3, III-4, and III-5 are also statistically likely to be offspring of a homozygous carrier. This explains the high proportion of mutation carriers in generation III.

CAD, five unaffected subjects, and seven with CAD phenotype unknown due to young age. A genome-wide analysis of linkage was performed using Affymetrix 10K Gene Chips. We analyzed linkage using all single-nucleotide polymorphisms (SNPs) by applying two prespecified models of the trait locus—a conservative model that specified 90% penetrance, 1% phenocopies, and disease allele frequency of 0.001 and a stringent model that specified 99% penetrance, 0.1% phenocopies, and allele frequency of 0.0001 (*11*). Results under both models demonstrated significant evidence of linkage to a segment of chromosome 12p, and no other interval yielded a logarithm (base 10) of the odds ratio (lod score) greater than 1.5. Under the stringent model, the maximum multipoint lod score was 4.4 for linkage of CAD within the 2.7-cM interval flanked by loci rs2213177 and rs747726 (Figs. 1 and 2A; odds ratio 25,000:1 in favor of linkage). Results of linkage under the conservative model were similar. Linkage was confirmed by genotyping 11 highly polymorphic di- and tetranucleotide repeat markers this interval of 12p (Fig. 1), and virtually indistinguishable results were obtained when all markers were combined in the analysis. The observed lod scores approximate the theoretical maximum under the specified models. It is worth noting that the index case, who was the offspring of affected first cousins, was homozygous across this interval, implying that he was homozygous for the underlying disease-causing mutation.

The lod-1 interval spans only 750,000 base pairs and contains only six annotated genes: *ETV6*, *BCL2L14*, *LRP6*, *MANSC1*, *LOH12CR1*, and *DUSP16* (fig. S1). Among these, *LRP6* (LDL receptor–related protein 6) is noteworthy. LRP6 and its close paralog LRP5 serve as coreceptors with frizzled proteins (members of the G protein–coupled receptor family) for Wnt ligands (*12*). Mice deficient for *LRP5* develop hypercholesterolemia and impaired glucose tolerance on a high-fat diet (*13*), and LDL levels are markedly increased on the apolipoprotein E–deficient background (*14*). In addition, deficiency for either *LRP5* (in the human and mouse) or *LRP6* (in the mouse) results in early severe osteoporosis (*15*, *16*). This latter observation recalls the unexplained osteoporosis of the index case. Evaluation of kindred members identified two additional affected males with early hip fractures (ages 48 and 68) and low bone density in the three additional affected subjects studied; in contrast, bone density was normal in the one unaffected subject studied (table S1).

These findings motivated further evaluation of *LRP6*. Direct sequencing of all exons and intron-exon boundaries of *LRP6* in the index case revealed a single variant, a homozygous mutation that introduces a missense substitution, R611C (Fig. 2B). R611 lies in an epidermal growth factor (EGF)–like domain (fig. S2) and is conserved among LRP6 orthologs ranging from *Xenopus* to human (Fig. 2C); it is also found in mammalian LRP5, LRP2, and LRP3. This mutation precisely cosegregated with early CAD in the kindred, was absent among 400 unrelated Iranian and 3600 U.S. Caucasian control chromosomes, and is predicted to be deleterious by the PolyPhen and Sift programs. Sequencing of the other five genes in the lod-1 interval identified no other missense or splice site mutations.

We next considered the impact of this mutation on CAD risk factors. Analysis revealed complete linkage of $LRP6_{R611C}$ and high LDL, with a lod score of 5.5 (Fig. 2A, odds of 316,000:1 in favor of linkage). The difference in mean LDL levels between mutation carriers and noncarriers is significant (170 ± 12 mg/dl versus 98 ± 5 mg/dl, $P = 6 \times 10^{-6}$; Table 1). Because high LDL levels are found in all mutation carriers,

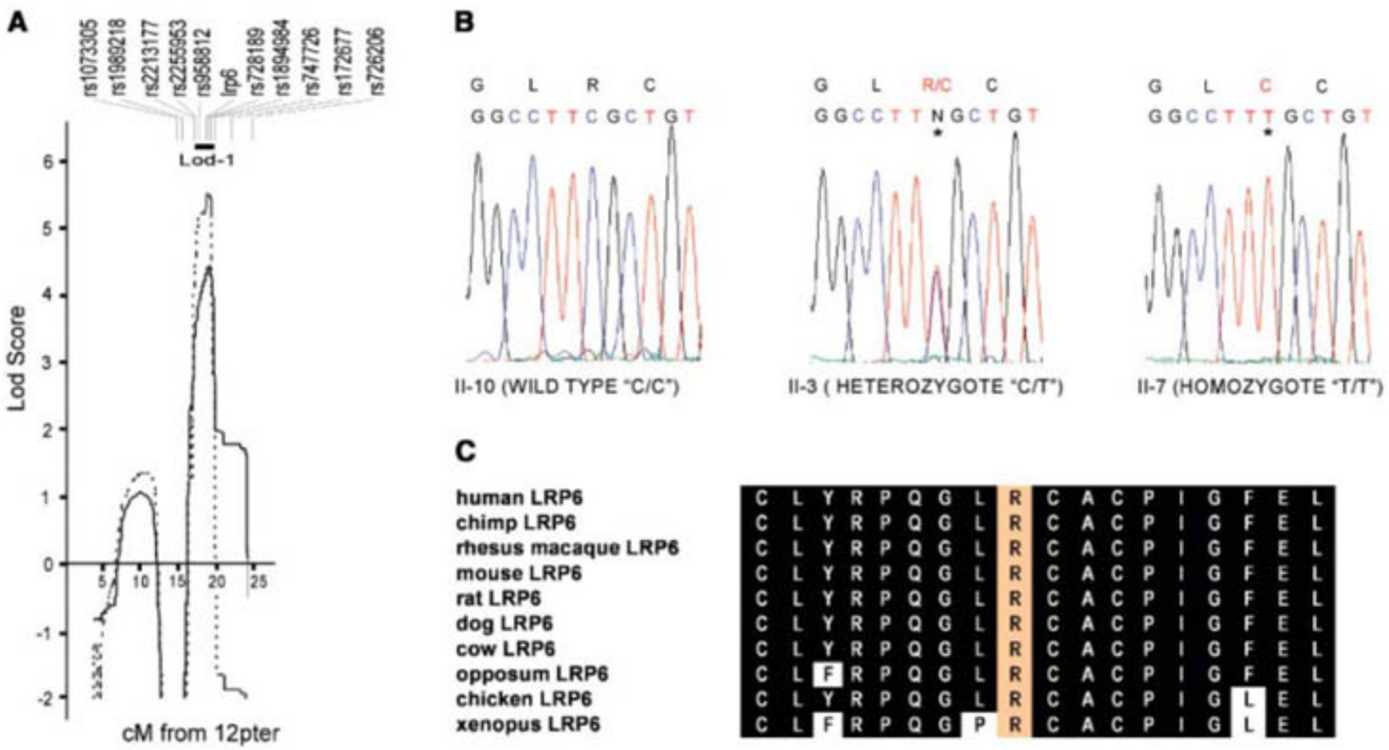

Fig. 2. Mutation in *LRP6* cosegregates with early CAD and high LDL. (**A**) Multipoint lod scores for linkage of early CAD and high LDL cholesterol to 12p. Multipoint lod scores for linkage of early CAD (solid line) or high LDL cholesterol (dashed line) to proximal 12p are shown under the stringent model of the trait locus (*27*). Lod scores were calculated with the use of all chromosome 12 SNP data from Affymetrix 10K chips (*27*). SNPs tightly linked to the location of the maximum lod score are indicated and the location of *LRP6* is shown. The lod score peak occurs at zero recombination with marker *rs958812* and the lod-1 interval spans 2.7 cM for both traits. (**B**) The DNA sequence of a segment of *LRP6* exon 9 is shown from an unaffected kindred member (left), a heterozygous mutation carrier (middle), and the homozygous index case (right). A single base substitution (asterisk) changes the wild-type cytidine to thymidine leading to substitution of cysteine for arginine at codon 611. (**C**) A portion of the amino acid sequence of the second EGF-like domain of LRP6 is shown from diverse vertebrate species. This segment is highly conserved and arginine is completely conserved from *Xenopus* to human.

Table 1. Comparison of phenotypes in carriers and noncarriers of LRP_{R611C}. Means ± standard deviation are shown for quantitative traits. All kindred members with measured values were included for LDL, triglyceride, HDL, and BMI measurements. For blood pressure, fasting blood glucose, and diabetes, results for subjects over age 40 are shown.

Trait	LRP_{R611C} carriers	Noncarriers	*P* value
LDL (mg/dl)	170 ± 12	98 ± 5	6×10^{-6}
Triglycerides (mg/dl)	209 ± 71	68 ± 20	1×10^{-5}
HDL (mg/dl)	57 ± 8	56 ± 7	0.4
BMI (kg/m^2)	24.3 ± 2.6	24.4 ± 1.6	0.13
Systolic BP (mmHg)	168 ± 21	116 ± 5	8×10^{-5}
Diastolic BP (mmHg)	100 ± 14	81 ± 7	0.0025
Fasting blood glucose (mg/dl)	159 ± 43	80 ± 3	0.001
Diabetes (yes/no)	11/4	0/5	0.005

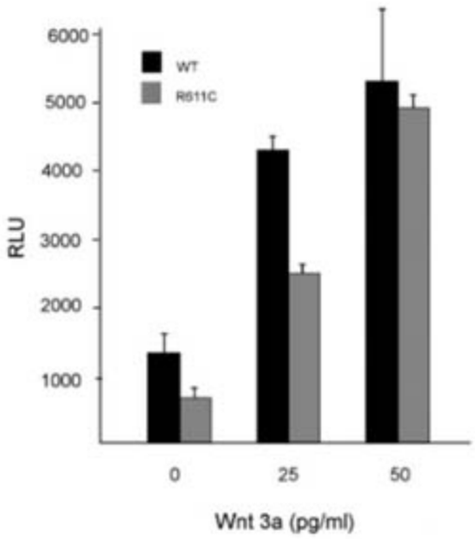

Fig. 3. $LRP6_{R611C}$ impairs Wnt signaling. NIH3T3 cells were transfected with plasmids encoding wild-type (WT) or mutant hemagglutinin-tagged LRP6 and Wnt reporter genes and incubated with indicated concentrations of purified Wnt 3a protein followed by an assay of Wnt signaling (LEF-1–dependent expression of luciferase) (*27*). The results are shown as mean and standard error of the mean of quadruplicate experiments. RLU, relative light units.

regardless of age, this trait can serve as a biomarker of the mutation in subjects too young to manifest CAD. Similarly, $LRP6_{R611C}$ imparts significant effects on triglyceride levels, blood pressure, fasting blood glucose, and prevalence of diabetes (Table 1). No significant effects were seen on HDL levels or body mass index. Finally, all five mutation carriers studied have low bone densities, each with values expected in less than 12.5% of the population ($P < 0.001$).

The functional significance of this *LRP6* mutation was explored by expression in NIH3T3 cells (*17*) (Fig. 3). In these cells, expression of LRP6 potentiates Wnt signaling, assayed as LEF-1 mediated expression of luciferase. In the absence of added Wnt 3a, $LRP6_{R611C}$ showed a 49% reduction of induced signaling compared with that of wild-type LRP6 ($P < 0.01$). The addition of low doses of Wnt 3a also showed markedly reduced signaling with $LRP6_{R611C}$ (42% reduction, $P < 10^{-5}$). At high doses of Wnt 3a, however, Wnt signaling through $LRP6_{R611C}$ does not differ significantly from that of the wild type ($P = 0.48$). Measurement of total LRP6 expression by Western blotting and cell surface expression measured by specific binding to Dkk-1 demonstrate similar levels of wild-type and mutant LRP6 (fig. S3, A and B). These findings are consistent with an impaired biochemical function of $LRP6_{R611C}$.

Our findings establish a causal link between *LRP6* mutation and early CAD with high LDL, high triglycerides, hypertension, diabetes, and low bone density. The evidence includes strong a priori evidence of segregation of the disease as an autosomal dominant trait in this kindred, linkage of this trait and underlying risk factors to a single small genomic interval, identification of a single rare mutation in the linked interval that alters a highly conserved amino acid, biochemical evidence that the mutation impairs function of the encoded protein, and evidence from mouse models that mutations in orthologs and paralogs of the identified gene confer similar effects on risk factors. We anticipate that the mutation we identified is very rare in the population; to date we have found no other suggestive mutations in *LRP6* among 400 unrelated subjects with CAD. Nonetheless, as for other Mendelian forms of important medical traits—including cardiovascular risk factors, neurodegenerative diseases, and pain perception, among many others (*18*–*20*)—the findings from this rare kindred may provide key insight into pathways that cause disease and that may be manipulated for health benefit. These findings motivate further investigation of the genes and activity of this pathway to search for inherited or acquired variation in Wnt signaling in common forms of CAD and metabolic syndrome.

The impact of the *LRP6* mutation on multiple CAD risk factors is notable. Most mutation carriers over age 45 meet criteria for the metabolic syndrome. Although the observed effects on these risk factors are substantial, they are not individually as large as those seen with many previously defined Mendelian traits. For example, the mean LDL levels among *LRP6* mutation carriers are 170 mg/dl, versus a mean level of about 300 mg/dl among carriers of heterozygous loss-of-function mutations in the LDL receptor (*21*). Similarly, the hypertension and diabetes in this family typically appear in middle age, at ages that could easily be mistaken for "garden variety" forms of these risk factors. These observations suggest that it is the combined effects of these risk factors that account for the very high cardiovascular risk to mutation carriers.

Because loss-of-function mutations in *LRP5* (*12*, *15*) and *LRP6* (*16*) result in reduced bone density, the osteoporosis among LRP_{R611C} carriers lends further support to the functional significance of this mutation. Moreover, recent epidemiologic studies have found strong association of osteoporosis and CAD (*22*). Our observations suggest that osteoporosis and CAD can be pleiotropic consequences of impaired Wnt signaling, raising the question of whether the co-occurrence of osteoporosis and CAD might commonly identify individuals with inherited or acquired impairment in Wnt signaling.

Our findings underscore emerging evidence implicating effects of altered Wnt signaling on cardiovascular risk factors. Common intronic variants in the Wnt-responsive transcription factor *TCF7L2* result in altered insulin secretion and type II diabetes mellitus (*23*). Similarly, rare mutations in other Wnt-related transcription factors cause maturity onset diabetes of youth (*24*, *25*). The LRP_{R611C} mutation confers effects not only on many risk factors but on CAD outcomes as well. The ubiquitous expression of *LRP6* (*26*) supports the possibility of pleiotropic effects in diverse tissues. Further investigation of Wnt signaling in patients with early CAD, metabolic syndrome, and its components may provide new insight into disease pathophysiology and approaches to prevention of these disorders.

References and Notes

1. C. J. Murray, A. D. Lopez, *Lancet* **349**, 1436 (1997).
2. J. M. Schildkraut, R. H. Myers, L. A. Cupples, D. K. Kiely, W. B. Kannel, *Am. J. Cardiol.* **64**, 555 (1989).
3. A. J. Lusis, *Nature* **407**, 233 (2000).
4. J. J. Nora, R. H. Lortscher, R. D. Spangler, A. H. Nora, W. J. Kimberling, *Circulation* **61**, 503 (1980).
5. I. Zavaroni, G. Reaven, *Diabetes Metab.* **17**, 109 (1991).
6. P. Poulsen, A. Vaag, K. Kyvik, H. Beck-Nielsen, *Diabetologia* **44**, 537 (2001).
7. M. E. Marenberg, N. Risch, L. F. Berkman, B. Floderus, U. de Faire, *N. Engl. J. Med.* **330**, 1041 (1994).
8. J. Johansson, M. Viigimaa, M. Jensen-Urstad, I. Krakau, L. O. Hansson, *J. Intern. Med.* **252**, 551 (2002).
9. H. Tunstall-Pedoe *et al.*, *Lancet* **355**, 688 (2000).
10. Expert Panel on Detection, Evaluation, and Treatment of High Blood Cholesterol in Adults, *JAMA* **285**, 2486 (2001).
11. T. A. Mansfield *et al.*, *Nat. Genet.* **16**, 202 (1997).
12. X. He, M. Semenov, K. Tamai, X. Zeng, *Development* **131**, 1663 (2004).
13. T. Fujino *et al.*, *Proc. Natl. Acad. Sci. U.S.A.* **100**, 229 (2003).
14. K. Magoori *et al.*, *J. Biol. Chem.* **278**, 11331 (2003).
15. Y. Gong *et al.*, *Cell* **107**, 513 (2001).
16. C. Kokubu *et al.*, *Development* **131**, 5469 (2004).
17. B. Mao *et al.*, *Nature* **411**, 321 (2001).
18. B. Caughey, P. T. Lansbury, *Annu. Rev. Neurosci.* **26**, 267 (2003).
19. J. J. Cox *et al.*, *Nature* **444**, 894 (2006).
20. E. G. Nabel, *N. Engl. J. Med.* **349**, 60 (2003).
21. J. L. Goldstein, M. S. Brown, *Science* **292**, 1310 (2001).
22. P. A. Marcovitz *et al.*, *Am. J. Cardiol.* **96**, 1059 (2005).

23. S. F. Grant *et al.*, *Nat. Genet.* **38**, 320 (2006).
24. Y. Horikawa *et al.*, *Nat. Genet.* **17**, 384 (1997).
25. K. Yamagata *et al.*, *Nature* **384**, 458 (1996).
26. S. D. Brown *et al.*, *Biochem. Biophys. Res. Commun.* **248**, 879 (1998).
27. Materials and methods are available as supporting material on Science Online.

28. We thank members of the kindred studied for their invaluable participation in this project. Research supported in part by an NIH KO8 award (to A.M.) and grants P50 HL55007 and P01DK68229 from NIH (to R.L.).

Supporting Online Material
www.sciencemag.org/cgi/content/full/315/5816/1278/DC1

Materials and Methods
Figs. S1 to S3
Tables S1 and S2
References

16 October 2006; accepted 1 February 2007
10.1126/science.1136370

Emulating Membrane Protein Evolution by Rational Design

Mikaela Rapp,[1]* Susanna Seppälä,[1]* Erik Granseth,[1,2] Gunnar von Heijne[1,2]†

How do integral membrane proteins evolve in size and complexity? Using the small multidrug-resistance protein EmrE from *Escherichia coli* as a model, we experimentally demonstrated that the evolution of membrane proteins composed of two homologous but oppositely oriented domains can occur in a small number of steps: An original dual-topology protein evolves, through a gene-duplication event, to a heterodimer formed by two oppositely oriented monomers. This simple evolutionary pathway can explain the frequent occurrence of membrane proteins with an internal pseudo–two-fold symmetry axis in the plane of the membrane.

Membrane protein evolution is often accomplished by gene-duplication and gene-fusion events (*1*), and high-resolution membrane protein structures have disclosed an unanticipated number of cases where homologous N- and C-terminal domains are related by an approximate two-fold symmetry axis either perpendicular to or in the plane of the membrane. In the former case, each domain has an even number of transmembrane helices and the two domains are oriented parallel to each other in the membrane, whereas in the latter case each domain has an odd number of transmembrane helices and the two domains are antiparallel. Representative examples of membrane proteins with parallel domains are LacY (*2*), GlpT (*3*), the Sav1866 ABC transporter (*4*), AcrB (*5*), EmrD (*6*), and the ADP/ATP carrier (*7*); among membrane proteins with antiparallel domains are LeuT (*8*), SecY (*9*), BtuCD (*10*), AQP1 (*11*), GlpF (*12*), AmtB (*13*), the ClC H^+/Cl^- exchange transporter (*14*), and NhaA (*15*).

A particularly notable mode of gene duplication–based membrane protein evolution was suggested recently by an analysis of proteins in the small multidrug-resistance (SMR) family (*16*). The best-studied SMR protein is EmrE from *E. coli*, an inner-membrane drug-efflux pump with four transmembrane helices. EmrE likely has a dual topology with identical copies of the protein forming an antiparallel homodimer (or higher oligomer) composed of N_{in}-C_{in} and N_{out}-C_{out} monomers (*16*–*20*), although some data suggest a parallel N_{in}-C_{in} dimer (*21*, *22*). Membrane protein topology is largely governed by the positive-inside rule (*23*)—i.e., loops rich in Lys and Arg residues tend to orient toward the cytoplasm. EmrE has only a weak K+R bias (*24*), as would be expected for a dual-topology protein, and it is encoded by a singleton gene with no homologous genes nearby on the chromosome. In contrast, many genes encoding SMR proteins, in both *E. coli* and other bacteria, appear as pairs on the chromosome, and the two encoded proteins have large but opposite K+R biases and therefore likely insert into the membrane with opposite orientations (*16*). These findings immediately suggest an evolutionary scenario in which a singleton gene encoding a dual-topology protein undergoes a gene duplication, after which the two resulting proteins become fixed in opposite orientations by evolving opposite K+R biases. Possibly, oppositely oriented proteins occasionally mutate back to a dual topology (*25*). In a final step, the two oppositely oriented proteins may fuse into a single polypeptide that folds into an antiparallel structure

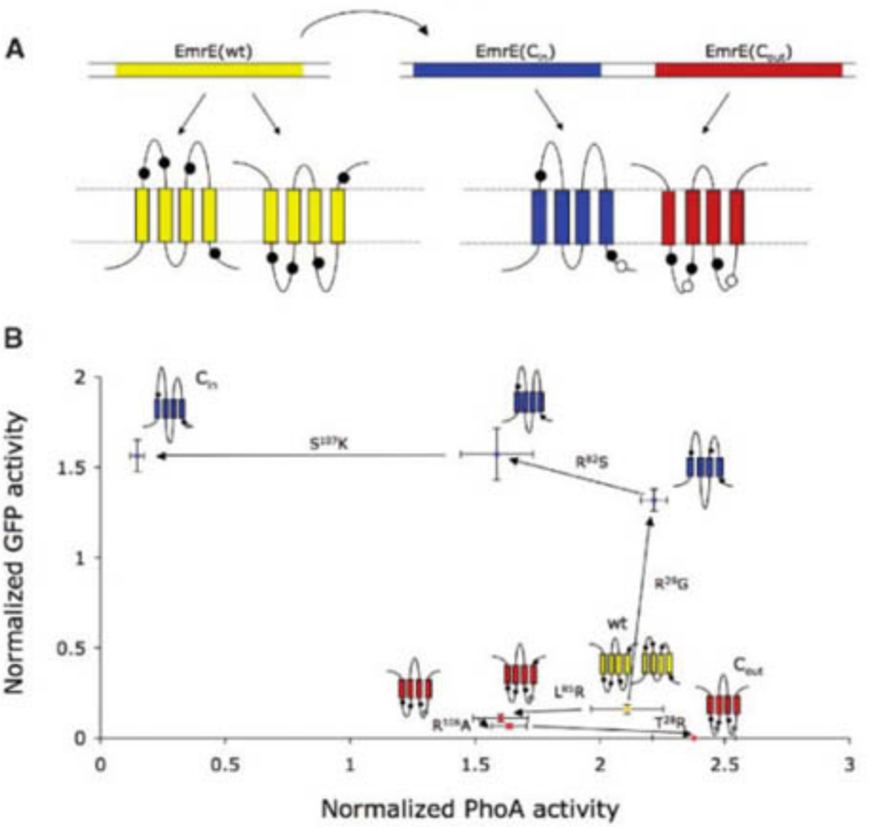

Fig. 1. (**A**) Conversion of the wild-type (wt) dual-topology protein EmrE to two oppositely oriented proteins, EmrE(C_{in}) and EmrE(C_{out}). Black circles indicate positively charged residues present in wild-type EmrE; white circles indicate positively charged residues added by mutagenesis. The mutations in EmrE(C_{in}) are R29G, R82S, and S107K, and the mutations in EmrE(C_{out}) are T28R, L85R, and R106A. (**B**) PhoA activities and GFP fluorescence levels for C-terminal PhoA and GFP fusions to the indicated EmrE mutants [normalized against the median PhoA activity or GFP fluorescence of a large set of *E. coli* inner-membrane protein PhoA and GFP fusions (*26*)]. High PhoA activity and low GFP fluorescence indicate a periplasmic localization of the C terminus, whereas low PhoA activity and high GFP fluorescence indicate a cytoplasmic localization. Error bars show standard errors in the mean value determinations.

[1]Center for Biomembrane Research, Department of Biochemistry and Biophysics, Stockholm University, SE-106 91 Stockholm, Sweden. [2]Stockholm Bioinformatics Center, AlbaNova, SE-106 91 Stockholm, Sweden.

*These authors contributed equally to this work.
†To whom correspondence should be addressed. E-mail: gunnar@dbb.su.se

with a pseudo–two-fold symmetry axis in the plane of the membrane (*16*).

EmrE provides an ideal case to test this evolutionary scenario. According to the dual-topology model, two oppositely oriented EmrE monomers form the active homodimer. We reasoned that mutants of EmrE designed to insert into the inner membrane with a unique N_{in}-C_{in} or N_{out}-C_{out} orientation should therefore be nonfunctional when expressed alone but should complement each other when coexpressed, hence emulating the proposed gene-duplication and topology-evolution steps. In contrast, should the active protein be a parallel homodimer, as has been suggested (*21*), molecules with N_{in}-C_{in} and N_{out}-C_{out} orientations would not be expected to complement each other. Further mutation of functionally important residues in the N_{in}-C_{in} or N_{out}-C_{out} mutant might allow the design of active heterodimers incorporating single-site mutations that would inactivate wild-type homodimeric EmrE, reflecting a wider scope for evolutionary fine-tuning of oppositely oriented heterodimers as compared with dual-topology homodimers.

To push EmrE toward the N_{in}-C_{in} and N_{out}-C_{out} orientations, we manipulated the K+R bias (Fig. 1A). The orientation in the inner membrane of the various EmrE mutants was probed by making C-terminal fusions to the topology reporters green fluorescent protein (GFP) and alkaline phosphatase (PhoA) (*26*). The different fusion constructs all express to similar levels (fig. S1A), and the GFP and PhoA activities show that construct EmrE(C_{in}) indeed has an N_{in}-C_{in} topology, whereas construct EmrE(C_{out}) adopts the opposite orientation (Fig. 1B).

Expression of EmrE makes *E. coli* resistant to high levels of ethidium bromide (EtBr) and other cationic hydrophobic drugs (*27*). We found that cells expressing wild-type EmrE (that was not fused to GFP or PhoA) grow well in 0.25 mM EtBr (Fig. 2A and fig. S1B), whereas cells transformed with empty vector do not (see fig. S2 for growth at different concentrations of EtBr and fig. S3 for growth curves in 0.25 mM EtBr). The expression of EmrE(C_{in}) and EmrE(C_{out}) individually (in single or double copy) does not confer resistance to EtBr. Notably, however, coexpression of EmrE(C_{in}) and EmrE(C_{out}) restores EtBr resistance to the same level as seen with wild-type EmrE (Fig. 2A, green bar), strongly suggesting the formation of a functional, antiparallel heterodimer.

The EtBr-resistance levels conferred by expression of the mutants that are intermediate between wild-type EmrE and EmrE(C_{in}) or EmrE(C_{out}) are also consistent with the proposed evolutionary scenario (Fig. 2A). For cells expressing the two intermediates on the way to EmrE(C_{out})—EmrE($L^{85}\rightarrow R^{85}$) (hereafter, L85R) and EmrE(L85R, R106A)—the growth rate drops with the number of mutations, as expected. For cells expressing the intermediates on the way to EmrE(C_{in})—EmrE(R29G) and EmrE(R29G, R82S)—the growth rate remains close to that of wild-type EmrE and only with the addition of the final mutation (S107K) in EmrE(C_{in}) does the growth rate drop to near zero, mirroring the GFP/PhoA fusion protein results that indicate a mixed orientation of both intermediates.

Although these results are in full agreement with the proposed dual topology of wild-type EmrE, taking the activities of the wild-type EmrE GFP and PhoA fusions at face value suggests that these fusions have a predominantly N_{out}-C_{out} orientation (Fig. 1B). This prompted us to measure growth rates in the presence of EtBr also for cells expressing the GFP-reporter fusions. In contrast to the results for the nonfused constructs, cells expressing wild-type EmrE-GFP grow less well in EtBr than do cells expressing the C_{in} intermediates EmrE(R29G)-GFP and EmrE(R29G,

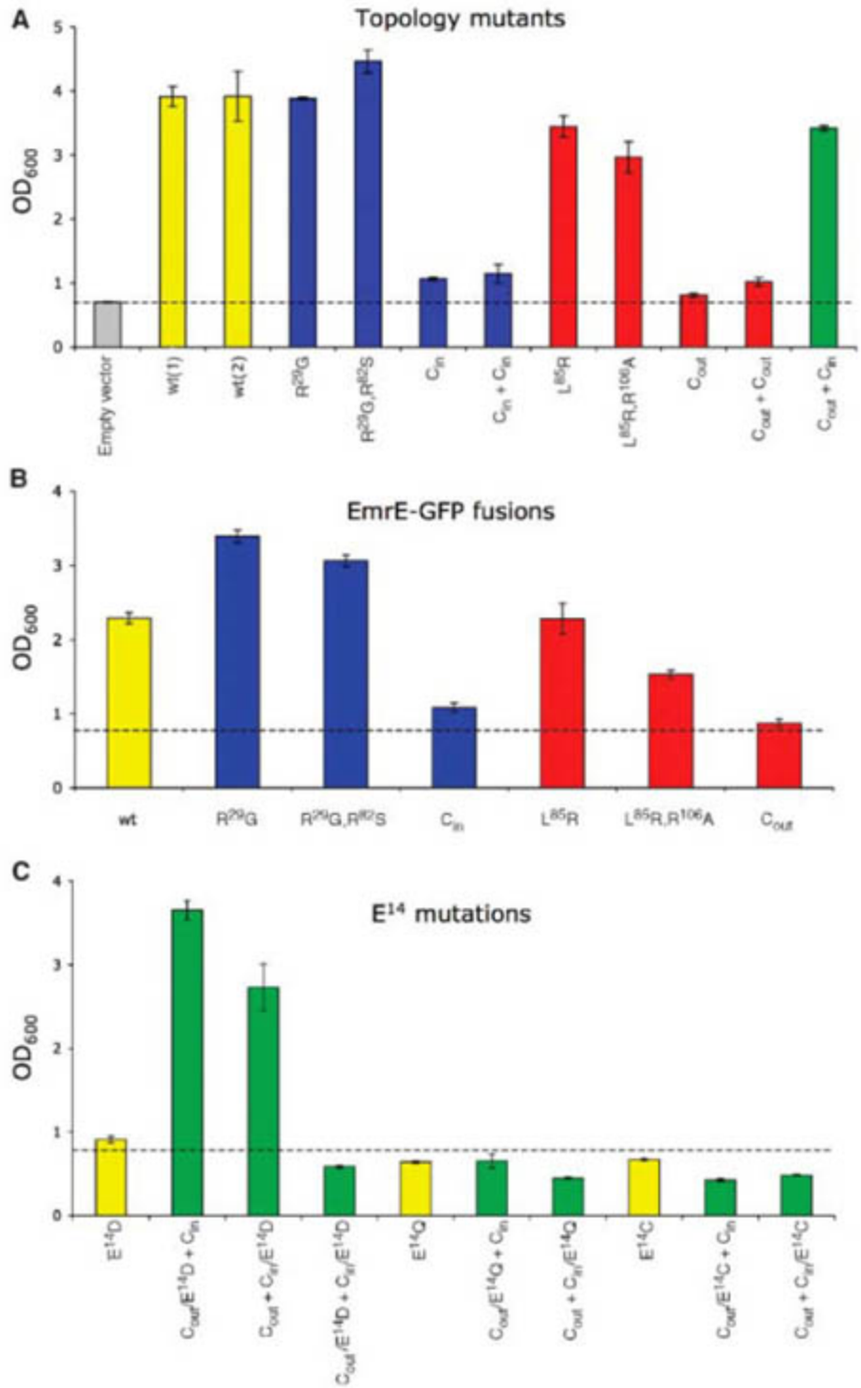

Fig. 2. (**A**) Optical density at 600 nm (OD_{600}) after 4 hours of growth in 0.25 mM EtBr of cells expressing the indicated EmrE mutants (not fused to GFP or PhoA). See Fig. 1 for color code. Green bar, coexpressed EmrE(C_{in}) + EmrE(C_{out}). The dashed line indicates the OD_{600} of cells transformed with empty pET Duet-1 vector (gray bar). Bars wt(1) and wt(2) show results for wild-type EmrE cloned into the first and second multiple-cloning site in the vector. (**B**) OD_{600} after 4 hours of growth in 0.25 mM EtBr of cells expressing the indicated EmrE-GFP fusions. (**C**) OD_{600} after 4 hours of growth in 0.25 mM EtBr of cells expressing the indicated EmrE mutants (not fused to GFP or PhoA). In all panels, error bars show standard errors in the mean value determinations.

R82S)-GFP; cells expressing EmrE(C_{in})-GFP do not grow, as expected (Fig. 2B). Among the C_{out} intermediates, EmrE(L85R)-GFP confers the same level of EtBr resistance as wild-type EmrE-GFP, whereas cells expressing EmrE(L85R, R106A)-GFP grow less well; those expressing EmrE(C_{out})-GFP grow no better than background.

The simplest explanation for these growth patterns is that the C-terminal GFP moiety causes a shift toward more C_{out} orientation, which is "corrected" by the C_{in}-promoting mutations R29G and R82S, precisely as indicated by the GFP and PhoA activity measurements in Fig. 1B. It is not unexpected that C-terminal reporter fusions, although normally highly reliable indicators of C-terminal orientation (*28*), can have a subtle effect on the orientation of finely balanced dual-topology proteins. Indeed, the same reasoning might also explain the predominant C_{in} orientation seen for an EmrE-Myc-His_6 construct with reduced in vivo activity (*22*), in which positively charged His and Lys residues in the C-terminal tag may favor the C_{in} topology but leave enough C_{out}-oriented protein to confer a certain degree of drug resistance.

A small number of residues are conserved throughout the SMR family. To test whether such residues are required in both or only in one subunit of the dimer, we focused on Glu^{14} in EmrE, a residue intimately involved in the proton-driven extrusion of substrate from the cell (*29*). Glu^{14} is totally conserved in all SMR proteins with low K+R bias, but is replaced by Asp in a small number of N_{out}-C_{out} homologs that presumably form active heterodimers (fig. S4). Indeed, cells coexpressing constructs EmrE(C_{out}/E14D) and EmrE(C_{in}) grow in EtBr at the same rate as cells expressing wild-type EmrE (Fig. 2C and figs. S2 and S3). Cells coexpressing the alternate combination EmrE(C_{out}) and EmrE(C_{in}/E14D) are also EtBr resistant but grow more slowly than the first combination, possibly explaining why Asp^{14} has so far only been found in N_{out}-C_{out}–oriented EmrE homologs. As seen for the homodimeric EmrE(E14D) mutant (*29*), cells coexpressing EmrE(C_{in}/E14D) and EmrE(C_{out}/E14D) do not grow in EtBr. Thus, Glu^{14} can be replaced by Asp in one but not in both monomers in the EmrE dimer. Mutations in the EmrE(C_{out}) or EmrE(C_{in}) monomers that do not conserve the negative charge at residue 14 (E14Q and E14C) do not support growth in EtBr when coexpressed with either EmrE(C_{in}) or EmrE(C_{out}).

Our results show that an evolutionary path connecting a dual-topology protein to a pair of oppositely oriented homologs can be emulated by rational protein design based on the positive-inside rule, and that once a heterodimer of oppositely oriented subunits has appeared, additional mutations that render the original dual-topology protein nonfunctional can be selected in one of the two monomers. With such a readily accessible evolutionary pathway available, it is no surprise that many membrane proteins show signs of internal duplication and approximate two-fold in-plane symmetry in their three-dimensional structures.

References and Notes

1. T. Shimizu, H. Mitsuke, K. Noto, M. Arai, *J. Mol. Biol.* **339**, 1 (2004).
2. J. Abramson *et al.*, *Science* **301**, 610 (2003).
3. Y. Huang, M. J. Lemieux, J. Song, M. Auer, D. N. Wang, *Science* **301**, 616 (2003).
4. R. J. Dawson, K. P. Locher, *Nature* **443**, 180 (2006).
5. S. Murakami, R. Nakashima, E. Yamashita, A. Yamaguchi, *Nature* **419**, 587 (2002).
6. Y. Yin, X. He, P. Szewczyk, T. Nguyen, G. Chang, *Science* **312**, 741 (2006).
7. E. Pebay-Peyroula *et al.*, *Nature* **426**, 39 (2003).
8. A. Yamashita, S. K. Singh, T. Kawate, Y. Jin, E. Gouaux, *Nature* **437**, 215 (2005).
9. B. van den Berg *et al.*, *Nature* **427**, 36 (2004).
10. K. P. Locher, A. T. Lee, D. C. Rees, *Science* **296**, 1091 (2002).
11. H. Sui, B. G. Han, J. K. Lee, P. Walian, B. K. Jap, *Nature* **414**, 872 (2001).
12. D. Fu *et al.*, *Science* **290**, 481 (2000).
13. S. Khademi *et al.*, *Science* **305**, 1587 (2004).
14. R. Dutzler, E. B. Campbell, M. Cadene, B. T. Chait, R. MacKinnon, *Nature* **415**, 287 (2002).
15. C. Hunte *et al.*, *Nature* **435**, 1197 (2005).
16. M. Rapp, E. Granseth, S. Seppälä, G. von Heijne, *Nat. Struct. Mol. Biol.* **13**, 112 (2006).
17. P. J. Butler, I. Ubarretxena-Belandia, T. Warne, C. G. Tate, *J. Mol. Biol.* **340**, 797 (2004).
18. I. Ubarretxena-Belandia, J. M. Baldwin, S. Schuldiner, C. G. Tate, *EMBO J.* **22**, 6175 (2003).
19. S. J. Fleishman *et al.*, *J. Mol. Biol.* **364**, 54 (2006).
20. Y. Elbaz, S. Steiner-Mordoch, T. Danieli, S. Schuldiner, *Proc. Natl. Acad. Sci. U.S.A.* **101**, 1519 (2004).
21. M. Soskine, S. Mark, N. Tayer, R. Mizrachi, S. Schuldiner, *J. Biol. Chem.* **281**, 36205 (2006).
22. S. Ninio, Y. Elbaz, S. Schuldiner, *FEBS Lett.* **562**, 193 (2004).
23. G. von Heijne, *EMBO J.* **5**, 3021 (1986).
24. Single-letter abbreviations for the amino acid residues are as follows: A, Ala; C, Cys; D, Asp; E, Glu; F, Phe; G, Gly; H, His; I, Ile; K, Lys; L, Leu; M, Met; N, Asn; P, Pro; Q, Gln; R, Arg; S, Ser; T, Thr; V, Val; W, Trp; and Y, Tyr.
25. T. Kikukawa, T. Nara, T. Araiso, S. Miyauchi, N. Kamo, *Biochim. Biophys. Acta* **1758**, 673 (2006).
26. Materials and methods are available as supporting material on *Science* Online.
27. M. Putman, H. W. van Veen, W. N. Konings, *Microbiol. Mol. Biol. Rev.* **64**, 672 (2000).
28. D. O. Daley *et al.*, *Science* **308**, 1321 (2005).
29. H. Yerushalmi, S. Schuldiner, *J. Biol. Chem.* **275**, 5264 (2000).

30. Supported by grants from the Swedish Research Council, the Marianne and Marcus Wallenberg Foundation, and the Swedish Foundation for Strategic Research to G.v.H.

Supporting Online Material

www.sciencemag.org/cgi/content/full/1135406/DC1
Materials and Methods
Figs. S1 to S4
References

21 September 2006; accepted 16 January 2007
Published online 25 January 2007;
10.1126/science.1135406
Include this information when citing this paper.

Local Interactions Select for Lower Pathogen Infectivity

Michael Boots* and Michael Mealor

Theory suggests that the current rapid increase in connectivity and consequential changes in the structure of human, agricultural, and wildlife populations may select for parasite strains with higher infectivity. We carried out a test of this spatial theory by experimentally altering individual host movement rates in a model host/pathogen system by altering the viscosity of their environment. In our microevolutionary selection experiments, the infectivity of the virus was, as predicted by the theory, reduced in the most viscous populations. We therefore provide empirical support for the theory that population structure affects the evolution of infectious organisms.

Because of the importance of the evolution of parasites and pathogens to human, agricultural, and wildlife systems, there is a well-developed theory that focuses on how transmission and increased mortality due to infection (virulence) may evolve (*1*–*4*). The classic theory of parasite evolution shows that natural selection will act to maximize the epidemiological basic reproductive number R_0: the number of secondary infections resulting from one infected host in a naïve host population (*1*–*4*). Clearly, parasite transmission acts to increase R_0, whereas virulence acts to decrease it by reducing the infectious period. One component of transmission that may evolve in the parasite is the probability of successfully infecting a susceptible host upon contact (infectivity). In the absence of constraints on selection, we would predict that the parasite would evolve maximal infectivity and zero virulence (*1*–*4*). This classic theory makes the assumption that the host populations are homogeneously mixed, and therefore each susceptible host has an equal probability of being infected by any infectious individual within the population. However, many natural host/parasite systems can be characterized by both localized transmission, where secondary infections are more frequent in individuals neighboring infected hosts, and patchy host distributions. Theory that examines the importance of local interactions (*5*–*9*) has predicted that spatial structure in host populations can constrain the evolution of parasite infectivity. When

Department of Animal and Plant Sciences, University of Sheffield, Western Bank, Sheffield S10 2TN, UK.

*To whom correspondence should be addressed. E-mail: m.boots@sheffield.ac.uk

interactions are predominantly local, highly infectious strains tend to "self-shade," so that susceptibles are rapidly exploited locally, causing infectious individuals to be surrounded by other infecteds. In contrast, strains with a lower infectivity produce, as they spread, a structure within the host population in which there is a higher local proportion of susceptible individuals next to infected ones. In this way, strains with lower infectivity gain an advantage as strains with high infectivity pay the cost of surrounding themselves with infected individuals (*5*–*7*). There is therefore an optimal transmission rate that balances maximizing infectivity with the maximization of susceptible individuals in the vicinity of the infected ones. Neighboring infected individuals may also tend to be infected by the same strain or closely related strains, and therefore local interactions tend to increase competition with offspring and kin, leading to different evolutionary outcomes (*10*–*13*).

Up until now, the study of parasite evolution in spatially structured populations has predominantly been a theoretical exercise. That said, there are some empirical host/parasite systems in which differences in spatial structure have been implicated as possible causes of differences in parasite characteristics. For example, serial passage experiments frequently result in increased parasite virulence (*14*, *15*). One explanation for this is that each passage involves mixing the host population and disrupting any spatial restrictions on transmission (*3*). Also, there is some correlative evidence that parasites with the capacity for long-distance dispersal tend to possess a higher virulence than parasites transmitted over short distances (*16*–*18*). Evolutionary experiments with fragmented populations have also shown the importance of spatial structure and extinctions to the evolution of pathogen life histories (*19*). However, we know of no manipulative evolutionary experiments that alter the spatial structure within host populations and examine the evolution of a parasite. Here we present the results of a microevolutionary selection experiment in which the infectivity of an insect larval virus was examined in replicated host microcosms having environments with different viscosities. The susceptible host individuals lived within their food medium, and therefore the more viscous environments led to lower individual movement rates and, as a consequence, more local interactions. We show that, as predicted by the spatial theory, infectivity was indeed reduced in the more viscous populations, where there were more local interactions and localized transmissions.

Larvae of the phycitiid moth species *Plodia interpunctella* (*Plodia*) are infected with a species-specific granulosis virus (PiGV). The virus persists in microcosms with *Plodia* and usually has minor effects on the host population dynamics (*20*–*22*). Natural infection occurs orally, with the cannibalism of PiGV-infected host cadavers being a major route of infection (*23*). The susceptible larvae live within the food medium, and therefore the movement of the larvae can be altered by using food mediums of different viscosities. This in turn changes the spatial structure of host/parasite populations, with the high mobility in soft mediums allowing greater larval mixing as individuals disperse across a larger part of their total environment. In contrast, larvae with lower movement will tend to encounter more of the same individuals and therefore PiGV transmission will be more localized. We manipulated the viscosity of the larval medium as described in the methods in the supporting online material (SOM) to create three levels of food viscosity: soft, intermediate, and hard. We then measured the movement rates of *Plodia* larvae within the three food mediums. Increasing the viscosity of the food caused a significant change in the distance that the larvae moved (Fig. 1) [analysis of variance (ANOVA) square root(distance) $F_{2,82} = 57.6$, $P < 0.01$]. Pairwise comparisons reveal that movement in soft food was significantly faster than in both intermediate and hard food, whereas movement in intermediate food was faster than in the hard food (Fig. 1). Our manipulation of the food medium therefore had the desired effect of significantly altering the movement rates. However, our aim was also not to affect the quality of the food in any other way. In a second set of experiments, we showed that the different mediums did not affect the individual performance of larvae, in terms of either development time (ANOVA $F_{2,177} = 0.23$, $P = 0.79$) or pupal weight (ANOVA $F_{2,121} = 0.22$, $P = 0.80$).

In order to test the theoretical predictions, we carried out microevolutionary laboratory experiments in which the virus was maintained in populations with different spatial structures. Host/parasite microcosms were established (see methods in SOM) and maintained on the foods of three different viscosities for 40 weeks (about eight host generations). They were then destructively sampled, and the infectivity of the extracted viral particles was assessed (SOM) by challenging *Plodia* larvae from the original large outbred stock population with virus extracted from each of the microcosms. Infectivity is easily determined by recording the proportion of host individuals that show infection after exposure, because in this system there is no recovery from this overt infection and the infected larvae neither grow nor mature. We can accurately estimate the concentration of the virus solution with which the individuals are challenged and therefore calculate the infectivity per virus particle (SOM). With infection occurring through cannibalism of infected larvae within the microcosms, large numbers of virus particles are likely to be taken up, and the risk of infection will be dependent on the infectivity of the particles themselves. This may contrast with many other systems in which the number of infective particles released into the environment is the major component of transmission, and therefore productivity is more important. The theory would predict that reduced movement and the consequent increase in local interactions in the population would select to lower transmission itself, and therefore in our system may act on individual virus infectivity.

A comparison of the average infectivity of single virions within the three food mediums revealed a clear effect of food medium viscosity (Fig. 2) [ANOVA log(infectivity), $F_{2,9} = 11.83$,

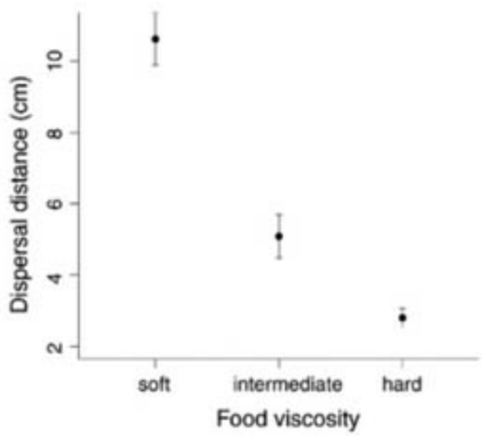

Fig. 1. Distance that larvae moved within the different food mediums. Increasing the viscosity of the food caused a significant change in the dispersal distance of the larvae [ANOVA square root(distance) $F_{2,82} = 57.6$, $P < 0.01$]. Pairwise comparison reveals that movement in soft food (mean ± 1 SE = 10.63 ± 0.73 cm) was significantly faster than in both intermediate (5.09 ± 0.61 cm) ($t = 6.42$, $P < 0.01$) and hard food (2.8 ± 0.26 cm) ($t = 10.57$, $P < 0.01$), and movement in intermediate food was faster than in hard food ($t = 3.36$, $P < 0.01$).

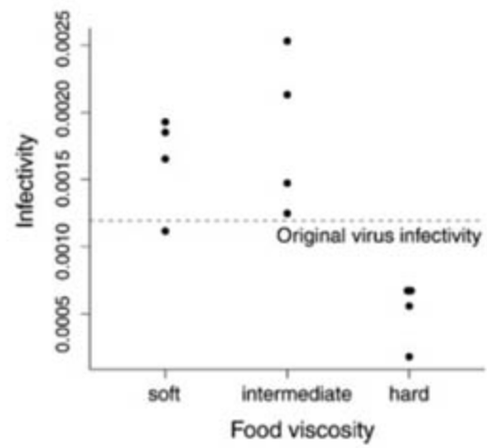

Fig. 2. Bioassay results indicating the infectivity of PiGV taken from *Plodia* populations fed on soft, intermediate, and hard food. The mean infectivity (calculated by dividing the percentage of mortality within bioassays by the number of virions present within the solution) of PiGV from soft and intermediate populations was 0.00164 (±SE 0.000183) and 0.00185 (±0.000295), which were both significantly greater than the mean infectivity of 0.000518 (±0.000117) from hard food (soft/hard coefficient comparison, $t = 4.04$, $P < 0.01$; intermediate/hard, $t = 4.37$, $P < 0.01$) [ANOVA log(infectivity), $F_{2,9} = 11.83$, $P < 0.01$].

$P < 0.01$]. From Fig. 2 and from pairwise contrasts, it is clear that the virus in the hard food microcosms was selected to become less infective than the virus in the other food mediums. We therefore have evidence for selection for lower infectivity in populations with the lowest movement rates. The infectivity of the virus in the soft and intermediate food types remained at the level of the original stock virus (Fig. 2), which suggests that although the virus in the hard food was selected for lower infectivity, there was no change in either the soft or the intermediate food mediums. Our soft treatment is the standard food medium on which *Plodia* is routinely maintained in the laboratory and is therefore the environment that the original virus will have experienced. We would not therefore have expected selection of the virus in the soft food. The lack of response in the intermediate food may simply indicate that the selection pressure was not strong enough in this treatment. However, the theoretical work (*5*) is indicative of a nonlinear effect of local interactions on transmission, and the lack of a response at the intermediate level supports this. Overall we have evidence that the hard food medium reduced the movement of the individual larvae, and the data are consistent with the prediction that this change in population structure selected the original virus for lower infectivity.

Spatial structure is often modeled with nonmotile host individuals regularly spaced on a lattice and parasite transmission as either completely local or completely global (*1*, *2*). Clearly, the spatial characteristics of the *Plodia* populations are much more complex than the simple, often regular spatial populations that are assumed in theoretical models (*4*–*6*). However, in our microcosms, restricting the movement of the larvae does lead to more localized transmission. We would argue that the small number of hosts locally available for infection causes self-shading by the more infective strains and favors the evolution of lower infectivity (*1*–*3*). The restriction in larval movement also forces individuals to remain in aggregations that are initially created in large part by females laying their eggs in batches. Our manipulation resulted in some changes in the population dynamics in the viscous populations and may have had other effects that we have not measured. However, we have shown that there was no effect of our manipulation on individual larvae apart from on their movement. It seems unlikely that genetic drift or bottlenecks can explain the results, given the size of the total viral population. Moth population sizes were somewhat lower in the hard food microcosms, but significant numbers of individual larvae were still infected (SOM), and we found no evidence of overall maladaptation in the virus from the hard food, with no significant difference in the concentrations of viruses extracted (SOM). Increased local adaptation to related host individuals in the more viscous populations, leading to increased maladaptation to the stock host population, is also unlikely because host reproduction is global. This last point emphasizes the fact that our spatial manipulation is relatively subtle because only the larval movement was manipulated while the adults still mixed within the populations. We would argue that this is therefore a particularly important result because it shows that such a relatively subtle change in mixing, within otherwise highly mixed systems, can lead to measurable changes in the evolution of parasites.

Our study shows how an experimental approach that changes the dispersal ability of individuals allows the empirical manipulation of population structures within a homogenous environment. Because spatial structure is increasingly recognized in theoretical models to be crucial to evolutionary outcomes (*24*), there is a pressing need for more manipulative experiments to test these predictions in other contexts. Given that most systems have an important spatial component and that many natural systems are more "spatial" than the one we used, we would argue that even more attention to population structure in evolutionary studies is warranted. In terms of pathogens, processes (including globalization) that increase the connectivity within host populations may alter the selection pressures on infectious organisms. As populations become more mixed, we might expect that not only will there be an increase in the extent of disease outbreaks but also the potential emergence of more infective strains of parasites.

References and Notes

1. R. M. May, R. M. Anderson, *Proc. R. Soc. London Ser. B* **219**, 281 (1983).
2. H. J. Bremerman, H. R. Thieme, *J. Math. Biol.* **27**, 179 (1989).
3. S. Levin, D. Pimental, *Am. Nat.* **117**, 308 (1981).
4. U. Dieckmann, J. A. J. Metz, M. W. Sabellis, K. Sigmund, *Adaptive Dynamics of Infectious Diseases* (Cambridge Univ. Press, Cambridge, 2002).
5. M. Boots, A. Sasaki, *Proc. R. Soc. London Ser. B* **266**, 1933 (1999).
6. M. Boots, A. Sasaki, *Ecol. Lett.* **3**, 181 (2000).
7. M. Boots, P. J. Hudson, A. Sasaki, *Science* **303**, 842 (2004).
8. Y. Haraguchi, A. Sasaki, *J. Theor. Biol.* **203**, 85 (2000).
9. D. A. Rand, M. Keeling, H. B. Wilson, *Proc. R. Soc. London Ser. B* **259**, 55 (1995).
10. X. X. van Baalen, D. A. Rand, *J. Theor. Biol.* **193**, 631 (1998).
11. W. D. Hamilton, R. M. May, *Nature* **269**, 578 (1977).
12. R. Ferriere, R. E. Michod, *Proc. R. Soc. London Ser. B* **259**, 77 (1995).
13. R. Ferriere, R. E. Michod, *Am. Nat.* **147**, 692 (1996).
14. D. Ebert, E. A. Herre, *Parasitol. Today* **12**, 96 (1996).
15. D. T. John, R. A. John, *J. Parasitol.* **80**, 149 (1994).
16. P. W. Ewald, *Epidemiol. Infect.* **106**, 83 (1991).
17. P. W. Ewald, *Sci. Am.* **268**, 86 (1993).
18. P. W. Ewald, *Evolution of Infectious Disease* (Oxford Univ. Press, 1994).
19. B. Kerr, C. Neuhauser, B. J. M. Bohannan, A. M. Dearn, *Nature* **442**, 75 (2006).
20. M. Boots, M. Begon, *Func. Ecol.* **7**, 528 (1993).
21. S. M. Sait, M. Begon, D. J. Thompson, *J. Anim. Ecol.* **63**, 541 (1994).
22. S. M. Sait, M. Begon, D. J. Thompson, *J. Anim. Ecol.* **63**, 861 (1994).
23. M. Boots, *Ecol. Ent.* **23**, 118 (1998).
24. U. Dieckmann, R. Law, J. Metz, Eds., *The Geometry of Ecological Interactions* (Cambridge Univ. Press, Cambridge, 2000).

25. We thank R. Finlay and H. Rae for technical assitance and J. Antonovics, D. Bowler, A. Pedersen, and J. Rolff for comments on the manuscript. This work was supported by a Natural Environment Research Council (NERC) studentship to M.M. and a NERC Advanced Fellowship to M.B.

Supporting Online Material

www.sciencemag.org/cgi/content/full/315/5816/1284/DC1
Materials and Methods
Table S1
References

2 November 2006; accepted 28 December 2006
10.1126/science.1137126

Stepper Motor Controller

The PriorPCI2 High Speed Stepper Motor Controller features a new compact (175 mm by 106 mm) design, standard six-axis control of XY, focus, and three filter wheels, shutter control for three shutters, and a 16-bit analog (0 to 10 V) output for piezo control. Other significant upgrades include four transistor-transistor logic (TTL) input/outputs for complete TTL macro control of all axes. As with the original PriorPCI, the new device features encoder inputs for the high-precision stage and focus movements, microstepping resolution down to 0.01 μm for XY and 0.002 μm for focus, and compatibility with the complete line of Prior microscope automation products.

Prior Scientific For information 800-877-2234 www.prior.com

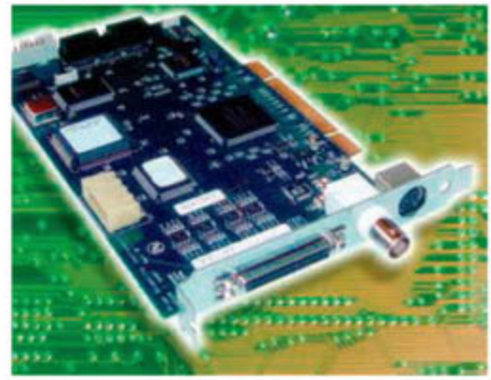

Cell Culture Flasks

NUNC Cell Culture Flasks are pre-coated with either poly-D-lysine or collagen I to save time and increase productivity in cell culture laboratories. The uniform application of the surface treatments facilitates reproducible cell culture performance by enhancing cell attachment, growth, and differentiation in serum-free and serum-containing media. The Cell Culture Flasks have an angled neck to enable easy access to the entire growth surface with pipettes or cell scrapers. The neck also allows for complete drainage of the flask and prevents the contents from splashing into the neck when stacked horizontally. A unique closure system allows for opening and closing the flask by a one-third turn of the cap.

Thermo Fisher Scientific/NUNC

For information 800-446-2543 www.nuncbrand.com

Spectrophotometers

The Biowave II+ and the Lightwave II+ ultraviolet/visible spectrophotometers feature enhanced 3 nm bandwidth and the manufacturer's novel Gifford optics with no moving parts. The xenon source combines high energy output and longer lamp life. A large, wide-view graphical display and integral menu-driven software make these instruments easy to use and provide flash scan capability, fixed wavelength, and kinetics and concentration measurements, all with flexible data manipulation options. Up to 90 methods can be stored. Results can be printed to the optional printer or exported to a computer via USB or Bluetooth.

WPA For information +44 (0) 1223 873318 www.wpaltd.co.uk

Gel System

The E-Gel CloneWell SYBR Safe gels and E-Gel iBase Power System, when used together, allow users to extract DNA bands of interest from gel without additional purification steps, saving time while maximizing the amount of DNA recovered. The gels feature two rows of wells; samples are loaded into the top row and electrophoresis carried out until the band of interest moves into the bottom row, from which it can be retrieved with a pipette. The power system has a built-in power supply and fits on the Safe Imager Blue-Light Transilluminator so the user can safely watch the DNA bands migrate on the gel. DNA recovered from CloneWell gels is compatible with all common cloning methods.

Invitrogen For information 800-955-6288 www.invitrogen.com

Mass Spectrometry Identification Tool

SimGlycan is an innovative glycan mass fingerprinting tool that matches mass spectrometry spectra data with its own comprehensive fragmentation database to predict the structure of glycans. It makes use of a proprietary search algorithm and generates a ranked list of the most likely glycan structures. It provides complete information for each structure, including glycan class, reaction, pathway, and enzyme. The program is supported on Windows 98/2000/ME/XP.

Premier Biosoft International For information 650-856-2703 www.PremierBiosoft.com

TIRF Microscope Illuminator

A new multicolor, multi-angle illuminator allows simultaneous multi-channel laser total internal reflectance fluorescence (TIRF) illumination. The TIRF illuminator allows up to three discrete laser lines to be used simultaneously for illumination, each with its own critical angle. In TIRF, the light's angle of incidence dictates how deeply the evanescent wave penetrates into tissue, and lasers of different wavelengths require varying angles to operate at their peak. In comparison with other TIRF systems, in which laser light of various wavelengths passes through a single fiber, necessitating switching lasers and adjusting the critical angle to achieve maximum performance, the Olympus illuminator makes use of three separate fibers to maximize results. It is easy to operate because the lasers are adjusted once, at the beginning of the experiment, and do not need to be adjusted again. The illuminator allows more efficient TIRF ratio experiments and faster measurement of rapid intracellular processes because the only temporal limitation on taking measurements is the 1–millisecond time it takes to switch lasers on and off. The illuminator is compatible with a wide variety of common gas and diode lasers.

Olympus America For information 800-455-8236 www.olympusamerica.com/microscopes

Literature

Precision Optical Filters for Fluorescence Microscopy is a multi-media CD catalog of fluorescence filter sets. It introduces QuantaMax, a line of durable, stable, high signal-to-noise sets, as well as a variety of new sets for fluorescent protein and fluorescence resonance energy transfer applications. These new products complement an extensive selection of dye-specific filter sets for all single and multi-label microscopy applications.

Omega Optical For information 802-254-2690 www.omegafilters.com

Newly offered instrumentation, apparatus, and laboratory materials of interest to researchers in all disciplines in academic, industrial, and government organizations are featured in this space. Emphasis is given to purpose, chief characteristics, and availability of products and materials. Endorsement by *Science* or AAAS of any products or materials mentioned is not implied. Additional information may be obtained from the manufacturer or supplier by visiting www.science.labvelocity.com on the Web, where you can request that the information be sent to you by e-mail, fax, mail, or telephone.

EUROPE'S BRAIN GAIN

With major boosts in science funding, Europe hopes to become a hot spot of innovative science and technology. **By Gunjan Sinha**

A glimpse at the numbers and one can understand why Europe's scientists migrate toward richer pastures. European countries spend far less than the United States and some Asian countries on research and development—widening the innovation gap. Two years ago, the EU's statistical office Eurostat showed that government and industry invested 1.9 percent of gross domestic product (GDP) on research and development in 2004—significantly less than Japan at 3.18 percent and the United States at 2.66 percent.

The bad news, however, has instigated change. Late last year, legislators firmed their commitment to the Lisbon strategy of 2000, which set a goal to transform the EU into a competitive knowledge-based economy. The European Council approved the 7th Framework Programme (FP7)—the EU's chief instrument for funding science and technology research from 2007 through 2013.

FP7 allocates €53 billion (currently €1 = $1.32) over seven years to better integrate Europe's fractured research scene—a 40 percent increase over the previous program. While most money will go to applied research projects, FP7 allocates more than €7 billion to another agency for which scientists have fought hard: the European Research Council (ERC), an agency akin to the US National Science Foundation. Run by scientists, the ERC will dole out money solely for basic research.

FP7 is part of a suite of initiatives intended to spur innovation across Europe. Not only is the European Parliament offering more money to scientists to encourage them to collaborate, individual member countries are also expanding their budgets. That means more grant money and fellowships will be available to scientists in the near future.

Biotechnology is also getting a boost. In some countries, new legislation is making it easier for European companies to grow. In others, programs that teach young scientists how to be entrepreneurs are expanding. The hope is that within a decade not only will science drive innovation, but the continent will also become a destination hot spot for the world's most talented scientists.

The European Parliament has pledged more money for collaborative research projects, and individual member countries are also boosting their budgets.

EU's Push to Compete

Antonio Rothfuchs knows firsthand the challenges of working as a medical scientist in Europe. He earned both his undergraduate and graduate degrees at the Karolinska Institutet in Stockholm before landing at the US National Institutes of Health for his postdoc in 2004.

Rothfuchs wanted to experience working abroad. But many young scientists in Sweden face temporary unemployment after finishing their Ph.D.'s

"In Sweden there is a lot more competition for funds that cover, at best, only part of your research costs," Rothfuchs wrote in an essay published in *Euroscience News* last year. After completing a postdoc, finding financial support to set up your own research lab is difficult, he says, even if you have finished successfully. In the United States, the odds are greater that a scientist will be able to launch his or her own lab, sometimes with startup money from a university.

The problem isn't one of neglect but one of scale. Sweden, in continued »

UPCOMING FEATURES

Careers in Cancer Research — April 6

Careers for Postdoc Scientists: Transferable Careers — April 20

Biotech and Pharma — April 27

fact, leads Europe in R&D spending—the nation spent 3.74 percent of GDP in 2004. But with only 9 million citizens, Sweden is tiny. Consequently grants tend to be much smaller. In 2006 the US National Institutes of Health had a $28 billion budget—80 times larger than that of the Swedish Research Council.

Rothfuchs's experience is typical of many European scientists. And while countries do support young scientists or full professors with various special grants, junior level scientists face sparse choices. Permanent positions or grant money to transition from working under a supervisor to independent research are scarce—many leave and don't return.

"We would prefer it if contract decisions were made based on the quality of the science and not on the scientist's age or how long they've been working."
—Birgit Müller

Europe Boosts Funding and Other Initiatives

By making more money available on top of what governments already offer, the EU's new funding scheme hopes to at least slow the exit stream. Scientists initially criticized FP7 because the proposed budget falls €20 billion short of the amount anticipated. The budget will, however, increase incrementally. By 2010 FP7 sets a goal to spend 2.6 percent of the EU's GDP on R&D projects. By 2013, FP7 calls to raise that value to 3 percent. Taxpayers will contribute one-third of the funds; the rest will come from businesses.

Most grants will go to applied research projects, which are organized into categories. The largest, "Cooperation," gets €32.4 billion and addresses information and communication technologies, health, and transport. The "People" category, which includes the Marie Curie grants for young scientists, provides €4.8 billion for training, work abroad, and luring expatriates back to Europe. "Capacities" contains some €4.1 billion for new research infrastructure such as radiation sources, data banks, and telescopes.

The last category, "Ideas," covers the ERC, a new agency that funds basic research. The ERC additionally offers grants to support scientists at different career stages. A European postdoc, for example, can now apply for a Starting Independent Researcher grant to launch his or her own lab. Applicants who are two to eight years postdoctorate are eligible and the grants amount to up to €2 million over five years—as many as 250 of these might be offered each year. Grants will also be available to support advanced scientists and are not restricted to European scientists. Researchers must, however, conduct their research within the EU.

The ERC "is a great thing," comments **Birgit Müller,** a geoscientist at Geophysical Institute, University of Karlsruhe in Germany. "In most grant proposals you have to show the immediate application of the research and most grants are for one to three years. In terms of basic research, that is very short."

But some are skeptical that the EU will achieve its investment goals. While some countries such as Sweden and Finland already spend more proportionally than the EU average on R&D, others such as Bulgaria and Romania spend less than 0.5 percent. "I think we will struggle as a union to reach 2.6 percent," says **Tony Mayer,** governing board member at Euroscience—an agency representing European scientists. Obviously to reach that goal, stronger countries will have to make up for weaker ones. Some countries such as Germany, France, and Britain, however, do stand out in this regard.

Germany

In 2006 the Deutsche Forschungs Gemeinshaft (DFG)—Germany's primary research funding body—increased its budget to €1.6 billion. The nation spent 2.5 percent of GDP on R&D, a figure comfortably above the EU average of 1.9 percent, and the federal government pledged to boost R&D spending to 3 percent of GDP by 2010.

In 2005 DFG also implemented an initiative to encourage German universities to compete for funds. Called the Excellence Initiative, it dedicates €1.9 billion of DFG's budget from 2006 through 2011 toward programs to raise the international profile of German science. These include: up to €1 million per year for new graduate schools, €6.5 million yearly for each of 30 "excellence clusters" that increase cooperation between universities and other research centers, and money available to universities that develop strategies to boost themselves to world-class status. The federal government covers 75 percent of the program and state governments cover the rest. An accompanying "pact for research and innovation" guarantees 3 percent increases for Germany's nonuniversity research institutes, including the Max Planck Society, through 2010.

Changes are also under way to support the country's mid-career scientists. Under current regulations, scientists with temporary posts at publicly funded institutions can only work a maximum of 12 years in the public system. The rules were intended to promote mobility. But with so few permanent positions available and industry's preference to hire young scientists who are more trainable (Germans, who typically do not finish continued »

» **EuropaBio**
www.europabio.org

» **European Research Council**
erc.europa.eu

» **Euroscience**
www.euroscience.org

» **Institute of Biotechnology at Cambridge**
www.biot.cam.ac.uk

» **National Institute of Allergy and Infectious Diseases**
www.niaid.nih.gov

» **The Wellcome Trust**
www.wellcome.ac.uk

» **World Stress Map Project**
www-wsm.physik.uni-karlsruhe.de

MINISTERIO DE SANIDAD Y CONSUMO

Instituto de Salud Carlos III

RESEARCH PROGRAM LEADERS

The "Carlos III" Institute of Health *(ISC III)* - the public body responsible for promoting biomedical and health -science research in Spain - has positions available for **Six Research Directors** to direct programs in the following key research areas:

- ❑ Nanomedicine (Ref.:Nano)
- ❑ Epidemiology and Public Healthcare (Ref.:EPSP)
- ❑ Infectious Diseases of the Respiratory System (Ref.: EISR)
- ❑ Rare Diseases (Ref.: ER)
- ❑ Stem Cell Biology (Ref.:BCT)
- ❑ Cell Therapy (Ref.:TC)

Responsibilities

Include the planning, development and initiation of strategic lines of research and the direction and coordinated management of research projects.

Successful candidates

Will be experienced investigators accustomed to taking on scientific challenges, leading teams of researchers, and managing resources.

The ISC III offers

- ❑ An opportunity to join a prestigious institution at a critical stage of its development.
- ❑ Integration into a highly qualified and motivated team.
- ❑ Independence in research and management.
- ❑ € 60.000 gross per year (basic + performance-related bonus).
- ❑ A human, economic and technical resource infrastructure to support the establishment of new research teams.
- ❑ Immediate incorporation.

Requirements

A PhD in biomedical discipline.

An outstanding scientific record, with proven research experience in at least one of the areas indentified above, verified by an excellent record of publications in international scientific journals.

Social skills and experience in strategic planning, resource management, leadership and research training.

Excellent communication skills in English, both spoken and written.

Complete terms and conditions of this offer and instructions on how to apply can be found at www.isciii.es
Closing date for the applications: March 23, 2007.

Max Planck Institute for Neurological Research

MAX-PLANCK-GESELLSCHAFT

with Klaus-Joachim-Zülch-Laboratories
of the Max Planck Society and the Faculty of Medicine
of the University of Cologne
Director Prof. Dr. D. Yves von Cramon

University of Cologne

Medical Faculty
Dean Prof. Dr. Joachim Klosterkötter

The Max-Planck-Institute for Neurological Research invites applications for a Group Leader position

Selbständige Nachwuchsgruppe der Max-Planck-Gesellschaft (Independent Junior Research Group)

The Max Planck Institute for Neurological Research and the Medical Faculty of the University of Cologne has opening for a Group Leader position, funding for a research group (Selbständige Nachwuchsgruppe der Max-Planck-Gesellschaft / Independent Junior Research Group) dedicated to neurological and oncological research. While there is no particular restriction on the research area, there is the expectation that the successful candidate has a particular expertise in molecular imaging.

Currently, the following technologies / methods are available at the Institute: **human brain PET and MRT, animal PET and animal MRT, optical imaging, autoradiography, electron microscopy, histology, immunohistochemistry and invasive imaging / neuromonitoring.** In 2007, a **combined human brain PET-MR System** will be installed.

Cologne and its rich scientific environment in North-Rhine-Westphalia provide many opportunities of interactions with the University of Cologne and the Universities in the region, including the teaching of courses.

The Group Leader position and funding is guaranteed for five years with the possibility of extension.

The Max Planck Society and the University of Cologne aim to increase the representation of women and therefore explicitly encourage applications from female scientists.

Deadline for applications is March 28, 2007. For further details and the application procedure please visit www.nf.mpg.de/careers.

schooling until their early 30s, are at a disadvantage in this regard), mid-level scientists are often left with little choice except to go abroad, says Müller. "We would prefer it if contract decisions were made based on the quality of the science and not on the scientist's age or how long they've been working."

France

Two years ago thousands of French scientists marched through the streets of Paris to protest what many saw as a crisis. Even though France already spends 2.16 percent of GDP on R&D, studies were showing that both the quantity and quality of French research was declining. Relative to other countries, France produces fewer new patents and biotech startups. Put off by low wages and scarce lab resources, young people were choosing other careers.

The French government responded by passing a package bill last year that includes several measures to lure young people into labs and to spur innovation. The research budget will grow from €19.9 billion in 2005 to €24 billion in 2010. Along with providing more money, the new law simplifies research management and empowers a new National Research Agency (ANR) to grant funds for projects based on merit reviews, a novelty in France. The proposed ANR budget for 2007 is €1 billion.

With ANR grant money, researchers can allocate funds to employ postdocs or technicians on temporary contracts and also to purchase equipment and consumables. As such ANR's model departs from traditional funding. To date most funds have been distributed via the public research organizations (PROs), quasiautonomous institutes with their own laboratories and permanent staff. These institutes typically fund groups on a yearly basis, but there is little relation between scientific results and funding.

The government also created a new Industrial Innovation Agency with a budget of €1.7 billion through 2008. Its aim is to support large-scale industrial R&D programs aimed at new technology-rich products or services that target a significant market.

Career Initiatives sponsored by The Wellcome Trust

- **Sir Henry Wellcome Postdoctoral Fellowships** enable newly qualified scientists to embark on independent research careers.
- **Flexible Travel Awards** to enhance opportunities for collaboration, mobility, and interdisciplinary training for experienced scientists.
- **Ph.D. programmes for clinicians** to provide world-class training for clinical academic researchers to complement existing Research Training Fellowship support.
- **Fellowships in Public Health and Tropical Medicine** supporting researchers from developing countries to gain research experience and training relevant to health in those countries.

"The framework money is forcing countries to come up with matching money."
—Tony Mayer

The United Kingdom

By contrast, the UK lags behind Germany and France. Public and private sector investment in R&D hovers around 2 percent of GDP.

But the numbers don't account for funds available through charitable trusts such as Wellcome and Cancer Research UK—two foundations with annual budgets that together add another £1 billion.

After the Bill and Melinda Gates Foundation, The Wellcome Trust is the second largest charitable trust in the world. It invests 85 percent of its annual budget in bioscience projects in the UK, of which 20 percent goes toward fellowships. "You could pretty much go from cradle to grave on Wellcome Trust Fellowships," says **Sohaila Rastan,** director of science funding. Because the trust is independent, it can be flexible. Grants are available to scientists without permanent positions and can run as long as seven years (see the Career Initiatives box for a list of new fellowships). The key criterion for winning a grant is excellence, says Rastan.

Money from charitable trusts, however, doesn't typically pay for research infrastructure such as laboratory upgrades and new equipment. In Europe, the primary source for facility upgrades and new equipment—the type of resources likely to attract top-notch scientists—is government money. In 2004, the British government published a 10-year plan for science and innovation that calls to boost science spending to 2.5 percent of GDP by 2014.

In a sense, "The framework money is forcing countries to come up with matching money," says Mayer of Euroscience. "And that's a good thing because the bulk of research investment is from the member countries in the form of salaries, equipment, bricks and mortar."

Biotechnology

The same force that has held back European science has also worked against European biotech—a lack of funds. While biotech startups are able to access seed money through private sources or government, many are unable to raise subsequent cash to grow. A study by UK-based Critical Limited, a consulting company, shows that while the number of biotech companies in Europe and the United States is almost equal, European companies are much smaller and have very few products in later stages. The industry employs over 190,000 people in the United States. In Europe the industry accounts for about 97,000 jobs. American companies also spend three times more on R&D and receive almost three times more venture capital funding. Two-thirds of European companies employ 20 or fewer people.

In terms of size and number of products, continued »

Max Planck Institute for Marine Microbiology

Research Scientist Position(s) in Marine Biogeochemistry

The Max Planck Institute for Marine Microbiology, Bremen, Germany, invites applications for two scientist positions in our Biogeochemistry Group. The Biogeochemistry Group studies geochemical and microbiological processes in marine sediments with emphasis on carbon, sulfur, oxygen, and metal cycling. We are looking for highly motivated scientists with post-doctoral experience who demonstrate an interest in collaborative research, the participation in ocean-going research cruises, and exposure to diverse research fields represented at the Max Planck Institute for Marine Microbiology. The successful candidates will be invited to develop their own projects as well as join ongoing and planned multidisciplinary research projects at the institute.

Candidates for either position should have a relevant background in biology, geology or chemistry, preferably with post-doctoral experience in marine geochemistry, microbiology, and/or stable isotope mass spectrometry. We are seeking to fill at least one of the positions with a scientist who has experience in stable isotope mass spectrometry and its applications to geochemical and/or microbiological problems.

We offer 2- to 3-year full-time appointments. The salary is according to the German system for public employees (E 13 TVöD). One position is available immediately and the other will become available in July 2007.

Further information can be obtained at www.mpi-bremen.de or from Dr. Timothy Ferdelman.

Applications should include a curriculum vitae, a list of publications, a description of future research objectives, and a list of three references. Electronic applications will not be accepted. Written applications are invited until April 13, 2007 and should be sent to:

Max Planck Institute for Marine Microbiology
Administration, Celsiusstr. 1, D-28359 Bremen, Germany

MAX-PLANCK-GESELLSCHAFT

FNP
Foundation for Polish Science

Homing Programme

2nd Call for Proposals

The Foundation for Polish Science invites applications from **Ph.D.s returning from an extended scientific stay abroad.** Homing Programme is a 2-year grant with possible extensions, awarded to facilitate the return of young researchers to Poland. It consists of a stipend for the laureate and a subvention for scientific project and international cooperation.

The closing date for applications is **30 April 2007**

For further information and application forms visit: **www.fnp.eu**

The programme is cofunded through the EEA Financial Mechanism

Grant for Postdoctoral Positions in Sweden

The grant will enable researchers with Swedish or non-Swedish doctorates (PhDs or equivalent) to work at Swedish higher education institutions or research establishments. The programme will span two years. Research areas: Natural Sciences, Engineering Sciences, Humanities, Social Sciences and Educational Sciences.

Application documents will be posted on the website at the end of February. The last application date is 29 March 2007.

www.vr.se

Vetenskapsrådet

MediTrans

- Targeted Delivery of Nanomedicine -

MediTrans is a multidisciplinary Integrated Project dealing with targeted nanomedicines. Within its framework, platform technologies will be developed with broad applicability towards disease treatment, as exemplified by the choice for chronic inflammatory disorders (like rheumatoid arthritis, Crohn's disease and multiple sclerosis) and cancer as target pathologies. Novel and rationally designed nanomedicines will be prepared by loading emerging, candidate and established carrier systems (like fullerenes, polymeric micelles and liposomes, respectively) with different types of drugs, and by endowing the agents with superior targeting properties and optimised (triggerable) release profiles. In parallel, MRI probes will be developed that report on the *in vivo* localisation of the nanomedicines, on the kinetics of drug release and on the efficacy of the intervention (image-guided drug delivery).

The MediTrans consortium consists of 30 partners from 9 EU member states (including 1 new member state) and 3 associated states, and it comprises 13 industrial companies, 11 universities and 6 research institutes. Its total budget is 16.1 M€, with 11 M€ as an EC contribution and 5.1 M€ as industrial support.

The MediTrans project has clear potential to forward targeted nanomedicines to the clinic and it will contribute to an improved structural collaboration between industry and academia. The Department of Pharmaceutics at Utrecht University is involved in almost every work package of MediTrans, it is in charge of WP1 (Nanocarrier design; Prof. Wim Hennink) and it is responsible for the overall co-ordination of the project (Prof. Gert Storm). For several work packages and project lines of MediTrans, the Department is now recruiting talented, motivated and internationally oriented PhD students with a (bio-) chemical, a (bio-) pharmaceutical, or a (bio-) medical background.

Interested and properly qualified candidates are invited to send their application, including a CV, a letter of motivation, and the names and contact details of two independent referees to Prof. Gert Storm, Department of Pharmaceutics, PO Box 80082, 3508 TB Utrecht, The Netherlands (Email: G.Storm@pharm.uu.nl).

"European biotech is about 10 years behind the US," says **Adeline Farrelly** at EuropaBio.

Several governments have, however, launched initiatives to help biotech companies grow faster and remain in business. In 2004, for example, the French government adopted legislation that gives startups a tax break. Any company that raises more than €5 million through an IPO and spends more than 15 percent of its operating costs on R&D is exempt from paying social security tax for employees involved in R&D projects. The measure can save companies up to 20 percent in employee costs, which they can reinvest in the company.

Called Young Innovative Company Status (YIC), the measure was initially conceived by France Biotech—an umbrella organization representing the industry in France—and the French Strategic Council for Innovation. Other European countries are following France's lead. Belgium adopted a YIC scheme in 2006; Sweden, Portugal, and Hungary also are considering similar schemes.

France biotech has proposed other initiatives that would offer shareholders who invest in small and medium sized enterprises tax-breaks (see the Biotech Tax Breaks box for details).

Such incentives are steps in the right direction, says **Christopher Lowe,** director of the Institute of Biotechnology at Cambridge University. "Governments need to make sure that the regulatory and financial climate is right to allow these developments to take place." Lowe points to the UK as an example. Forty percent of all publicly traded European biotech companies have roots in the UK, making it the clear leader in Europe's biotechnology scene. The closest rivals are Germany and Swizerland at 11 percent each. Many companies sprung up 10 years ago, says Lowe, when startups were especially unconstrained by political policy.

"In Britain, there's a long history of entrepreneurship."
—Christopher Lowe

Helga Nowotny

Lowe also points to culture's role in Britain's relative success. "There's a long history of entrepreneurship here," says Lowe, who has experienced a similar spirit in Scandinavia. Many of Sweden's universities, for example, have set up technology transfer divisions to promote entrepreneurship. Last year Karolinska Institutet began offering undergraduate courses in bio-entrepreneurship and plans to expand the courses into a graduate program.

Integration Issues Still Loom

While the influx of cash will certainly improve the profile of European science, it's not enough, says **Helga Nowotny,** vice-president of the ERC. Despite the European Commission's efforts to harmonize laws among member countries, regulations still vary. Research is fractured and that holds back frontier science.

"Even if R&D funding goes up, there is no direct way to translate this into more innovation," she cautions. "R&D policies don't stand alone." Governments need to facilitate, she says. To start, that means working harder toward greater legislative harmony, especially in the life sciences, and toward mobility-friendly pension systems and tax incentives for business, for example.

These issues don't negate the need for funds, they only highlight the need to nurture Europe's potential in other ways, Nowotny says. Europe very well may become a scientific powerhouse in the future. "We have some very good research institutions and much to offer in terms of quality of life." And many changes already under way reflect steps in the right direction. Germany's Excellence Initiative, which promotes competition among universities to create elite institutions, is a good example she says.

"I also see the ERC contributing with new opportunities to lure European researchers back," Nowotny adds. "We have to transform the brain-drain of scientists into 'brain circulation' both within Europe and beyond."

Gunjan Sinha is a freelance writer living in Berlin, Germany.

» **Visit www.sciencecareers.org and plan to attend upcoming meetings and job fairs that will help further your career.**

Biotech Tax Breaks

Young Innovative Listed Enterprise (YILE) status is a new initiative proposed by France Biotech and the French Strategic Council for Innovation to encourage public investment in biotechnology. To qualify a company would need to have raised more than €5 million via an IPO on a regulated or managed European market; spend more than 15 percent of its operating costs on R&D; employ less than 250 employees; and have a turnover of less than €50 million or a balance sheet total of no more than €43 million. If adopted by the French government, YILE companies will be able to offer shareholders the following tax benefits for the eight years following listing on market:

» full exemption from capital gains tax for direct or indirect shareholders.

» full exemption from France's net wealth tax (ISF) for shares held directly or indirectly.

» full exemption from inheritance tax for shares held directly or indirectly.

EMBL

The European Molecular Biology Laboratory (EMBL) is an international research organisation with its Headquarters Laboratory in Heidelberg, Germany and four additional Units in Hinxton (the European Bioinformatics Institute, EBI), Grenoble, Hamburg, and Monterotondo. For our Outstation in Monterotondo we are searching for a

Group Leader

Mouse Biology Unit at EMBL, Italy

The Group Leader will lead an independent research group in the EMBL Mouse Biology Unit in Monterotondo, near Rome. We seek a dynamic, independent group leader with an excellent track record and demonstrated experience or interest in mouse genetics and physiology, and a desire to join a multidisciplinary environment. We encourage applicants working on diverse questions in organismal biology with an emphasis on models of human disease, using modern genetic and genomic approaches.

EMBL offers a highly collaborative, uniquely international culture. It fosters top quality, interdisciplinary research by promoting a vibrant environment consisting of young independent research groups with access to outstanding graduate students and post-doctoral fellows.

Further information on the position can be obtained from the Head of Mouse Biology Unit, Nadia Rosenthal (rosenthal@embl.it).

EMBL is an inclusive, equal opportunity employer offering attractive conditions and benefits appropriate to an international research organisation.

To apply, please email a CV with a concise description of current research interests and future plans as well as 2-3 recommendation letters, quoting ref. no. S/06/173 in the subject line, to:
application@embl.de

www.embl.org

EUROPE

GRANTS

Set up your laboratory

in Croatia, Czech Republic, Estonia, Poland, Portugal or Turkey

EMBO Installation Grants

The aim of this scheme is to strengthen science in the participating countries. The grants will help scientists to relocate, set up their labs and rapidly establish a reputation in the European scientific community.

Award

- → €50,000 annually for three to five years
- → Participation in EMBO Young Investigator networking activities

Eligibility

- → First-class scientific background and publication record
- → Job offer in participating country at time of application

Initial participating countries

→ Croatia → Czech Republic → Estonia
→ Poland → Portugal → Turkey

Application deadline: 15 April 2007
N.B. Applicants must apply jointly with the receiving institute.

EMBO

www.embo.org/sdig

Call for Fellowship Applications

Templeton Research Fellows Program:
Philosophers and Physicists Collaboration on the Nature of Quantum Reality
at
IQOQI – The Institute for Quantum Optics and Quantum Information
Austrian Academy of Sciences, Vienna, Austria

Program Director: Professor Anton Zeilinger

Scientists and philosophers who have been engaged at the junction of physics, philosophy, and religious studies are invited to apply for a Residential Templeton Research Fellowship in Vienna. Physicists should have a strong philosophical background or inclination, and vice versa. Applications will be considered as openings occur. The start of a fellowship term is flexible to accommodate the plans of the individual fellow. Applicants should send a full CV with publication list, a list of scientific talks and conference contributions, and a recent photo, together with a statement of specific research interests, and any relevant accompanying material. The selection of Fellows will be made by an international and multi-disciplinary panel of judges.

For further information, please refer to:
http://www.iqoqi.at/news/opportunities/files/templeton_fellows.pdf

Please send application materials by e-mail or regular mail to the following address:

Templeton Research Fellows Program
Attn: Ms. Andrea Aglibut
Institute for Quantum Optics and Quantum Information
Austrian Academy of Sciences
Boltzmanngasse 3
A-1090 Vienna
Austria
e-mail: andrea.aglibut@oeaw.ac.at

Roche

Pharmaceuticals

Project Leader in Vascular Biology

Who we are:
At Roche, we believe passionately in what we do, and that our products make a difference in people's lives. We are a successful business that can offer exciting career opportunities to you, both locally and internationally, in a supportive and rewarding culture. We know that our people are responsible for our success and we value our employees, aiming to create a work environment where feeling valued, respected and empowered is a daily experience.

Headquartered in Basel, Switzerland, Roche is one of the world's leading research-focused healthcare groups in the fields of pharmaceuticals and diagnostics. As a supplier of innovative products and services for the early detection, prevention, diagnosis and treatment of disease, the Group contributes on a broad range of fronts to improving people's health and quality of life. Roche is a world leader in diagnostics, the leading supplier of medicines for cancer and transplantation and a market leader in virology.

The Position:
You will lead a multidisciplinary team of technicians and associate scientists with a proven track record in drug discovery and basic research. The team's mission is to identify and evaluate potential drug targets in vascular inflammation, in the pursuit of truly novel medicines for atherosclerosis.

Who you are:
You have a PhD and/or MD and a strong background in drug discovery, with at least five years' experience in pharmaceutical research and significant experience in atherothrombosis research. Your area of expertise is physiology/pharmacology, with a strong background in animal models of atherosclerosis. Successful research on mechanisms of atherosclerotic lesion instability is documented by your excellent publication record. Previous exposure to therapeutic approaches using apolipoproteins or apolipoprotein mimetics would be an advantage.

You should also have experience in working with high-profile scientific leaders and be able to represent Roche at scientific meetings and in academic and industry consortia. Previous experience in working in cost-effective, cross-functional, interdisciplinary groups in a matrix organisation and the ability to work in a goal-oriented manner within strict time constraints are additional pre-requisites for this position.

If you are interested in this position please apply online at: http://careers.roche.com, Job ID 3395 and attach full supporting documentation (CV, diplomas).

TECHNISCHE UNIVERSITÄT MÜNCHEN

The Department of Chemistry at the Garching campus of the Technische Universität München invites applications for a

Professorship in the field of Protein Chemistry (W2 tenure track).

The successful candidate is expected to work on fibrillar proteins, with a focus on the analysis of the underlying structural and functional principles, their assembly, pathogenic fibril formation, or material properties. Candidates are expected to have demonstrated excellence in research in one or several of these areas.

The professorship is associated with the newly established Cluster of Excellence "Munich center for integrated protein science, CIPS-M" as part of the Excellence Initiative of the federal government of Germany. The successful candidate will complement the research focus "Biological Chemistry" of the Department of Chemistry. A commitment to teaching (at least partly in German) is essential. Promotion to tenure is possible after a maximum of 5 years.

Preconditions for employment are successful completion of academic studies at an institute of higher education, pedagogical aptitude, Ph.D./doctorate and a postdoctoral lecturing qualification or certification of an equivalent academic achievement, which may have been obtained both in line with an Assistant Professorship and outside a university environment. At the time of appointment, applicants should not be older than 52 years. Under certain circumstances the age limit may be lifted (see Art. 10 Abs. 3 Satz 2 BayHSchPG).

In cases of equal eligibility, preferential consideration will be given to disabled candidates.

The TUM is striving to increase the proportion of women in research and education and thus expressly invites qualified female scientists to apply for this position.

Applications with the usual supporting information (curriculum vitae, certificates, list of publications, indicating the five most relevant publications, and a resume of planned research activities, etc.) should be submitted by **15 April 2007** to: **Technische Universität München, Dekan der Fakultät für Chemie, Lichtenbergstr. 4, 85747 Garching, Germany,** and in parallel electronically to: **w2protein@ch.tum.de**.

GRADUATE PROGRAM

Frontiers in Genetics

National Center of Competence in Research
Nationales Forschungsschwerpunkt
Pôle de Recherche National

International Doctoral Training Program

Frontiers in Genetics proposes an international program for doctoral training supported by the Swiss National Science Foundation. The program is based at the **University of Geneva** but includes participating members at the Universities of Lausanne, Zurich and Basel, at the Swiss Federal Institutes of Technology in Lausanne and Zurich, at the Swiss Institute for Experimental Cancer Research (Lausanne) and the Friedrich Miescher Institute (Basel). The program accepts students towards a PhD degree starting in **October 2007** and provides a strong background in molecular genetic, genomic and proteomic approaches for the study of modern biological problems.

We are seeking outstanding candidates with a degree in biological or physical sciences and a commitment to a career in research. The students selected will receive stipends for four years, subject to completion of all program requirements.

Applicants should download and send the application form, a letter describing their interests, background and research experience, an official transcript of their university curriculum with grades, and contact information of 3 persons who can supply letters of recommendation, to:

Dr Caroline Laemmli, NCCR Executive Officer
National Center of Competence in Research *Frontiers in Genetics*
30, Quai Ernest-Ansermet
CH - 1211 Geneva 4, Switzerland

The **application deadline is April 30, 2007** for admission in Fall 2007.

Application form and additional information on:
www.frontiers-in-genetics.org

Participating members: Stylianos E. Antonarakis, Silvia Arber, Konrad Basler, Denis Duboule, Susan Gasser, Marie Gomez, Ernst Hafen, Pedro Herrera, François Karch, Ulrich K. Laemmli, Joachim Lingner, Serge Nef, Ivan Rodriguez, Ariel Ruiz I Altaba, Botond Roska, Ueli Schibler, David Shore, Pierre Spierer, Françoise Stutz, Bernard Thorens, Didier Trono, Jean-Dominique Vassalli, Walter Wahli.

The **Ruhr University Bochum** invites applications for the positions of

three Directors (W3) of the Interdisciplinary Centre for Advanced Materials Simulation (ICAMS)

in combination with Professorships in the areas of

Micromechanical modelling of macroscopic material behaviour: The main focus of this department is modelling material behaviour at the macroscopic scale. Continuum methods are extended and combined with atomistic and mesoscale concepts. A proven track record in research on mesoscale processes such as dislocation dynamics, texture evolution, microstructural damage accumulation and fracture mechanics is expected.

Scale-bridging thermodynamic and kinetic simulations at the mesoscopic scale: This department covers the mesoscale with special emphasis placed on microstructure, phase transformations, precipitation processes and interface dominated material properties. Simulation tools include statistical mechanics, Monte Carlo simulations and phase field modelling.

Simulation of material behaviour at the atomistic scale: The research objective of this department is the description of fundamental material properties, thermodynamic quantities and surface reactions at the atomistic scale. A strong focus on coupling atomistic level simulations to mesoscale materials properties is expected. Phenomena such as defect properties and microstructural evolution are in the focus of interest. Knowledge in the areas of DFT, empirical potentials and MD and/or the development of empirical potentials is required.

For all three positions (starting date: January 2008) proven track records in bridging length and time scales and the willingness to collaborate with the other two groups and with industry are expected. ICAMS is a newly founded interdisciplinary institute for modelling and simulation of advanced engineering materials including soft matter. ICAMS aims at predicting the macroscopic behaviour of engineering materials from atomistic properties and microstructure with the intention to provide tools allowing improved and accelerated development of new materials. ICAMS is funded and financed by leading German companies, the Federal State of North-Rhine Westfalia and the Ruhr University Bochum. ICAMS is designed to be a strong multidisciplinary centre consisting of three endowed chairs (encompassing several positions for research assistants and PhD students) and three associated advanced study groups which link ICAMS-activities with existing theoretical and experimental expertise. ICAMS' mission is to establish new research and educational programmes in the area of materials simulation, combining expertise from natural sciences, mathematics and engineering. ICAMS will have strong interactions with the material scientists at the Ruhr University Bochum, with leading institutes in materials research and with industry. ICAMS will also educate a new generation of materials engineers trained in advanced materials simulation techniques. We seek candidates with an outstanding international reputation, the ability to lead an institute and to collaborate with industry, experience in the acquisition of research funds and in teaching at the university level. The Ruhr University Bochum is committed to equal opportunity in employment and gender equality in its working environment. To increase equal gender distribution in all job categories and at all levels, we strongly encourage applications from qualified women. Female applicants will be given preferential consideration when their level of qualification, competence and professional achievements equals that of male candidates, unless arguments based on the personal background of a male co-applicant prevail. Applications from appropriately qualified handicapped persons are also encouraged.

Applications, including a curriculum vitae, a list of publications and a statement of research interests and plans, should be sent by April 13th, 2007 to: **Dr. E. Weiler, Rector of the Ruhr University Bochum, concerning ICAMS, Ruhr-Universität Bochum, D-44780 Bochum**. Potential candidates will be invited to participate in a scientific colloquium on 15th-17th of May 2007.

*icrea
Institució Catalana de Recerca i Estudis Avançats

CATALAN INSTITUTION FOR RESEARCH AND ADVANCED STUDIES

Senior Research Positions 2007

ICREA announces the opening of 25 senior research positions in different fields.

Minimum requirements are a Ph.D. degree obtained before May 2003, preferably with four years of international exposure at the doctoral and/or post-doctoral level. However, **only those candidates with an outstanding research record and excellent leadership capabilities will be considered.**

Successful applicants will have a **permanent contract** with ICREA and will work at universities, research centres and other cooperating institutions in Catalonia. Salaries will be in line with those paid at Catalan universities.

ICREA research professors will be subject to an evaluation of research progress and general performance after a three-year period, and subsequently every five years. A positive evaluation will lead to a salary increase.

For further details visit **www.icrea.eu**.

Junior – Academia Research Contracts 2007

ICREA announces the opening of 15 junior – academia research contracts in different fields.

Minimum requirements are a Ph.D. degree obtained before May 2005, preferably with two years of international exposure at the doctoral and/or post-doctoral level. Applicants should be around 34 years old at the time of their application, although consideration will be given to older candidates in special circumstances.

Successful applicants will have a **five-year contract** with ICREA and will work at universities, research centres and other cooperating institutions in Catalonia. Salaries will be at the level of a first-year professor (*Professor Titular*) in the Catalan public university system.

ICREA researchers will be evaluated after their contracts have been in effect for four years. Researchers whose performance is outstanding may be eligible for a permanent ICREA senior position at the end of their five-year contract. The number of such positions will be limited.

For further details visit **www.icrea.eu**.

Applications and deadline

Applications for both calls must be submitted electronically via ICREA's website **www.icrea.eu**. The website provides all the information needed to apply. **Deadlines:** Senior Call – 20 April 2007 · Junior - Academia Call – 27 April 2007.

***ICREA** is a foundation jointly sponsored by the Ministry of Innovation, Universities and Enterprises of the Government of Catalonia (*Generalitat de Catalunya*) and by the Catalan Research and Innovation Foundation. ICREA's main goal is to support high-level research in Catalonia by creating new research positions.

MEETINGS

Vizier
Industrial platform

VIZIER MEETING

Viruses, crystal structures, and drug-design

1st Industrial and Scientific Meeting of the European Project VIZIER
27th April 2007 – Marseille, France.

The European integrated project VIZIER (for Comparative Structural Genomics of **Vi**ral Enzymes **I**nvolved in **R**eplication) involves **23 European laboratories** and targets > 200 RNA viruses genomes in order to determine three-dimensional structures of proteins involved in their replication. These enzymes are high priority targets for the **development of new antiviral compounds**. RNA viruses are a major **health concern:** they are responsible for the majority of viral diseases (Hepatitis, Dengue, Flu, Measles…), and potential bio-terrorism agents. The VIZIER project federates complementary scientific specialties encompassing bioinformatics, virology, genomics, protein engineering, crystallography, biochemistry, and medicinal chemistry.

The audience of the "special event" on Friday 27 April will learn about progress made during the first two years of VIZIER. **Epidemiological aspects** of **emerging diseases** will be debated in the perspective of viruses and vectors adaptation to climatic and way of life changes. The VIZIER scientists will describe the **last structural genomics results**. The industry will present recent advances in the development of **antiviral compounds**. Some "success stories" involving VIZIER results will be detailed (SARS, Chikungunya, West-Nile and Dengue, Caliciviruses).

For more information on the VIZIER project, including list of partners, and list of invited speakers, please see: ***www.vizier-europe.org***

PRIZES

BODOSSAKI FOUNDATION

PRIZE ANNOUNCEMENT 2008

For the year 2008, the Bodossaki Foundation has decided to award four (4) prizes, of **22.000 Euros each,** to scientists of up to 40 years old, of Greek nationality, parentage or descent, in the following fields:

(1) Mathematics
(2) Theories, Methods and Techniques, of Biomedical Applications of Informatics and Telecommunications
(3) Economics/Political Science
(4) Targeted Drug Development

For further information please contact:

The Bodossaki Foundation
23A, Vassilissis Sofias Avenue
GR-106 74 Athens
tel:+30.210.322-2042
fax:+30.210.3237971
e-mail:katerina@bodossaki.gr

www.bodossaki.gr

WWW.NIH.GOV
Positions @ NIH
THE NATIONAL INSTITUTES OF HEALTH

DIRECTOR, PSI STRUCTURAL GENOMICS KNOWLEDGEBASE
National Institute of General Medical Sciences (NIGMS)

NIGMS is seeking an individual to serve as the Director of the PSI Structural Genomics Knowledgebase (SG-KB), a key component of the Protein Structure Initiative (PSI). The PSI is a national research program in the emerging field of structural genomics. The long-range goal of the PSI is to make the three-dimensional atomic-level structures of most proteins easily obtainable from knowledge of their corresponding DNA sequences. The PSI SG-KB will serve as a headquarters for scientific data and knowledge generated by the PSI-funded centers, so that they may be widely available to the scientific community. Information about the PSI may be found at: http://www.nigms.nih.gov/Initiatives/PSI.htm.

Requirements: The position will be a part-time temporary assignment for up to two years, with the possibility of an extension for up to two additional years. Individuals at an accredited U.S. public or private college or university, or technical institution of higher learning are eligible to apply. Students and employees from foreign universities are not eligible for consideration. Individuals detailed to the NIGMS remain employees of the outside organization, and may only serve in an advisory or consultative capacity.

Candidates must have a Ph.D. or equivalent degree in a field relevant to the position. The ideal candidate will have scientific knowledge and research experience in one or more of the following fields: molecular biophysics, structural biology, genomics, bioinformatics, and computational biology. In addition, candidates should possess experience in broad networking interactions and collaborations in the above research fields, a proven track record in directing and/or managing a large scientific database or large research project, as well as strong leadership ability and effective communication skills.

How to Apply: To be considered for this position, send to the e-mail address below a CV, bibliography, and a vision statement (not to exceed three pages) that presents your views on how to maximize the usefulness and impact of the Knowledgebase for the greater biological community.

NIGMSCV@mail.nih.gov

Applications must be received by the closing date: **March 30, 2007**. The National Institutes of Health inspires public confidence in our science by maintaining high ethical principles. Individuals detailed to NIH are subject to Federal government-wide regulations and statutes, as well as agency-specific regulations described at http://ethics.od.nih.gov. We encourage you to review this information. You may contact Kimberly Allen with questions regarding this announcement on 301-594-2755.

Department of Health and Human Services
National Institutes of Health
National Cancer Institute

The Center for Cancer Research (CCR), National Cancer Institute (NCI), National Institutes of Health (NIH), is seeking applicants for an available Staff Scientist position.

The selected individual will provide senior scientific support for Drs. Carol Clayberger and Alan Krensky on studies related to the regulation of expression of the chemokine RANTES (Mol Cell Biol. 2007; 27:253-66; J Clin Invest. 2002;110:119-26; J Biol Chem. 2002;277:30055-65; Immunity. 1999;10:93-103). The successful candidate will have a doctoral degree with at least five years experience post degree. Candidate must have a strong background in molecular biology with training in transcriptional regulation and epigenetics. Experience with animal models and/or immunology is preferred. All applicants should submit a letter indicating their interest; a statement of research interests; current curriculum vitae and complete bibliography; and the names and addresses of five references (include email addresses) by **March 30, 2007**.

Applications should be sent to: **nciccrjobs@mail.nih.gov**. Please indicate **"Clayberger Staff Scientist"** in the subject line.

Staff Scientist (Core Laboratory)

The National Institute of Allergy and Infectious Diseases (NIAID), a major research component of the NIH and the Department of Health and Human Services, is recruiting for a Staff Scientist (Core Laboratory) in the Bacterial Toxins and Therapeutics Section, Laboratory of Bacterial Diseases (LBD). The LBD has an active program in basic research seeking to understand genetic and biochemical mechanisms underlying microbial pathogenesis. The research has the long term goal of developing vaccines and therapeutics for bacterial infections. Currently, a principal focus is anthrax.

Responsibilities of the position include: 1) demonstrate detailed knowledge of the genetics and physiological behavior of Bacillus anthracis, 2) develop genetic tools for alteration of bacterial genes and study of gene expression, 3) study the role of toxins, capsule, and proteases in the virulence of B. anthracis, 4) develop procedures for the safe study of highly virulent bacterial agents in BL3 laboratory conditions, and 5) instruct and supervise others in safe operation of BL3 laboratories.

The successful individual will ideally possess an M.D. or Ph.D. degree and have proven experience with genetic manipulation of B. anthracis. Furthermore, the individual should have the ability and prior experience in working with highly infectious agents under BL3 containment conditions. Individuals selected for this position must undergo background checks and be certified to work with Category A Select Agents and will receive vaccination for anthrax and other agents.

Salary is commensurate with research experience and accomplishments.
Please send CV/Bibliography, selected reprints, and names of three references to **Ms. Patricia Vasilatos, Bldg. 33, Room 1W10A, 33 North Drive, MSC 3202, Bethesda, MD 20892-3202**. Applications must be received by **April 2, 2007**.

University of California Davis, School of Medicine

and the

Shriners Hospitals for Children Northern California

Postdoctoral Fellowship Openings

The Institute for Pediatric Regenerative Medicine (IPRM), a collaborative initiative of The University of California Davis School of Medicine and Shriners Hospitals for Children Northern California, is recruiting for postdoctoral fellows in the laboratories of:

Paul Knoepfler, Ph.D. This opening is for a fellow to study genetic and epigenetic regulation of murine and human ES cells. Postdoctoral fellows will have the opportunity to obtain experience and training in molecular genetics, transgenic technology, genomics, and ES cell biology. Candidates should have experience and publications in developmental and stem cell biology, biochemistry, and/or molecular biology.

Wenbin Deng, Ph.D. The fellow will study molecular mechanisms of nervous system development and disease. Emphasis is on signaling mechanisms of neuronal and glial cell death, excitotoxic, oxidative and inflammatory forms of injury to the developing brain, stem cell biology and regenerative medicine. Candidates will have the opportunity to obtain experience and training in animal models of human disease, neural culture techniques, and biochemical/molecular and morphological methods.

Candidates must have a Ph.D and/or M.D. Candidates should forward a letter to the appropriate PI describing their research, current interests, curriculum vitae, reprints of 3 publications, names and addresses of at least 3 references to: Human Resources, c/o Paul Knoepfler, Ph.D. or Wenbin Deng, Ph.D. (depending on lab of interest), 2425 Stockton Blvd., Sacramento, CA 95817 or fax (916) 453-2388. The positions will remain open until filled.

University of California Davis & Shriners Hospitals for Children are EOE/Drug Free Workplace

MASSACHUSETTS GENERAL HOSPITAL HARVARD STEM CELL INSTITUTE

The Center for Regenerative Medicine (CRM) at Massachusetts General Hospital invites applications for a tenure-track assistant professor position. Outstanding scientists in the field of stem cell biology who have the demonstrated ability to develop a strong independent research program will be considered. Successful candidate(s) will be members of the **Harvard Stem Cell Institute** and faculty of Harvard University. Candidates must hold a PhD and/or MD and have a history of innovative, interactive research. Women and minority candidates are urged to apply.

Applicants should send an electronic copy of (1) letter of interest (2) research plan and (3) current curriculum vitae to **Dr. David Scadden c/o Chris Shambaugh: cpasker@partners.org**. Three letters of recommendation should also be sent directly to:

Center for Regenerative Medicine Search Committee
Attention: Chris Shambaugh
Massachusetts General Hospital
185 Cambridge St.
CPZN 4265A
Boston, MA 02114

MGH is an Equal Opportunity/Affirmative Action Employer.

CHAIR OF GENETICS

The Albert Einstein College of Medicine invites applications and nominations for the position of Professor and Chair of the Dept of Molecular Genetics. Founded in 1964 as the first Department of Genetics in a medical school, it currently comprises 8 primary and 10 cross-appointed faculty using genetic strategies to study humans, mice, yeast, flies, and worms.

With the opening in late 2007 of the new 200,000 square foot Center for Genetic and Translational Medicine, the distinguished scientist selected to be the Lois and Saul Kramer Chair of Genetics will have the opportunity to recruit several new faculty immediately and to guide the development of a program that emphasizes both human genetics and model organisms. The Department hosts specialized facilities for various microarray experiments, genotyping, cell culture, DNA sequencing, and genome imaging (FISH/SKY). We seek an outstanding scientist with broad experience for appointment as full professor with tenure to the Lois and Saul Kramer endowed Chair.

Einstein offers an extremely interactive environment with numerous, well-equipped core facilities subsidized by the College (http://www.aecom.yu.edu/home/shared.asp). There are currently 750 medical students, 325 graduate students, and 360 postdoctoral fellows in training. A new strategic plan, recently developed by the Dean and faculty of Einstein, calls for the growth and development of cutting-edge technologies focused on selected human diseases, with Genetics as a major emphasis. The diversity of the populations served by the College of Medicine in the Bronx and its hospital affiliates throughout New York City provides extraordinary opportunities for an imaginative and committed leader to enhance the well-being of the human condition through genomic research.

Interested applicants should send a letter of interest and C.V. in electronic format to: **Dr. Pamela Stanley, Chair, Genetics Search Committee, Albert Einstein College of Medicine, Jack and Pearl Resnick Campus, 1300 Morris Park Avenue, 312 Belfer, Bronx, New York, 10461. Tel: (718) 430-3346, E-mail: stanley@aecom.yu.edu.**

We particularly welcome applicants who will add diversity to our academic leadership and faculty. Equal Opportunity Employer.

ALBERT EINSTEIN COLLEGE OF MEDICINE
Advancing science, building careers

College of Biological Science

13 Tenure Track Positions

UNIVERSITY of GUELPH

CHANGING LIVES IMPROVING LIFE

The College of Biological Science is the largest unified bioscience institution in Canada and comprises over 90 faculty including nine Canada Research Chairs, 3,000 graduate and undergraduate students, and with an annual external research income in excess of $32M. The College has recently taken occupation of a $144M, 390,000 sq ft Science Complex, with outstanding facilities for research and teaching including an Advanced Analysis Centre for proteomics, genomics and bioimaging. Exceptional state-of-the-science facilities are available for experimentation in controlled environments involving plants (Phytotron), aquatic organisms (Aqualab) and aquatic mesocosms (Limnotron). An animal wing, part of the Univeristy's Animal Care Facilty, that is suitable for acute and chronic housing of rodents is strategically located within the Human Health and Nutritional Science Department. As part of a strategic plan to maintain the College at the forefront of life science, we are seeking to recruit outstanding individuals to a series of targeted, tenure-track positions at the Assistant Professor level. Successful applicants will be expected to establish a strong, independent research program involving innovative approaches and contribute to wider, interdisciplinary research goals. The College takes pride in the excellence of its students, and applicants should be able to articulate a commitment to the highest standards of pedagogy and will be expected to participate in undergraduate and graduate education. Candidates must have a PhD, preferably with postdoctoral experience, a strong record of publications in peer-reviewed journals, and ideally some experience in undergraduate/graduate teaching. Further details on specific positions can be obtained by contacting the individuals indicated next to each area. Visit our website at **http://www.uoguelph.ca/cbs/**

Human Health, Nutrition, Physiology and Biomechanics (five positions):

Candidates are sought with proven experience in nutrition, biomechanics and physiology and applications to human health. Three positions are in association with a new Guelph-Humber program in nutrition, fitness and health. The biomechanist must be able to combine biomechanics/bioengineering principles and anatomy to address chronic health issues. The physiologist needs a strong understanding of systemic cardiopulmonary physiology as well as nutrition and exercise interactions. The nutritionist will be required to integrate nutritional sciences with lifestyle and physical activity topics and to have a good knowledge of nutraceuticals and functional foods.

The College is also looking for candidates for two additional positions; one in the area of nutragenomics as it pertains to human health. The second position is for a physiologist with interest areas that compliment those of the Department of Human Health and Nutritional Sciences (cardiovascular, neural, skeletal muscle, metabolic physiology). Contact Dr. Terry Graham, email terrygra@uoguelph.ca

Comparative Animal Physiology

We seek individuals with a background in comparative physiology and with expertise in developmental biology or neurophysiology. The position will enhance existing strengths in environmental physiology, comparative biochemistry, endocrinology, neuroendocrinology and biomechanics with a strong focus on aquatic organisms. Contact Dr. Don Stevens, email dstevens@uoguelph.ca

Functional Genomics

We seek individuals with expertise in integrating broad gene and/or protein expression data sets to understanding complex processes of physiological regulation and evolutionary adaptations in animals. Opportunities exist to collaborate with a large group of comparative animal physiology, ecology and evolutionary biology researchers with a strong focus on aquatic organisms. Contact Dr. Patricia Wright, email patwrigh@uoguelph.ca

Evolutionary Biology

We seek individuals with expertise in evolutionary biology, particularly those that use theoretical and modeling approaches, which complement our existing strengths in evolutionary ecology, evolutionary genetics and molecular systematics. Opportunities exist to participate in new graduate teaching and research initiatives in bioinformatics, biodiversity, and applied evolution. Contact Dr. Moira Ferguson, email mmfergus@uoguelph.ca

Co-evolutionary Ecology

We seek individuals with a research focus on interactions, dynamics and reciprocal co-evolution among species in ecological communities. We are particularly interested in novel applications of co-evolution, such as emerging problems in the evolution of infectious disease, pests, pathogens and/or non-native species as well as the ability to span multiple levels of organization. Contact Dr. John Fryxell, email jfryxell@uoguelph.ca

Ecosystem Ecology

We seek individuals that investigate coupled biological-physical processes in natural or human-influenced systems and who can link their research in ecosystem ecology to our existing strengths in physiological, population and community ecology. The successful candidate will use modern analytical techniques in combination with field approaches to investigate the functioning of ecosystems, the responses of ecosystems to changing environments and climate change, ecosystem consequences of biodiversity, and biogeochemical cycling. Contact Dr. Denis Lynn, email ddr@uoguelph.ca

Cellular Microbiology

We seek a candidate of exceptional promise who will apply contemporary integrated approaches in microbiology and cellular biology to investigate the interactions between microorganisms and eukaryotic host cells. Applications will be considered from individuals asking leading edge biological questions in any system involving bacteria, eukaryotic microorganisms or viruses. Contact Dr. C. Whitfield, email cwhitfie@uoguelph.ca

Prokaryotic or Eukaryotic Developmental Biology

We seek a candidate of exceptional promise who will apply contemporary approaches to address leading edge biological questions in developmental biology. Applications will be considered from individuals investigating any biological system including those studying microbes, plants or animals. Contact Dr. C. Whitfield, email cwhitfie@uoguelph.ca

Structural Biology-Electron Microscopy

We seek a candidate of exceptional promise who will exploit cryo-electron microscopy and allied structural biology approaches to investigate leading edge biological questions.Applications will be considered from individuals investigating any important prokaryotic or eukaryotic system. Contact Dr. C. Whitfield, email cwhitfie@uoguelph.ca

Applicants should submit three copies of their curriculum vitae, including the names of three referees, and a letter of application to the

Dean's Office,
College of Biological Science,
University of Guelph,
Guelph, ON, Canada N1G 2W1

Committees will be looking at applications from March 31st. General enquiries can be made to the Dean, Professor Michael Emes email memes@uoguelph.ca tel. 519-824-4120 ext. 56102.

All qualified candidates are encouraged to apply; however, Canadians and permanent residents will be given priority.

The University of Guelph is committed to an employment equity program that includes special measures to achieve diversity among its faculty and staff. We therefore particularly encourage applications from qualified aboriginal Canadians, persons with disabilities, members of visible minorities and women. All appointments will be subject to financial approval by the University.

We are investing in the future of cancer research –

Come Join Us!

Earle A. Chiles Research Institute
Robert W. Franz Cancer Research Center
Providence Cancer Center
Portland, Oregon

Set in the beautiful Pacific Northwest, nestled between the Oregon Coast and Mt. Hood, stands Portland's Earle A. Chiles Research Institute and Providence Cancer Center. Our unique setting in a community-based academic center fosters collaboration between our outstanding laboratory and clinical investigators. Combined with our access to large numbers of cancer patients, this creates an ideal translational research environment. Our emphasis lies in moving discoveries from the laboratory bench to the patient's bedside.

With a proven track record in the field ofimmunotherapy, this group of NIH-funded investigators has done groundbreaking work in tumor immunology. Laboratory and clinical translations have included work with cancer vaccines, adoptive immunotherapy, defining the biology of immune reconstitution during vaccination, novel cytokine-based therapy, and the use of immunomodulatory antibodies in patients with melanoma, breast, lung and prostate cancer. If you would like an opportunity to develop your own basic science ideas, with a focus on moving them from the laboratory to the patient, we would like to hear from you.

Faculty members with laboratory-based programs include:

- Bernard A. Fox, PhD
  Generation and effector mechanisms of anti-tumor T cells
- Hong-Ming Hu, PhD
  Presentation of tumor antigens and immune escape mechanism
- Edwin B. Walker, PhD
  Immunological monitoring; memory T cell regulation in cancer
- Andrew D. Weinberg, PhD
  Immunomodulation with OX40 agonists

Faculty members with clinical-based research programs focused on melanoma, gastrointestinal malignancies, genitourinary malignancies, and lung cancer include:

- Walter J. Urba, MD, PhD
- Brendan D. Curti, MD
- Todd Crocenzi, MD

Our new building, which will open in early 2008, will eventually triple the size of our research facility. There will be state-of-the-art facilities for preclinical tumor models, basic science research, human immunological monitoring, and an infrastructure to perform all phases of clinical research.

We have the following research opportunities available:

- Established laboratory investigators
- Clinical investigators interested in collaborating with laboratory investigators
- Scientists looking for first independent position

For more information or to submit a resume or CV, please call our director, Walter J. Urba, at **503-215-6259** or email **Walter.Urba@providence.org**.

http://providencecareers.org/PS37

PROVIDENCE
Health & Services

Providence Health & Services is an Equal Opportunity Employer.

USF HEALTH

UNIVERSITY OF SOUTH FLORIDA

http://www.health.usf.edu · 12901 Bruce B. Downs Blvd, MDC 02 · Tampa, FL 33612

Associate Dean for Graduate and Postdoctoral Affairs

University of South Florida - Health College of Medicine

University of South Florida Health invites nominations and applications for the position of an Associate Dean for Graduate and Postdoctoral Studies, College of Medicine. University of South Florida is the third largest university in the southeast and among the top 20 largest in the nation with over 42,000 students. The Carnegie Foundation ranks USF in the top tier of national research universities, generating more than $310 million annually in extramural funding.

Reporting to the Vice Dean for Research, Graduate and Postdoctoral Affairs, the Associate Dean has full administrative and fiscal responsibility for the successful operation of the various components of the graduate program. In addition, the Associate Dean provides leadership with respect to the vision of graduate education within the College/School through shared academic governance, is responsible for identifying and recommending institutional responses to new trends in higher education and postdoctoral training and is charged with the development of new program initiatives that seek to expand graduate student access and enrollment and increase the number of postdoctoral trainees.

Minimum qualifications include an earned doctorate in one of the biomedical sciences from an accredited institution and five years experience at the Associate Professor level or higher. Preferred qualifications and experience are: experience with strategic planning and the development and promotion of graduate and certificate programs in the biomedical science; academic experience at the Full Professor level; and a distinguished record of scholarly activity, continuous extramural funding, and requisite teaching experience in a medical/graduate curriculum. A record of sustained accomplishments, evidence of leadership in his/her field and a demonstrated commitment to graduate education and postdoctoral training is also desired, as is the ability to promote and function successfully in an environment of collaborative collegiality and diversity and a knowledge of trends and issues challenging higher education.

Applications, nominations and letters of interest should be e-mailed by June 1, 2007 to **Ms. Vanessa Ayer (vayer@health.usf.edu)**. The review of materials will begin immediately and will continue until the position is filled. For more information about this position and the application process, please visit this website: **http://research.health.usf.edu/employment.html**

USF Health is committed to increasing its diversity and will give individual consideration to qualified applicants for this position with experience in ethnically diverse settings, who possess varied language skills, or who have a record of research issues that support/benefit diverse communities or teaching a diverse student population. The University of South Florida is an Equal Opportunity / Affirmative Action / Equal Access Institution. For disability accommodations, contact Vanessa Ayer 813-974-8349 within 5 days of an event. According to Florida law, search records, including applications and search committee meetings, are open to the public.

VCU

Virginia Commonwealth University

SENIOR ASSOCIATE DEAN FOR RESEARCH

School of Engineering

Virginia Commonwealth University seeks a senior associate dean for research in its School of Engineering and invites applications/nominations for this position. The School of Engineering was founded in 1996 and stands as a remarkable example of public-private partnership. The School currently comprises five departments - biomedical engineering, chemical and life science engineering, computer science, electrical and computer engineering, and mechanical engineering. Its current enrollment is 1100 undergraduate and 200 graduate students with a faculty of 45.

The Position: Reporting to the dean of the School of Engineering, the senior associate dean will be responsible for providing vision and leadership in achieving the School's objectives for substantial growth in the size and scope of sponsored research. Over the next seven years, the School will increase its undergraduate enrollment by 70%, its graduate enrollment by 50%, and its faculty by 100%. The senior associate dean for research will develop and implement programs to enable the School to increase its annual external research funding from $5 million to $20 million over the same period. Working with the dean and faculty the senior associate dean for research will assist in the recruitment and retention of outstanding junior faculty and senior faculty capable of achieving this objective. The School's strategic plan places particular emphasis on growth of basic and applied research related to clinical medicine. The senior associate dean for research will work closely with his/her counterparts in the VCU Schools of Medicine, Dentistry, and Pharmacy to develop proposals for major grants in this area. The senior associate dean will be a member of the senior leadership team for the School and University and will represent the School in all matters related to its research mission.

Qualifications: An earned doctorate in engineering or a related discipline is required. The successful candidate will have demonstrated management and leadership accomplishments in a progression of faculty and administrative roles and demonstrated success in leading interdisciplinary teams on major projects. She/he will have established an outstanding record of teaching and externally-funded research sufficient for a tenured appointment in one of the School's academic departments. Strong skills in written and oral communication are essential. Experience in an industrial research and development setting is highly desirable.

Application/Nominations: Applicants should submit a statement of interest and curriculum vitae along with four references to: **Chair, Senior Associate Dean of Research Search Committee, Virginia Commonwealth University, School of Engineering, 601 West Main Street, P.O. Box 843068, Richmond, Virginia 23284.** Letters of nomination may be mailed to the same address. The search will continue until the position is filled.

VCU is an Equal-Opportunity Affirmative Action Employer.
Women, minorities and persons with disabilities are strongly encouraged to apply.

Weill Cornell Medical College

Faculty Positions in Theoretical Neuroscience

The Institute for Computational Biomedicine at the Weill Cornell Medical College (Manhattan campus) invites applications for tenure-track faculty positions at the Assistant Professor level or higher. Applicants should have a broad range of achievements in theoretical approaches to systems biology, with a strong emphasis on neuroscience. He/she will be expected to build an exciting, first-rate research program, to participate in the training of graduate students and postdoctoral fellows, and to interact with a thriving, and rapidly growing, group of theorists and experimentalists, working at all levels of systems biology - molecular, cellular, multicellular and behavioral.

Junior Fellow Positions in Theoretical Neuroscience

The Institute for Computational Biomedicine also invites applications for Junior Fellow positions. These are targeted for young scientists of outstanding promise, typically at the advanced postdoctoral level - scientists with the drive, perseverance, and history of accomplishments to suggest that they will, in the long run, make fundamental contributions to scientific understanding. Once chosen, Fellows are free to pursue lines of inquiry that interest them within the field. The fellowship offers the opportunity to pursue research independently and intensely, free from the burdens of a standard faculty position (teaching, grant writing, administrative responsibilities, etc.). Current positions are for 2-3 years and target theoretical neuroscience; successful and productive Fellows will be considered prime candidates for tenure-track faculty positions.

Applications for both faculty and fellow positions should be received by Oct. 1, 2007 and include a curriculum vitae, a two-page summary of past research and future plans, and reprints of two or three key publications. The application and three letters of recommendation should be sent to:

Cornell Junior Fellow/Theoretical Neuroscience Faculty Search Committee
c/o Jennifer Cameron
Manager of Faculty Recruitment
Weill Cornell Medical College
1300 York Avenue, Box 27
New York, NY 10021

For information about the Institute for Computational Biomedicine (ICB), see:
http://icb.med.cornell.edu

For information about neuroscience research at Weill Cornell, see:
http//neuroscience.med.cornell.edu/

Cornell is an Equal Opportunity/ Affirmative Action Employer.

The University of North Dakota
School of Medicine & Health Sciences
501 N Columbia Road Stop 9037
Grand Forks, ND 58202

UND

CHAIR
DEPARTMENT OF ANATOMY AND CELL BIOLOGY

The University of North Dakota School of Medicine and Health Sciences invites applications and nominations for the position of CHAIR of the Department of Anatomy and Cell Biology. We seek an outstanding medical scientist with a strong research record, including extramural support, and a commitment to excellence in teaching undergraduate, graduate and professional medical and allied health education. The candidate will be expected to complement, expand and strengthen existing areas of research in the department and may utilize the state-of-the-art imaging facilities, including a Zeiss LSM 510 META confocal system and a Hitachi 7500 TEM and 4700 field emission SEM. A new MicroPET and Cyclotron, a dedicated small animal research facility and a Genomics and Proteomics facility are available at the University of North Dakota School of Medicine and Health Sciences. The applicant should possess interpersonal and leadership skills in mentoring faculty, directing students and performing administrative duties.

The Chair will oversee a department whose active research interests include neurosciences, and cell and cancer biology. The department offers M.S., Ph.D., and M.D./Ph.D. degrees and numerous traditional anatomical courses at the graduate level, instructs first and second year medical students, and provides undergraduate courses to allied health and non-majors. Further information is available at: **http://www.med.und.nodak.edu/depts/anatomy/**

The University is located in Grand Forks and currently enrolls over 12,000 students. Grand Forks is a family-friendly community in a region offering excellent and rapidly expanding cultural, recreational, and sporting activities. To learn more about the University of North Dakota and Grand Forks visit: **http://www.und.edu** and **http://www.grandforksgov.com**.

Review of applications will begin **March 1, 2007** and the search will remain open until the position is filled. Applicants should submit a detailed curriculum vitae, a letter of interest outlining prior experience, research interests, teaching philosophy, plans for the future and the names and addresses of three references to: **Joshua Wynne, M.D., Professor of Internal Medicine, Executive Associate Dean, Associate Dean for Academic Affairs, and Chair of the Search Committee, c/o Office of the Dean, School of Medicine and Health Sciences, University of North Dakota, Stop 9037, Grand Forks, North Dakota 58202-9037,** or E-mail electronically to: **acbsearch@medicine.nodak.edu**.

The University of North Dakota is an Equal Opportunity/Affirmative Action Institution.

THE UNIVERSITY OF FLORIDA COLLEGE OF MEDICINE

Chair, Department of Neuroscience

The University of Florida College of Medicine invites applications and nominations for the position of Professor and Chair in the Department of Neuroscience. The department has a mission within the college of both research and teaching responsibilities. The department has 24 primary faculty members with research interests in all aspects of neuroscience (**www.neuroscience.ufl.edu**). The department is housed within the McKnight Brain Institute (**www.mbi.ufl.edu**), a state-of-the-art facility for research and teaching in neuroscience and neuroscience-related disciplines. The successful candidate will have a Ph.D., M.D., or M.D./Ph.D. degree. We seek an accomplished scholar with a distinguished record of research, international recognition, leadership, and administrative skills.

The review of applications will begin on **March 30, 2007** and will continue until the position is filled. Applicants should provide a letter of application, curriculum vitae and the names of three references via email to **NS-search@phys.med.ufl.edu** or by mail to: **Charles E. Wood, Ph.D., Chair, Search Committee, Box 100274, Department of Physiology and Functional Genomics, University of Florida, Gainesville, FL 32610-0274**.

The University of Florida is an Equal Opportunity Institution.

City of Hope

FACULTY POSITIONS
Hematopoietic Stem Cell and Leukemia Research
City of Hope National Medical Center

As part of its ongoing expansion, the City of Hope National Medical Center/Beckman Research Institute and Comprehensive Cancer Center have established a new Department of Hematopoietic Stem Cell and Leukemia Research. The mission of this department is to build a program of excellence in basic and translational hematopoietic stem cell and leukemia biology, and provide an infrastructure to translate novel therapeutic approaches from the laboratory to the clinic. We invite applications for faculty positions at the Assistant or Associate Professor level. Exceptionally well-qualified candidates at a more senior level may also be considered. Potential areas of research emphasis include, but are not limited to, self-renewal and differentiation of normal and leukemia stem cells, identification of key molecular mechanisms of transformation; preclinical studies of molecular targets; hematopoietic stem cell-based therapeutics, and human ES cell based modeling of normal and leukemic hematopoiesis. This program will complement and support our outstanding clinical Hematopoietic Malignancies and Hematopoietic Cell Transplantation Program.

Appointees will have a primary appointment in the Department of Hematopoietic Stem Cell and Leukemia Research, within the Division of Hematology and Hematopoietic Cell Transplantation, and may also be appointed to City of Hope's NCI-designated Comprehensive Cancer Center. Generous start-up packages will be available. Appointees may also participate in the Graduate School of Biological Sciences. The Beckman Research Institute provides an environment that encourages interdisciplinary, collaborative interactions with a rich set of core resources (described in **http://www.cityofhope.org/bricoh/shared_resources.asp**). Candidates should have a Ph.D. or M.D. degree, postdoctoral experience, and the potential to establish, or to have established, an independent research program. Applicants should submit a curriculum vitae, a statement of research interests and plans, and the names, addresses and telephone numbers of at least three references (who may, optionally, submit their letters), to:

Hematopoietic/Leukemia Stem Cell Search Committee, c/o Dr. Ravi Bhatia M.D., Director
Department of Hematopoietic Stem Cell and Leukemia Research
Division of Hematology and Hematopoietic Cell Transplantation
City of Hope National Medical Center
1500 E. Duarte Road, Duarte, CA 91010-3000
E-mail: bnotthoff@coh.org

The City of Hope is an Equal Opportunity Employer. Women, minorities, veterans, and disabled persons are encouraged to apply.

ASSISTANT/ASSOCIATE/ FULL PROFESSOR DIABETES, CANCER, NEUROSCIENCES

The Wayne State University Department of Pharmaceutical Sciences invites applications for a 12-month, tenured or tenure-track position at the assistant, associate or full professor level. Applicants should possess a PhD in pharmaceutical sciences or a related discipline, or an MD or equivalent degree. Preference will be accorded applicants with interdisciplinary research interests complimentary to existing departmental research programs in diabetes, cancer and neurosciences. Outstanding candidates from other areas will be strongly considered. The successful applicant is expected to develop a vigorous, externally funded research program and provide high-quality teaching in the PhD and PharmD programs. Highly competitive start-up, compensation and benefits are offered. The department occupies state-of-the-art labs in a new building on the School of Medicine-Detroit Medical Center campus, with outstanding opportunities for translational research collaborations. Visit **www.cphs.wayne.edu/psc.html** for department information. Application review will begin in late March and continue until the position is filled, with an anticipated start date of Fall 2007. Candidates are asked to submit an electronic application including cover letter, curriculum vitae and research plan through the WSU Online Hiring System **http://jobs.wayne.edu** and search under Department H1822-Pharmaceutical Sciences. Wayne State University is a premier institution of higher education offering more than 350 academic programs through 14 schools and colleges to more than 34,000 students in metropolitan Detroit. *Wayne State University is an Equal Opportunity Employer.*

Department of Health and Human Services
National Institutes of Health
National Institute on Aging

Statistical Genetics Director

The National Institute on Aging, a major research component of the National Institutes of Health (NIH) and Department of Health and Human Services, is recruiting for a Staff Scientist-Facility Head who will serve as the Statistical Genetics Director of the Laboratory of Genetics (LG) of the Intramural Research Program (IRP). The incumbent will be responsible for collaborating in and coordinating statistical genetic and epidemiological analyses of aging-related human conditions and diseases. The collaborative research includes the adaptation or development of new analytic programs with participation in an interactive group studying genetic and epidemiological data for selected aging-related phenotypes in the Baltimore Longitudinal Study of Aging; in other outbred populations; and, in the Sardinian "founder population". Accordingly, the duties of this position require the applicant to hold a Ph.D. and have at least 2 years of additional postdoctoral experience in statistical genetics. Applicants must have a record of scientific accomplishments, including excellence in statistical genetic analyses and qualifications to develop, update, and manage statistical staff and analysis software.

Salary is commensurate with experience and accomplishments. The salary range for Staff Scientists is $79,397 - $159,657. A full Civil Service package of benefits (including retirement, health, life and long term care insurance, Thrift Savings Plan, etc.) is available. Applicants must send curriculum vitae, bibliography, and three letters of recommendation to: Chair, LG Staff Scientist — Statistical Genetics Search Committee; Vacancy # **NIA-IRP-07-01**; c/o Peggy Grothe, Intramural Program Specialist; Office of the Scientific Director, National Institute on Aging, 5600 Nathan Shock Drive, Baltimore, MD 21224. Applications must be received before **April 30, 2007**. If additional information is needed, please call 410-558-8012 or email: **grothep@grc.nia.nih.gov.**

DHHS and NIH are Equal Opportunity Employers

Faculty Position in Vascular Biology

Our rapidly growing vascular biology program is interested in dynamic and enthusiastic professionals who will become future leaders in the field of endothelial biology. As part of the expansion, a new state-of-the-art 300,000 square-foot research building has been opened recently to house the Children's Research Institute and expanded facilities for Medical College of Wisconsin faculty. It is expected that the tenure-track appointment will complement existing research expertise in the Institute. Eligible candidates are expected to be Ph.D. or M.D./Ph.D. and will be hired at the rank of Assistant Professor. Candidates with K or R00 level funding are preferred but not required. An attractive start-up package will be provided to facilitate program development. Please submit résumé, research plan, and names of three references to:

Ramani Ramchandran, Ph.D.
Associate Professor
Medical College of Wisconsin
Department of Pediatrics, Genetics Division
CRI Developmental Vascular Biology Program
Translational and Biomedical Research Center
CRI C3420
8701 Watertown Plank Road • P.O. Box 26509
Milwaukee, WI 53226
Email: rramchan@mcw.edu

Children's Hospital and Health System™ — Medical College of Wisconsin
Children's Specialty Group™

EOE/AA M/F/D/V

香 港 大 學
THE UNIVERSITY OF HONG KONG

Founded in 1911, The University of Hong Kong is committed to the highest international standards of excellence in teaching and research, and has been at the international forefront of academic scholarship for many years. Of a number of recent indicators of the University's performance, one is its ranking at 33 among the top 200 universities in the world by the UK's Times Higher Education Supplement. The University has a comprehensive range of study programmes and research disciplines, with 20,000 undergraduate and postgraduate students from 50 countries, and a complement of 1,200 academic members of staff, many of whom are internationally renowned.

Research Assistant Professorships and Post-doctoral Fellowships

Applications are invited for a number of positions as Research Assistant Professor (RAP) (Ref: RF-2006/2007-435) and Post-doctoral Fellow (PDF) (Ref: RF-2006/2007-436), at the University of Hong Kong, on or before February 29, 2008. Appointments will be made for a period of 2 to 3 years.

RAP and PDF posts are created specifically to bring new impetus and vigour to the University's research enterprise. Positions are available from time to time to meet the strategic research needs identified by the University. In this round of advertisement, RAP/PDF positions are available in the following Faculties/Departments/School/Centres/Institute:

- School of Humanities
- Centre for the Advancement of University Teaching
- Faculty of Education
- Civil Engineering
- Law
- Anatomy
- Biochemistry
- Centre for Cancer Research
- Centre for Reproduction, Development and Growth
- Clinical Oncology
- Medicine
- Molecular Chinese Medicine Lab and BioScreening Unit
- Obstetrics and Gynaecology
- Orthopaedics and Traumatology
- Pathology
- Psychiatry
- Research Centre of Heart, Brain, Hormone and Healthy Ageing
- School of Chinese Medicine
- Chemistry
- Earth Sciences
- Ecology and Biodiversity
- Institute of Molecular Technology for Drug Discovery and Synthesis
- Physics
- Zoology
- The Hong Kong Jockey Club Centre for Suicide Research and Prevention

Research Assistant Professors
The main focus of an RAP's duty is research. RAPs can however be assigned some teaching duties, up to 50% of the normal teaching load. Applicants should be research active and have a proven publication record. A highly competitive salary commensurate with qualifications and experience will be offered, with a contract-end gratuity and University contribution to a retirement benefits scheme (totalling up to 15% of basic salary). Annual leave, and medical/dental benefits will also be offered.

Post-doctoral Fellows
PDFs are expected to devote full-time to research. Applicants should be doctoral degree holders having undertaken original research that has contributed to the body of knowledge. A highly competitive salary commensurate with qualifications and experience will be offered. Annual leave and medical benefits will also be available.

Procedures
Prospective applicants are invited to visit the following webpage <https://www.hku.hk/apptunit/> to view the full list of the research areas and their home Faculties/Departments/Schools/Centres for which RAP/PDF positions are currently available. Before preparing an application they should contact the Head of the appropriate academic unit to ascertain that their research expertise matches the research area for which a vacant RAP/PDF post is available.

Applicants must submit a completed University application form, which should clearly state **which position** they are applying for; and in which **academic discipline**. They should also provide further information such as details of their research experience, publications, research proposals, etc.

Further particulars and application forms (272/302 amended) can be obtained at https://www.hku.hk/apptunit/; or from the Appointments Unit (Senior), Registry, The University of Hong Kong, Hong Kong (Fax (852) 2540 6735 or 2559 2058; E-mail: senrappt@hkucc.hku.hk). **Closes March 31, 2007**. Candidates who are not contacted within 3 months of the closing date may consider their applications unsuccessful.

The University is an equal opportunity employer and is committed to a No-Smoking Policy

Dunedin, New Zealand

Postdoctoral Fellowship

(Mathematical Modelling of Polar Marine Hydrodynamics)

(Three year Fixed-term)

UNIVERSITY of OTAGO

Te Whare Wānanga o Otāgo

Department of Mathematics and Statistics

Applications are invited to fill a Postdoctoral Fellowship position supported on the Marsden Fund grant Advances in Ocean Wave/Sea-Ice Interaction: Towards an Operational Model and tenable from 3 September 2007. The successful applicant will have completed a PhD related to the mathematical modelling of heterogeneous floating compliant bodies such as ice floes and/or very large floating structures. They will have a first degree in Mathematics and experience in variational methods, integral equations, numerical solution of differential equations and algebraic systems, and complex variable theory methods such as the Wiener-Hopf technique.

Specific enquiries about this vacancy or the Department may be directed to Professor Vernon Squire, Pro-Vice-Chancellor, Division of Sciences, Tel +64 3 479 7977, Fax +64 3 479 9045, Email vernon.squire@stonebow.otago.ac.nz

Reference Number: A07/30 Closing Date: Friday 16 March 2007.

APPLICATION INFORMATION

With each application you must include an application form, an EEO Information Statement, a covering letter, contact details for three referees and one copy of your full curriculum vitae. **For an application form, EEO Information Statement and a full job description go to: www.otago.ac.nz/jobs Alternatively,** contact **the Human Resources Division, Tel +64 3 479 8269, Fax +64 3 479 8279, Email** job.applications@otago.ac.nz

EEO Employers Group Equal opportunity in employment is University policy.

www.otago.ac.nz/jobs

TENURE-TRACK FACULTY POSITION IN NEUROSCIENCE

As part of an ongoing major expansion in biomedical research, Virginia Commonwealth University Medical Center invites applications for tenure-track faculty positions (F2060-F2062) in the areas of cellular, molecular or translational neuroscience or neurogenetics. Candidates should have an active neuroscience research program with a record of sustained research productivity. More senior candidates should have current extramural funding. Candidates will be considered for the rank of assistant to full professor, based upon qualifications and experience. Applicants should have a M.D., Ph.D. or equivalent degree and will be expected to contribute to the University's teaching mission as well as develop vigorous collaborative efforts with other VCU researchers. Departmental affiliation will depend on the applicant's area of research and interests. VCU neuroscience research is divided across several programs having national prominence in terms of NIH-funded research ranking. Major areas of strength include developmental neuroscience and signal transduction (Dept. of Biochemistry), psychiatric genetics and substance abuse research (Depts. of Pharmacology/Toxicology and Psychiatry, Institute for Drug and Alcohol Studies and Virginia Institute for Psychiatric and Behavioral Genetics), traumatic brain injury (Depts. of Anatomy and Neurobiology and Neurosurgery), and epilepsy (Dept. of Neurology). However, this search also invites outstanding applications from other aspects of neuroscience, especially neurodegenerative disease and neuro-oncology. More information about the University and this open position can be found at **www.vcu.edu** and **www.pubinfo.vcu.edu/facjobs/**.

Applicants should submit a CV, names and e-mail addresses of three references, and a summary of research and teaching interests to: **Michael F. Miles, M.D., PhD., Departments of Pharmacology/Toxicology and Neurology, Virginia Commonwealth University, P.O. Box 980599, Richmond, VA 23298-0613.** Materials should be submitted electronically to: **Mr. Harold Greenwald, haroldg@vcu.edu**. Review of applications will begin immediately and continue until the positions are filled but submission by June 15, 2007 is recommended for full consideration.

VCU is an Equal Opportunity/Affirmative Action Employer and encourages women, minorities and persons with disabilities to apply.

Wheaton College

for Christ and His Kingdom

Faculty Opening Fall 2007

Position in either

NUTRITION or MOTOR CONTROL, DEVELOPMENT & LEARNING

The Applied Health Science Department of Wheaton College is searching for an outstanding full-time, tenure track faculty member at the assistant or associate professor level with expertise in nutrition or motor control, development and learning. The person will be expected to teach in his/her area of specialty, develop elective courses, and maintain a scholarship agenda. The department is focused on human health and lifestyle; experience in the applied/clinical setting is preferred and a doctorate is required.

Deadline for applications is April 12, 2007.

The appointment is intended to begin July 1, 2007.

Applicants should send curriculum vita and a description of their teaching philosophy and research interests to: **Dr. David Ianuzzo, Chair; Applied Health Science Department; Wheaton College; 501 College Avenue; Wheaton, IL 60187** or e-mail **david.ianuzzo@wheaton.edu**.

Additional application materials will be sent to eligible candidates.

Wheaton College is an evangelical protestant Christian liberal arts college whose faculty members affirm a Statement of Faith and the moral and lifestyle expectations of our Community Covenant. The College complies with federal and state guidelines of nondiscrimination in employment; women and minorities are encouraged to apply.

Sr. Scientist II – Protein Crystallographer

E2700-1531

The National Renewable Energy Laboratory is recruiting outstanding candidates for a Structural Biologist position. We are particularly interested in candidates with expertise in x-ray crystallography, and strong interests in understanding the structure, dynamics and function of biological and biomimetic systems related to renewable energy. For additional duties, requirements and application instructions, please see our website at:

www.nrel.gov/employment

NREL

NREL is an equal opportunity employer and drug-free workplace.

VCU Medical Center

Virginia Commonwealth University is recruiting a director of the VCU Molecular Imaging Center. The candidate should have an MD and/or PhD in a relevant discipline, have an established record of external funding in human imaging research with a clear path to clinical translation and have demonstrated experience interacting within a multidisciplinary team. Substantial resources will be available to recruit additional faculty, staff and needed equipment. Appointment will be to a tenure-track or tenured position at the level of associate or full professor in an appropriate department. The candidate will be expected to recruit, organize and lead an active, research-oriented center consisting initially of PET and MR facilities and ultimately incorporating all imaging modalities. Experience in clinical imaging research is desired but not critical. The candidate will also be expected to establish and foster collaborations with multiple research groups at our large academic medical center and to develop a strong external funding base for imaging research. Interested candidates should send their curriculum vitae, letter of interest indicating their current and future research goals, and names of three references to: **Kenneth Kendler MD** at **Kendler@vcu.edu** or **Department of Psychiatry, VCU, PO Box 980126, Richmond VA, 23298 USA.**

VCU is an Equal Opportunity/Affirmative Action Employer. Women, minorities, and persons with disabilities are encouraged to apply.

TEXAS TECH UNIVERSITY
HEALTH SCIENCES CENTER
School *of* Medicine™

Endowed Chair/Tenure Track Faculty Position for Oncology and Cancer Research

The Texas Tech University Health Sciences Center and the Southwest Cancer Treatment and Research Center in Lubbock are seeking applications for a tenure track clinical scientist position at open rank. The successful candidate will hold primary appointments in an appropriate clinical department and the Department of Cell Biology and Biochemistry as well as in the Graduate School of Biomedical Sciences and will be the recipient of an endowed chair for oncology and cancer research. We seek outstanding candidates, with recognized clinical skills and leadership ability to establish a robust clinical cancer and translational research program that will have strong interactions within a group of basic cancer biologists with interests in tumor biology, signal transduction, immunology, cell cycle, drug resistance and proteomics. Candidates must hold an M.D. or M.D./Ph.D., have post-doctoral experience, a strong record of cancer research achievement, preferably with current national-level funding, be willing to spend a majority of their effort on research activities, and be eligible for a Texas medical license.

Applicants should include a cover letter, current CV, a summary of clinical and research accomplishments and interests, and names and contact information for four references to:

Dr. H.W. Weitlauf
Professor and Chair
Department of Cell Biology and Biochemistry
Texas Tech University Health Sciences Center
3601 4th Street, Lubbock, Texas 79424
Phone: (806) 743 2701
email: harry.weitlauf@ttuhsc.edu

Applications from women and minority candidates are particularly encouraged.

Faculty Positions in Environmental Toxicology of the Nervous System
Department of Pharmacology and Toxicology
Center for Environmental Health
Stark Neurosciences Research Institute
Indiana University School of Medicine

The Department of Pharmacology and Toxicology of the Indiana University School of Medicine in Indianapolis in partnership with the Center for Environmental Health (CEH) and the Paul and Carole Stark Neurosciences Research Institute (SNRI) announces a search for new faculty in the areas of molecular mechanisms underlying the impact of environmental toxins on the nervous system. This effort is part of a major expansion of environmental health research over the next several years. The partnering organizations seek outstanding individuals for faculty positions at the **Assistant or Associate Professor** level. More senior individuals with exceptional credentials may be considered. A Ph.D. and/or M.D. degree and at least 3 years of postdoctoral research experience are required, and strong evidence of productivity and grant support are desirable. Of primary interest are candidates who employ pharmacological, molecular, genomic/proteomic and/or chemical approaches to the study of the impact of environmental toxins on physiological and pathological processes with emphasis in the neurosciences. Competitive start-up packages include ample laboratory space and access to exceptional core research facilities. Successful candidates will be expected to develop strong extramurally supported research programs, contribute to an already strong, collaborative research environment, and to excel in mentoring graduate and postgraduate trainees. More information about the department and partnering centers can be found on our websites (**pharmtox.iusm.iu.edu**, **ceh.iu.edu** and **snri.iusm.iu.edu**). Interested individuals should send a curriculum vitae, a research prospectus, and the names and addresses of 3 references. Application materials will only be accepted in electronic format by submission to the attention of: **Neurotoxicology Search Committee** at **cehinfo@iupui.edu**.

We encourage applications from women and other underrepresented groups. In addition, it is the University's policy to provide reasonable accommodations for qualified persons with disabilities. Indiana University is an EEO/AA Employer, M/F/D.

INSTITUT PASTEUR

Institut Pasteur, Paris, France

POSTDOCTORAL FELLOWSHIPS
Institut Pasteur, Paris, France

Founded in 1887 by Louis Pasteur and located in the heart of Paris, the Institut Pasteur is a world-renowned private research organization. The Pasteur Foundation of New York is seeking outstanding Fellowship Applicants. Candidates may apply to any laboratory within 10 departments: Cell Biology and Infection; Developmental Biology; Genomes and Genetics; Immunology; Infection and Epidemiology; Microbiology; Neuroscience; Parasitology and Mycology; Structural Biology and Chemistry; and Virology. See website for details.

Fellowship package is $60,000 per year for three years. *U.S. citizenship required.* This is a biannual call; next application deadline: **September 7, 2007**.

e-mail: Pasteurus@aol.com.
Website: http://www.pasteurfoundation.org

From physics to nutrition

For careers in science, turn to *Science*

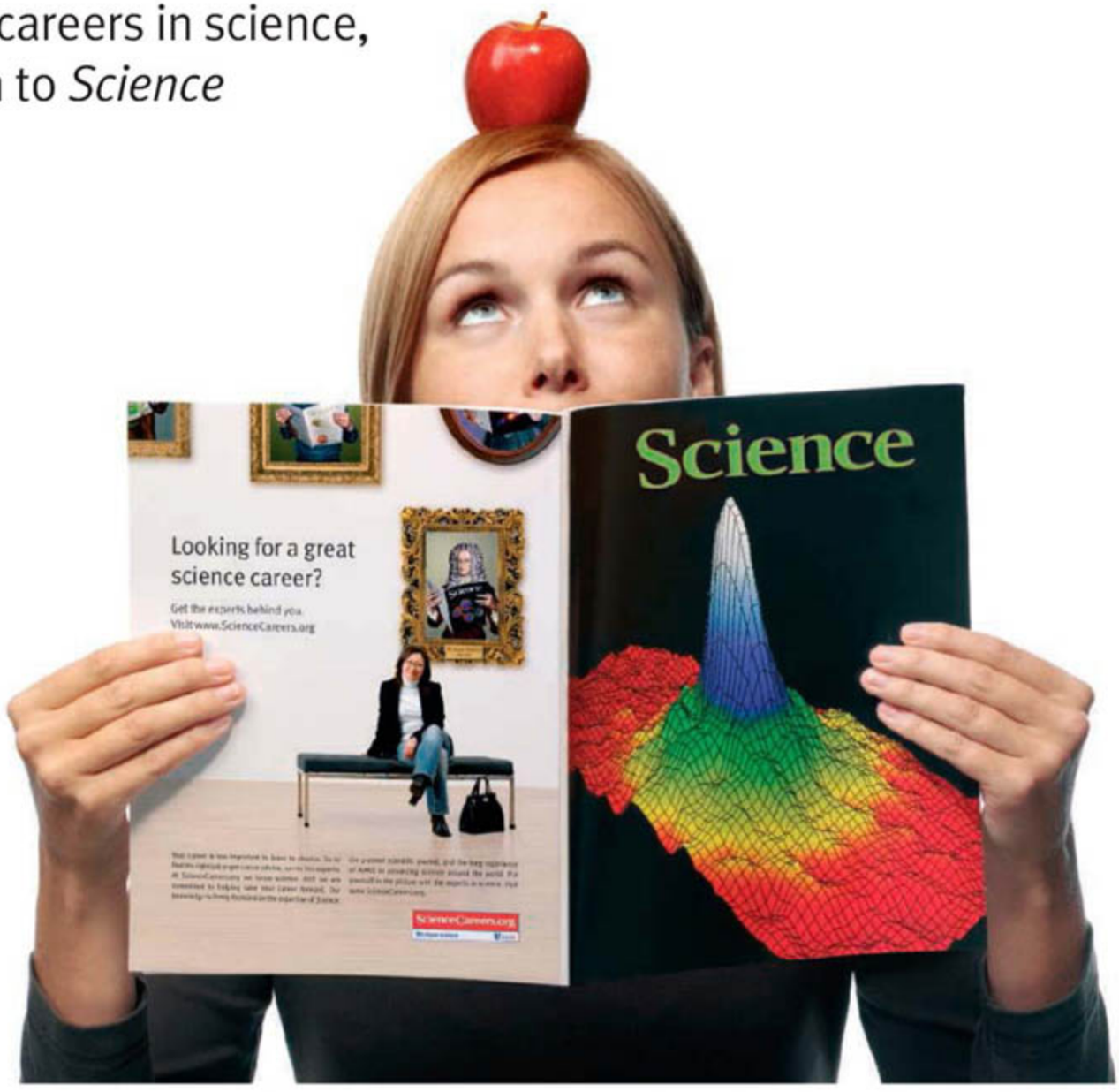

If you want your career to bear fruit, don't leave it to chance. At ScienceCareers.org we know science. We are committed to helping you find the right job, and to delivering the useful advice you need. Our knowledge is firmly founded on the expertise of *Science*, the premier scientific journal, and the long experience of AAAS in advancing science around the world. ScienceCareers.org is the natural selection. **www.sciencecareers.org**

Features include:

- Thousands of job postings
- Career tools from Next Wave
- Grant information
- Resume/CV Database
- Career Forum

ScienceCareers.org
We know science AAAS

POSITIONS OPEN

ASSISTANT PROFESSOR
Anatomy

The Department of Biological Sciences at San José State University (SJSU) seeks applicants for a **TENURE-TRACK** position to start on August 21, 2007.

Applicants must have a Ph.D. degree in the anatomical or physiological sciences and experience in cadaver-based anatomy. Ability to teach courses in histology, embryology, and/or neuroanatomy is desirable. The successful candidate will participate in teaching anatomy and physiology courses for nonmajors and will teach in courses for biology majors and graduate students. Applicants must have a proven record or potential for excellence in teaching. The successful candidate must address the needs of a student population of great diversity, in age, cultural background, ethnicity, primary language, and academic preparation. Applicants must have research experience and publications in their discipline. The successful candidate must have the ability to establish an extramurally funded research program involving undergraduates and M.S. graduate students. Research collaborations with other Department faculty are encouraged. Opportunities for external collaboration include nearby biotechnology companies, Bay area universities, Moss Landing Marine Laboratories, and NASA Ames Research Center.

For consideration, send a letter of application, curriculum vitae, official university graduate and undergraduate transcripts, a statement of teaching interests/philosophy and research interests, and at least three original letters of reference with contact information to the **Anatomy and Physiology Search Committee** at the: **Department of Biological Sciences, San José State University, One Washington Square, San José, CA 95192-0100.** Please include job requisition number JOID 012169 on all correspondence. Review of applications will commence on March 15, 2007, and continue until the position is filled. **Website: http://www.sjsu.edu/depts/Biology.** *SJSU is an Equal Opportunity/Affirmative Action Employer committed to the core values of inclusion, civility, and respect for each individual.*

PHARMACEUTICAL SCIENCES FACULTY POSITIONS
University of Southern Nevada
College of Pharmacy
South Jordan, Utah Campus

The University of Southern Nevada College of Pharmacy has established a program in the Salt Lake City, Utah, area and is seeking applicants for full-time faculty positions at the Utah campus in the areas of biochemistry/medicinal chemistry and pharmaceutics. Responsibilities include teaching in blocks and electives related to your discipline, participating in research and scholarly endeavors, and providing service to the College and the community.

Minimum requirements include a Ph.D. degree in biochemistry, immunology, medicinal chemistry, pharmaceutics, or a related discipline. Successful candidates should have excellent communication skills and an interest in creative and nontraditional teaching methods. Documented evidence of research or other scholarly initiatives is required. Salary and rank will depend on qualifications and experience.

Submit a letter of interest, curriculum vitae, statement of educational philosophy, and contact information for three professional references to: **Tyler Rose, Ph.D., University of Southern Nevada College of Pharmacy, 10920 S. River Front Parkway, South Jordan, UT 84095; e-mail: trose@usn.edu.**

An Affirmative Action/Equal Opportunity Employer.

POSTDOCTORAL POSITION
Cancer Research

For *U.S. citizen/permanent resident* for training grant funding at Johns Hopkins University School of Medicine. Please send curriculum vitae and three references to: **Dr. L. Resar, Johns Hopkins University School of Medicine, 720 Rutland Avenue, Ross Research Building, Room 1025, Baltimore, MD 21205, e-mail: lresar@jhmi.edu.**

POSITIONS OPEN

ASSISTANT/ASSOCIATE PROFESSOR

The Department of Neuroscience, Cell Biology, and Physiology at Wright State University (WSU), Dayton, Ohio, invites applications for a tenure-track faculty position at the Assistant or Associate Professor level. The successful candidate will have research interests that compliment the research strengths of the Department and the newly established Comprehensive Center for Neuroscience (CCN) in the Boonshoft School of Medicine. Specifically, the successful candidate will pursue research in the function, structure, development, and/or modification of synapses and circuits in the spinal cord or motor systems. Preference will be given to candidates using genetic animal models to study the formation and maturation of synapses and synaptic circuits. Candidates are expected to teach neuroscience in graduate and medical school courses. Requirements for the position include: a Ph.D. degree, an excellent record of research accomplishments, ability to direct innovative independent research, competitive funding potential, and a strong commitment to high quality teaching. Applicants for the Assistant rank must have at least two years of postdoctoral training and a record of publications demonstrating excellence in research and potential for obtaining extramural grant funding. Applicants for the Associate rank must have at least four years as an Assistant Professor and a record of publications and grants demonstrating a sustained quality research program with a national reputation for excellence and supervision of graduate students. Review of applications will begin March 15, 2007, and continue until the position is filled. Interested applicants should submit curriculum vitae, statement of research and teaching interests, up to three representative reprints and/or preprints, and at least three references to: **Dr. Francisco Alvarez, Chair NCBP Faculty Search Committee, Department of Neuroscience, Cell Biology and Physiology, 235C Biological Sciences Building, Wright State University, 3640 Colonel Glenn Highway, Dayton, OH 45435** or **e-mail: ncbp@wright.edu.** *WSU is an Affirmative Action/Equal Opportunity Employer.*

FACULTY in TUMOR IMMUNOLOGY

The San Antonio Cancer Institute, an NCI-designated Cancer Center, seeks tumor **IMMUNOLOGISTS** to join the Division of Medical Oncology, Department of Medicine at the University of Texas Health Science Center at San Antonio (UTHSCSA). A strong record of accomplishment in basic research is essential. Candidates must qualify for appointment as **ASSISTANT PROFESSOR or HIGHER.** Significant resources and excellent collaborations are available to establish a competitive research program. UTHSCSA offers excellent benefits and competitive salaries. Send a cover letter outlining future research interests, curriculum vitae, and three references in hard copy to: **Search Committee for Tumor Immunology, Division of Medical Oncology, UTHSCSA, 7703 Floyd Curl Drive, MSC 7884, San Antonio, TX 78229-3900,** or electronically to **e-mail: saci@uthscsa.edu.** *All faculty appointments are designated as security-sensitive positions. UTHSCSA is an Equal Employment Opportunity/Affirmative Action Employer.*

POSTDOCTORAL FELLOW POSITION

A Postdoctoral position is available to study the role of the Parkinson's disease-related protein alpha-synuclein using yeast. This position is available immediately. Applicants must have a Ph.D. with experience in yeast genetics, molecular and cellular biology, and microscopy. All interested applicants should forward curriculum vitae/bibliography and list of three references to: **Stephan Witt, Ph.D., Department of Biochemistry and Molecular Biology, Louisiana State University Health Sciences Center, 1501 Kings Highway, Shreveport, LA 71130; e-mail: swittl@lsuhsc.edu, fax: 318-675-5180.** Further details can be found at **website: http://www.shrevebiochem.com.**

Louisiana State University Health Science Center is an Affirmative Action/Equal Opportunity Employer.

POSITIONS OPEN

CHAIR, DEPARTMENT of BIOLOGY
Howard University

The Department of Biology at Howard University is seeking candidates for the position of Chair of the Department. The Department consists of 26 full-time faculty members, 44 graduate students, and 800 undergraduate students, granting B.S., M.S., and Ph.D. degrees. Candidates must have a Ph.D. degree in a biological science accompanied by significant record of teaching experience, research productivity, and grants acquisition. Qualified candidates should also have experience in planning, budgeting, and all other aspects of fiscal affairs as well as a clear vision for the Department and an understanding of and commitment to the mission of Howard University. The area of specialization of the candidate is open. Applicants should send curriculum vitae that includes a clear statement of educational and administrative philosophy, and arrange for three letters of reference to be sent. The deadline for receipt of all materials is 15 March 2007. Please send materials to:

Dr. James Lindesay, Chair
Biology Search Committee
Office of the Dean
College of Arts and Sciences
Locke Hall, Room 101
Howard University
Washington, DC 20059

Founded in 1867, Howard University is a comprehensive research-oriented institution. It has a rich history and tradition of providing top-quality educational programs for more than 10,000 undergraduate, graduate, and professional students. Its multiple academic schools are supported by highly rated technological ancillary units. The University owns and operates a 500 bed teaching hospital, an FM radio station, and a public television station. The College of Arts and Sciences is the flagship academic unit at the University that facilitates more than thirty major programs of study through the natural sciences, social sciences, humanities, and fine arts divisions. The Graduate School develops the research abilities of students seeking degrees at the Master's and doctoral levels. *Howard University is an Equal Opportunity Employer.*

VISITING ASSISTANT PROFESSOR POSITIONS
in Marine Ecology and Genetics (Two Positions)
Claremont McKenna, Pitzer, and Scripps Colleges

The Joint Science Department of Claremont McKenna, Pitzer, and Scripps, three liberal arts colleges in the Claremont Colleges Consortium in Southern California, seeks to hire two visiting Assistant Professors for the 2007-2008 academic year, beginning August 2007. Teaching responsibilities for position one include an upper-division course in marine ecology, a nonmajors' course in marine biology, and a lecture section of the organismal/evolutionary semester of introductory biology. For position two, responsibilities include an upper-division genetics course and laboratory sections of both halves of the introductory biology course. Participation in research, particularly directing undergraduate research projects is encouraged. A Ph.D. in biology or related subject, and prior teaching experience are required.

Please submit curriculum vitae and a statement of interest, specifying which position is of interest to you, and arrange to have three letters of reference sent to: **Temporary Biology Positions, W.M. Keck Science Center, 925 N. Mills Avenue, Claremont, CA 91711-5916. Telephone: 909-621-8298.** Inquiries to **Dr. Emil Morhardt, e-mail: emorhardt@jsd.claremont.edu.** Review of applications begins March 19, 2007. The positions will remain open until filled.

In a continuing effort to enrich its academic environment and provide equal educational employment opportunities, the Claremont Colleges actively encourage applications from women and members of historically underrepresented groups in higher education.

POSITIONS OPEN

PHYSIOLOGY EDUCATION SPECIALIST

Applications are invited for a tenure-track **ASSISTANT PROFESSOR** in the Department of Biological Sciences at Northern Arizona University (NAU), **(website: http://www.nau.edu/biology** for more information on the Department and the position).

Successful candidates will have a Ph.D. in physiology or a related field, two years of college level teaching experience or equivalent, a record of scholarly activity in physiology pedagogy, and a demonstrated ability to work effectively with people from a variety of culturally diverse backgrounds. Preference will be given to candidates with a demonstrated ability to enter our teaching rotation and effectively deliver physiology education in an undergraduate and graduate setting. Specific teaching responsibilities may include human anatomy and physiology, animal physiology, advanced human physiology, and/or pathophysiology. The successful candidate is expected to establish a program in teaching-related scholarly activity including (1) assessment of teaching effectiveness, (2) effective application of modern pedagogical methods, and (3) being a departmental leader for pedagogical improvement. Applicants should submit curriculum vitae and a statement of teaching philosophy, and have three letters of recommendation sent to: **Physiology Search Chair, Department of Biological Sciences, P.O. Box 5640, Northern Arizona University, Flagstaff, AZ 86004.** The search will remain open until position is filled or April 1, 2007; however the committee will begin reviewing applications on March 5, 2007. The successful candidate is expected to start August 20, 2007.

NAU is an Affirmative Action/Equal Employment Opportunity/Minorities, Women, Persons with Disabilities, Veterans Employer.

Veterans Affairs San Diego Healthcare System, a progressive, state-of-the-art university-affiliated teaching facility, is seeking Anatomic Pathology/Clincial Pathology Board-certified **PATHOLOGIST.** The Department of Pathology, in this College of American Pathologists-accredited clinical laboratory, is recruiting for a **CHIEF OF ANATOMIC PATHOLOGY**. Candidate will possess excellent clinical and organization skills. Responsible for all surgical pathology, autopsies, cytological examinations of the body fluids, exudates, and aspirates; responsible for coordination of all elements of anatomic pathology; and training of anatomic pathology residents. Maintains expertise for consultation and guidance in matters pertaining to anatomic pathology and cytopathology and is responsible for ensuring all activities meet requirements for accrediting agencies. Candidate should qualify for appointment as faculty to the Pathology Department of University of California San Diego School of Medicine. Salary/rank commensurate with experience and established Veterans Affairs salary scales. Medical license in any state. *Non-U.S. citizens will only be considered if this search yields no qualified candidates.* Recruitment/relocation incentive may be authorized. Education Debt Reduction Program funding may be available. Send curriculum vitae to: **Lorraine Conn, Mail Code 113, Veterans Affairs San Diego Healthcare System, 3350 La Jolla Village Drive, San Diego, CA 92161 (telephone: 858-518-7259).** *Affirmative Action/Equal Opportunity Employer.*

POSTDOCTORAL FELLOW POSITION

The Anatomy and Physiology Department invites applications for the position of Postdoctoral Fellow in the Tumor Physiology Laboratory **(website: http://www.vet.k-state.edu/employment/index.htm).** Ph.D. in cancer biology or biochemistry is required. Submit electronically curriculum vitae, short essay describing scientific experiences and/or future study, names of two to three references to: **Dr. Masaaki Tamura (e-mail: mtamura@vet.k-state.edu).** Screening of applications will begin February 26, 2007, and continue until position is filled. *Kansas State University (KSU) is an Equal Opportunity, Affirmative Action Employer. KSU actively seeks diversity among its employees.*

POSITIONS OPEN

DEPARTMENT HEAD and PROFESSOR
Environmental Health Science
College of Public Health
The University of Georgia

The Department of Environmental Health Science, in the recently established College of Public Health at the University of Georgia **(website: http://www.uga.edu/publichealth/ehs/)** Athens, Georgia, seeks an established scholar to lead the Department. Candidates must have an earned Doctorate, and achievement sufficient to merit appointment as full professor. Minimum qualifications include (1) evidence of leadership and likelihood of success in an academic setting; (2) demonstrated success in securing external research funding; (3) a willingness to foster multidisciplinary collaboration, and (4) interpersonal skills to effectively interact with students, faculty, staff, and administrators.

The Department supports an active research program and offers degrees at the Bachelor's, Master's, and doctoral levels. The successful candidate will be expected to provide vision and leadership for the continued growth and development of the Department. There are substantial opportunities for research collaborations with other programs, institutes, and centers.

Screening of applications will begin immediately. To be assured of full consideration, application must be received by April 30, 2007. Please send a letter indicating your research interests, your administrative and supervisory experience and philosophy, a list of four references (references will be contacted only with the applicant's knowledge), and curriculum vitae to: **Chair, Search Committee, Department of Environmental Health Science/College of Public Health, 206 Environmental Health Science Building, The University of Georgia, Athens, GA 30602-2102.**

The University of Georgia is an Equal Opportunity/Affirmative Action Employer.

The Department of Pharmacology and Toxicology, School of Pharmacy, University of Kansas, is recruiting a tenure-track **ASSISTANT PROFESSOR** to begin as early as the fall of 2007. The successful applicant will teach pharmacology to graduate students and pharmacy students, obtain NIH and other external funding to support an active research program in neuropharmacology (preferably in neurotransmitter receptor systems and signaling broadly defined), show evidence of ability to collaborate across departments and campuses, and provide service via select committee obligations. A Ph.D. in a biological or pharmaceutical science with postdoctoral experience in neuropharmacology is required. Send curriculum vitae, research plan, and three letters of reference to: **Nancy Muma, Department of Pharmacology and Toxicology, School of Pharmacy, University of Kansas, 1251 Wescoe Hall Drive, 5064 Malott Hall, Lawrence, KS 66045.** In addition, upon receipt of the materials, you will be sent instructions for completing required sections of the online Faculty and Academic Staff Application Data Form. The review of applications will begin March 1, 2007, and continue until the position is filled. *Equal Opportunity/Affirmative Action Employer*

Two **POSTDOCTORAL ASSOCIATE** positions are available immediately at the Scripps Research Institute to investigate drug development for filarial parasitic infection and the development of molecular biological tools to study pandemic influenza. Highly motivated individuals with a Ph.D. in molecular biology or parasitology are encouraged to apply. For the former position, experience with *C. elegans* is required. Competitive salary and benefit package commensurate with experience will be provided. Interested candidates should submit curriculum vitae, a statement of research interests, and contact information for three references to: **Kim D. Janda, Ph.D., Departments of Chemistry and Immunology and Worm Institute for Research and Medicine (WIRM), The Scripps Research Intitute, 10550 North Torrey Pines Road, BCC-582, La Jolla, CA 92037;** or by **e-mail: kdjanda@scripps.edu.**

POSITIONS OPEN

CAREER OPPORTUNITY

The Veterans Affairs San Diego Healthcare System is currently seeking **PHYSICIAN** applications for the Chief of Pathology and Laboratory Service. Assignment is approximately 50 percent administrative and supervisory and 45 percent clinical and teaching, in this University of California San Diego School of Medicine affiliate. Responsibilities include oversight and direction of a clinical laboratory performing 2.5 million tests annually, anatomic pathology, and cytopathology; pre-analytical, analytical, and post-analytical procedures for clinical and anatomic pathology departments; accountability for the training of residents in the graduate medical education program; coordination of teaching and patient care conferences; and leadership to a Department of over 100 full-time employees, contract employees, and students, including direct supervision of nine staff, five physicians, and four administrative/technical personnel. We offer excellent education, teaching, research, and clinical practice opportunities in an interdisciplinary collaborative setting. Academic appointment with the affiliate is an expectation. Comprehensive benefits package. *Must be U.S. citizen.* Recruitment/relocation incentive may be authorized. Education Debt Reduction Program funding may be available. Send curriculum vitae and direct questions to: **Jan Stock, Human Resources Specialist, telephone: 858-552-8585, ext. 7859, Veterans Affaris San Diego Healthcare System, 3350 La Jolla Village Drive, San Diego, CA 92161.** *Equal Opportunity Employer.*

ENDOWED PROFESSORSHIP in PHYSIOLOGY EDUCATION
Department of Physiology
University of Kentucky Medical Center
Website: http://www.mc.uky.edu/physiology

We seek an established authority in biomedical education to fill the newly endowed Donald T. Frazier Professorship in Physiology. Applicants must have a Ph.D., M.D., or equivalent degree, a strong record of accomplishment in medical or science education, and extramural funding in educational, basic, or translational research. This is a tenured or tenure-track faculty position at a rank appropriate to the applicant's career stage. The successful candidate will promote existing programs in professional, graduate, and undergraduate education and in science outreach and will stimulate innovative new initiatives to enhance our educational mission. We are particularly interested in applications from women, minorities, and people with disabilities. Qualified individuals are encouraged to forward curriculum vitae, a concise statement of educational philosophy and research interests, and the names of three references to: **Ms. Bonnie Emerich, Department of Physiology, University of Kentucky Medical Center, 800 Rose Street, Room MS-508, Lexington, KY 40536-0298.** *The University of Kentucky is an Affirmative Action/Equal Opportunity Employer.*

POSTDOCTORAL FELLOW/LEUKEMIA RESEARCH

An excellent opportunity for career development with conversion to a Junior Faculty appointment. This position will study signal transduction, degradation, and transcriptional regulation by the AML1, AML/ETO, and TEL/AML proteins. A strong knowledge of hematopoiesis and molecular and cellular biology is required. Please send curriculum vitae and three reference names to: **Andrew S. Kraft, M.D., Director, Hollings Cancer Center, 86 Jonathan Lucas Street, P.O. Box 250955, Charleston, SC 29425. E-mail: hccjobs@musc.edu.** Please reference ad 1005.

POSTDOCTORAL POSITION available at the Department of Urology, New York University School of Medicine to study bladder cancer, urinary tract infection, and kidney stones using biochemical and genetic tools. A Ph.D. and three years of strong research experience in general biology, biochemistry, and molecular biology are required. Please e-mail cover letter, curriculum vitae, and referee information to **e-mail: xue-ru.wu@med.nyu.edu** for consideration.

POSITIONS OPEN

RESEARCH EPIDEMIOLOGIST

Lincoln Park Zoo, in partnership with the Association of Zoos and Aquariums and USDA-Animal and Plant Health Inspection Service, is establishing a Zoonotic Emerging Disease Surveillance Center as part of the Davee Center for Veterinary Epidemiology and Endocrinology at Lincoln Park Zoo. This position will be the **PROGRAM COORDINATOR** for this initiative. Primary duties include (1) development and management of existing and new Association of Zoos and Aquariums (AZA) disease surveillance and monitoring programs (avian influenza, West Nile virus, TB) and (2) development of other AZA-based epidemiological research in conjunction with the Davee Center mission and strategic objectives. Successful candidates must have a demonstrated ability to design, conduct, and communicate the results of research and applied programs in epidemiology; demonstrate a basic understanding of ecology and endocrinology for collaborative purposes; and demonstrate a commitment to wildlife conservation through management of wild and captive populations, and willingness to participate in the Department's team approach to conservation research projects. Preference of medical degree (M.D./D.V.M.) and postgraduate epidemiology training or Ph.D. in epidemiology or a closely related biological discipline. More information available at **website: http://www.lpzoo.org.** Send resume, copies of college transcripts, and letter of interest to: **Human Resources Department, Lincoln Park Zoo, 2001 North Clark Street, Chicago, IL 60614.**

RESEARCH FELLOWSHIP
Cardiac Electrophysiology

The University of Vermont College of Medicine is seeking well-qualified candidates for a research fellowship in cardiac electrophysiology. The research will be performed in concert with the University Cardiac Electrophysiology group at Fletcher Allen Health Care. The Cardiac Electrophysiology group is a research-oriented group interested in coordinated basic and clinical research into the mechanisms of cardiac arrhythmias and the development of improved tools and techniques for interventional treatment of cardiac arrhythmias. The group has experience in electrophysiologic research at the ion channel, isolated myocytes, and whole organ levels. There is excellent opportunity for collaboration with a world class group studying intracellular calcium handling and heart failure. Applications are encouraged from those with either an M.D. or Ph.D. Please send curriculum vitae and three references to: **Peter S. Spector, M.D., McClure 1 Cardiology, 111 Colchester Avenue, Burlington, VT 05401, telephone: 802-847-4539, fax: 802-847-8818, e-mail: peter.spector@vtmednet.org.**

Additional job postings not featured in this issue can be viewed online at **website: http//www.sciencecareers.org.** New jobs are added daily!

MARKETPLACE

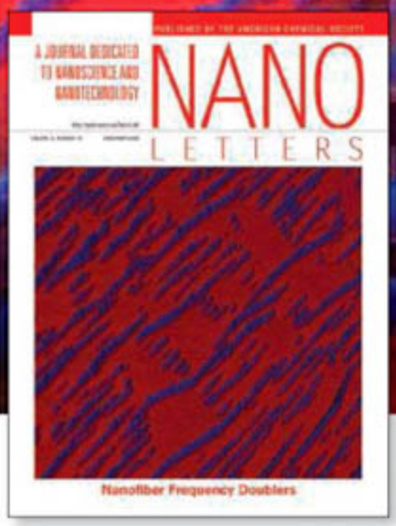

9.847 ISI® impact factor

#1 in nanoscience & nanotechnology

http://pubs.acs.org/NanoLett

#1 in nanoscience & nanotechnology with a 9.847 ISI® impact factor

In the new category of nanoscience & nanotechnology, *Nano Letters* leads the way with a big ISI® impact factor of **9.847**, as reported in the 2005 ISI® Journal Citation Reports®. The Journal received 13,040 citations, a 77% increase over 2004.

Nano Letters is a Rising Star

Thomson Scientific® has named *Nano Letters* as a "Rising Star" journal in 10 out of 12 periods in the past two years. "Rising Star" journals are those journals that achieved the highest percentage increase in total citations during the previous bimonthly period, out of all chemistry journals indexed by Thomson Scientific.

Co-Editor: A. Paul Alivisatos
University of California, Berkeley

Co-Editor: Charles M. Lieber
Harvard University

2007 Subscription Information
Volume: 7, 12 issues
Print Edition ISSN: 1530-6984
Web Edition ISSN: 1530-6992
Institutional Subscription Rate: $1,424
(Outside North America: $1,518)

To view a sample issue of *Nano Letters* and lists of most-cited and most-accessed articles, go to http://pubs.acs.org/NanoLett

Most-cited articles published in 2005 from *Nano Letters*:

Immunotargeted Nanoshells for Integrated Cancer Imaging and Therapy
Loo, C.; Lowery, A.; Halas, N.; West, J.; Drezek, R.
Nano Lett; (Letter); **2005**; *5*(4); 709-711. DOI: 10.1021/nl050127s

Cytotoxicity of Colloidal CdSe and CdSe/ZnS Nanoparticles
Kirchner, C.; Liedl, T.; Kudera, S.; Pellegrino, T.; Munoz Javier, A.; Gaub, H. E.; Stolzle, S.; Fertig, N.; Parak, W. J.
Nano Lett; (Letter); **2005**; *5*(2); 331-338. DOI: 10.1021/nl047996m

Nanoscale Morphology of High-Performance Polymer Solar Cells
Yang, X.; Loos, J.; Veenstra, S. C.; Verhees, W. J. H.; Wienk, M. M.; Kroon, J. M.; Michels, M. A. J.; Janssen, R. A. J.
Nano Lett; (Letter); **2005**; *5*(4); 579-583. DOI: 10.1021/nl048120i

Gold Nanocages: Bioconjugation and Their Potential Use as Optical Imaging Contrast Agents
Chen, J.; Saeki, F.; Wiley, B. J.; Cang, H.; Cobb, M. J.; Li, Z.-Y.; Au, L.; Zhang, H.; Kimmey, M. B.; Li, X. D.; Xia, Y.
Nano Lett; (Letter); **2005**; *5*(3); 473-477. DOI: 10.1021/nl047950t

Highly Efficient Multiple Exciton Generation in Colloidal PbSe and PbS Quantum Dots
Ellingson, R. J.; Beard, M. C.; Johnson, J. C.; Yu, P.; Micic, O. I.; Nozik, A. J.; Shabaev, A.; Efros, A. L.
Nano Lett; (Letter); **2005**; *5*(5); 865-871. DOI: 10.1021/nl0502672

ACS AuthorChoice Free Access

ACS AuthorChoice is a new option for open access.
For details go to **http://pubs.acs.org/4authors/authorchoice**

JOIN THE ACS NANO CYCLE OF EXCELLENCE

contribute | *publish* | *review*

ACS PUBLICATIONS
HIGH QUALITY. HIGH IMPACT.

LESS SAMPLE.

MORE STORY.

Sensitive and sensible, BioSource™ ELISA Kits deliver relevant data from as little as 50 µl. Or fewer than 10,000 cells if you're working with phosphoELISA™ Kits. We offer a wide range of ELISA and phosphoELISA™ Kits for measuring cytokines and phosphorylated proteins—with the exacting sensitivity and reproducibility you need. And faster incubation times. What are you waiting for? See how far your sample can go with BioSource™ ELISA Kits at **www.invitrogen.com/elisa**.

invitrogen™